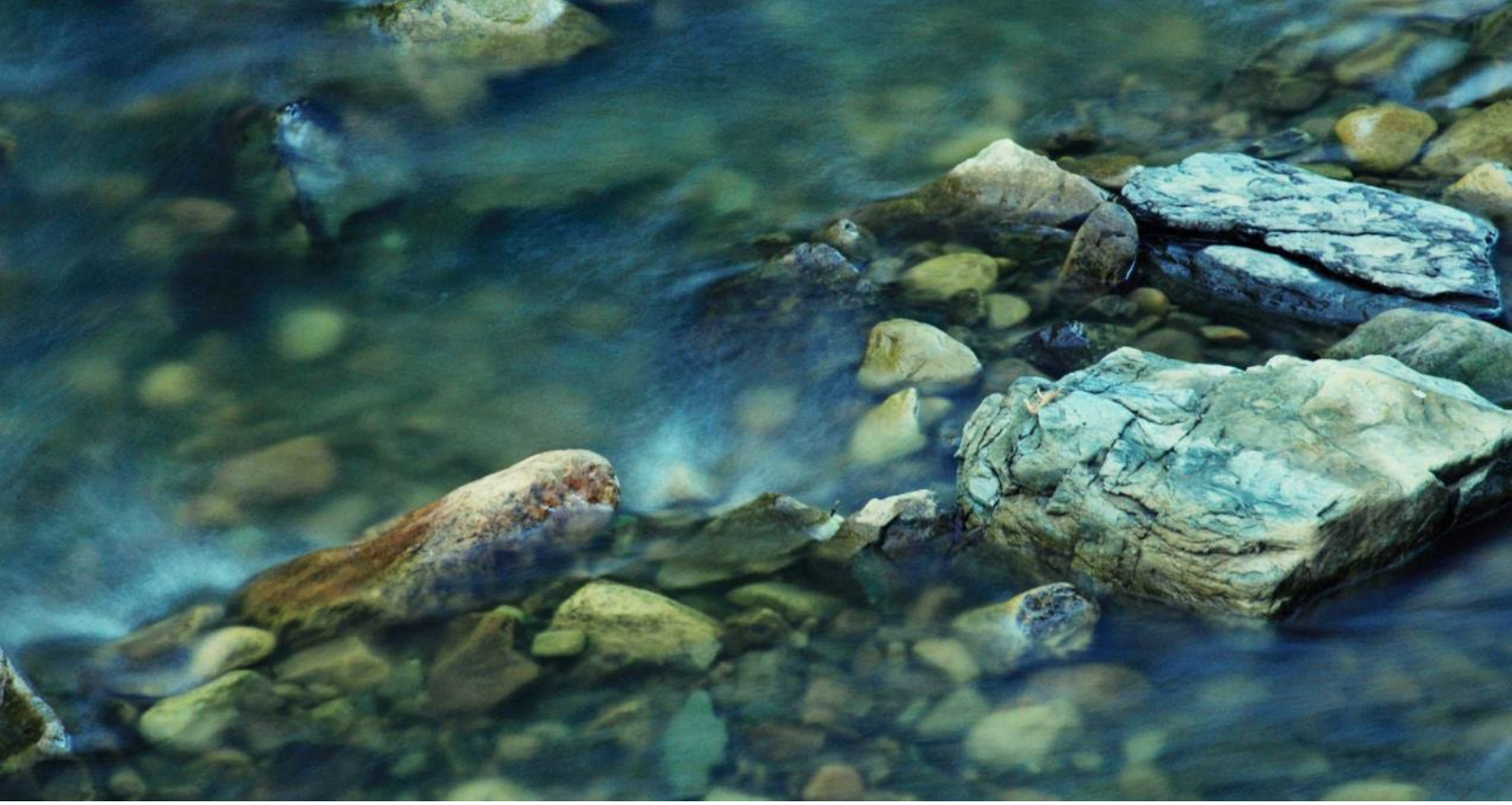

July 2023
Grand Lake Sedimentation Study

Revised Updated Study Report

Prepared for

GRDA
Grand River Dam Authority

July 2023
Grand Lake Sedimentation Study

Revised Updated Study Report

Prepared for
Grand River Dam Authority
P.O. Box 409
Vinita, Oklahoma 74301

Prepared by
Anchor QEA, LLC
660 West Washington Avenue
Suite 302
Madison, Wisconsin 53715

Simons & Associates
P.O. Box 607
Midway, Utah 84049

TABLE OF CONTENTS

TABLES

FIGURES

EXHIBITS

LIST OF ABBREVIATIONS AND TERMS

µm	micrometer
1D	one-dimensional
2D	two-dimensional
3D	three-dimensional
AASHTO	American Association of State Highway and Transportation Officials
ADCP	acoustic Doppler current profiler
BC	boundary condition
cfs	cubic feet per second
cm	centimeter
cm/s	centimeters per second
FERC	Federal Energy Regulatory Commission
ft^2	square feet
ft^3	cubic feet
ft/ft	vertical feet per horizontal foot
g/cm^3	grams per cubic centimeter
GIS	Geographic Information System
GPS	Global Positioning System
Grand Lake	Grand Lake O' the Cherokees
GRDA	Grand River Dam Authority
HEC-RAS	Hydrologic Engineering Center's River Analysis System
HEC-SSP	Hydrologic Engineering Center Statistical Software Package
H&H	hydrology and hydraulics
ISR	Initial Study Report
ITR	Independent Technical Review
lb/ft^2	pounds per square foot
$lb/ft^2/hr$	pounds per square foot per hour
LiDAR	Light Detection and Ranging
mm	millimeter
N/A	not applicable
NED	National Elevation Dataset
NGVD29	National Geodetic Vertical Datum of 1929
NSE	Nash-Sutcliffe Efficiency
OM	Operations Model
Ops	operations
OWRB	Oklahoma Water Resources Board
Pa	Pascal

PBIAS	Percent Bias
pcf	pounds per cubic foot
PD	Pensacola Datum
Project	Pensacola Hydroelectric Project
REAS	Real Estate Adequacy Study
RM	river mile
RMSE	root-mean-square deviation
RSR	RMSE-Observations Standard Deviation Ratio
RTK	Real-Time Kinematic
SBP	Sub-Bottom Profiler
SMD	Study Modification Determination
SPD	Study Plan Determination
SSC	suspended sediment concentration
STM	sediment transport model
TPU	total propagated uncertainty
UHM	Upstream Hydraulic Model
USACE	U.S. Army Corps of Engineers
USDA	U.S. Department of Agriculture
USGS	U.S. Geological Survey
USP	Updated Study Plan
USR	Updated Study Report
USSD	U.S. Society on Dams
UWSFL	University of Wisconsin Soil and Forage Laboratory
WEST	WEST Consultants, Inc.
WSE	water surface elevation
WSLH	Wisconsin State Laboratory of Hygiene

Executive Summary

Anchor QEA, LLC (formerly FreshWater Engineering), and Simons & Associates were retained to support the Grand River Dam Authority (GRDA) as subconsultants to Mead & Hunt for the Federal Energy Regulatory Commission (FERC) relicensing of the Pensacola Hydroelectric Project (Project). Anchor QEA's and Simons & Associates' role, with Mead & Hunt's support, is to perform a Sedimentation Study to determine the rates and locations of sedimentation throughout the Grand Lake O' the Cherokees (Grand Lake) watershed and associated tributaries.

This task culminated in the development of a sediment transport model (STM) using the Hydrologic Engineering Center's River Analysis System (HEC-RAS) fluvial modeling software. Data needed for model development range from topographic information to stream discharge volumes, water surface elevations (WSEs), and sediment parameters both in the lake and streambeds and moving into the system through major tributaries. Anchor QEA evaluated publicly available data sources to compile parameters necessary for model development and to determine where additional field work was required to fill data gaps.

WEST Consultants, Inc. (WEST), provided assistance in the Sedimentation Study. Initially, WEST completed an Independent Technical Review (ITR) of the STM and Initial Study Report. The ITR comments and recommendations are documented in a technical memorandum completed in April 2022 (WEST 2022). WEST provided technical support in the development and calibration of the STM for the Updated Study Report (USR). This effort included providing recommendations to improve model calibration and statistical methods to measure how the model is performing and developing a script to adjust the HEC-RAS geometry to account for consolidation of the future sediment deposits within the reservoir. WEST provided quality assurance reviews of the STM developed for the USR.

Topographic and bathymetric data are available from a range of sources. Grand Lake itself was surveyed by the Oklahoma Water Resources Board in 2009, then again by the U.S. Geological Survey (USGS) in 2019. Upstream surveys of the Neosho River, Spring River, and Elk River were performed as part of the 1998 Real Estate Adequacy Study (REAS), and USGS surveyed those reaches again in 2017. Topographic information was available from surveys performed in support of the 1998 REAS and Light Detection and Ranging (LiDAR) flights conducted in 2011. Other topographic information was obtained from the USGS National Elevation Dataset one-third, arc-second datasets where LiDAR information was unavailable. Circa-1940 topographic maps were digitized for analysis of conditions at the time of dam construction. Additionally, stage-storage curves were available from circa-1940 U.S. Army Corps of Engineers as-built drawings as well as the more recent Grand Lake bathymetry surveys.

Other data are available from USGS gaging stations located throughout the Grand Lake watershed. WSE data and stream discharge information are available along the Neosho, Spring, and Elk rivers, as well as on Tar Creek. These stations also provide sediment transport data in the form of suspended sediment concentration (SSC) measurements taken throughout the period of record at each gage.

Data gaps existed within the period of record for the USGS gaging stations within the Grand Lake watershed, and the gaging network lacked spatial density. As a result, the study team developed a field monitoring system to track WSE throughout the study area and fill data gaps. A set of 16 monitoring locations were selected, and HOBO pressure loggers were installed at each site in December 2016. Over the last 4.5 years, pressure and temperature were recorded at 30-minute intervals. The record provided a detailed dataset of water levels that were used for model development and calibration.

Other data gaps identified were related to sediment properties. Sediment conditions within the basin were evaluated using grab samples to evaluate grain size distributions. In general, the streambeds consist of gravel with limited sand; the lake is primarily silt and clay. Due to the presence of cohesive material (silt and clay) in the lake, Anchor QEA also collected core samples for SEDflume erosion analysis. The erosion analysis was used to determine parameters for sediment movement as part of model development.

Subsurface investigations included sub-bottom profiler (SBP) surveys and core sampling. SBP surveys and core sampling were used to estimate the thickness of deposited silt and clay material in the region of the delta feature. Core samples were also used to provide sediment grain size information and evaluate approximate date of deposition through cesium-137 analysis. Findings indicated a thick layer of cohesive material that is in continual flux, i.e., **not consistently depositional on the delta feature.**

Sediment transport rates were the final missing parameters. The aforementioned SSC measurements occur only occasionally, and samples taken during large flow events are limited. Researchers were also unable to find bedload sediment transport measurements at any location in the watershed. Anchor QEA field work included trips to gather additional SSC measurements to help close data gaps in the record. Technicians also sampled bedload sediment transport and found that even under large flows, the **bulk of sediment transport occurs as cohesive silt and clay in suspension rather than along the bed**.

Hydraulic calibration of the model consisted of tuning roughness parameters to match measured peak WSEs for a range of flow events. Events that occurred between July 2007 and April 2017 were used for hydraulic calibration. Model tuning relied on adjusting hydraulic roughness coefficients and flow roughness factors. Calibration datasets included the USGS gages throughout the model domain,

high water marks, and the Anchor QEA monitoring stations. Model results showed good agreement with the gaged locations.

HEC-RAS has limited capabilities to accurately model cohesive sediment. GRDA discussed this at length in the Updated Study Plan submitted in April 2022 and proposed using a quantitative analysis of bathymetric change in addition to an STM focused on the upper regions of the study area.

In issuing their Determination on Request for Study Modifications (FERC 2022), FERC allowed development of the quantitative analysis and also agreed that HEC-RAS could be used to model portions of the study area above river mile 100, and that trapping efficiency and modeled sediment outflows could be used to evaluate sedimentation within the lower portion of the reservoir.

GRDA used a quantitative analysis of sedimentation to evaluate future deposition within the study area. A relationship between hydraulic bed shear stress as evaluated using a fixed bed HEC-RAS model and measured sediment deposition was developed for this purpose. After evaluation, the results indicated that sediment deposition would occur primarily on the downstream face of the delta feature, which follows typical evolution patterns of such deposits. The end result is that the delta feature is not expected to grow in height over the coming license period.

Sediment model calibration showed reasonable agreement with measured sediment deposition between the circa-1940 datasets and more modern surveys. Discrepancies are attributable to measurement uncertainties, particularly due to the significant limitations of the circa-1940 survey information.

Predictive 50-year simulations included analyses of *High* and *Low Sedimentation* simulations to account for the uncertainties of the available datasets. The calibrated sediment inflows were used to evaluate expected results under both *Baseline* and *Anticipated Operations*; the *High* and *Low Sedimentation* simulations were used to bound the maximum and minimum sedimentation volumes that could reasonably occur in the upcoming license period under anticipated Project operations. These analyses showed that the sediment primarily accumulates on the downstream face of the delta feature, as predicted by literature sources such as Vanoni (2006). The predicted geometry was then imported to the one-dimensional (1D) Upstream Hydraulic Model (UHM) to evaluate impacts to water levels.

Evaluation with the 1D UHM allowed assessment of changes to water levels based on sedimentation. The 1D UHM was used to evaluate the July 2007 flow event and a synthetic 100-year event on the Neosho River for three separate starting pool elevations.

Model results were compared to determine the relative impacts of 50 years of sediment accumulation under expected loading, *High Sedimentation* versus *Low Sedimentation* rates, and *Baseline* versus *Anticipated Operations*. The results indicated that **sediment loading, a natural**

phenomenon outside GRDA's control, generally has the largest impact on upstream water levels in the Neosho River, overshadowing any impacts caused by Project operations. The impacts to water levels in the City of Miami for all evaluations are immaterial. Project operations, sediment loading, and future geometry show immaterial changes to water levels in the vicinity of the City. GRDA does not control the volume of incoming sediment, and the simulations indicate that, much like the findings of the Hydrologic and Hydraulic Study, nature dictates incoming sediment loads and therefore water levels in the study area, *not* Project operations.

The sedimentation model inputs and outputs have been made available to relicensing participants for download upon request.

1 Introduction

The Sedimentation Study has been divided into three main stages—data collection, model development, and sedimentation predictions. During the initial stage, the study team collected data that were publicly available, analyzed data gaps, and created and executed plans to gather additional information. Model development used the field data to develop and calibrate the sediment transport model (STM). Sedimentation predictions will use the calibrated model to estimate the future deposition and erosion patterns within the study area to help evaluate future flood risks in the basin.

As discussed in the *Updated Study Plan Sedimentation Study* (USP; Anchor QEA et al. 2022), a three-level approach was implemented in conducting the Sedimentation Study. This approach includes qualitative geomorphic analysis, quantitative engineering and geomorphic analysis, and computer modeling (Figure 1). Qualitative geomorphic analysis considers the general trends in the system and how the stream has evolved over time. The quantitative engineering and geomorphic analysis uses measured data and hydraulic shear stress model results to determine the amount of sediment deposited or eroded in the study area, and computer modeling uses Hydrologic Engineering Center's River Analysis System (HEC-RAS) sediment transport features to evaluate sedimentation within the study area. Each individual component of this approach is intended to provide validation to the other components to ensure reasonable and reliable results are obtained.

Figure 1
A Conceptual Schematic of the Three-Level Approach for Analyzing Geomorphology, Sediment Transport, and Sedimentation Processes

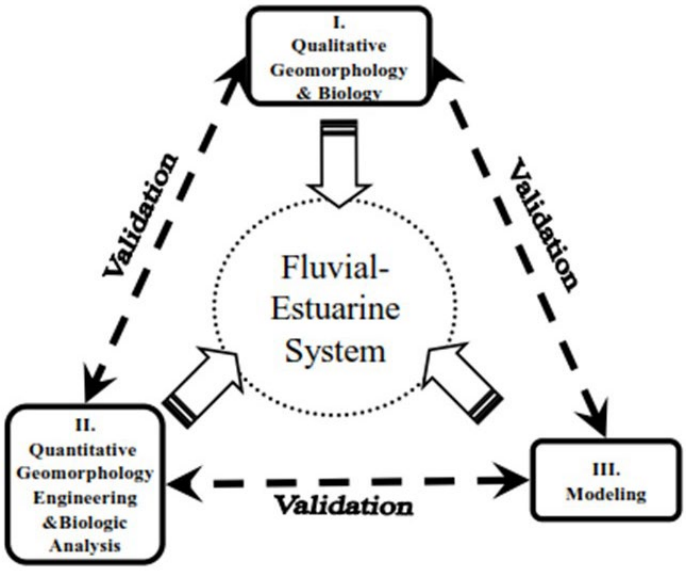

Note: Validation must occur between all three levels to ensure that reasonable results have been achieved.

1.1 Study Goals and Objectives

The primary goal of the Sedimentation Study is to determine the potential effect of the Pensacola Hydroelectric Project (Project) operations on sediment transport, erosion, and deposition in the lower reaches of tributaries to Grand Lake upstream of Pensacola Dam. Additionally, the Sedimentation Study is designed to provide an understanding of the sediment transport processes and patterns upstream of Grand Lake on the Neosho, Spring, and Elk rivers, as well as on Tar Creek. An STM will provide estimates of overall sedimentation trends and impacts of sedimentation in the project boundary.

1.2 Study Area

The Pensacola Dam is located near Langley, Oklahoma. It impounds the Neosho River, forming the Grand Lake reservoir (often referred to as Grand Lake O' the Cherokees). The Grand Lake reservoir is split between four counties, including Craig, Ottawa, Delaware, and Mayes in northeastern Oklahoma. The main tributaries that flow into the reservoir are the Neosho, Spring, and Elk rivers. Honey, Drowning, Duck, and Horse creeks also flow into the lake. Additional minor tributaries include Sycamore and Tar creeks.

1.3 Study Plan Proposals and Determinations

Grand River Dam Authority (GRDA) is currently relicensing the Project. A timeline of study plan proposals and determinations is as follows:

1. On April 27, 2018, GRDA filed its Proposed Study Plan (PSP) to address sedimentation modeling in support of its intent to relicense the Project.
2. On September 24, 2018, GRDA filed its Revised Study Plan (RSP).
3. On November 8, 2018, the Federal Energy Regulatory Commission (FERC) issued its Study Plan Determination (SPD) for the Project.
4. On January 23, 2020, FERC issued an Order on the Request for Clarification and Rehearing, which clarified the timeline for certain milestones applicable to the relicensing study plan.
5. On September 30, 2021, GRDA filed its Initial Study Report (ISR).
6. On December 29, 2021, GRDA filed its response comments on the ISR. This document included the following two attachments relevant to the Sedimentation Study:
    a. Appendix D – Sedimentation ISR (updated)
    b. Appendix E – Proposed Modified Study Plan for Sedimentation Study
7. On January 14, 2022, GRDA held a technical meeting for the Sedimentation Study. A summary of the technical meeting was filed with FERC on January 20, 2022.
8. On April 27, 2022, GRDA filed Response Comments on Sedimentation Study and Submission of USP for Approval with FERC. The document included the following three attachments:
    a. Attachment 1 – GRDA Response Comments on Sedimentation Study Plan

b. Attachment 2 – Independent Technical Review (ITR) of HEC-RAS STM
c. Attachment 3 – USP

9. On May 27, 2022, FERC issued its Determination on Request for Study Modifications for the Pensacola Hydroelectric Project. This Study Modification Determination (SMD) focused on the Sedimentation Study.
10. On September 30, 2022, GRDA filed the Updated Study Report (USR).

FERC's May 27, 2023, SMD approved GRDA's USP (also referred to by FERC as the second proposed plan modification) with the following modifications:

1. Extend the proposed downstream modeling limit for HEC-RAS to the U.S. Route 59 crossing at river mile (RM) 100.
2. Analyze the effects of sediment on storage capacity in Grand Lake using hydraulic outputs from the Upstream Hydraulic Model (UHM) and the U.S. Army Corps of Engineers (USACE) sediment trapping efficiency calculations downstream of RM 100.
3. Run the UHM using starting reservoir elevations of 740 feet, 745 feet, and 750 feet Pensacola Datum (PD).
4. Run the UHM with the predicted channel geometries and starting reservoir elevations using the simulated 100-year inflow event and the historical July 2007 inflow event.

As documented in this Revised USR, dated July 2023, GRDA has completed FERC's requested modifications.

2 Description of Data

2.1 Existing Data

A significant amount of the necessary data was available to the study team at the beginning of the project. Sources included USACE, the U.S. Geological Survey (USGS), past studies in Grand Lake, and surveys performed by the Oklahoma Water Resources Board (OWRB).

2.1.1 Terrain Information

Multiple datasets were available for potential use in this analysis. The earliest data are survey information from circa 1940. The most recent dataset was collected in 2019. All datasets considered for the study are discussed in chronological order in the following subsections.

Sedimentation deposition and erosion rates are key to the Sedimentation Study. Having reliable survey data collected at a ***known date*** is crucial to develop a useful STM. Without accurate information about the time interval between surveys, it is impossible to estimate a rate of change to calibrate a model. During calibration, model parameters are adjusted to reflect measured changes. For example, if those changes occur over a period of 10 years, the resulting parameters would be significantly different than if the same measured changes occurred over 70 years. Therefore, GRDA has documented the available data and assessed both: 1) the reliability of the data; and 2) whether a ***known date*** of data collection can be established.

2.1.1.1 Circa-1940 Data

The circa-1940 dataset comprises the following three available data sources:

1. 1938 USACE topographic maps with 5-foot contours (USACE 1938)
2. 1941 USACE Pensacola reservoir envelope curve computation folder (USACE 1941)
3. 1942 USACE Pensacola reservoir revised envelope curve computation folder (USACE 1942)

The 1938 USACE maps were used in the 1941 and 1942 USACE computations. The 1941 information does not include cross sections in plotted or tabular format. Rather, the data are presented as elevation/area and elevation/width relationships. The 1942 information includes plotted cross sections, but no data are available below the Neosho River/Spring River confluence.

Because the ***known date*** of the data collection can be established, these three data sources were used to create a single circa-1940 representation of Pensacola Reservoir and the upstream area. The information is imprecise and has significant limitations. Nevertheless, GRDA recognizes that this dataset represents the best available data for conditions at the time of dam construction and used it as the basis for model development in this study.

2.1.1.2 1969 USACE Data

During the Sedimentation Study Technical Meeting, the 1988 Flood Insurance Study was mentioned as a potential source for historical bathymetric information. GRDA reviewed the Flood Insurance Study and found that the bathymetry came from a 1969 USACE study (USACE 1969). GRDA analyzed the data. Even though the ***known date*** of the data collection can be established, unfortunately the data only extend from RM 134.6 upstream to RM 136.9. This 2.3-mile segment of historical bathymetric data is too short for use in STM calibration and validation. Thus, GRDA did not use the 1969 USACE data in STM calibration and validation.

2.1.1.3 1996 Expert Report

The 1998 Real Estate Adequacy Study (REAS; USACE 1998) states that modeling data (i.e., bathymetry) from Pensacola Dam to Twin Bridges State Park were taken from the Rule 26 Expert Report for the Grand (Neosho) River Upstream of Pensacola Dam (see Section VII, Subsection D of the Hydraulic Analysis section of the 1998 REAS). GRDA obtained the 1996 Expert Report (DeVries 1996) from USACE. The following three presentations of bathymetric data were in the 1996 Report:

1. River thalweg elevation profiles
2. Cross-section plots
3. HEC-2 printouts of cross-section data

The report does not state the source of the bathymetric data presented. Therefore, the ***known date*** of the data cannot be established. GRDA compared these data sources against each other. Multiple thalweg elevation profiles were presented in the report. One thalweg profile did not match the other profiles. The other profiles matched each other, matched the inverts of the cross-section plots, and matched the inverts in the HEC-2 printouts. Therefore, the one outlying thalweg profile was disregarded.

Next, the 1996 Expert Report data were compared to the 1998 REAS data. Results of the comparison are displayed in Figure 2. The 1998 REAS claims that data below Twin Bridges were taken from the 1996 Expert Report. However, the two datasets are significantly different. The 1998 REAS data clearly did not come from the 1996 Expert Report dataset.

The 1996 Expert Report profile was also compared to the 1941 envelope curve profile to see if the 1996 data originated from the 1941 data. The 1941 profile is also displayed in Figure 2. The 1996 and 1941 data are significantly different from each other. Furthermore, the 1996 Expert Report thalweg is significantly lower than the 1941 thalweg. GRDA considered whether a misreported datum could be the issue, but the differences are on the order of 10 feet or more. This significant decrease in elevation from the 1941 thalweg to the thalweg reported in the 1996 report could only be the result of significant erosion in the lower portion of the reservoir, which is entirely unrealistic.

Summary

1. The ***known date*** of collection for data presented in the 1996 Expert Report cannot be established.
2. The 1996 report data do not match the 1998 REAS data, invalidating the claim that the 1998 REAS data downstream of Twin Bridges came from the 1996 report data.
3. The 1996 report data do not match the 1941 data; the 1996 report data could not have been sourced from the 1941 data.
4. Regardless of the collection date of the 1996 report data, significant and unrealistic erosion would have had to occur after 1941 for the dataset to be valid.

For these reasons, GRDA discarded the 1996 Expert Report data.

Figure 2
1996 Expert Report Thalweg Comparison

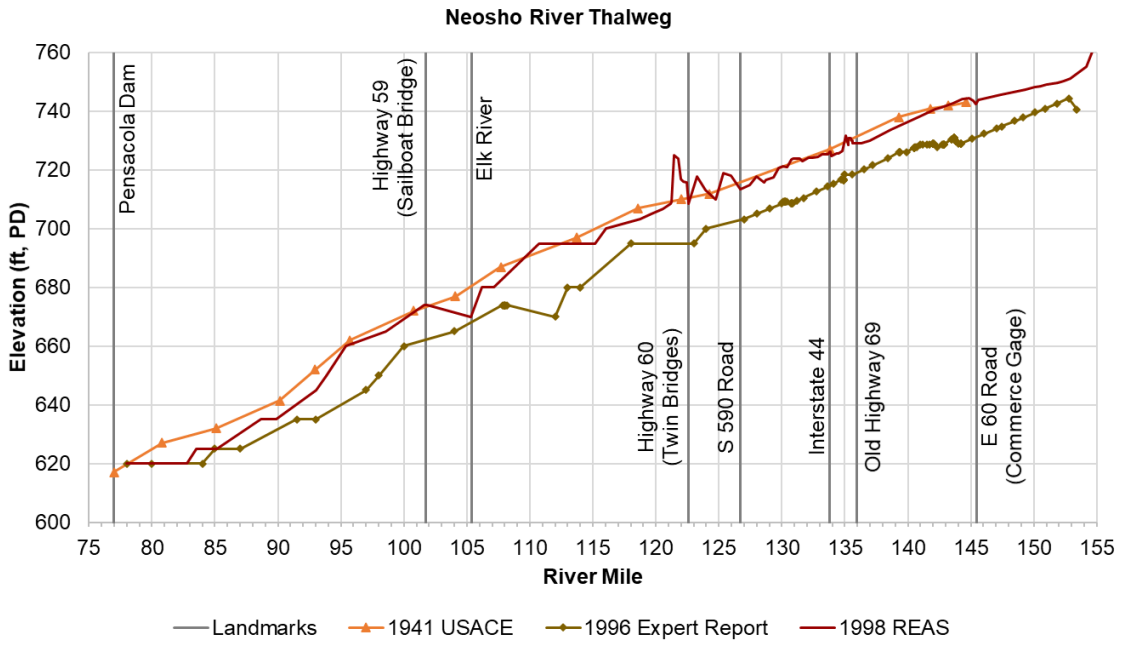

2.1.1.4 1998 Real Estate Adequacy Study Data

Multiple datasets were presented in the 1998 REAS and are discussed individually in the following subsections.

2.1.1.4.1 Grand and Neosho Downstream Data

The REAS hydrographic survey limits extend downstream to RM 120.1 (approximately 2 miles downstream of the Spring River confluence) along the Neosho River. Data below RM 120.1 were not surveyed as part of the REAS study but were included in the study's analysis. Plate 3 from the 1998

REAS, which documents REAS survey extents, is presented as Figure 3. The solid blue sections represent the area surveyed as part of the REAS.

Figure 3
Hydrographic Survey Limits for REAS

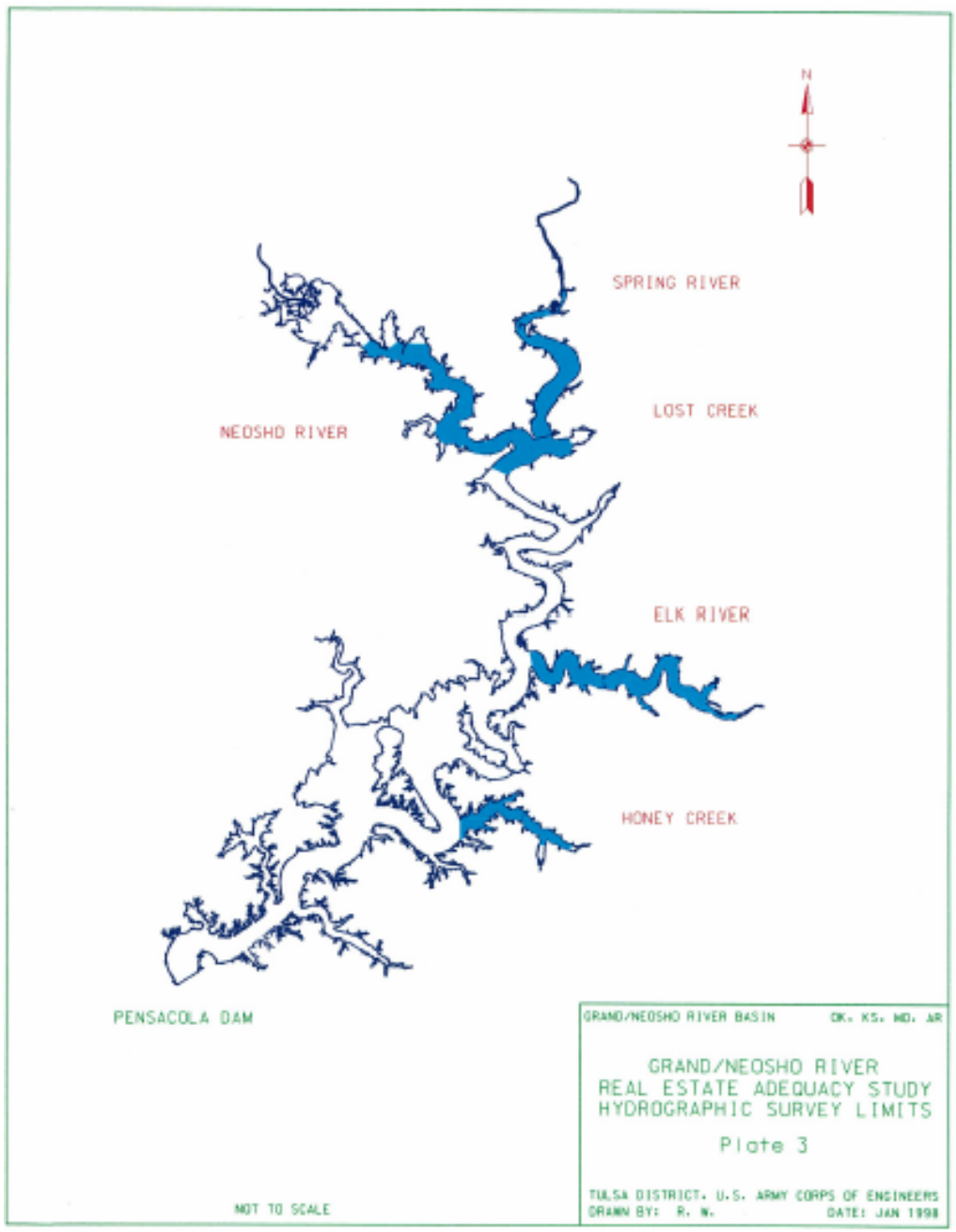

Source: USACE (1998)

As discussed in Section 2.1.1.3, the 1998 REAS states that the 1996 Expert Report downstream data have been invalidated by comparing the two datasets. This fact calls the validity of the REAS downstream data into question. Furthermore, that means the ***known date*** of the data collection cannot be established.

GRDA compared the downstream REAS data to the 1941 envelope curve data in hopes that they would match. This would indicate that the REAS data were from 1941 and would assign a date to the dataset, making it usable for STM calibration and validation. Unfortunately, the downstream data presented in the REAS do not match the 1941 data. Thus, the survey date of the REAS data below RM 120.1 remains unknown. Furthermore, the REAS thalweg is lower than the 1941 thalweg in multiple locations within the downstream reach. Assuming that the REAS data were collected after 1941, that would require erosion in the lower portion of the reservoir, which is extremely unlikely given that low flow velocities and shear stress typically result in sediment depositions within reservoirs.

Summary

1. The REAS directly states that the downstream data were not collected as part of the 1998 study effort.
2. The REAS states that the downstream data came from the 1996 Expert Report. This claim has been invalidated by a comparison of the two datasets.
3. The ***known date*** of collection for the downstream REAS data cannot be established.
4. Unrealistic erosion would have had to occur for the downstream REAS data to be valid.
5. The downstream REAS data do not match any other available datasets. If the data matched, the collection date could be established.

For these reasons, GRDA discarded the downstream portion of the REAS data.

2.1.1.4.1.1 The City's Claims Regarding the Downstream Data

The City of Miami has used the downstream portion of the REAS data to make unsubstantiated claims regarding sedimentation rates and patterns of deposition in the study area. The City claimed that "comparison of the pre-dam river profile with recent bathymetric surveys indicates significant sediment deposition near the head of Grand Lake," and then jumped to the conclusion that sediment deposition in Grand Lake "increases upstream flooding along the Neosho and Spring Rivers."

The foundation of the City's claims is a presumed 1998 date of the downstream REAS data, which cover Grand Lake and extend upstream to RM 120.1. As discussed in Section 2.1.1.4.1, the REAS explicitly states that the downstream data are not from 1998 and were not surveyed as part of the REAS data collection. Regardless, GRDA investigated the City's claims regarding sediment deposition in the study area.

Figure 4 displays multiple thalweg profiles. Even assuming that the "1998" REAS profile was surveyed in 1998 (which it was not), comparison of the datasets would suggest that sediment deposition patterns have changed significantly in ways that cannot be explained solely by the construction of the dam or Project operations.

Figure 4
Historical Neosho River Thalweg Comparison

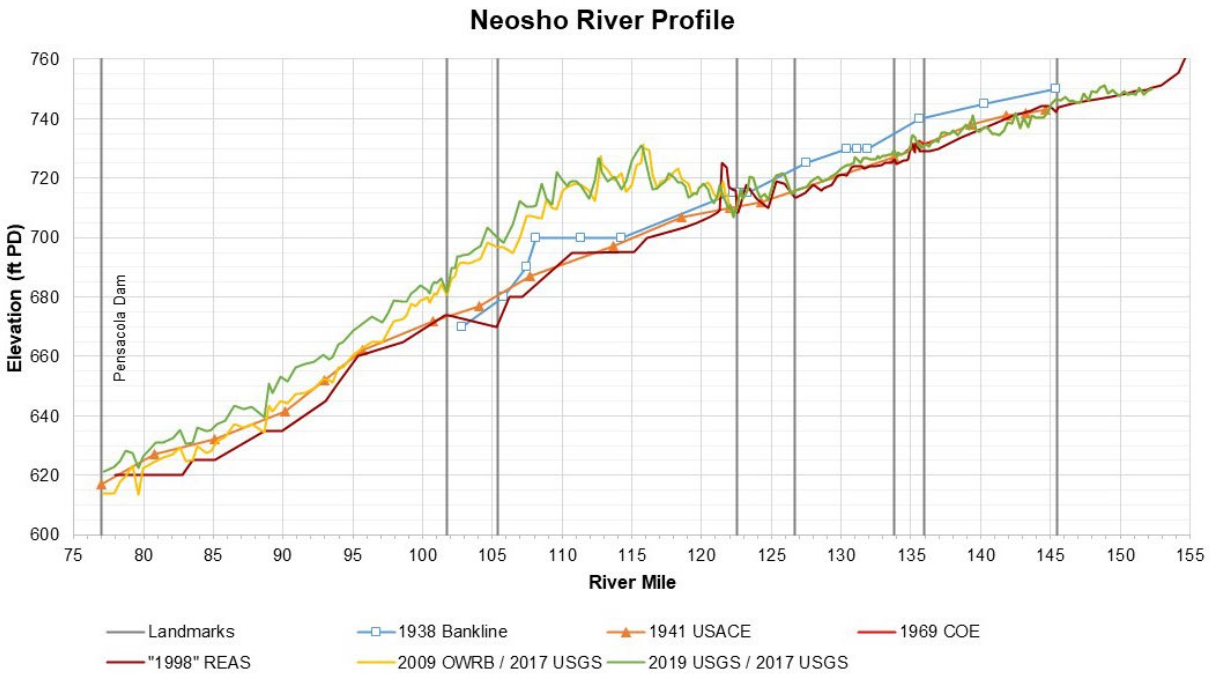

Note: This plot covers the Neosho River from RM 152.2 at the upstream end to the Pensacola Dam at RM 77.12 on the downstream end.

As shown in Figure 4, the City's claims regarding sediment deposition and erosion patterns would require significant and unrealistic changes since completion of the dam. For a moment, assume that despite the USACE REAS documentation clearly stating otherwise, the City's assumption that the downstream REAS data are from 1998 is correct. If the City is correct, that would mean the following:

1. From 1940 to 1998, sediment eroded in the delta feature region and near the dam.
2. From 1998 to 2009, the sedimentation pattern reversed, and 20 to 30 feet of sediment accumulated at the delta feature in only approximately 11 years.
3. From 2009 to 2019, sedimentation patterns changed again, with virtually no sediment depositing on the top of the delta feature.

This thought experiment reveals how the City's assumptions, which contradict USACE documentation, are flawed.

To further show how the City's assumptions are flawed, GRDA evaluated sediment loading to the reservoir (also referred to as sediment inflow to the reservoir) since completion of the dam in 1940. Using the sediment rating curves developed with USGS data and the field data collected by GRDA, the portion of sediment that entered the study area from 1940 to 1998, 1998 to 2009, and 2009 to 2019 is calculated, assuming that the downstream REAS data were collected in 1998. Sediment loading calculations are presented in Table 1.

Table 1
Relative Sediment Delivery and Measured Deposition Thickness at the Delta Feature by Specified Time Period (if the "1998" REAS Data Are to be Believed)

Time Period	Number of Years	Percentage of Total Sediment Loading	Apparent Deposition in Region of the Delta Feature
1940–"1998"	58	68%	~0 feet
"1998"–2009	11	14%	20–30 feet
2009–2019	10	13%	~0 feet on the top, ~2–3 feet on the downstream face

Most of the deposition (68%) should have occurred between 1940 and "1998"—a period of 58 years—based on historical sediment loading rates. However, the thalweg comparison shows virtually no deposition in the region of the delta feature for this period. Then in the 11 years between "1998" and 2009 with no change in the regulated operations of the reservoir, when only 14% of the deposition should have occurred, there was 20 or 30 feet of deposition at some specific locations within the region of the delta feature. Then in the 10 years between 2009 and 2019, when 13% of the deposition should have occurred, there was 2 to 3 feet of deposition on the downstream face of the delta feature. The City offers no scientific explanation for the complete disconnection between sediment loading and deposition.

Summary

1. The City of Miami has made unsubstantiated claims about sedimentation rates and patterns in the study area.
2. The foundation of the City's claims is based on a presumed (but demonstrably erroneous) 1998 date of the downstream REAS data, which cover Grand Lake and extend up to RM 120.1.
3. The REAS explicitly states that the downstream data are not from 1998.
4. A comparison of the thalweg profiles shows the flaws in the City's assumptions.
5. A comparison of sediment loading to deposition depths shows the flaws in the City's assumptions.
6. The City has offered no scientific data to substantiate their assumptions.

For these reasons and the reasons stated in the previous section, GRDA cannot accept the City's claim that the downstream portion of the REAS data is from 1998.

2.1.1.4.2 Neosho and Spring Upstream Data

As displayed in Figure 3, the REAS hydrographic survey limits extend downstream to RM 120.1 along the Neosho River. The Spring River is also included within the upstream REAS survey limits.

In their ITR, WEST Consultants, Inc. (WEST), used the average channel bed profile to compare several datasets against each other, including the REAS geometry (Figure 5). This method of analysis is more representative of overall channel geometries than the simple thalweg profile, because it accounts for portions of the channel that are outside of the thalweg. WEST concluded that the portion of the REAS dataset above RM 120.1 can be used for this study. GRDA agreed that this portion of the REAS dataset can be used in STM development as a calibration dataset. However, there is no quality control documentation in the REAS for this data (see Section 2.1.1.4.4) and the data were obtained using less accurate techniques compared to the more recent datasets. Thus, there is a significant amount of uncertainty regarding this dataset, which influenced the accuracy of the STM calibration and validation.

Determining the rate of sediment accumulation in the study area is critical, and surveyed data with a known collection date is required to calculate rates of sediment accumulation. Although the upstream REAS dataset met the threshold for usability in the STM, the lack of quality control documentation in the REAS casts doubt on the accuracy of the dataset. Nevertheless, because the ***known date*** of the data collection has been established, GRDA recognizes that this dataset represents a usable, comprehensive historical dataset and used the upstream REAS data for STM calibration and validation.

Figure 5
Historical Neosho River Average Channel Bed Comparison

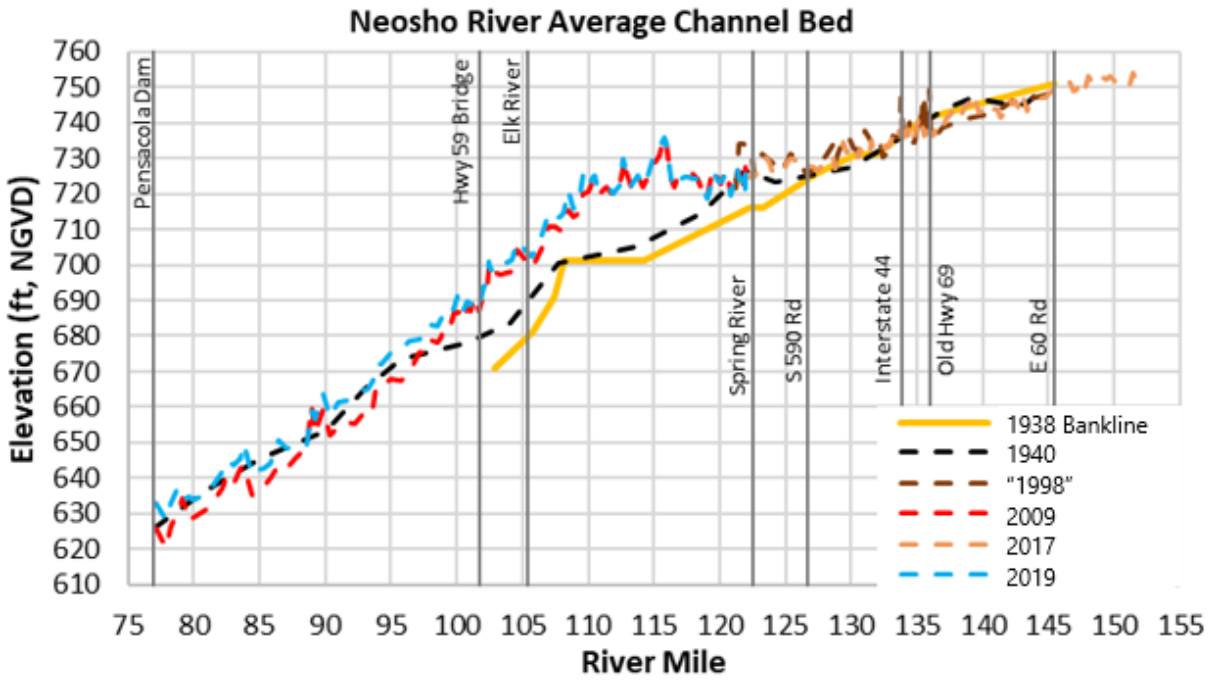

Source: WEST's ITR technical memorandum (WEST 2022)

2.1.1.4.2.1 The City's Recommendations Regarding the Upstream Data

Regarding the upstream REAS data, the City states the following:

> The Neosho River upstream of the City has changed very little since 1940. It may be appropriate to replace the 1998 survey data with the 2019 [sic – the survey is from 2017] survey data for the reach upstream of the City. (City of Miami 2022).

The City proposed to discard the upstream REAS data, which are at least documented in some form, while keeping the least reliable, incorrectly documented data within the REAS—the downstream data that cover Grand Lake. ***The City proposed discarding the only section of the REAS dataset that is based on surveys completed during the 1998 study***. Furthermore, discarding the upstream 1998 REAS data would have prevented GRDA from performing calibration and validation of the STM in the upstream reach. Implementing the City's proposal would have resulted in an STM with less predictive capability.

Therefore, GRDA rejected the City's proposal to discard the documented upstream portion of the REAS dataset.

2.1.1.4.3 Elk River Data

As displayed in Figure 3, bathymetry on the Elk River was collected as part of the REAS hydrographic survey. However, there was an obvious issue with the collected data.

A USGS gaging station (07189000 Elk River near Tiff City; USGS 2021a) on the Elk River is located at RM 14.22 on the Highway 43 Bridge. In the REAS dataset, the channel invert at that location is 753.90 feet PD. This is implausible, because that invert elevation is higher than water surface elevations (WSEs) recorded by USGS. REAS documentation states that the survey was performed in July 1997. The USGS reported WSEs were less than 753.90 feet PD at the site for all but 3 days in July 1997, with a low WSE of 752.94 feet PD reported on July 31, 1997 (Figure 6). This is clearly an impossible result, because it suggests the water surface was below ground. As a result, no HEC-RAS model can ever predict the correct WSE at the site during low flow events.

Although the ***known date*** of the data collection has been established, the data are not reliable. For this reason, GRDA did not use the Elk River REAS data in the STM.

Figure 6
Elk River Thalweg Comparison and WSE Measurement

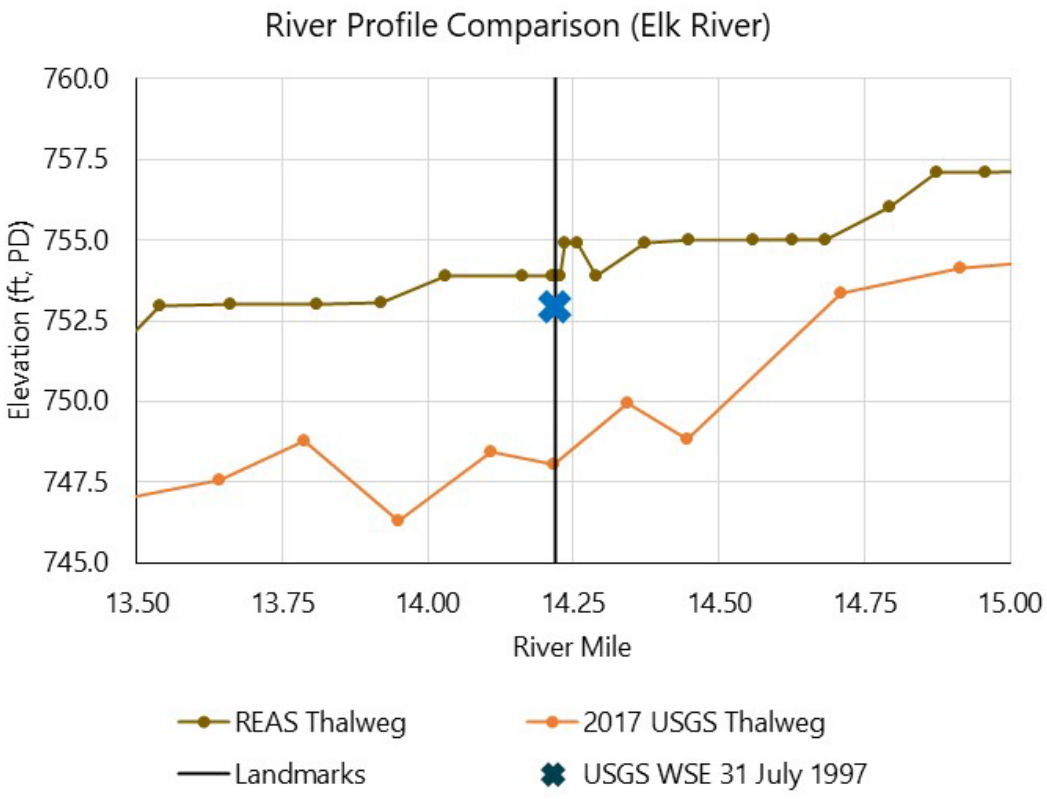

2.1.1.4.4 USACE Stance on Reliability

Given the concerns with the REAS dataset below RM 120.1, GRDA contacted USACE to discuss the REAS data. David Williams, PhD, PE, CFPM, D.WRE, of the Tulsa District stated the following in an email dated January 26, 2022:

> I do have concerns about the applicability of the cross-sectional survey that was used in the 1998 study (for the reasons that have been described), and I have no issue w/ sharing these concerns.

His stated reasons were as follows:

> I did speak with an engineer who previously worked for the Tulsa District, and he pointed out that the survey wasn't subjected to a rigorous QA/QC process.

The City itself acknowledged there are problems with the data, suggesting that the datum shift may have been incorrectly applied. In their March 2022 comment submission (City of Miami 2022), the City wrote the following:

> Tetra Tech's review of the REAS dataset indicates that it is about 2 feet higher than other surveys, raising the possibility that the REAS dataset was incorrectly adjusted from Pensacola Datum (PD) to NGVD29.

The City then stated that if that issue is resolved, "the REAS dataset probably may be reliable." The City provided no technical arguments for why the data are reliable or why the datum issue does not call the reliability of the data into question.

GRDA agreed that a datum shift is likely one problem with the data, as evidenced by a plot provided by USACE (Figure 7). In the figure, the vertical axis (on the left) is "Elevation in Feet (NGVD)," but the chart title at right is "20,000 cfs Envelope Curve PD Datum." GRDA compared the streambed in the figure to the channel invert in the REAS data and determined that the vertical datum of the displayed data is PD. This type of error (listing two datums in the same figure) confirms inadequate quality control of the data and contradicts the City's argument that the full REAS dataset "probably may be reliable" (a heavily caveated assertion that itself demonstrates the City's lack of confidence in its own assertion).

Figure 7
USACE Figure Showing Mislabeled Vertical Datum

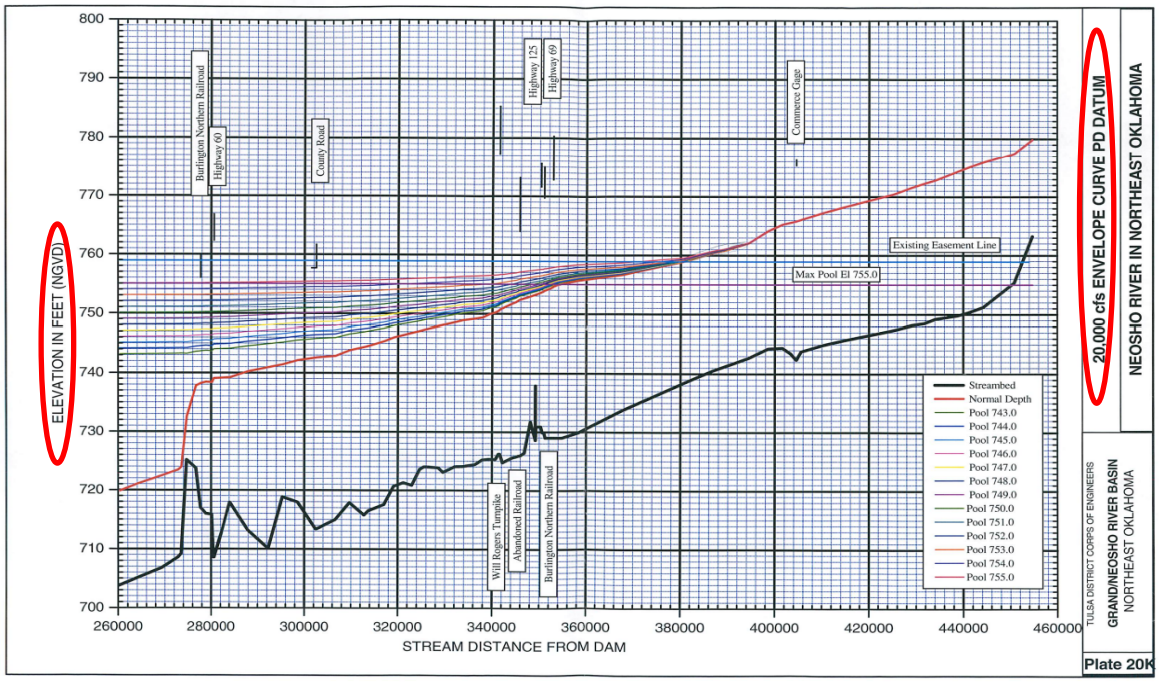

Note: Figure provided by USACE showing thalweg profile of the Neosho River in the vicinity of Miami, Oklahoma; red outlines added to highlight conflicting vertical datum labels.

The City's argument for inclusion of the full REAS dataset did not rely on technical criteria. The City cited use of the REAS in litigation as a reason to use the full REAS dataset as a basis for STM development. The fact that the REAS was used in litigation proceedings in the past has no bearing on whether the dataset is reliable or useful for the purposes of this study. The City claimed the delta feature was formed in an 11-year span between 1998 and 2009 but, as discussed in Section 2.1.1.4.1, the "1998" data are not actually from 1998. This fact undermines the City's claims regarding delta feature formation. The City's consultant could have easily performed a sediment loading analysis, which would have revealed the City's error. The City asserted that REAS data in the reservoir should be treated as representative of 1998 conditions, ignoring the USACE documentation in the REAS report. Any objective evaluation of the data shows that the REAS data below RM 120.1 cannot reasonably be used for this study.

Summary

1. USACE informed GRDA that the REAS was completed without proper quality control processes, and as a result, the data may not be reliable.
2. The City acknowledged that there are issues with the REAS yet provided no technical arguments for why those issues do not call the reliability of the data into question.

3. The City's claim that the delta feature was formed in an 11-year span between 1998 and 2009 relies on an undated dataset and thus is invalid.

Based on the information presented in Section 2.1.1.4.1 and the information in this section, GRDA discarded the downstream portion of the REAS data.

2.1.1.4.5 Conclusion on 1998 Real Estate Adequacy Study Data Reliability

Portions of the "1998" REAS dataset are usable while other portions are unusable, as summarized in the following:

1. The downstream data, which cover Grand Lake below RM 120.1, are not usable and were discarded for the purposes of this study.
2. The upstream data, which cover the Neosho River above RM 120.1 and the Spring River, are usable for this study.
3. The Elk River data are not usable and were discarded for the purposes of this study.

There is a significant amount of uncertainty regarding the usable data. The upstream REAS data meet the threshold of usability in the STM, but the lack of quality control documentation in the REAS casts doubt on the accuracy of the dataset and increases the level of uncertainty in the data. Nevertheless, because the ***known date*** of the upstream REAS data has been established, GRDA recognizes that this dataset represents a usable, comprehensive historical dataset and used the upstream REAS data for STM calibration and validation.

2.1.1.5 2009 Oklahoma Water Resources Board Survey

The 2009 Grand Lake bathymetry data were collected by OWRB using a single-beam echosounder. The coverage of the lake was extensive, with data collected along 1,680 virtual transects (OWRB 2009). The finalized dataset includes nearly 700,000 points. The 2009 OWRB report shows survey track lines; this figure is presented as Figure 8. The 2009 OWRB report includes a section devoted to the discussion of quality control/quality assurance. Intersecting transect lines and channel track lines were compared to assess the estimated accuracy of the survey measurements. OWRB documented that the data quality met or exceeded USACE's performance standards (USACE 2002), with a reported depth accuracy at the 95% confidence level of ±1.3 feet and a bias of 0.5 foot.

Figure 8
Data Density and Survey Track Lines Provided by OWRB in 2009 Grand Lake Survey Report

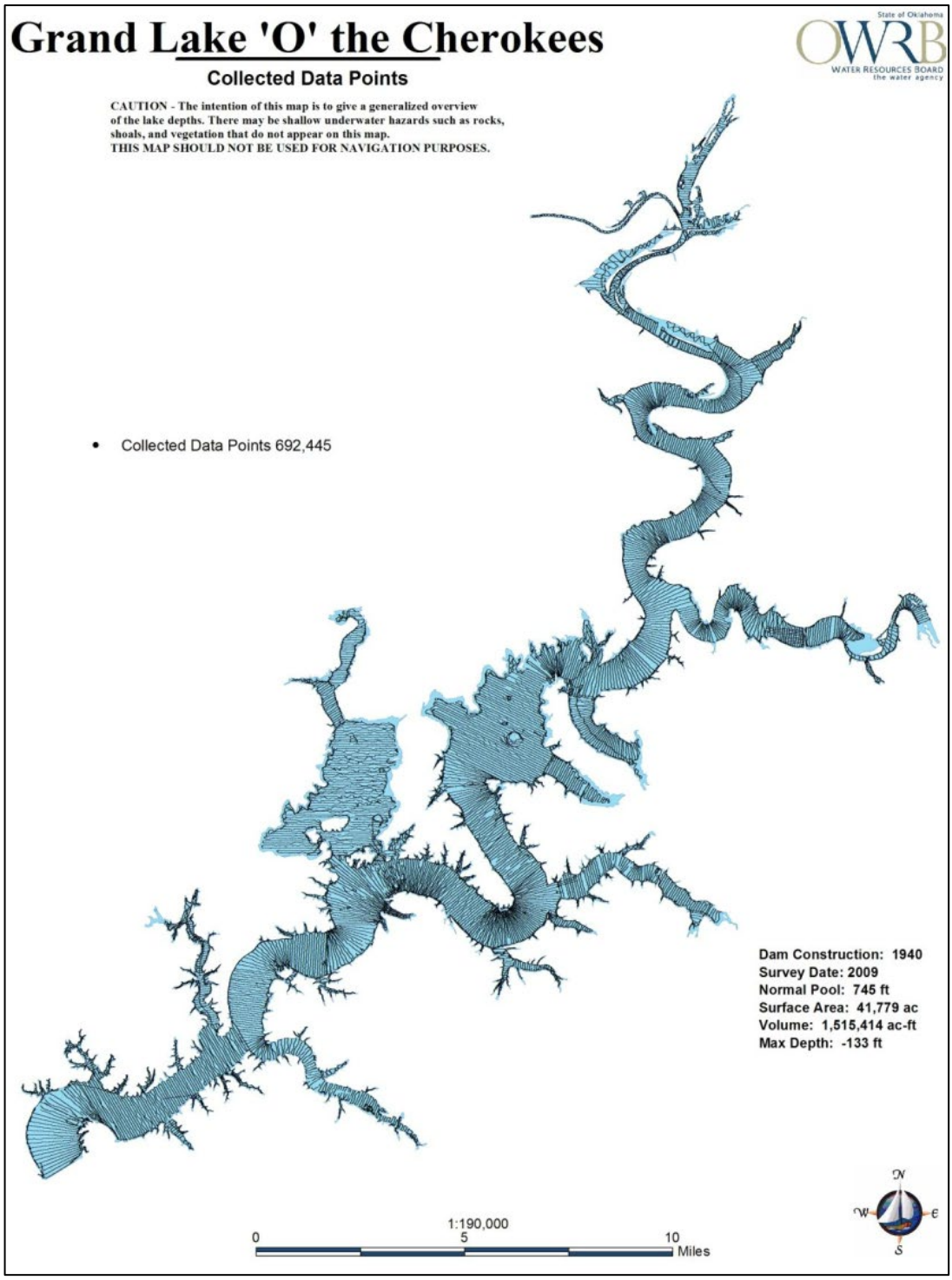

A review of typical reservoir deposition and siltation patterns shows that fine sediments can be transported far into a reservoir. van Rijn (n.d.) states that inflowing, sediment-laden water may travel under the relatively clear reservoir water as a plume (density or turbidity currents), bringing sediment far closer to the dam than would be allowed through shear stress alone. Zavala (2020) confirms this in a discussion of hyperpycnal flows, or density-driven flows, in which he states that incoming flows can transfer large volumes of sediment even without steep bed slopes. Hyperpycnal flows occur when a relatively denser gravity flow of sediment-laden water enters a marine or lacustrine body of water and the density of the moving water is greater than the density of the standing water, causing the denser, sediment-laden water to flow along the bed, as an underflow below the standing water.

2.1.1.5.1 Quality Concerns

The 2009 OWRB survey was not without problems. Although it is the best available dataset from this timeframe, it shows significantly more sedimentation than is realistic given incoming sediment loads. The total incoming sediment volume from 1940 to 2019 is approximately 234,974 acre-feet with an incoming sediment load of approximately 327,044,375 tons, which converts to a sediment density of 63.9 pounds per cubic foot (pcf). The same calculation based on volume change and sediment load from 1940 to 2009 results in a computed sediment density of approximately 115.5 pcf, whereas the 2009 to 2019 calculation results in a sediment density of 10.6 pcf. This disparity of calculated sediment densities between the 1940 to 2009 and 2009 to 2019 data demonstrates the issue with the bathymetric surveys compared to sediment load. The issue with this dataset is not simply that deposition was near the dam because hyperpycnal flows are capable of bringing sediment to the lower reservoir. The issue is the total volume of deposition given the incoming sediment load.

In an e-mail exchange with USGS, Jason Lewis (2022) indicated they had not found any major issues with the 2009 bathymetric dataset. He also stated the following:

> The 2009 dataset tends to show much greater variability in flat areas compared with 2019 data, so I suspect a lot of that has to do with correction processes such as GPS correction, temperature correction issues, and other issues such as boat movement.

The impossibly high deposition in the lower reservoir led GRDA to use only the portion above RM 100 for calibration purposes. The reservoir downstream of RM 100 was evaluated using only total change from 1940 to 2019 in analysis. This preserves a reasonable long-term estimate of total deposition where impacts are to the conservation pool while not discarding the entire 2009 dataset because it is the best available dataset.

Because the dataset has documented quality control and there is a ***known date*** of data collection, GRDA used the 2009 data for calibration and validation upstream of RM 100. However, as explained

above, deposition in the lower reservoir is not realistic given the sediment loading between 1940 and 2009, so the 2019 USGS survey was used for long-term evaluation below RM 100.

2.1.1.6 2017 USGS Upstream Survey

The 2017 USGS upstream survey data cover the Neosho, Spring, and Elk rivers. The 2017 USGS upstream survey data went through a thorough quality control process and, as a result, are considered a reliable data source. USGS calculated quality assurance statistics at the intersection of primary and control transects. The root-mean-square-error (RMSE) of the quality assurance data was less than 0.5 foot for all data collection methods on all rivers (Smith et al. 2017).

Because the dataset has documented quality control and there is a ***known date*** of data collection, GRDA can use the 2017 USGS data for STM calibration and validation.

2.1.1.7 2019 USGS Grand Lake Survey

As part of the FERC SPD, the 2019 USGS Grand Lake bathymetry data were collected by USGS using a multi-beam echosounder. The 2019 USGS survey data went through the highest levels of quality assurance and, as a result, are considered a reliable data source. USGS used literature-based methodologies for quality assurance. Quality assurance measures included beam-angle checks (required to verify that the multi-beam system is operating within USACE-approved standards), patch tests (used to identify and correct systematic errors), and uncertainty estimations (using total propagated uncertainty, or TPU). USGS reported that more than 95% of the TPU values were less than 0.30 foot, which is within the most stringent specifications for an International Hydrographic Organization Special Order survey (IHO 2008).

Yet the City found issue with the 2019 USGS dataset despite the rigorous quality assurance documented by USGS (2020). The City compared thalweg elevations between the 2009 and 2019 datasets and claimed that the aggradation rates were unrealistic (City of Miami 2022).

The City argued that seeing deposition near the dam is unreasonable and indicates there is no explanation for sediment moving that far into the reservoir. The literature is clear that density currents, and other transport mechanisms, operate in reservoirs and carry sediment far into impoundments (Lumborg and Vested 2008; van Rijn n.d.; Zavala 2020).

The City's comments do not cast doubt on the accuracy of the entire 2009 and 2019 datasets. Rather, the disregard for documented reservoir sediment transport phenomena demonstrate that the City's consultant misunderstands basic principles of sediment transport in reservoirs.

Because the dataset has documented quality control and there is a ***known date*** of data collection, GRDA used the 2019 USGS data for STM calibration and validation.

2.1.1.8 Topographic Surveys

Two primary data sources exist for overbank analyses. The first is topographic survey information gathered during the 1998 REAS (USACE 1998). The extents of this survey reach the Oklahoma and Kansas border along both the Neosho and Spring rivers and approximately 5 miles upstream of the Highway 43 Bridge on the Elk River. The second major overbank data source is Light Detection and Ranging (LiDAR) data from a mission flown in 2011 (Dewberry 2011). Where additional data were needed for overbank areas, they were obtained from the USGS National Elevation Dataset (NED) one-third, arc-second dataset (USGS 2017). These combined datasets covered the entire overbank portion of the study area.

2.1.1.9 Terrain Datasets

The information gathered from the above-referenced sources was compiled to make three terrain datasets. The datasets served as the basis for all STM geometry development. Although data for each were created from a patchwork of sources measured at different times, for simplicity of naming them, they will be referred to in this report by the year of the relevant Grand Lake survey. Upland topography is stable enough over time that it can be combined with bathymetry data taken at a different point in time. Terrain files contain both bathymetric and topographic information. Table 2 details the terrain names and relevant source materials.

Table 2
Summary of Datasets Used to Create the Three Primary Terrain Files Used in the Sediment Study

Terrain Name	Grand Lake Survey	Upstream Survey	Overbank Survey
"1998" Terrain	Unspecified Circa-1940 Data	1998 REAS	1998 REAS/2011 LiDAR/2017 NED
2009 Terrain	2009 OWRB	2017 USGS	2011 LiDAR/2017 NED
2019 Terrain	2019 USGS	2017 USGS	2011 LiDAR/2017 NED

Figure 9 shows the survey areas for each of the above-referenced surveys, except the 2019 USGS bathymetric survey of Grand Lake and the 1998 REAS survey. The extents of the 2019 Grand Lake survey are approximately the same as those of the 2009 OWRB survey.

Figure 9
Survey Extents of Various Data Sources for Sediment Transport Model Development

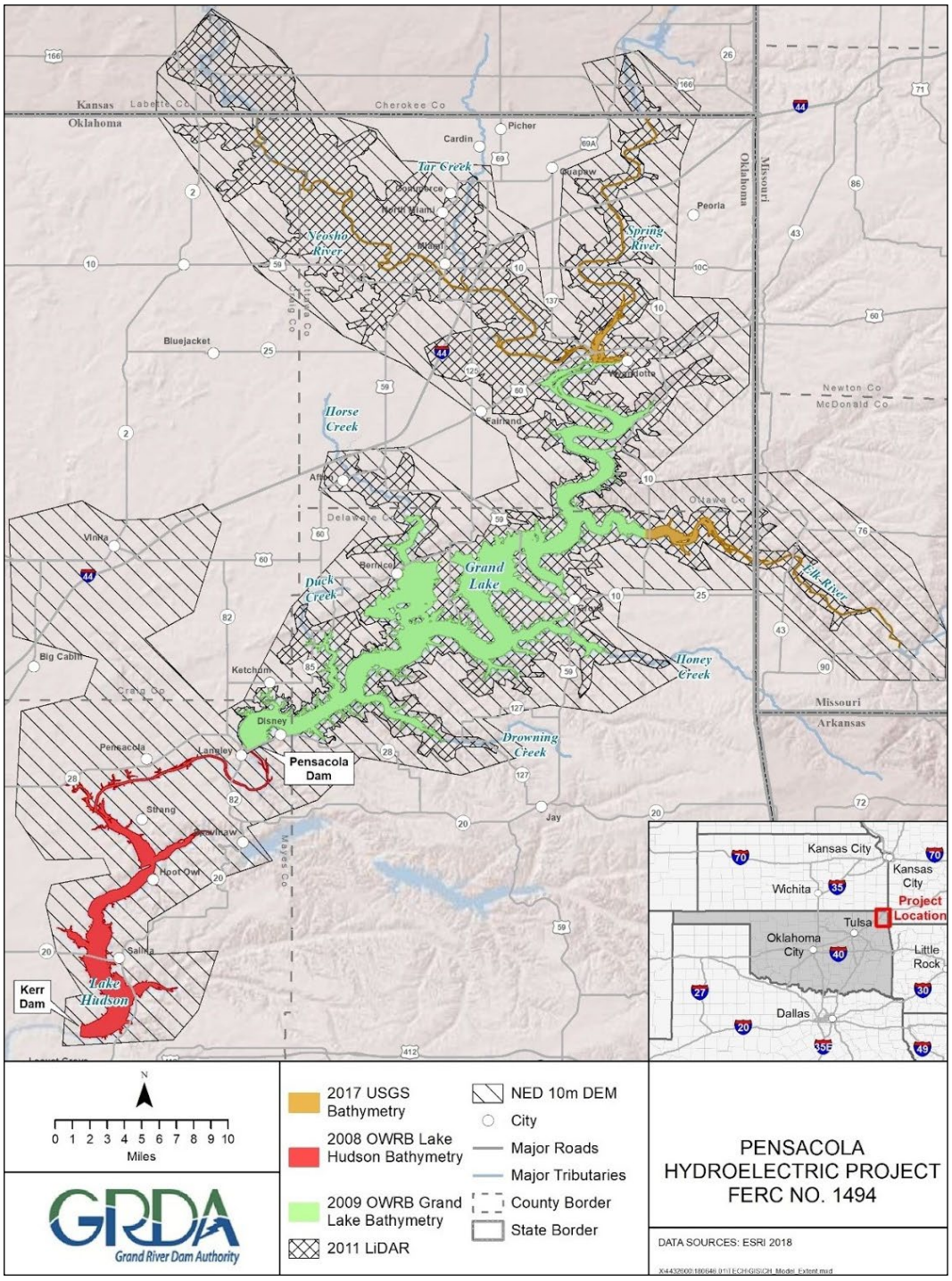

2.1.1.10 Stage-Storage Curves

Grand Lake stage-storage curves were available dating back to 1940. USACE created a capacity curve from as-built dimensions and surveys at that time. The 2009 OWRB survey of Grand Lake and the 2019 USGS survey of Grand Lake provide additional stage-storage curves. These were used to estimate the annual volume of sediment deposition within the Grand Lake reservoir as a ground-truthing measure.

2.1.1.11 ADCP Bathymetric Profile Comparison

USGS periodically performs discharge profile measurements near gage stations using an acoustic Doppler current profiler (ADCP), and data are available on request. Although the primary function of the ADCP sampling events is to generate current profiles, the ADCP also measures water depth along the sampling transect. Using the river stage at the time of the event, water depth can be converted to bed elevation. Comparing the multiple profiles taken at a similar location over several years can reveal sediment transport trends.

For each gage, ADCP profile locations vary from event to event. The data were projected onto a single profile line for comparison. The profile lines were placed to represent as many ADCP transects as possible. Given that the transects are not taken at exactly the same location, elevations near the banks are likely unreliable.

2.1.1.11.1 Neosho River near Commerce

Figure 10 displays the ADCP transects taken at the Neosho River near the Commerce USGS station. Only the 2017, 2018, and 2019 data are near enough spatially to be compared. The 2018 and 2019 transects in Figure 11 show a stair-stepping effect, which is likely due to poor Global Positioning System (GPS) signal and reporting. Change in volume cannot be analyzed due to the data gaps in the 2018 and 2019 transects.

Figure 10
Neosho River near Commerce USGS ADCP Transects

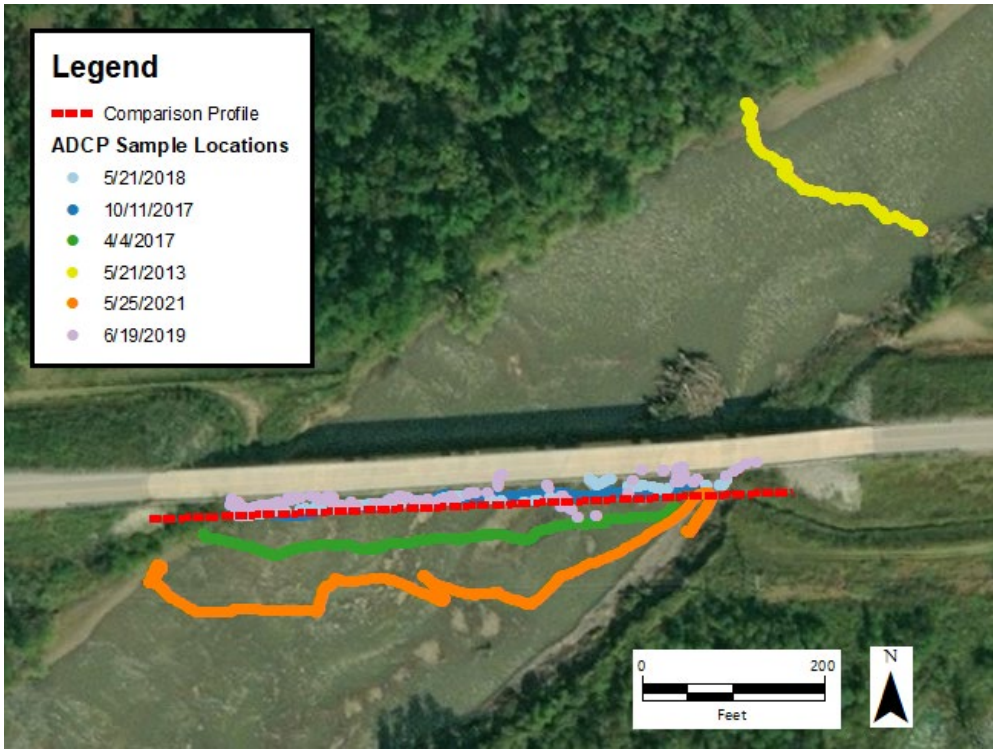

Figure 11
Neosho River near Commerce USGS ADCP Sections

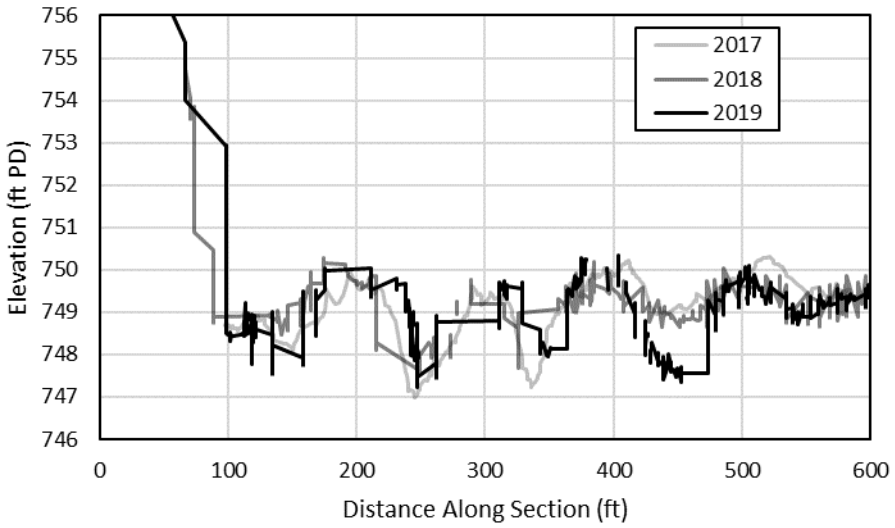

2.1.1.11.2 Neosho River at Miami

The Neosho River at Miami station has data from six sampling events spanning 2017 to 2021. The transects are spaced along approximately 50 feet of river as seen in Figure 12. Three high-quality transects equally spaced in time are displayed in Figure 13. There is almost no change in channel depth from 2017 to 2021.

Figure 12
Neosho River at Miami USGS ADCP Transects

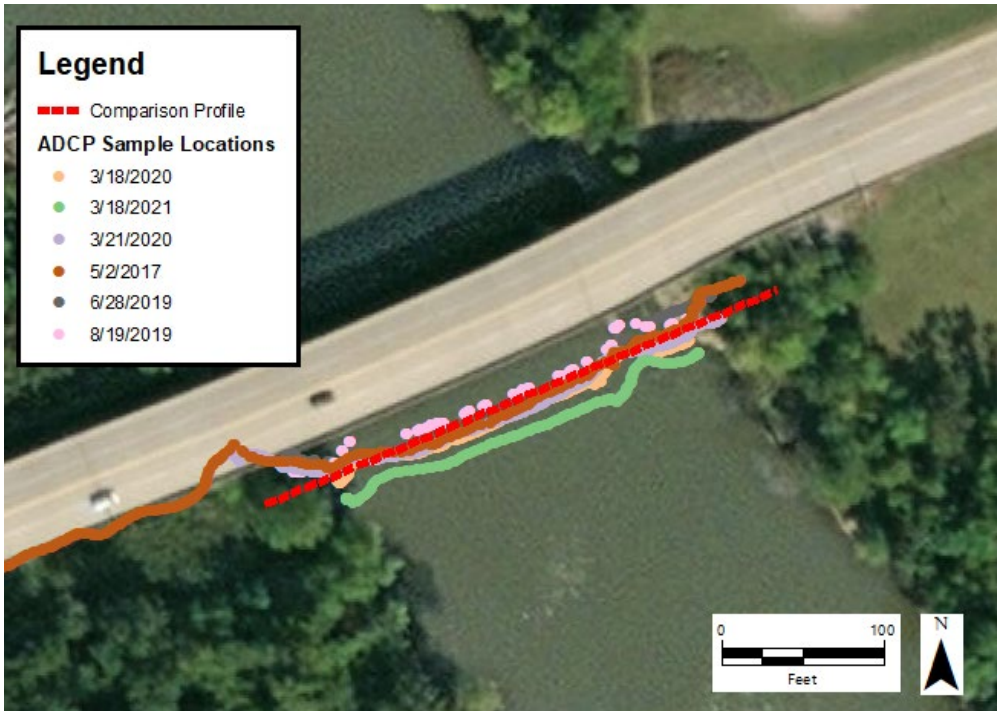

Figure 13
Neosho River at Miami USGS ADCP Sections

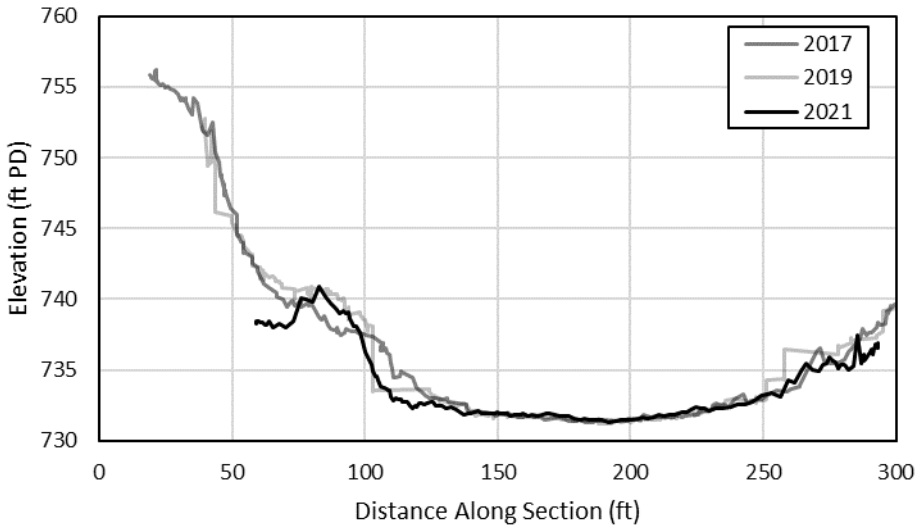

2.1.1.11.3 Tar Creek near Commerce

The Tar Creek near Commerce station has data available from four events ranging from 2004 to 2019, taken within 20 feet of each other as seen in Figure 14. The 2019 sample was removed due to data gaps. Figure 15 shows the transects from 2008, 2014, and 2017. Although the 2009 overbank topography is higher than 2014 and 2017, the three sections show a slightly increasing channel elevation, approximately 1 foot from 2008 to 2017.

Figure 14
Tar Creek near Commerce USGS ADCP Transects

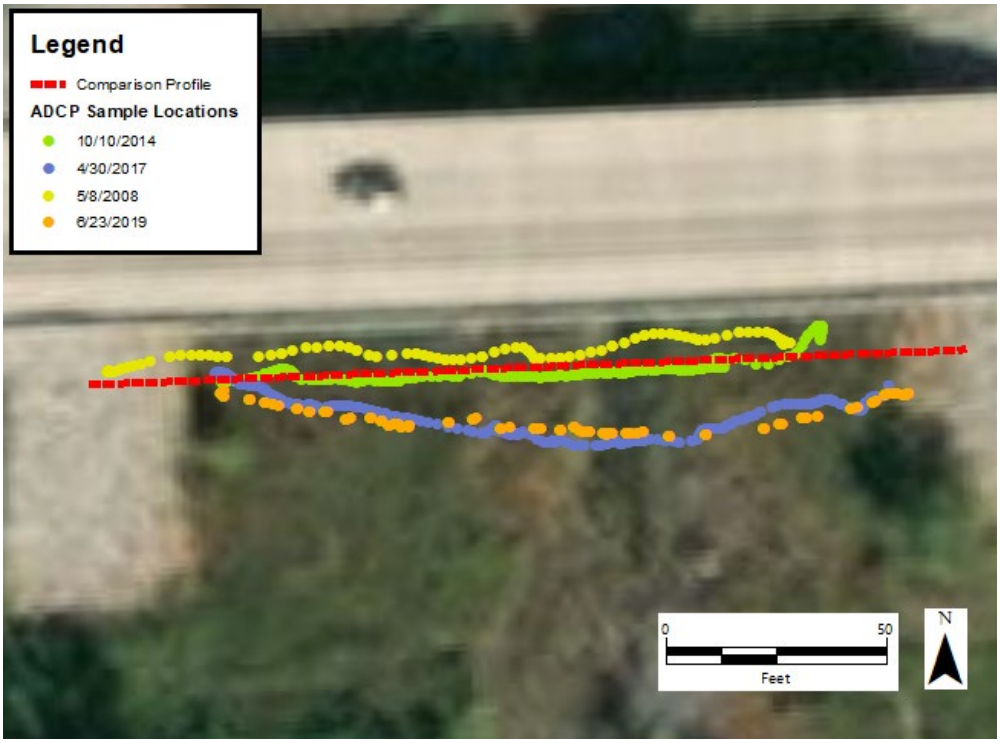

Figure 15
Tar Creek near Commerce USGS ADCP Sections

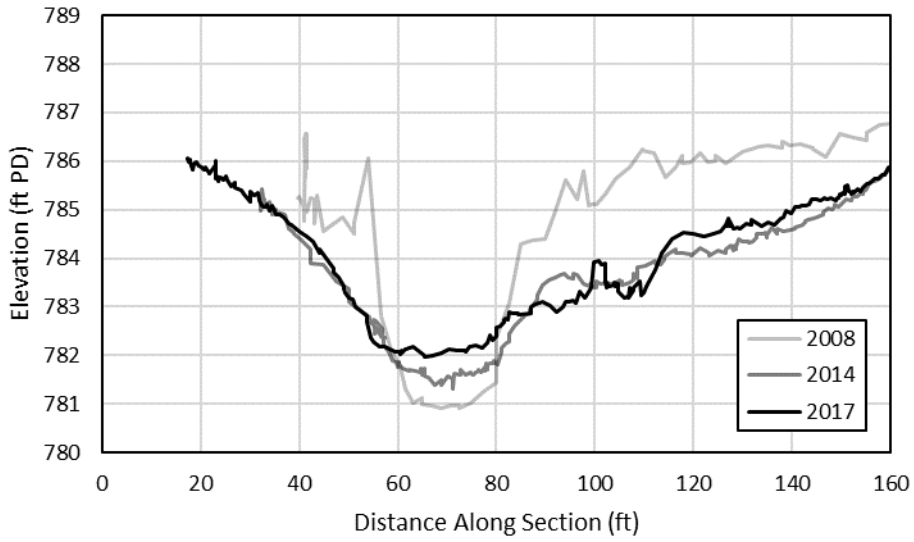

2.1.1.11.4 Tar Creek at 22nd Street Bridge

Two ADCP sample events were available from Tar Creek at 22nd Street Bridge, taken in 2013 and 2016, spaced approximately 10 feet apart as seen in Figure 16. The data showed no significant change in channel elevation from 2013 to 2016 (Figure 17).

Figure 16
Tar Creek at 22nd Street Bridge USGS ADCP Transects

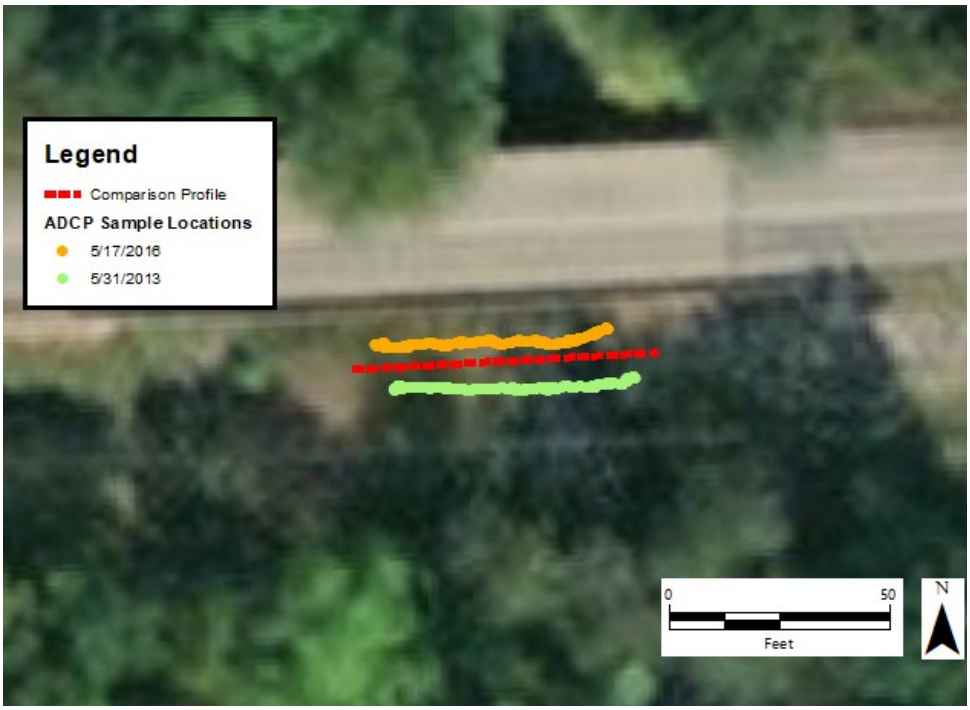

Figure 17
Tar Creek at 22nd Street Bridge USGS ADCP Sections

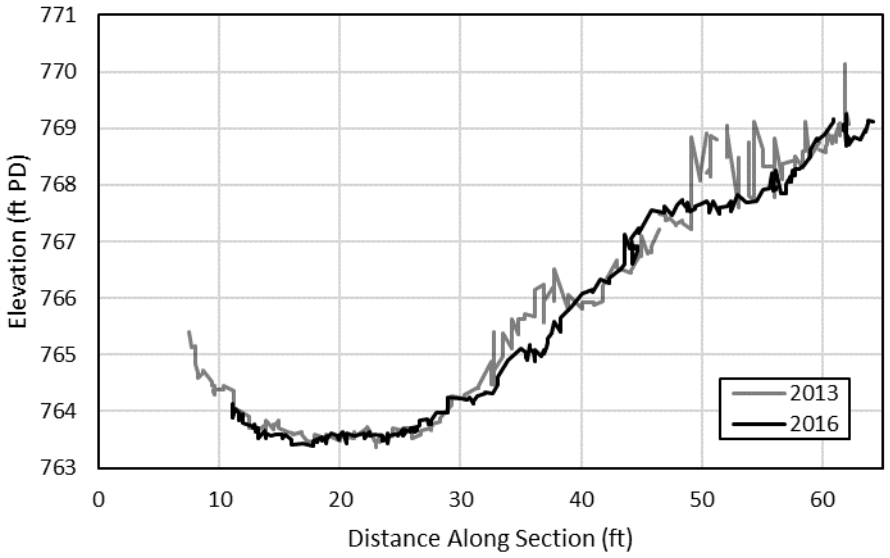

2.1.1.11.5 Spring River near Quapaw

The USGS has made ADCP data available from seven sampling events at Spring River near Quapaw station, taken from 2009 to 2015, spaced across approximately 60 feet of river as shown in Figure 18. The data from events taken from 2009 to 2015 show a different profile than those taken from 2016 to 2020. Figure 19 shows no change in channel elevation from 2009 to 2015, and Figure 20 shows an increasing channel elevation from 2016 to 2020. The distance between the transects accounts for some of the variation.

Figure 18
Spring River near Quapaw USGS ADCP Transects

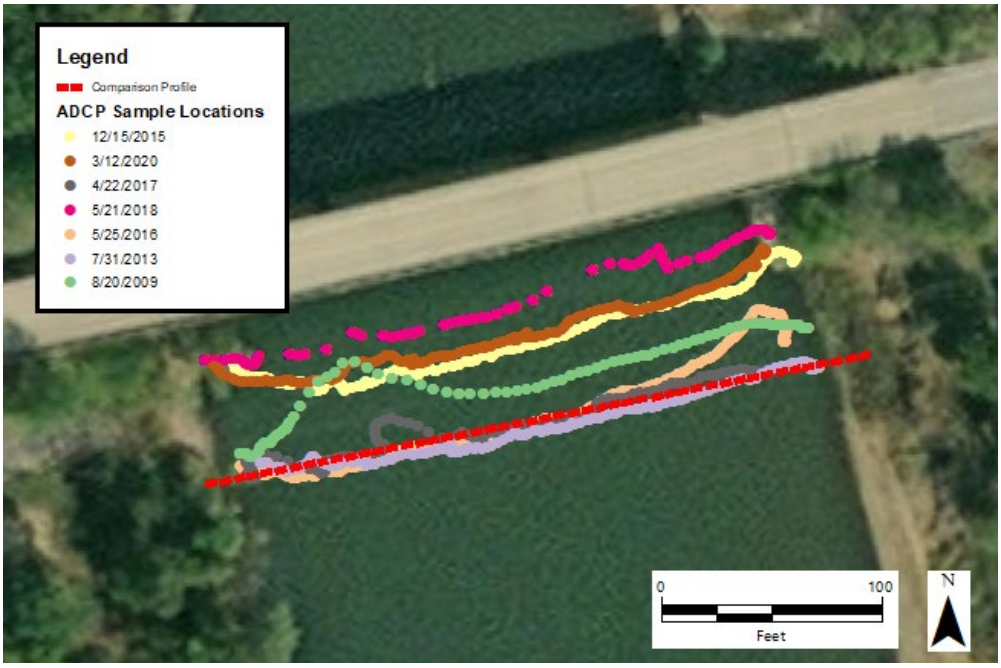

Figure 19
Spring River near Quapaw USGS ADCP Sections

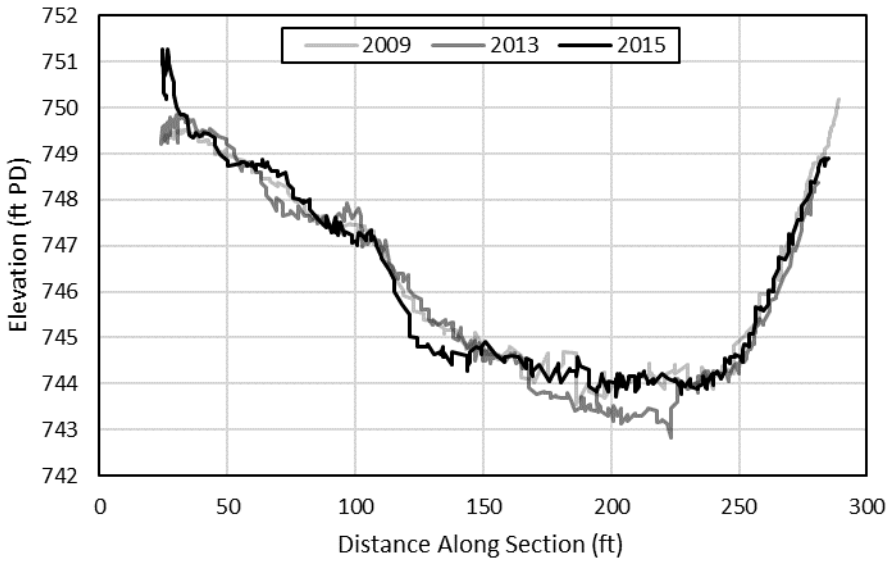

Figure 20
Spring River near Quapaw USGS ADCP Sections

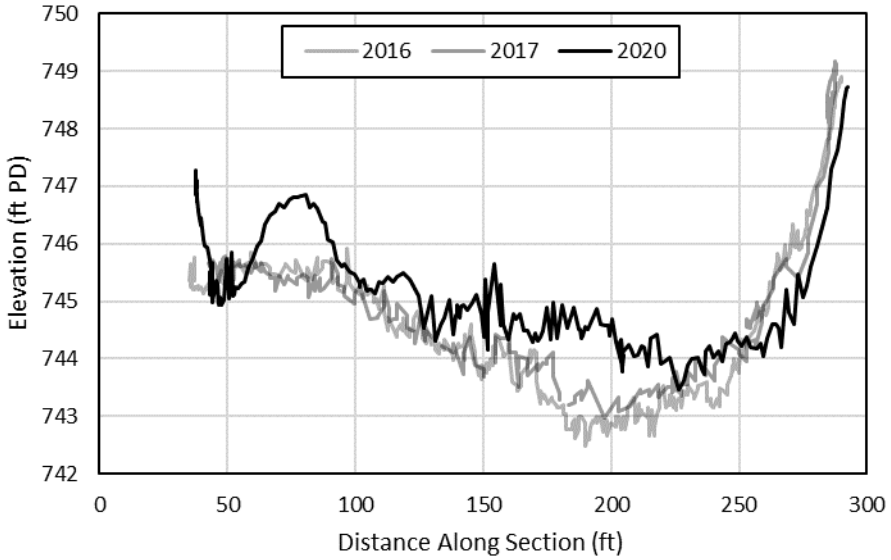

2.1.1.11.6 Elk River near Tiff City

Figure 21 shows USGS ADCP data from six sampling events at Elk River near the Tiff City USGS station. The transects are spaced approximately 50 feet apart, and span 2011 to 2022. High-quality datasets in close proximity to the comparison profile are shown in Figure 22. The sections show some movement in the existing sand bar between the sampling events, and an overall trend toward higher channel elevation.

Figure 21
Elk River near Tiff City USGS ADCP Transects

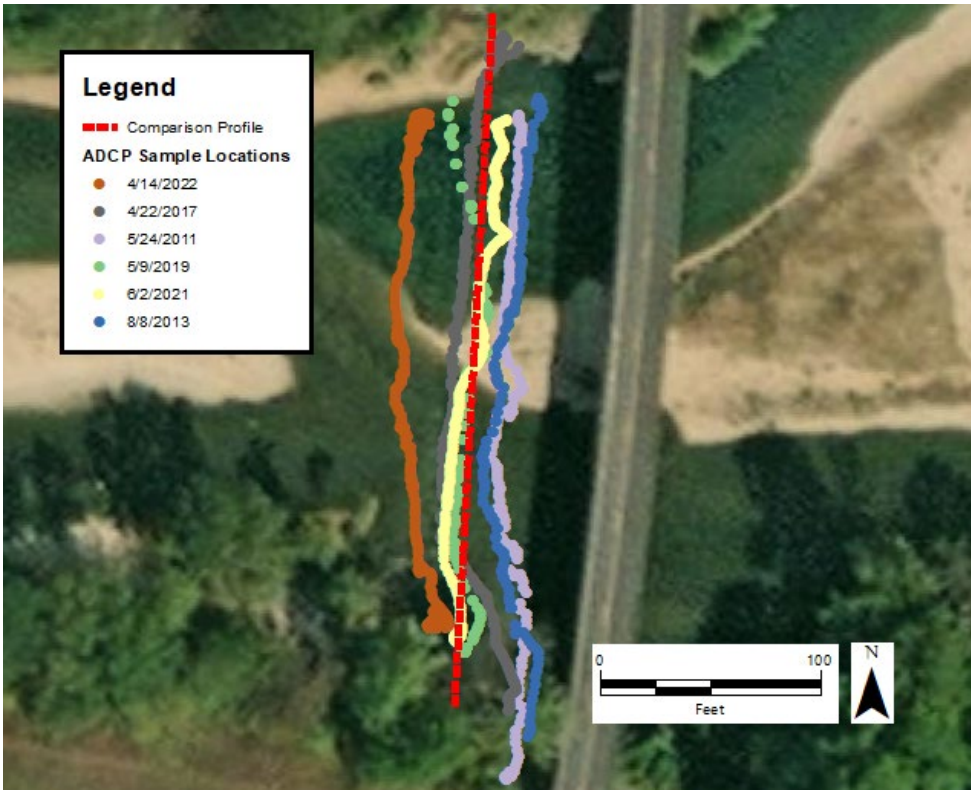

Figure 22
Elk River near Tiff City USGS ADCP Sections

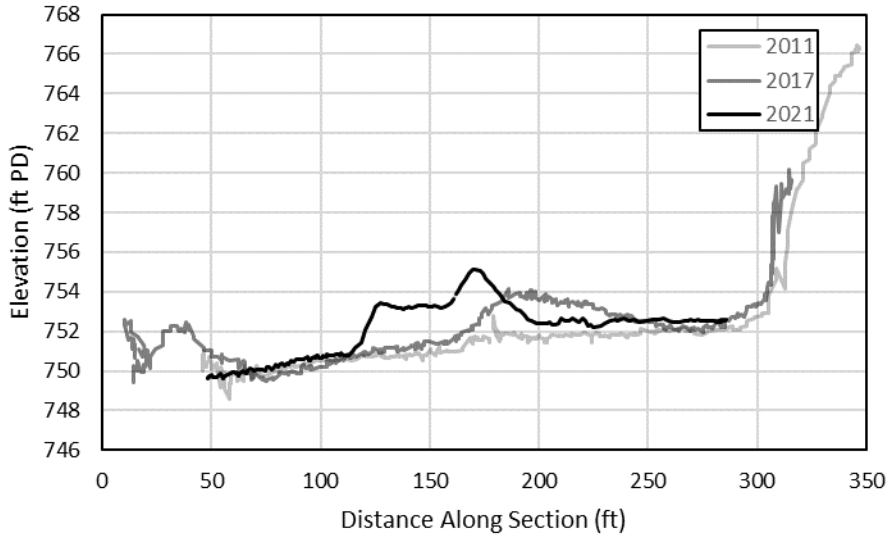

2.1.2 Water Surface Elevation, Discharge, and Flow Velocity

USGS provides monitoring gages in several locations within the study area watershed. These locations are shown in Figure 23, and station information is provided in Table3. Each station provides WSE information at regular intervals; most also list discharge volumes. These gage readings are available to the public through USGS websites (USGS 2021a, 2021b, 2021c, 2021d, 2021e, 2021f, 2021g).

Table 3
USGS Gages Present in the Grand Lake Watershed and Periods of Record for Parameters Relevant to the Study

USGS Station ID	Site Name	Period of Record		
		Discharge (Continuous Record)	WSE (Continuous Record)	SSC (Intermittent Record)
07185000	Neosho River near Commerce, Oklahoma	1990–Present	2007–Present	1944–2016
07185080	Neosho River at Miami, Oklahoma	N/A	2007–Present	N/A
07185090	Tar Creek near Commerce, Oklahoma	2007–Present	2007–Present	2004–2016
07185095	Tar Creek at 22nd Street Bridge at Miami, Oklahoma	1989–Present	2007–Present	1988–2006
07188000	Spring River near Quapaw, Oklahoma	1989–Present	2007–Present	1944–Present
07189000	Elk River near Tiff City, Missouri	1990–Present	2007–Present	1993–2009
07190000	Lake O' the Cherokees at Langley, Oklahoma	N/A	2007–Present	N/A

Note:
N/A indicates that the specific data type was not recorded at these locations.

Figure 23
Map of the Study Area Showing Locations of USGS Gaging Stations and Water Surface Elevation Monitoring Sites

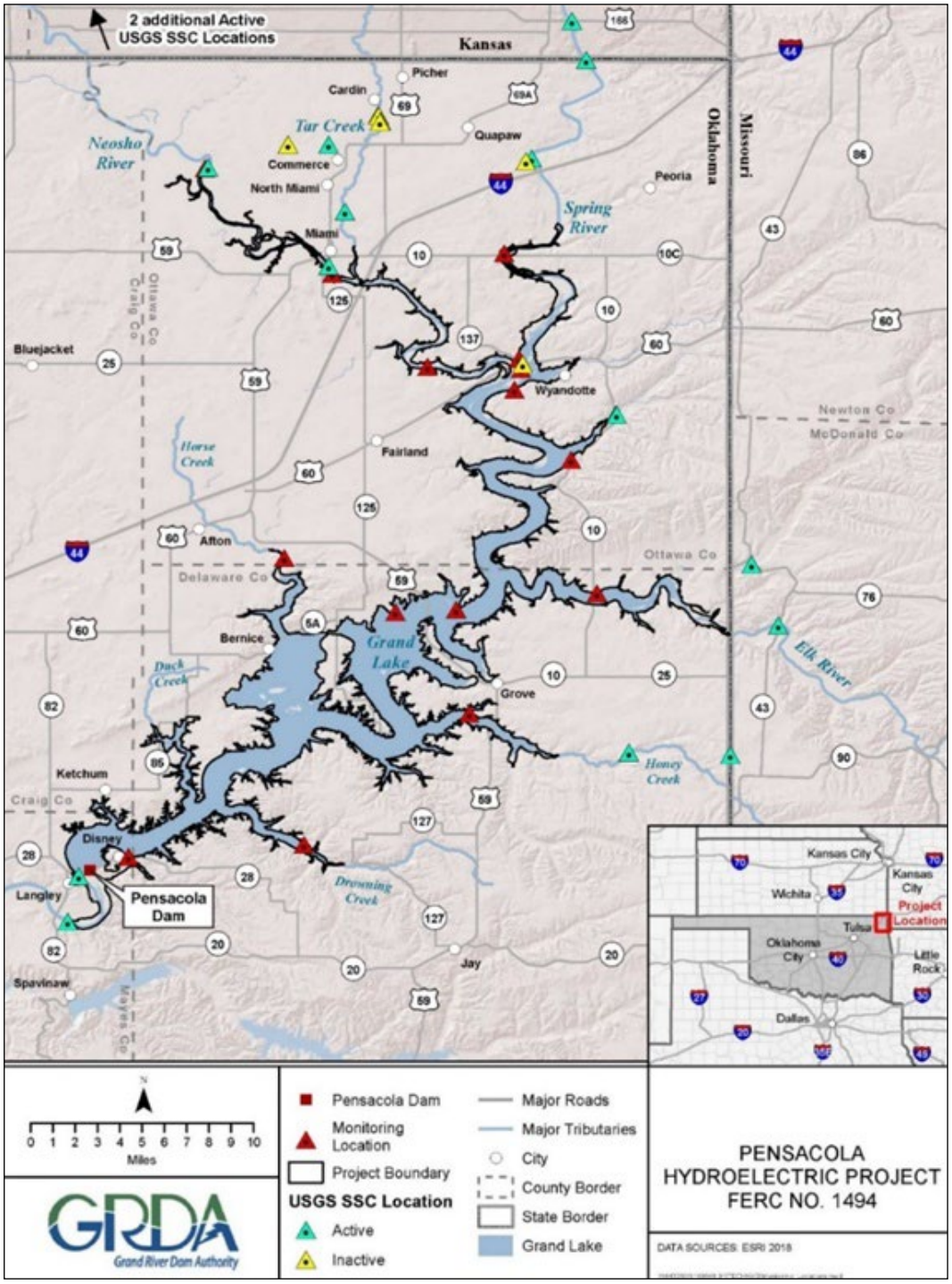

USGS also performs periodic discharge profile measurements at the gage stations. These typically use an ADCP. Table 4 provides a summary of the available ADCP data.

Table 4
Acoustic Doppler Current Profiler Data Available from USGS Measurements

USGS Station ID	Site Name	Period of Record	Range of Flows (cubic feet per second)
07185000	Neosho River near Commerce, Oklahoma	2006–Present	931–129,000
07185080	Neosho River at Miami, Oklahoma	2013–2017	172–57,100
07185090	Tar Creek near Commerce, Oklahoma	2008–2017	402–4,930
07185095	Tar Creek at 22nd Street Bridge at Miami, Oklahoma	2012–2016	398–2,400
07188000	Spring River near Quapaw, Oklahoma	2004–Present	639–62,600
07189000	Elk River near Tiff City, Missouri	2008–2017	2,340–24,800

2.1.3 Sediment Information

There are two primary components of sediment information needed for this study. The first is analysis of the bed sediments in the rivers and lake; the second is evaluation of sediment volumes moving into the study area from upstream sources.

2.1.3.1 Bed Sediments

Understanding and analysis of sediment transport through the rivers flowing into Grand Lake require knowledge of the sediment forming the bed of these streams. Only limited information was available regarding bed material of these streams. Several studies investigated sediment in the channel and upland areas within Grand Lake (e.g., Pope 2005; Andrews et al. 2009; Ingersoll et al. 2009; Juracek and Becker 2009; Smith 2016). Although the studies have produced a great deal of sediment analysis, they do not contain information that can be used to determine properties necessary for the proposed study such as critical shear stress or detailed grain size distributions.

Mussetter, in a 1998 report entitled *Evaluation of the Roughness Characteristics of the Neosho River in the Vicinity of Miami, Oklahoma*, photographically documented characteristics of the bed material forming the Neosho River and described the sediment as sand and gravel.

Mussetter (1998) observed the following regarding the bed material of the Neosho River (see Figure 24):

> Based on field observations and sediment samples taken from bank-attached bars and from the bed of the river, the bed material in the reach upstream from approximately the I-44 Bridge (RM 142) is composed primarily of gravel and sand. Downstream from I-44, the surface bed material at the time of the sampling in late 1996, which was performed when the discharge in the river was relatively low, was primarily silt and clay (Mussetter 1997). There are no obvious factors other than reduced flow velocities caused by backwater from Pensacola Dam that would cause the observed change in character of the river bed in the reach downstream from Miami. Prior to construction of the dam, the bed of the river downstream from Miami was most likely gravel and sand, similar to that found upstream.

Figure 24
Typical Sand and Gravel Material on a Point Bar Along the Left (North) Side of the Neosho River at Approximately RM 147

Source: Mussetter (1998)

In the conclusions of his report, Mussetter continues his observations and speculation regarding the bed of the Neosho River:

> The bed of the Neosho River through and upstream from Miami consists of a mixture of sand and gravel. In contrast, the bed is composed of finer-grained material in the reaches downstream from Miami due to the effects of backwater from Grand Lake. Samples taken from the bed surface at low flow in late 1996 consisted primarily of silt- and clay-sized material. Based on the characteristics of the upstream bed material, it is probable that the silt and clay is entrained and carried farther downstream into the reservoir during higher flows, and that the bed is composed primarily of sand.
> (Mussetter 1998)

The concept that the bed consists primarily of sand was apparently reinforced by the analysis of resistance to flow. In discussing the Manning's *n* values, which quantify resistance to flow in hydraulic modeling, Mussetter states the following:

> These values are consistent with observed values in other sand bed streams having dune bedforms. This result indicates that dunes, and therefore relatively high Manning's n values, must be present in the reach downstream from Miami during high flows under with-reservoir conditions.
> (Mussetter 1998)

As demonstrated in subsequent sections of this report, there are a number of factors that contribute to the observed change in character of the bed material from non-cohesive sand and gravel to cohesive silt and clay. Mussetter (1998) focuses only on the presence of Pensacola Dam, but there are other factors influencing those findings. These factors include backwater from bridges, geologic and geomorphic features, and the fact that the river is transporting almost exclusively cohesive silt- and clay-sized material with very little bedload transport of non-cohesive material. In addition, on the recession limb of hydrographs, some sediment being transported by the river may temporarily deposit before being flushed farther downstream during subsequent higher flows resulting in the transition of the bed surface from coarser material to finer and back to coarser again.

2.1.3.2 Sediment Transport

The second sediment analysis required is measurement of sediment volumes flowing into the system. Approximate sediment transport rates can be determined from USGS measurements of suspended sediment concentrations (SSCs; Figure 25). SSC provides a measurement of sediment loading, typically in milligrams per liter, of streamflow. That information can then be multiplied by discharge volumes to determine transport rates within the water column. Table 3 provides a summary of the

available period of record for SSC information. However, the datasets are small with samples collected on rare occasions; they do not represent continuous records like the discharge and WSE measurements.

Figure 25
Suspended Sediment Concentration Samples and Stream Discharges During Sampling on the Neosho River Near Commerce (USGS Gage 07185000)

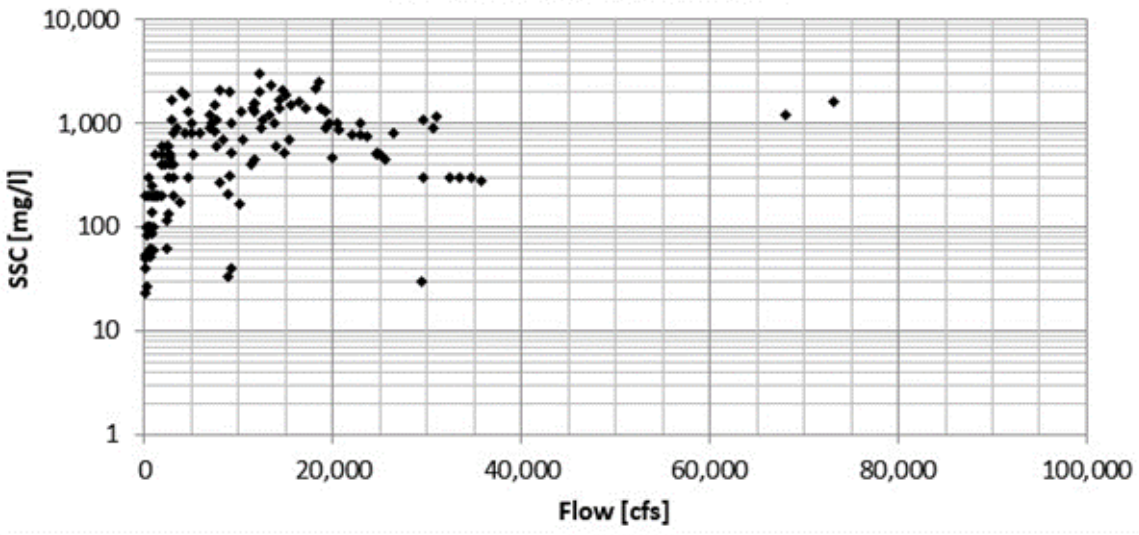

Note: Only two samples were collected at discharges above 40,000 cfs.

SSC measurements focus only on fine materials suspended in the water column. This typically includes silts and clays, with limited sand possible depending on turbulence at the sampling site. It does not, however, measure transport rates along the streambed. Bedload transport is generally dominated by sands, gravels, and cobbles that "roll" downstream along the streambed. This information is critical to understand the full sediment transport regimes of a watershed. Recorded sediment transport rates are limited to SSC calculations because bedload transport has not been reported within the Grand Lake watershed.

2.1.3.3 Contaminated Sediment

City of Miami, Miami Tribe, Eastern Shawnee Tribe, Ottawa Tribe, Seneca Cayuga Nation, Wyandotte Nation, and N. Larry Bork (counsel for the City of Miami citizens) provided a list of existing information to be used in their requested contaminated sediment transport study. The toxicity of the sediments is not within the scope of this study. However, existing data and information available from studies conducted of the Superfund site within the Tar Creek watershed were reviewed and incorporated in the study as appropriate.

2.2 Field Data Collection

Due to information gaps relevant to the study, field data collection was deemed necessary. This consisted primarily of WSE monitoring and sediment and water sampling to provide calibration information for eventual model development.

2.2.1 Water Surface Elevation Monitoring

Anchor QEA collected WSE data throughout the Project site (Figure 23). Sixteen monitoring locations were selected, and HOBO pressure loggers (Figure 26) were installed at each site in December 2016. The loggers record raw pressures and water temperatures at 30-minute intervals to provide a continuous WSE record throughout the basin. Data are stored in onboard memory; with 30-minute recording intervals, the memory capacity is approximately 1.2 years.

Figure 26
Photograph of HOBO Pressure Loggers and Mounting Chamber

Loggers were placed in a mounting chamber and attached to rebar driven into the bed at each location shown in Figure 23. The mounting chamber was constructed of PVC with threaded caps painted black to limit visibility and deter theft or vandalism. Rebar was driven into the bed to a sufficient depth to prevent the loggers from washing away during high flow events.

2.2.2 Sediment Grab Samples

The study team first collected surface samples of stream sediment throughout the watershed. A total of 62 samples were collected during a visit in December 2019 (Table5). Figure 27 shows the locations of the sediment samples. Exhibit 2 provides the plots of the gradations of the sediment grab samples.

Table 5
Surface Sediment Grab Sampling Locations by River and Reach

Stream	Samples Collected
Neosho River North of Spring River	20
Neosho River South of Spring River	9
Tar Creek	13
Spring River	10
Elk River	8
Sycamore Creek	1
Horse Creek	1

Figure 27
Location of Sediment Grab Sampling Efforts within the Grand Lake Watershed

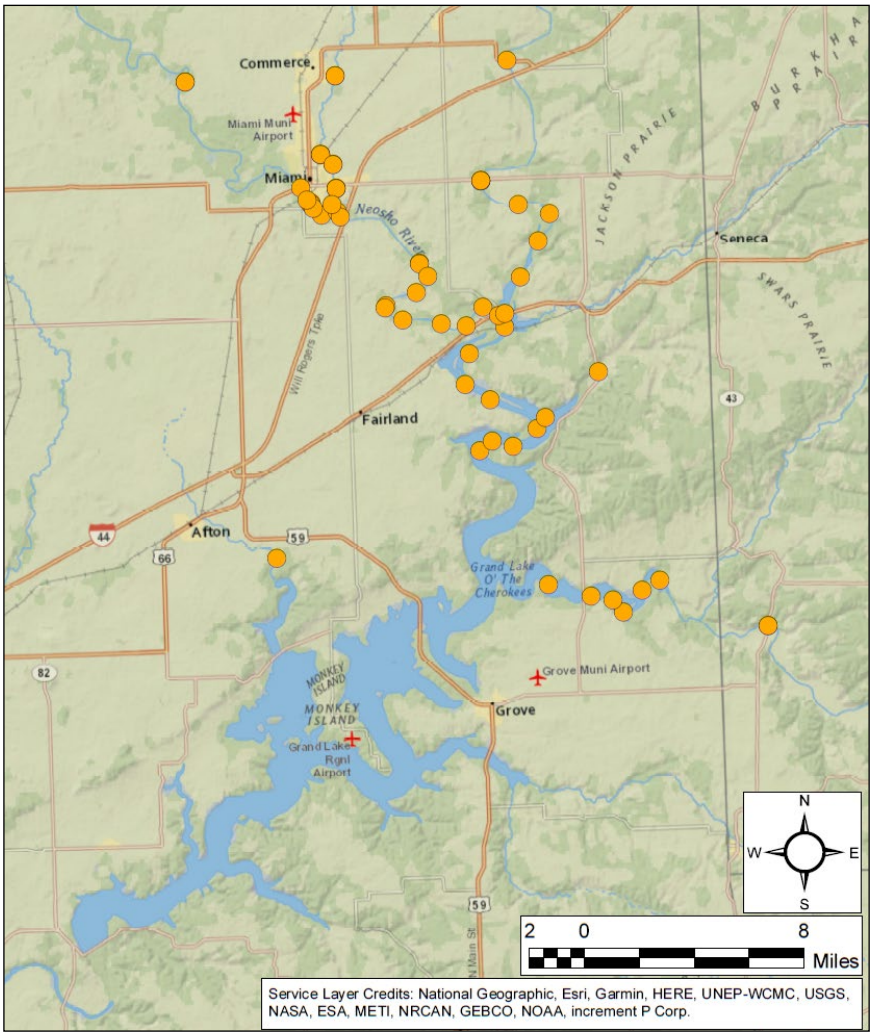

Samples were collected both in the overbank and in-channel areas. Overbank samples were gathered with shovels and in-channel samples were taken with either a PVC push-core sampler, a shovel, or an Ekman dredge (Figure 28). Once collected, the samples were placed into containers for analysis at the University of Wisconsin Soil and Forage Laboratory (UWSFL) in Marshfield, Wisconsin.

2.2.3 *SEDflume Core Sampling*

Cohesive sediment cores were collected during the study for erosion testing using SEDflume (see Exhibit 3). Despite initial reports indicating that Grand Lake watershed sediment transport was dominated by sands (Tetra Tech 2018), field information showed that cohesive sediments were prevalent throughout the basin and comprised the majority of sediment moving through the study area. As a result, plans were adapted to account for the presence of silts and clays, which are not eroded or transported in the same way as non-cohesive sediments such as sand and gravel.

Figure 28
Ekman Dredge Used for In-Channel Sediment Sampling

Sediment transport is generally dictated by bed shear stress. Bed shear is a function of bed slope and water depth. It is essentially a measure of frictional drag on the streambed. At low shear stress, sediment is held in place by gravitational forces. At the point of incipient motion, shear and gravitational forces are essentially balanced; the shear stress in this condition is known as the critical shear stress. Above critical shear, the bed sediment becomes mobile and can be transported. Below critical shear, sediment does not move and can settle out of the water column. Depending on sediment properties, critical shear stress can vary widely, with boulders having high critical shear values and fine sand exhibiting low critical shear stresses.

Non-cohesive sediments such as sand, gravel, and cobbles (Figure 29, top photograph) tend to have easily predictable critical shear stress. It is typically proportional to sediment density and grain size and is relatively constant through the entire sediment layer. Generally, grains move relatively independently of each other. As a result, these sediments are comparatively simple to evaluate and model.

Figure 29
Visual Comparison of Different Sediment Types

Note: Top—non-cohesive sand, gravel, and cobbles; bottom—cohesive silt and clay.

Modeling cohesive sediments is far more complex. Critical shear stress is determined primarily by the cohesive forces between silt and clay particles rather than individual grain sizes. This is complicated by the process of consolidation; as sediment is deposited in an area, it applies force to the underlying layers, compressing them and increasing the cohesion, making them less susceptible to erosion. The amount of time spent on the bed also affects consolidation and critical shear stress. Furthermore, erosion typically occurs as clumps break free of the surrounding sediment. Due to the changing resistance to erosion based on depth and the nature of cohesive sediment transport, it is considerably more difficult to accurately model and requires additional information.

Accurate collection of sediment information can be accomplished through erosion testing on SEDflume (Borrowman et al. 2006; McNeil et al. 1996). The SEDflume testing facility consists of an enclosed flume with a hole in the bed. An undisturbed sediment core sample is placed under the hole, and the surface of the core is raised to be flush with the flume bed. Water is pumped across the sample surface at a known shear stress; as the core erodes, a jack lifts it to keep the surface flush with the flume bed. The rate of erosion is the distance the jack moved per unit time of the test. Bed shear stress can then be increased to evaluate rates at a range of shear values. This test provides information about critical shear stress throughout the sediment core, allowing engineers to evaluate critical shear as a function of depth.

The study team collected core samples for SEDflume analysis in March 2020 (Figure 30). A total of 14 core samples were collected using a box push-core system (Figure 31). The box core was a clear plastic sleeve, which was pressed into the sediment bed. A pressure relief valve at the top of the core allowed air and water to escape as the core sank into the streambed. The resulting suction pressure kept the sample inside the sleeve as it was raised back to the water surface. The sample was then measured, sealed, and transported to the test laboratory for analysis.

Figure 30
SEDflume Core Sampling

Note: Left—technician pulling box core rig out of the bed; center—box core showing sediment fill and measuring depth of sample; right—several collected samples before shipment to the test facility.

Figure 31
Locations of SEDflume Core Samples Collected During the Sediment Investigation

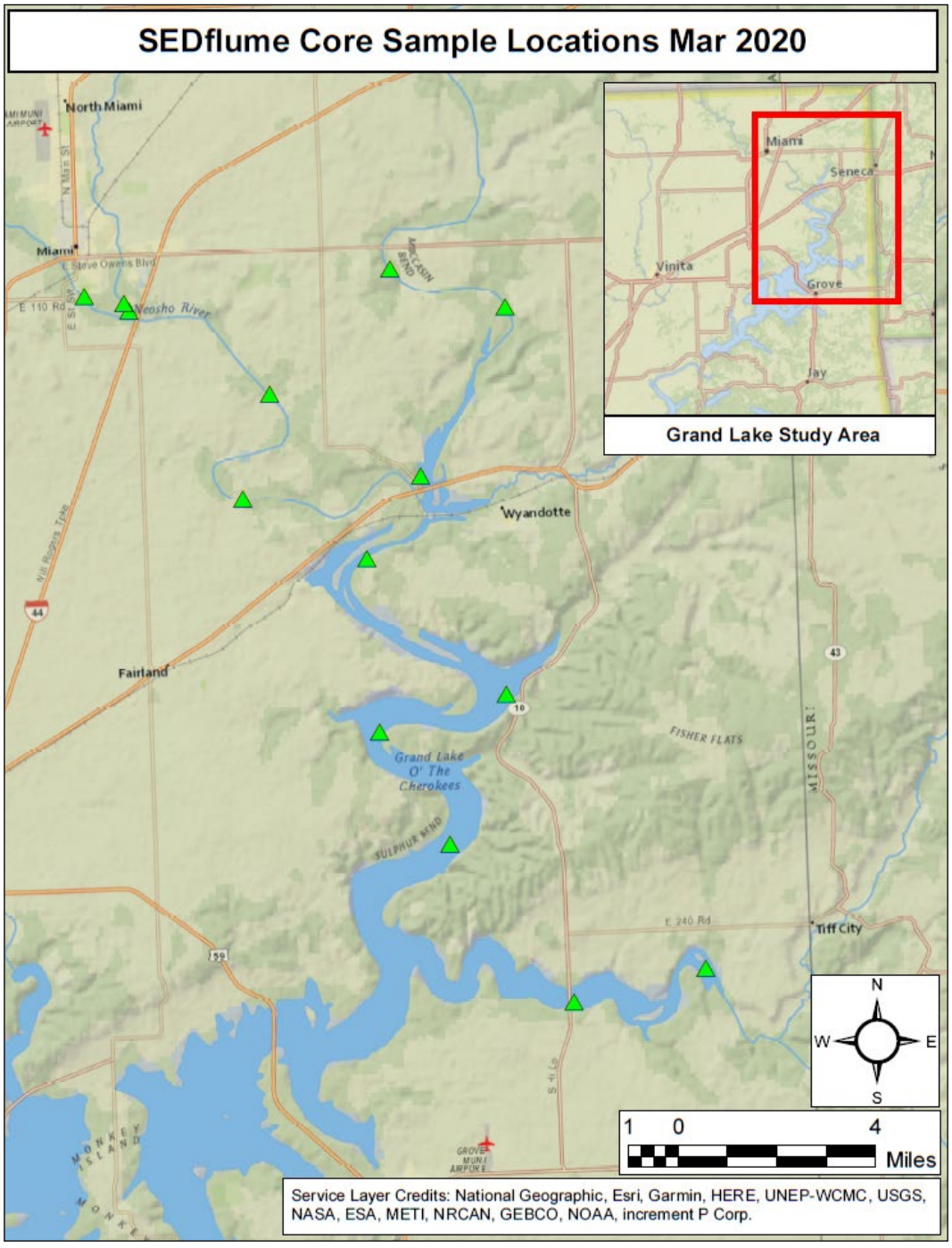

SEDflume analysis also provided particle size analysis. During testing, Integral Consulting used a Beckman Coulter LS particle size analyzer over a range of depths below the surface of the core for each sample.

2.2.4 Sediment Transport Measurements

Sediment transport measurements were also included in the sediment study. These consisted primarily of two forms of data: SSC and bedload transport quantification. Bedload samples were collected immediately following SSC sampling at each site. Dates of sampling efforts and discharges are provided in Table6.

Table 6
Sampling Dates and Discharge Measurements, per USGS Gaging Station Records

Date	Discharge (cubic feet per second)			
	USGS 07185000 Neosho River at E 60 Rd	**USGS 07185090 Tar Creek at Hwy 69**	**USGS 07188000 Spring River at E 57 Rd**	**USGS 07189000 Elk River at Hwy 43**
August 2019	15,500	10.0	1,240	537
May 2020	37,500	*	8,040	4,940
July 2020	2,930	5.29	3,480	*
April 2021	2,330	*	2,250	*
May 2021	18,900	750	16,500 23,400**	*
July 2021	41,600	500	14,700	*

Notes:
*Samples not taken at this location.
**Spring River was sampled twice during the May 2021 site visit.

2.2.4.1 Suspended Sediment Concentration

A D-74 depth-integrating water sampler was used to collect SSC samples (Figure 32). This sampler features a finned body with a nozzle pointing upstream and a vent pointing downstream. As it is lowered into the water, flow is allowed through the nozzle and into a sampling bottle. The sampler is lowered into the stream until it reaches the bed, then is raised; this is all done at a constant speed. Based on flow conditions at the site, researchers have an array of nozzle sizes and travel speeds to choose to ensure valid data (USGS 2006).

Figure 32
Sampling Equipment Used During Suspended Sediment Concentration Sampling Efforts

Notes: The D-74 water sampler is attached to the crane, and the SonTek M9 ADCP used to measure stream flows is in the lower right. Samples are placed in the carrier at left after collection.

Anchor QEA followed standard USGS protocols for equal width interval water sampling (USGS 2006). The field technicians used a SonTek M9 ADCP or timed a floating object moving a known distance to measure current profiles at each site before sampling began. Based on flow velocities and patterns, they selected appropriate nozzle sizes and descent and ascent velocities for the D-74 sampler following USGS standard procedures (USGS 2006). Following nozzle installation, a calibrated winch lowered the sampler to the stream and raised it at the specified rates. Samples were then capped and sent to the Wisconsin State Laboratory of Hygiene (WSLH) for SSC analysis.

Field notes and a detailed description of the process followed were provided in April 2022 as attachments to GRDA's response comment.

2.2.4.2 Bedload Transport

Anchor QEA used a Helley-Smith bedload sampler (Figure 33) to collect bedload transportation measurements. Sampling sites were the same as those used for SSC measurements to ensure capture

of all sediment (SSC and bedload) moving through the system under given flow conditions. The Helley-Smith sampler sits on the streambed with a rectangular opening pointed upstream. Saltating, sliding, and rolling sediment is transported at the bed surface into the opening and trapped in a mesh bag. USGS documentation provides guidelines for the use of this equipment; Anchor QEA followed USGS procedures (Edwards and Glysson 1999) to collect bedload sediment during site visits (Table 6).

Figure 33
Bedload Transport Measurements Collected Using the Helley-Smith Sampler

Field notes and a full description of the process followed were provided in April 2022 as attachments to GRDA's response comment (GRDA 2022).

2.2.5 Subsurface Investigations

GRDA also performed subsurface investigations of the delta feature. These included two primary components: sub-bottom profiler (SBP) surveying and vibracore sampling. The SBP survey covered

nine transects of the Neosho River and was completed in January 2022 (Figure 34). Vibracore sampling included multiple samples at each SBP transect and was completed in February 2022.

Figure 34
Locations of SBP Transects and Sediment Cores Collected by GRDA

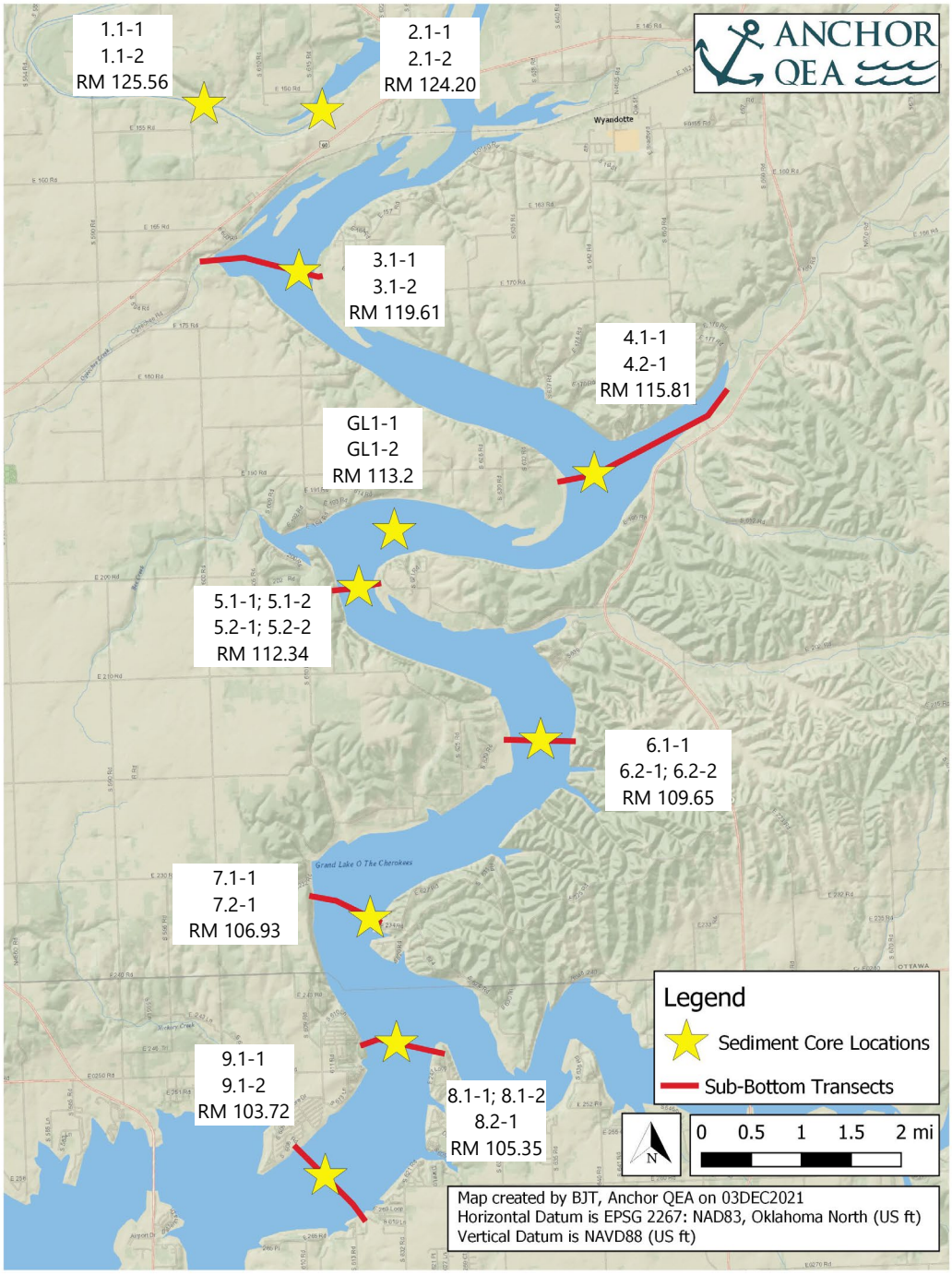

An SBP uses sonar pulses to determine depth of a waterbody. There is an emitter and a receiver on the SBP head unit, and by measuring the amount of time necessary for the emitted pulse to reach an object and return to the receiver, the SBP is able to measure the distance the pulse traveled. This allows the SBP to measure bathymetry, but the pulse is also powerful enough to penetrate a soft sediment bed, such as clay, silt, and sand before reaching a harder layer. Using the same principles, the SBP can then estimate the thickness of a soft sediment layer above gravel or bedrock.

Vibracoring uses a motorized head unit to press core tubes into the stream or lakebed. The combined weight and vibration of the head unit allows for deeper penetration than simply pressing the core tube into the bed or relying on gravity coring methods. Once collected, grain size analyses and other testing can be used to determine sediment properties as a function of depth in the sediment layers. The cores were used for two purposes: 1) to confirm SBP survey information and evaluate sediment composition; and 2) an attempt to determine approximate dates of deposition through the use of cesium-137 (Cs-137) analysis.

Cs-137 is an isotope that does not occur in nature. It is created by nuclear fission, which humans began developing in the 1940s. As nuclear weapons testing accelerated, atmospheric Cs-137 increased until a 1963 nuclear test ban treaty. The Cs-137 levels then dropped significantly. Atmospheric Cs-137 concentrations are well-correlated with Cs-137 concentrations in soil, showing the same pattern of increase from the 1940s to 1963, then a marked decrease.

Measurement of relative Cs-137 activity in sediment allows researchers to estimate deposition dates for sediment layers. In areas of continual deposition, Cs-137 analysis will find a pattern of increasing Cs-137 activity moving deeper in the column until reaching the 1963 layer. Below that layer, concentrations drop to zero by the 1940s. In disturbed areas or places with non-continuous deposition, there is usually no clear Cs-137 peak. The combination of SBP, vibracore samples, and Cs-137 provides insight into the volume, rate, and timeline of sediment deposition in the Neosho River.

2.2.6 Additional Bathymetric and Sediment Investigations

In December 2022, Anchor QEA performed an additional field investigation near the Miami Fairgrounds to evaluate the low-head dam at RM 135.25 on the Neosho River (Exhibit 8). This investigation included a bathymetric survey of the area immediately upstream and downstream of the structure. It also included additional vibracore sampling in the area upstream of the dam.

The Miami low-head dam has been in place for approximately 100 years and would serve as an effective barrier to downstream bedload sediment transport in the event that material reached the structure. The larger, heavier grains would build up along the upstream face of the dam because the river energy is insufficient to transport the sediment up and through or over the structure. Over time,

this would result in a sediment bed extending upstream of the dam that is approximately flush with the bed material immediately upstream of the dam face, as is found upstream of small dams in rivers where a significant quantity of coarse sediment is transported. The bathymetric survey was intended to evaluate whether that had occurred. Results are provided in Section 2.3.6.

Core sampling in the area was intended to determine the type of sediment at that location in the stream. Based on previous fieldwork, Anchor QEA expected to find an armor layer over finer material. Results are provided in Section 2.3.6.

2.3 Field Results

2.3.1 Water Surface Records

Anchor QEA has visited the site several times to collect and redeploy pressure loggers. Trips to collect WSE monitoring data were performed according to Table .

Table 7
WSE Monitoring Site Visit Dates and Logger Retrieval Rates

Date	Loggers Recovered
December 2016	16 Deployed
August 2017	13 of 16
March 2018	2 of 16
April 2019	12 of 16
December 2020	13 of 16

Anchor QEA retrieved the loggers on an approximately annual basis. Upon arrival at each monitoring station, Anchor QEA staff collected Real-Time Kinematic (RTK) GPS measurements of the WSE and surveyed any nearby benchmarks. The loggers were collected, and data were read from them using an optic USB interface. They were then relaunched and placed back in the field; staff measured depth to the loggers and depth to bed before leaving the site. After all loggers were retrieved, the data were processed to produce WSE readings from the pressure data.

The loggers recorded raw pressure measurements that had to be converted to water depths and then WSE. Because pressure readings include both water pressure and atmospheric pressure, it was first necessary to subtract ambient air pressure from the measurements. Records from the Grove Municipal Airport provided atmospheric pressure readings for processing. Python programs were used to subtract the raw readings to water pressure measurements; water density was then used to estimate the depth of the sensors according to Equation 1.

Equation 1

$$h = \frac{P}{\rho g}$$

where:

h	=	water depth
P	=	pressure
ρ	=	water density
g	=	acceleration due to gravity

Once water depths were established at the time of retrieval, logger elevation was set based on the measured WSE and recorded depth; data throughout the period of record were thus converted from the raw pressure recordings to WSE measurements (Figure 35). The calculated WSE readings were adjusted to match the RTK GPS measurements taken while on site.

Several loggers had data gaps in the record. At various sites, the loggers were washed away or vandalized, which prevented recovery. One additional data gap was due to an unforeseen high-water event that prevented recovery until after internal storage had been filled. Full datasets are available in Exhibit 1.

Figure 35
Sample Series

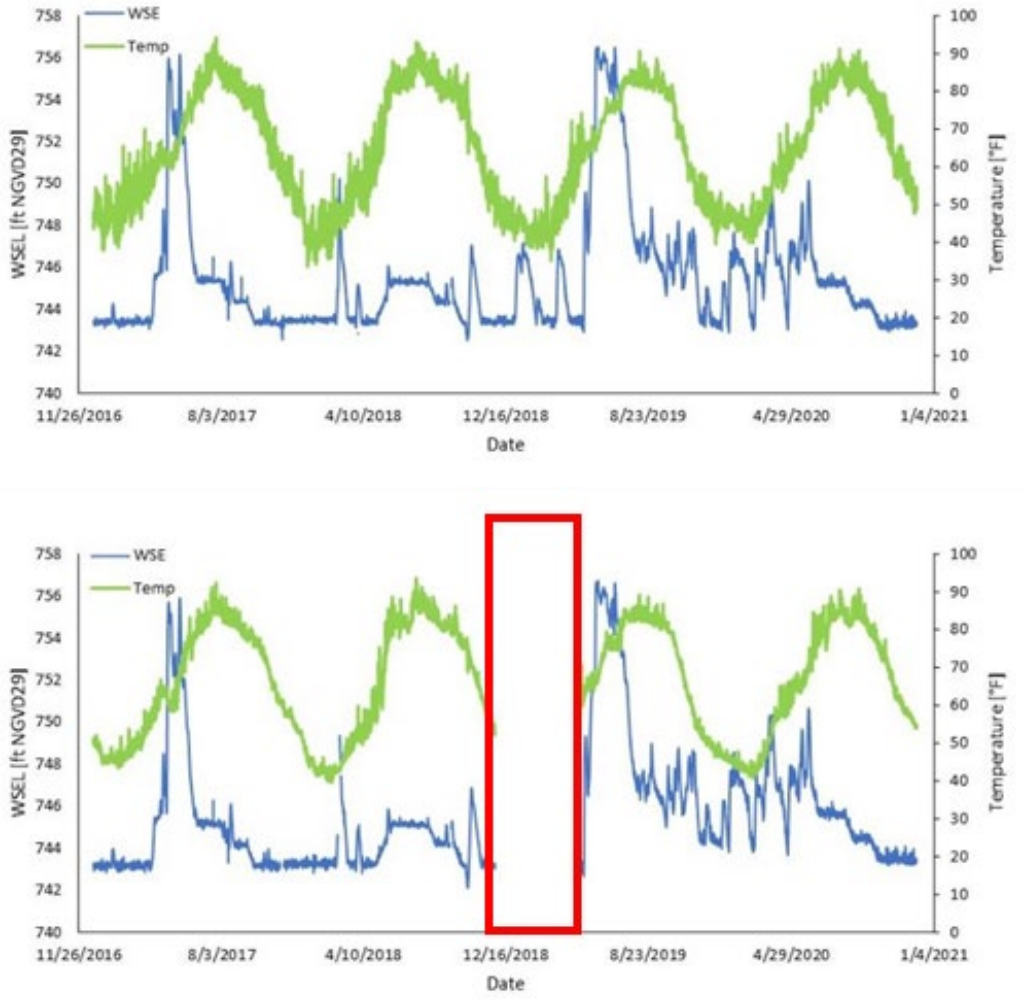

Note: Top: complete dataset; bottom: gap in record.

2.3.2 Sediment Grain Size Analysis

Following the December 2019 sediment grab sample collection, Anchor QEA sent 62 sediment samples to UWSFL for grain size analysis. The results of the analysis indicated a bi-modal size distribution, with a majority of streambed sediments consisting of gravels and coarse sediments and a majority of lakebed sediments composed of silt and clay. The results showed limited volumes of sand in either stream or lake sediments, with most of the lakebed being finer than sand and most of the riverbed being coarser than sand (Figure 36).

Figure 36
Particle Size Distributions within the Grand Lake Study Area

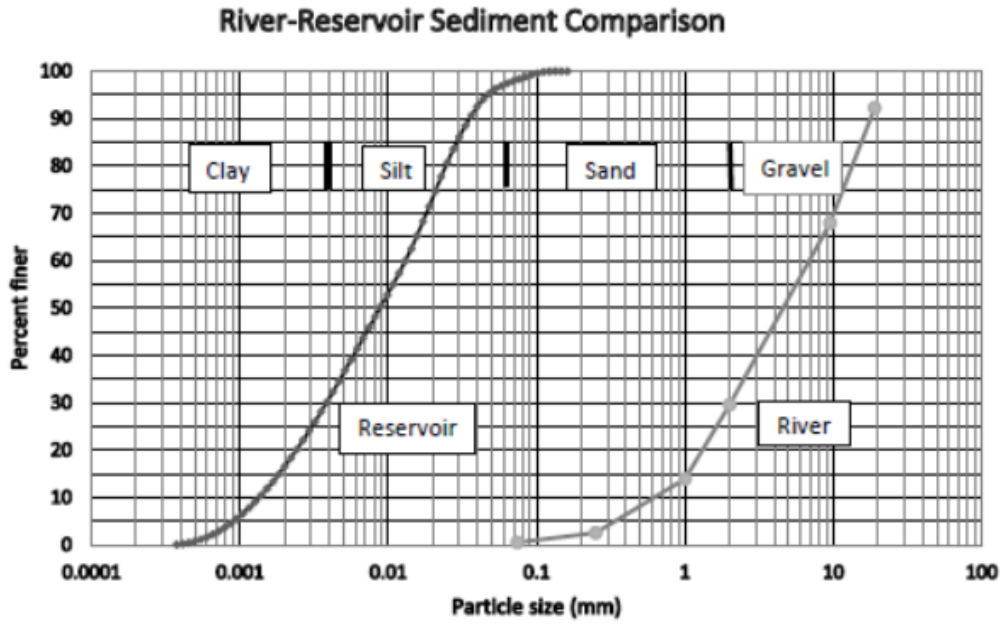

As shown in Figure 37, the beds of these streams consist primarily of gravel, with some sand. The surface of the streambeds appears to be armored by gravel and (in the case of areas of Tar Creek) larger particles. Hydraulic and sediment transport analyses, based on particle size distributions, will determine the extent to which these particles are transported downstream into the reservoir.

Figure 37
Sample Photographs Showing the Sediment in the Spring River, Tar Creek, Elk River, and Neosho River

Note: Clockwise from top left, the Spring River, Tar Creek, Elk River, and Neosho River.

Farther downstream, as the tributaries transition into lacustrine conditions, the character of the bed material changes dramatically. Samples collected from the reservoir bed appear to consist primarily of silt and clay (Figure 38).

Figure 38
Sediment Grab Samples Collected from the Reservoir Bed in Grand Lake

Full results for each sample are presented in Exhibit 2. These results show the significant variability in particle size distributions from reach to reach within streams and even significant differences between samples taken in close proximity.

2.3.3 SEDflume Test Results

SEDflume samples were tested by Integral Consulting at their Santa Cruz, California laboratory. Testing was performed according to the procedures described by McNeil et al. (1996) and Borrowman et al. (2006). The laboratory analysis of the samples included evaluation of erosion parameters, grain size distributions, and bulk density of the samples.

2.3.3.1 Erosion Parameter Analysis

Erosion of cohesive sediment is quantified by two key parameters: critical shear stress at which erosion begins, and the rate of erosion as a function of increasing shear stress greater than critical shear. A standard technology, SEDflume, has been developed to measure these parameters. The SEDflume is described as follows:

> A SEDflume is essentially a straight flume with an open bottom section through which a rectangular, cross-sectional core barrel containing sediment can be inserted [Figure 39]. The main components of the flume are the water tank, pump, inlet flow converter (which establishes uniform, fully developed, turbulent flow), the main duct, test section, hydraulic jack, and the core barrel containing sediment [Figure 40]. The core barrel, test section, flow inlet

section, and flow exit section are made of transparent acrylic so that the sediment–water interactions can be observed visually. The core barrel has a rectangular cross section, 10 by 15 cm, and a length of 60 cm. (Integral Consulting 2020)

Figure 39
SEDflume Schematic Showing Top and Side Views

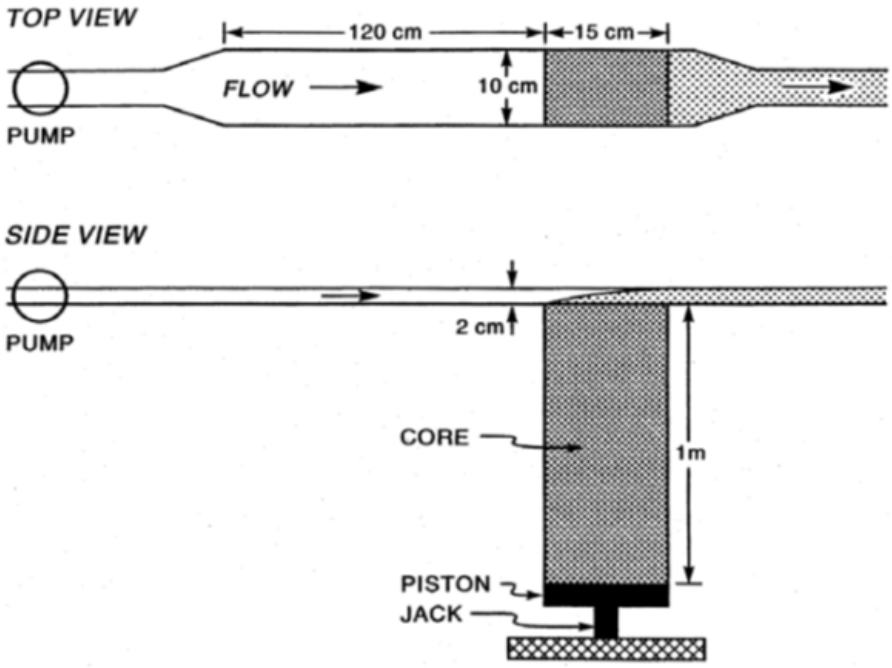

Source: Integral Consulting (2020)

Figure 40
Photograph of SEDflume Test System

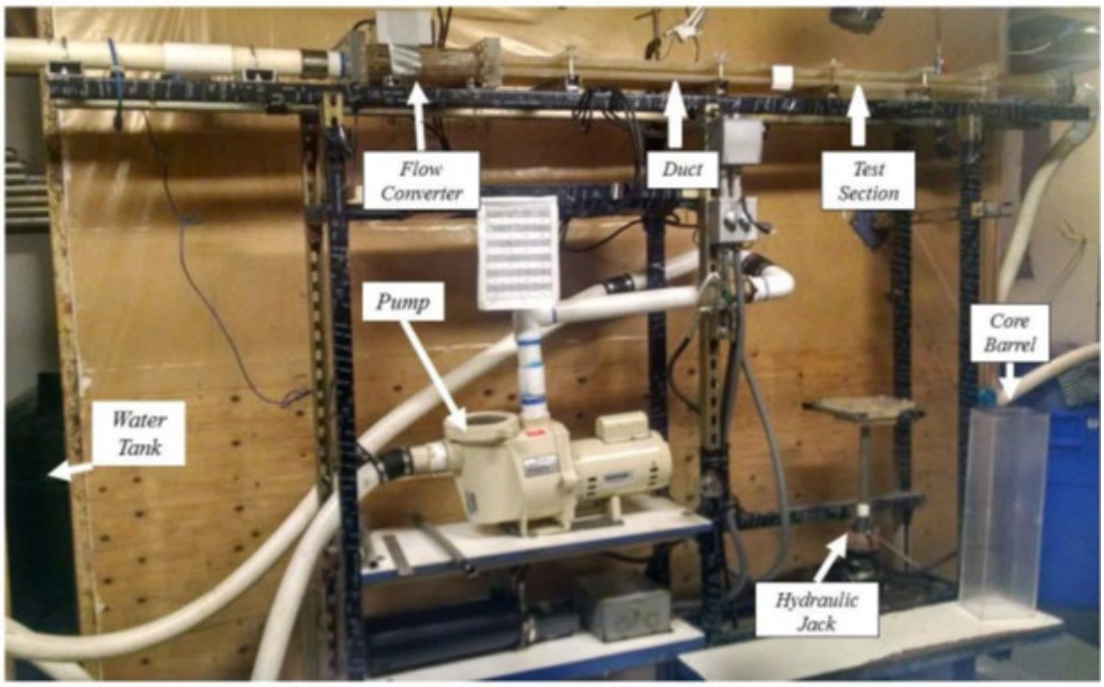

Source: Integral Consulting (2020)

In its report, Integral Consulting describes the process of conducting the laboratory testing with SEDflume, as follows:

> At the start of each test, a core barrel and the sediment it contains are inserted into the bottom of the test section. The sediment surface is aligned with the bottom of the SEDflume channel. When fully enclosed, water is forced through the duct and test section over the surface of the sediment. The shear stress produced by the flow and imparted on the particles causes sediment erosion. As the sediment on the surface of the core erodes, the remaining sediment in the core barrel is slowly moved upward so that the sediment–water interface remains level with the bottom of the flume. (Integral Consulting 2020)

Integral Consulting then describes the process of taking measurements to develop critical shear and erosion rate data:

> At the start of each core analysis, an initial reference measurement is made of the starting core length. The flume is then operated at a specific flow rate

> corresponding to a particular shear stress, and sediment is eroded (McNeil et al. 1996; Jepsen et al. 1997). As erosion proceeds, the core is raised if needed to keep the core's surface level with the bottom of the flume. This process is continued until either 10 minutes has elapsed or the core has been raised roughly 2 cm. (Integral Consulting 2020)

As the flow rate is increased through the flume and as sediment begins to erode from the surface of the core determines the critical shear value above which erosion occurs and below which no erosion occurs. Once the critical shear value is determined for that layer of sediment, the flow rate through the flume is increased and erosion measured over a range of flow or shear stresses. This process is repeated at different levels of the core sample below the surface to develop the critical shear and erosion rates through the depth of the sample. Tabulated results for each of the streams showing the critical shear erosion parameters determined using SEDflume can be seen in Table 8 through Table 11 and Figure 41 through Figure 44 show the erosion rates at the various applied shear stresses over the depth of the core sample for the associated streams.

Table 8
Physical Properties and Derived Critical Shear Stresses of SEDflume Sample NR-130 (Neosho River)

Sample Depth (cm)	Median Grain Size (µm)	Wet Bulk Density (g/cm^3)	Dry Bulk Density (g/cm^3)	Loss on Ignition (%)	τ_{no} (Pa)	τ_1 (Pa)	τ_c Linear (Pa)	τ_c Power (Pa)	Final Critical Shear (Pa)
0.0	8.34	1.49	0.84	3.7	0.2	0.4	0.84	0.33	0.33
5.9	5.20	1.56	1.01	6.8	0.4	0.8	0.44	0.29	0.40
8.6	7.01	1.64	1.10	5.0	---	---	---	---	---
Mean	**6.85**	**1.56**	**0.98**	**5.2**	**0.3**	**0.6**	**0.64**	**0.31**	**0.37**

Figure 41
Photograph of Core NR-130 (Neosho River) Aligned with Applied Shear Stresses and Associated Erosion Rates

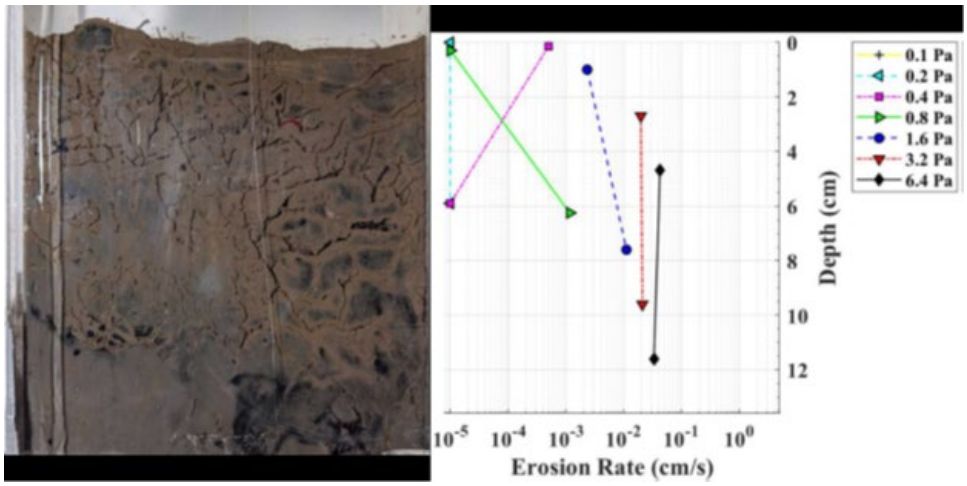

Source: Integral Consulting (2020)

Table 9
Physical Properties and Derived Critical Shear Stresses of SEDflume Sample TC-DS (Tar Creek)

Sample Depth (cm)	Median Grain Size (µm)	Wet Bulk Density (g/cm^3)	Dry Bulk Density (g/cm^3)	Loss on Ignition (%)	τ_{no} (Pa)	τ_1 (Pa)	τ_c Linear (Pa)	τ_c Power (Pa)	Final Critical Shear (Pa)
0.0	7.99	1.15	0.34	8.0	0.05	0.1	0.06	0.04	0.05
2.2	9.76	1.27	0.53	7.7	0.2	0.4	0.32	0.32	0.32
8.5	8.72	1.20	0.43	8.7	0.4	0.8	0.46	0.40	0.40
13.5	10.64	1.40	0.72	5.8	0.8	1.6	0.83	0.71	0.80
20.4	9.37	1.41	0.74	5.8	0.8	1.6	0.84	0.73	0.80
25.6	7.91	1.47	0.84	5.3	0.8	1.6	0.86	0.76	0.80
Mean	**9.07**	**1.32**	**0.60**	**6.9**	**0.5**	**1.0**	**0.56**	**0.49**	**0.53**

Figure 42
Photograph of Core TC-DS (Tar Creek) Aligned with Applied Shear Stresses and Associated Erosion Rates

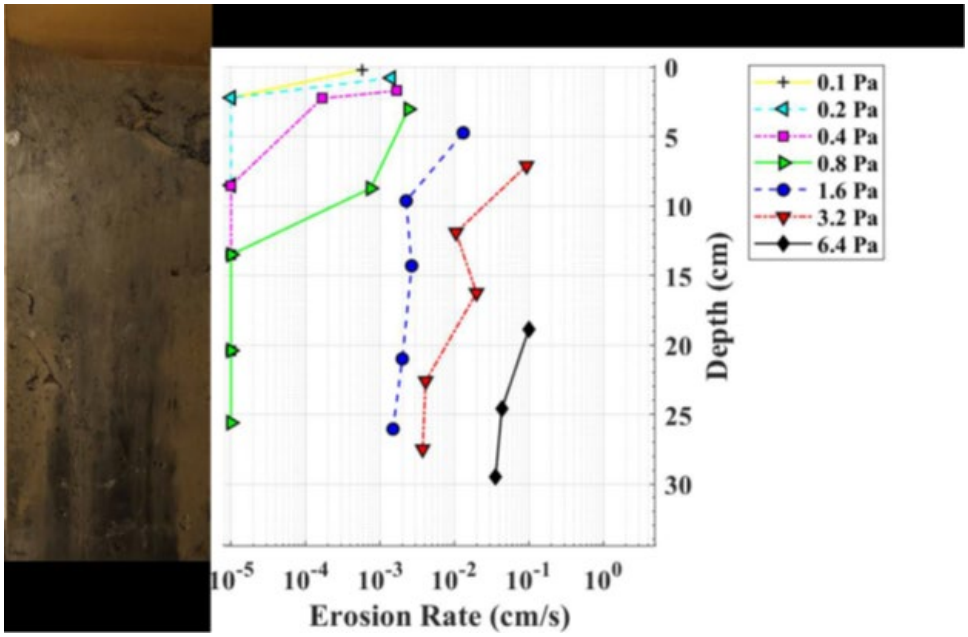

Source: Integral Consulting (2020)

Table 10
Physical Properties and Derived Critical Shear Stresses of SEDflume Sample SR-100 (Spring River)

Sample Depth (cm)	Median Grain Size (µm)	Wet Bulk Density (g/cm^3)	Dry Bulk Density (g/cm^3)	Loss on Ignition (%)	τ_{no} (Pa)	τ_1 (Pa)	τ_c Linear (Pa)	τ_c Power (Pa)	Final Critical Shear (Pa)
0.0	13.20	1.13	0.34	11.6	0.1	0.2	0.12	0.11	0.11
5.3	112.80	1.26	0.57	12.1	0.2	0.4	0.22	0.16	0.20
10	6.22	1.38	0.70	6.8	0.2	0.4	0.25	0.24	0.24
15.1	13.00	1.34	0.65	8.1	0.4	0.8	0.45	0.41	0.41
20.3	9.37	1.35	0.68	8.2	0.4	0.8	0.43	0.32	0.40
Mean	**30.92**	**1.29**	**0.59**	**9.4**	**0.3**	**0.5**	**0.29**	**0.25**	**0.27**

Figure 43
Photograph of Core SR-100 (Spring River) Aligned with Applied Shear Stresses and Associated Erosion Rates

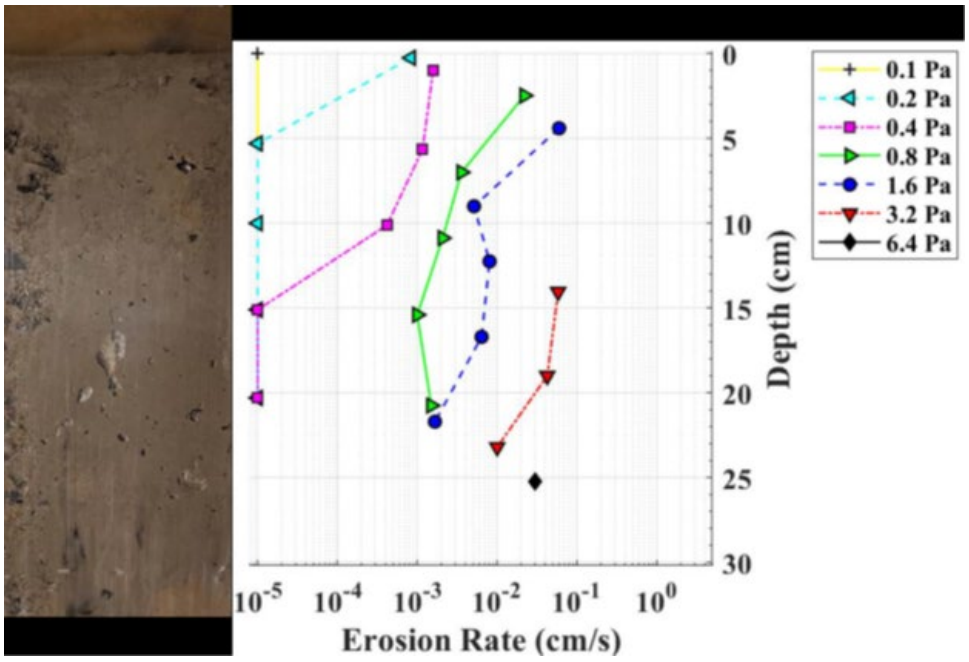

Source: Integral Consulting (2020)

Table 11
Physical Properties and Derived Critical Shear Stresses of SEDflume Sample ER-680 (Elk River)

Sample Depth (cm)	Median Grain Size (µm)	Wet Bulk Density (g/cm^3)	Dry Bulk Density (g/cm^3)	Loss on Ignition (%)	τ_{no} (Pa)	τ_1 (Pa)	τ_c Linear (Pa)	τ_c Power (Pa)	Final Critical Shear (Pa)
0.0	18.95	1.39	0.68	3.4	0.1	0.2	0.13	0.12	0.12
3.7	32.96	1.70	1.16	2.9	0.4	0.8	0.48	0.42	0.42
8.6	16.32	1.66	1.11	3.0	0.4	0.8	0.43	0.37	0.40
13.7	23.18	1.54	0.94	4.2	---	---	---	---	---
Mean	**22.85**	**1.57**	**0.97**	**3.4**	**0.3**	**0.6**	**0.35**	**0.30**	**0.31**

Figure 44
Photograph of Core ER-680 (Elk River) Aligned with Applied Shear Stresses and Associated Erosion Rates

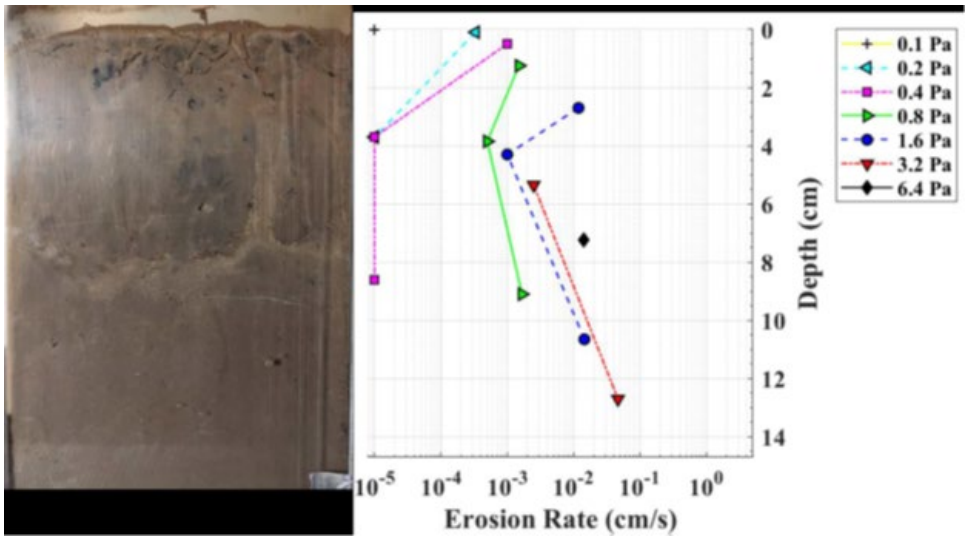

Source: Integral Consulting (2020)

A summary of erosion rates ratios developed by Integral Consulting (Figure 45) shows that erosion rates generally are significantly lower at deeper locations in the sediment columns than at the surface. Interval 1 refers to the top layer of the sediment cores, with each subsequent interval representing a deeper layer of material. Exact interval thicknesses vary, though most are 5 centimeters (cm) or less.

Figure 45
Intracore Erosion Rate by Interval for Each SEDflume Core Sample

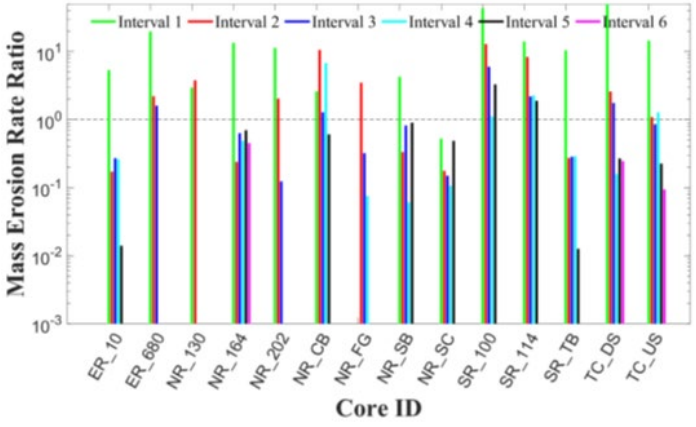

Source: Integral Consulting (2020)

The results of the tests showed expected critical shear patterns. Sediment near the top of the column is more recently deposited and therefore has had less time to consolidate; in general, it is more easily eroded. Lower in the sediment column, the particles have consolidated over time and under higher pressures due to the overlying material; critical shear stress is generally higher as one moves deeper into the core sample.

It is important to understand the high degree of variability of erosion rates as a function of depth below the sediment surface by looking at an example. A sample of the data is shown in Figure 46. The photograph on the left allows visual inspection of the core sample before erosion; the chart on the right provides erosion rate as a function of depth and applied shear stress. It indicates more resistance to erosion at deeper levels of the soil column. For example, at 0.4 pascal (Pa) of shear stress, the surface material eroded at a rate of approximately 4×10^{-3} centimeters per second (cm/s), but at 5 cm of depth, erosion was significantly lower (approximately 10^{-5} cm/s) for the same shear stress.

Figure 46
Example SEDflume Analysis Results

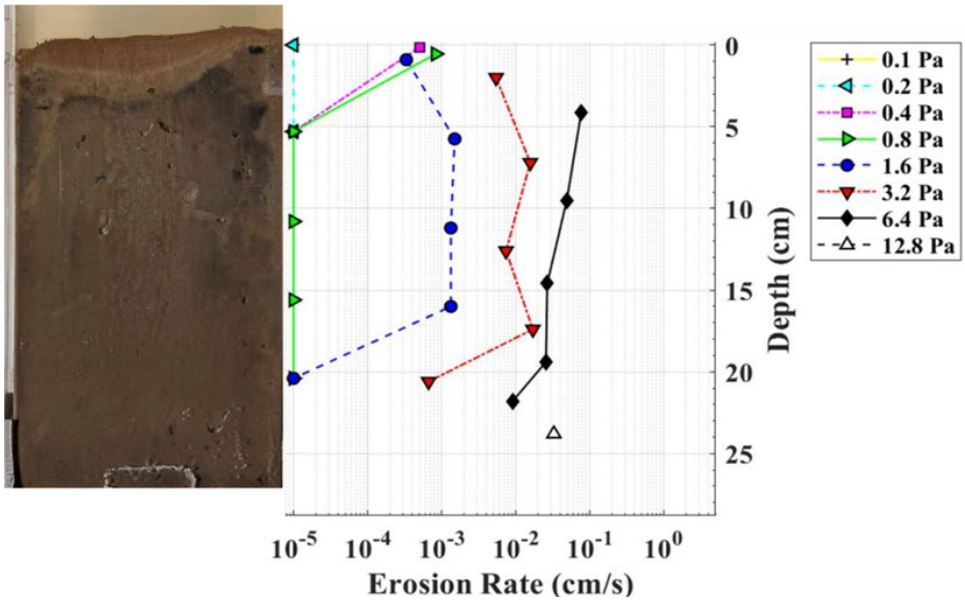

Note: Left: image of sediment core before erosion testing; right: graphical dataset showing erosion rates as a function of bed shear stress and depth in sediment column.
Source: Integral Consulting (2020)

This example and the previous summary of intracore erosion rates show a variation of several orders of magnitude over the depth of samples. This extreme variability affects the development of reasonable erosion parameters to be used in the STM.

2.3.3.2 Sediment Particle Size Analysis

During erosion of the samples, the testing facility used a Beckman Coulter LS particle size analysis system to collect sediment grain size information (Integral Consulting 2020). An example of the output is provided in Figure 47.

Figure 47
Sample Particle Size Analysis Output from SEDflume Analysis

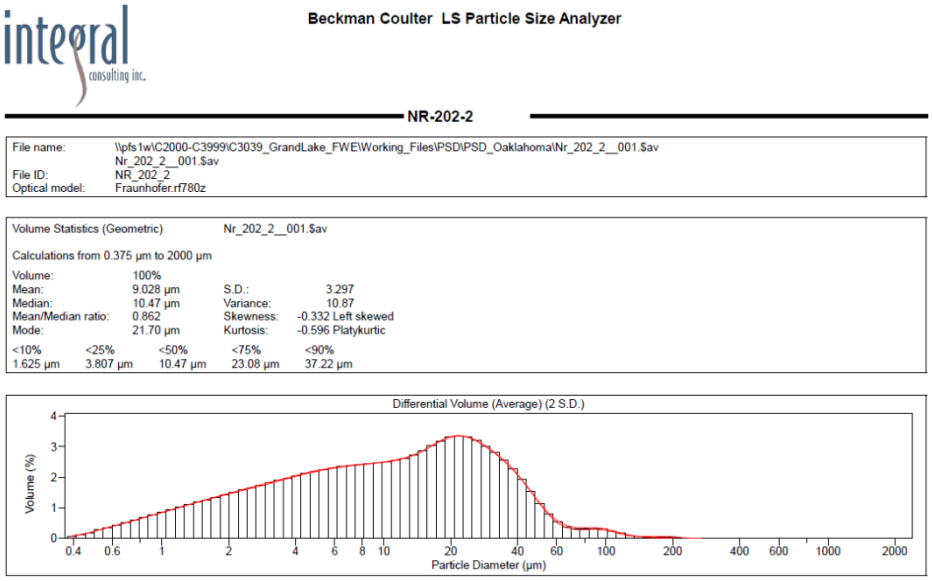

Source: Integral Consulting (2020)

The particle count analysis shows that most of these samples consist of silt- and clay-sized particles. These data were developed into particle size distribution curves relating sediment size to the percentage of the sample finer than the individual sizes to cover the entire range of sediment sizes in the sample. Figure 48 presents an example of this type of graph. A complete set of particle size distribution graphs for the samples is found in Exhibit 3.

Figure 48
Sample Particle Size Analysis Output from SEDflume Analysis Showing Cumulative Percent Finer Values for Core NR-130 (Neosho River)

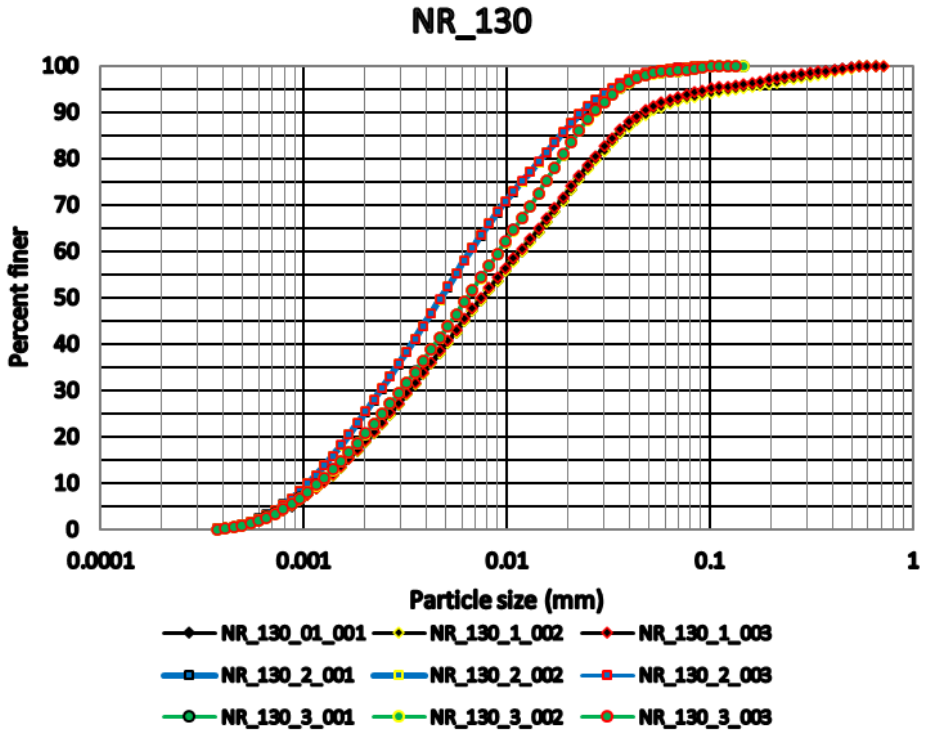

2.3.3.3 Sediment Deposit Bulk Density Analysis

A key factor in understanding silt and clay deposits is the density of sediment and how it varies vertically in the sediment column. Density, along with erodibility and the particle size distribution, are critical parameters for evaluating fluvial transport of this type of sediment.

Although density of sand and gravel deposits fits into a relatively narrow band and does not vary significantly over time, sediment deposits of silt and clay generally settle out of the water column at a low density and then gradually increase in density over time as water is compressed out of the sediment column. As more sediment deposits over the original layers, density of lower layers increases; the consolidation process continues over time until a maximum value is reached. In some situations, this can result in the formation of sedimentary rock such as claystone or shale.

As discussed above, this process also affects the strength or erodibility of sediment. The deeper, more consolidated layers tend to exhibit higher critical shear stress values than the more recently deposited layers near the bed surface.

Density is also the link between sediment transport and deposition. Incoming sediment load is quantified in weight (i.e., tons per day as the unit of sediment transport), whereas sediment deposition as measured by survey is defined in terms of volume. In the case of reservoir sediment deposits, the deposited volume can vary considerably over time and with the depth of the sediment layer.

Sediment density of the upper layer of the sediment deposit was determined in the analysis of sediment cores. Table 12 summarizes the range of sediment density values for the core samples.

Table 12
Density Results from Top Layer Testing of SEDflume Samples

Sediment Core	Minimum Dry Density		Maximum Dry Density		Mean Dry Density (pcf)
	pcf	% of Mean	pcf	% of Mean	
SED-ER-10	28.7	66.7	48.7	113.0	43.1
SED-ER-680	42.5	70.1	72.4	119.6	60.6
SED-NR-130	52.4	85.7	68.7	112.2	61.2
SED-NR-164	76.2	81.9	103.0	110.7	93.0
SED-NR-202	27.5	63.8	53.1	123.2	43.1
SED-NR-CB	37.5	74.1	64.9	128.4	50.6
SED-NR-FG	73.0	90.0	85.5	105.4	81.2
SED-NR-SB	30.6	62.8	62.4	128.2	48.7
SED-NR-SC	48.7	88.6	61.2	111.4	54.9
SED-SR-100	21.2	57.6	43.7	118.6	36.8
SED-SR-114	32.5	69.3	54.9	117.3	46.8
SED-SR-TB	29.3	73.4	46.2	115.6	40.0
SED-TC-DS	21.2	56.7	52.4	140.0	37.5
SED-TC-US	30.0	75.0	46.2	115.6	40.0
Minimum	**21.2**	**56.7**	**43.7**	**105.4**	**36.8**
Mean	**39.4**	**72.6**	**61.7**	**118.5**	**52.7**
Maximum	**76.2**	**90.0**	**103.0**	**140.0**	**93.0**

The summary table shows a significant degree of variability for the dry density values for the sediment cores. For example, the minimum dry density ranges from 21.2 to 76.2 pcf, and the maximum dry density ranges from 43.7 to 103 pcf. For reference, the bulk density of water is 62.4 pcf and solid rock at a specific gravity of 2.65 is 165.4 pcf. Laboratory results for each individual sample analysis are found in Exhibit 3. Assessment of the data does not reveal any readily apparent spatial trends in sediment density.

Sediment density may be correlated with depth below the surface of the sediment deposit due to the consolidation process as fine sediment deposits generally compress over time. Table 13 through Table 16 display the sediment density from the SEDflume samples in relation to sample depth for each of the streams. Corresponding graphs (Figure 49 through Figure 52) of sediment density with depth below the sediment surface for each stream show this general trend (noting that 1 gram per cubic centimeter [g/cm^3] is equivalent to 62.4 pcf—the density of water). Also shown in the graphs are D_{10}, D_{50}, and D_{90} (the sediment grain diameters that are larger than 10%, 50%, and 90% of the total sample, respectively) to give some perspective on sediment sizes found in the samples.

Table 13
Physical Properties of SEDflume Sample NR-130 (Neosho River)

Sample Depth (cm)	Median Grain Size (µm)	Wet Bulk Density (g/cm^3)	Dry Bulk Density (g/cm^3)	Loss on Ignition (%)
0.0	8.34	1.49	0.84	3.7
5.9	5.20	1.56	1.01	6.8
8.6	7.01	1.64	1.10	5.0
Mean	**6.85**	**1.56**	**0.98**	**5.2**

Figure 49
Physical Properties of SEDflume Sample NR-130 (Neosho River) with Depth

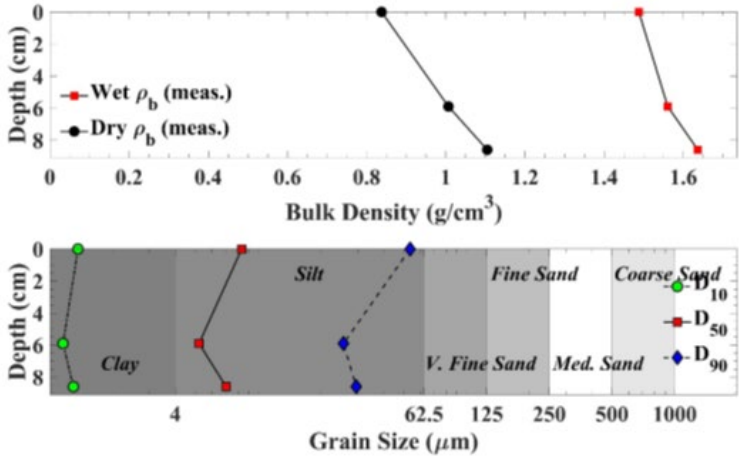

Table 14
Physical Properties of SEDflume Sample SR-100 (Spring River)

Sample Depth (cm)	Median Grain Size (µm)	Wet Bulk Density (g/cm^3)	Dry Bulk Density (g/cm^3)	Loss on Ignition (%)
0.0	13.20	1.13	0.34	11.6
5.3	112.80	1.26	0.57	12.1
10.0	6.22	1.38	0.70	6.8
15.1	13.00	1.34	0.65	8.1
20.3	9.37	1.35	0.68	8.2
Mean	**30.92**	**1.29**	**0.59**	**9.4**

Figure 50
Physical Properties of SEDflume Sample SR-100 (Spring River) with Depth

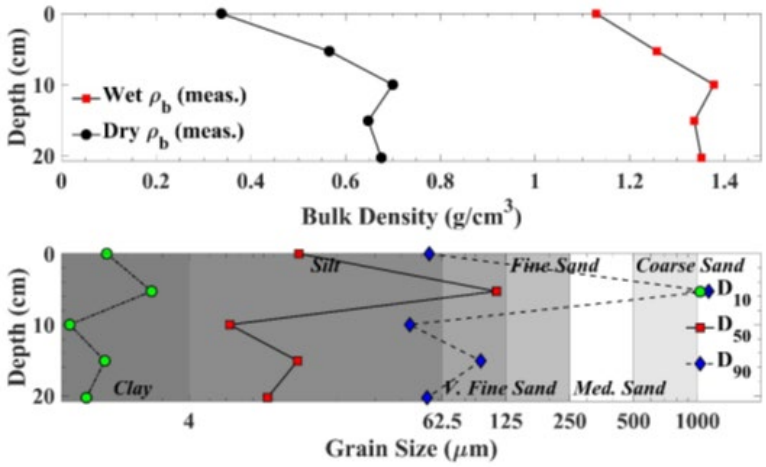

Table 15
Physical Properties of SEDflume Sample TC-DS (Tar Creek)

Sample Depth (cm)	Median Grain Size (µm)	Wet Bulk Density (g/cm^3)	Dry Bulk Density (g/cm^3)	Loss on Ignition (%)
0.0	7.99	1.15	0.34	8.0
2.2	9.76	1.27	0.53	7.7
8.5	8.72	1.20	0.43	8.7
13.5	10.64	1.40	0.72	5.8
20.4	9.37	1.41	0.74	5.8
25.6	7.91	1.47	0.84	5.3
Mean	**9.07**	**1.32**	**0.60**	**6.9**

Figure 51
Physical Properties of SEDflume Sample TC-DS (Tar Creek) with Depth

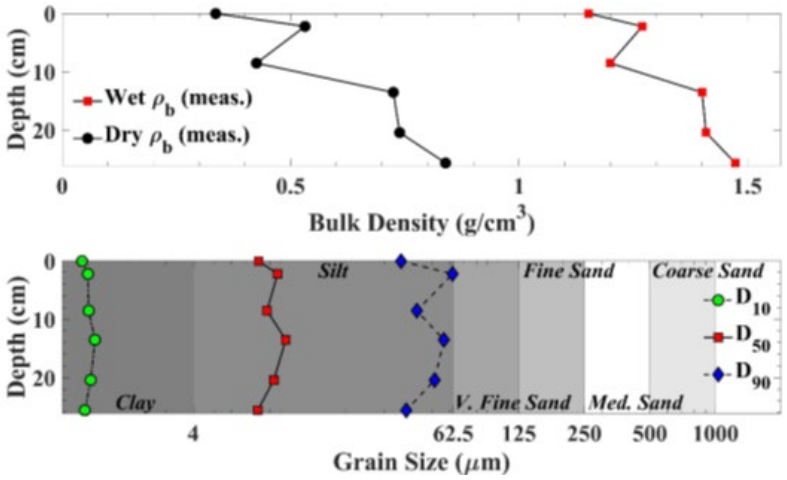

Table 16
Physical Properties of SEDflume Sample ER-680 (Elk River)

Sample Depth (cm)	Median Grain Size (µm)	Wet Bulk Density (g/cm^3)	Dry Bulk Density (g/cm^3)	Loss on Ignition (%)
0.0	18.95	1.39	0.68	3.4
3.7	32.96	1.70	1.16	2.9
8.6	16.32	1.66	1.11	3.0
13.7	23.18	1.54	0.94	4.2
Mean	**22.85**	**1.57**	**0.97**	**3.4**

Figure 52
Physical Properties of SEDflume Sample ER-680 (Elk River) with Depth

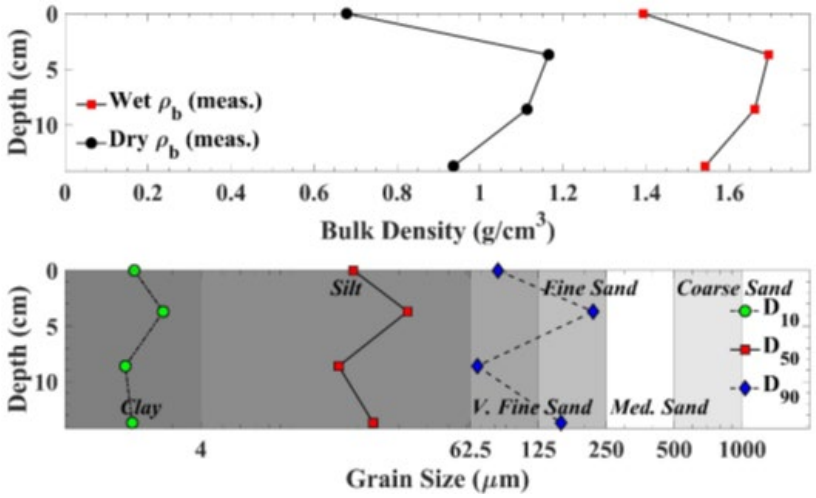

2.3.4 Sediment Transport Measurements

Sediment transport samples were collected during several site visits and delivered to appropriate laboratories for analysis.

2.3.4.1 Suspended Transport Results

SSC samples were processed by the WSLH. Sample analysis evaluated both total sediment concentration and concentration of sediment with grain sizes less than 63 micrometers (µm; upper limit of silt-sized particles) to assess the percentage of cohesive sediments moving through the system in suspension.

Several samples produced erroneous results due to laboratory processing errors, with cohesive sediment concentrations higher than total sediment concentrations. These results were discarded. Across all samples, particles smaller than 63 µm accounted for 82% of all suspended sediment.

Full reports of SSC sample analysis can be found in Exhibit 4.

2.3.4.2 Bedload Transport Results

During each SSC sampling trip, Anchor QEA collected bedload transportation measurements as well. At no point did the Helley-Smith sampler bag collect any sediment particles. Flow rates during sampling efforts are shown in Table 6. Data collected to date indicate that for the vast majority of flow conditions experienced on these rivers, very little bedload transport occurs. Bed material particle size distributions, coupled with shear stress calculations over a wider range of flows and standard STM parameters for non-cohesive sediment sizes, will be used in the model to develop a more

complete understanding of the relative contribution of bedload transport. Initial indications are that bedload transport does not represent a significant contribution to the overall sediment transport into Grand Lake.

2.3.5 Subsurface Findings

The SBP survey and vibracore sampling results provided information on deposition thicknesses in the area of the delta feature. The SBP survey was the initial field measurement, but it was also important to verify those results with vibracore samples.

The SBP will produce a visual output referred to as a "waterfall" that indicates the distances to different objects. The most powerful return signal is often the lakebed or streambed, and subsequent layers are somewhat weaker signals that are still visible in the data. Another type of signal is referred to as a "multiple," which is produced by pulses bouncing between the SBP sonar head and the bed, several times, resulting in a series of nearly parallel lines. An example image collected during the SBP survey at RM 112.34 showing this is provided in Figure 53.

Figure 53
Example SBP Waterfalls showing Layer Transitions and "Multiples"

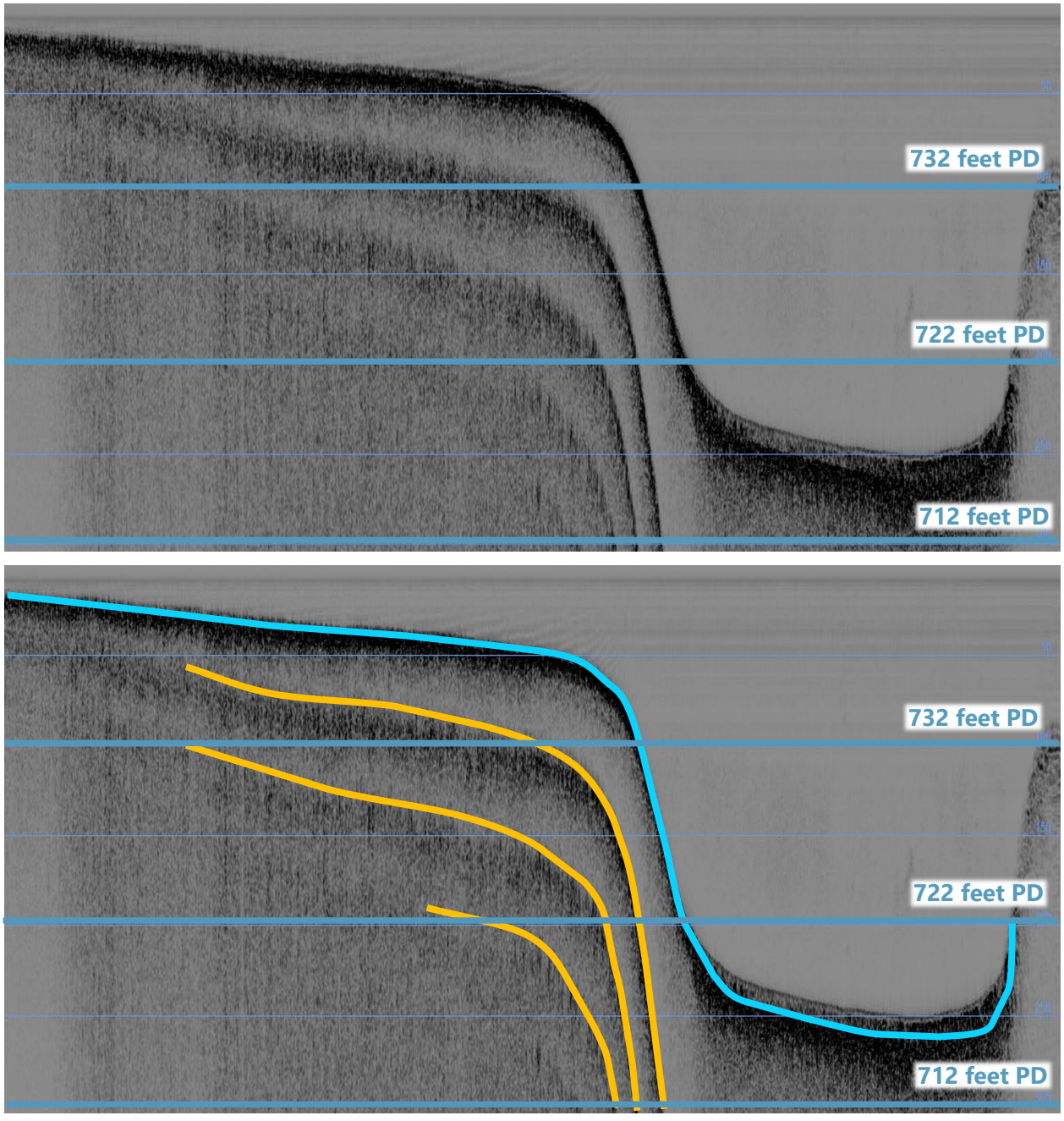

Notes: Waterfall images taken from SBP survey at RM 112.34 (approximately 1.5 miles upstream of Council Hollow)
Lower image is identical to upper, but locations of layer transitions and multiples are highlighted.
Teal line is the layer transition between soft and hard sediments
Orange lines are "multiples" or secondary reflections

The waterfalls produced during the Neosho River SBP survey showed layer transitions at approximately 2 to 3 feet below the bed surface. This indicated a thin layer of soft material over firmer sediments throughout much of the survey area. The interpretation was confirmed by an SBP expert, and the representative stated that a majority of the areas surveyed were not characterized by soft sediment beds (Figure 54).

Figure 54
Interpretation of SBP Survey Results at Stations 4 through 9

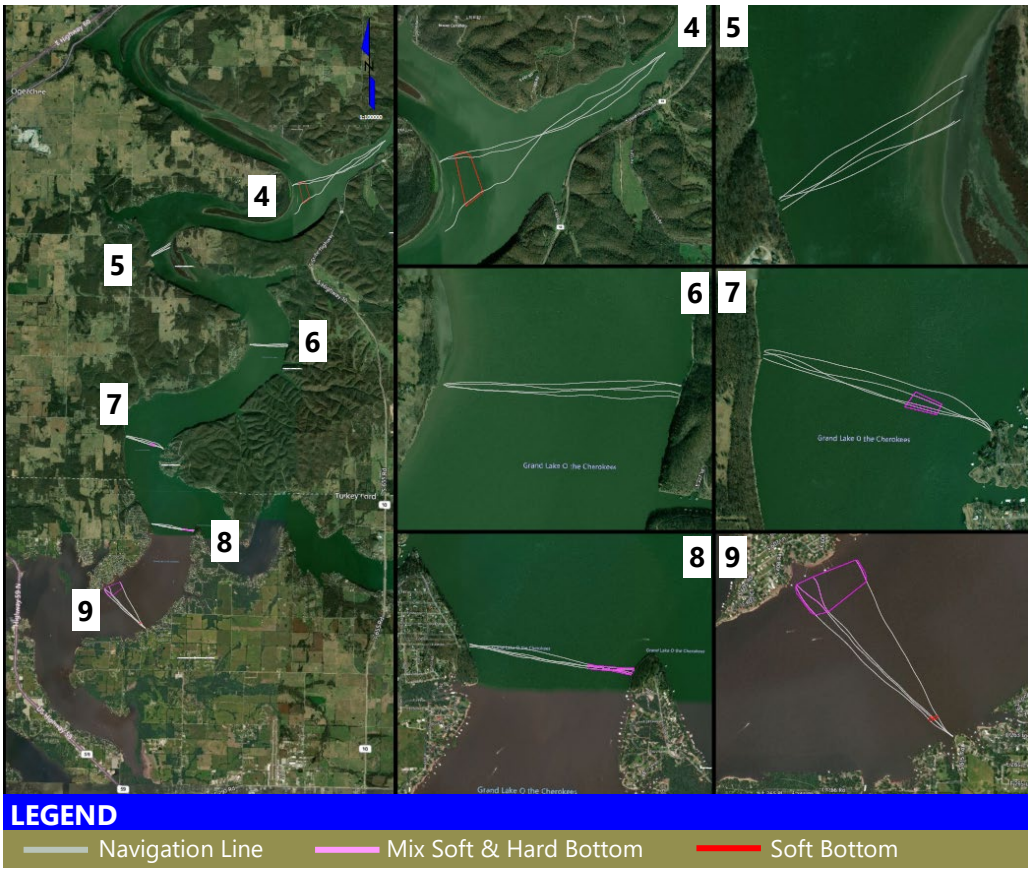

Source: Interpretation of SBP readings; station numbers adjusted from OARS original to reflect GRDA numbers.

Figure 54 shows the navigation lines from the field SBP survey. Where a mixture of soft and hard beds was noted by the SBP expert (for example at transect 9, bottom right), pink outlines were drawn. Red outlines indicate soft bottom materials (transect 4, top center). Areas not colored were interpreted to consist of hard bottom sediments. The vibracore sampling was performed to validate SBP survey results, and they indicated generally thicker layers of deposition than were reported by the SBP.

The vibracore pushed core tubes into the riverbed at the locations shown in Figure 55 using 16-foot coring tubes. These were chosen to align with the SBP survey discussed in Section 4.1 as a means of confirming interpretation of the results. SBP survey transects are shown in red with their relationship to the vibracore sample locations.

Figure 55
Locations of Sediment Cores Collected by GRDA

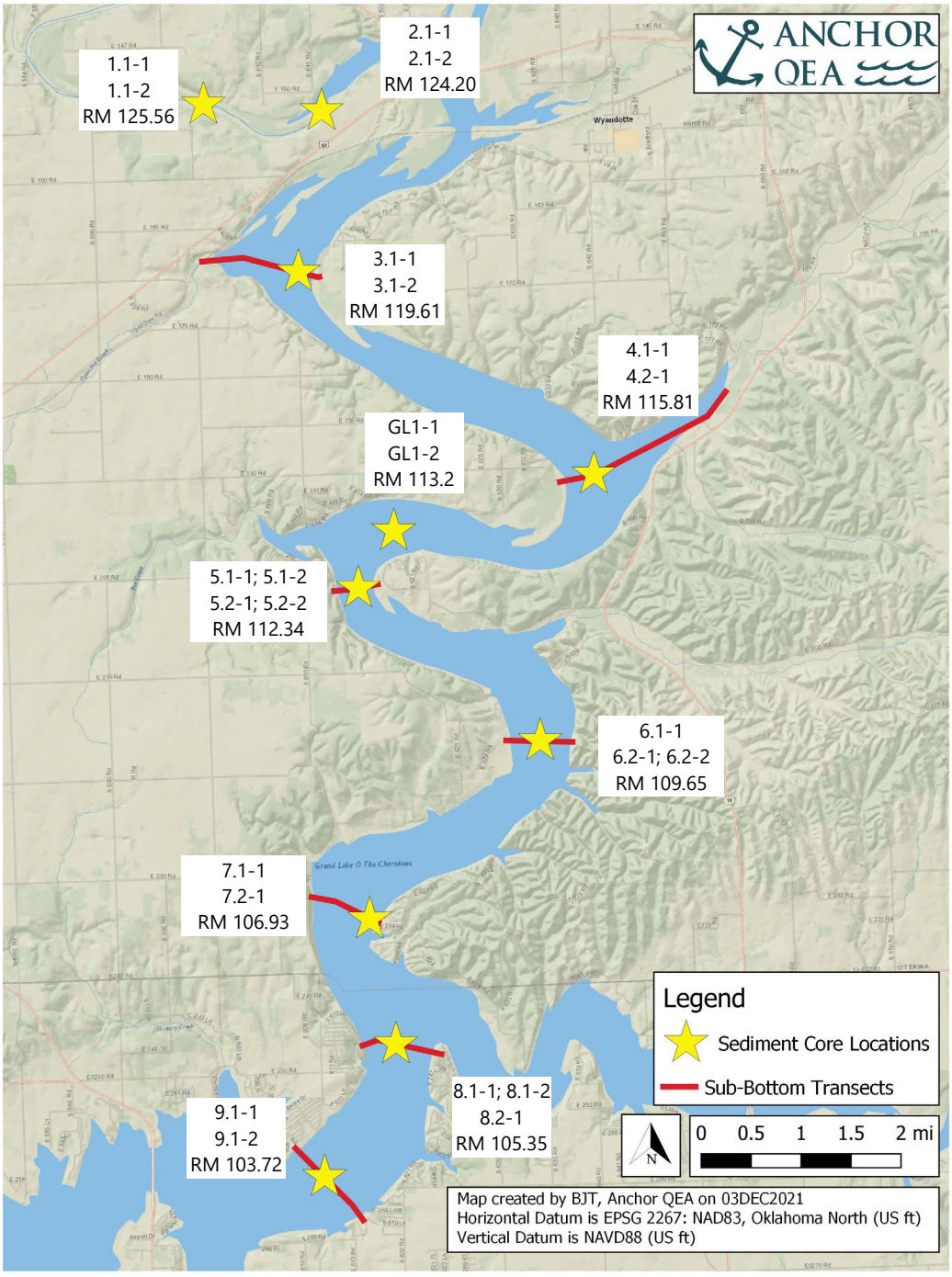

The vibracoring efforts produced 24 core samples for analysis. The cores were pushed to refusal, which ranged from 1.5 to 11 feet in the reach above the Elk River (Figure 56). In the lower reservoir,

one core penetrated approximately 12 feet of sediment before refusal. Two cores over 10 feet in length taken in the delta feature (RM 112.34) were evaluated for Cs-137 activity. Cores shorter than 10 feet or taken from the lower reservoir were analyzed only for grain size distribution (see Section 3.3). Figure 56 shows the maximum vibracore penetration depths at each site shown in Figure 55.

Figure 56
Maximum Vibracore Sample Penetration on Neosho River

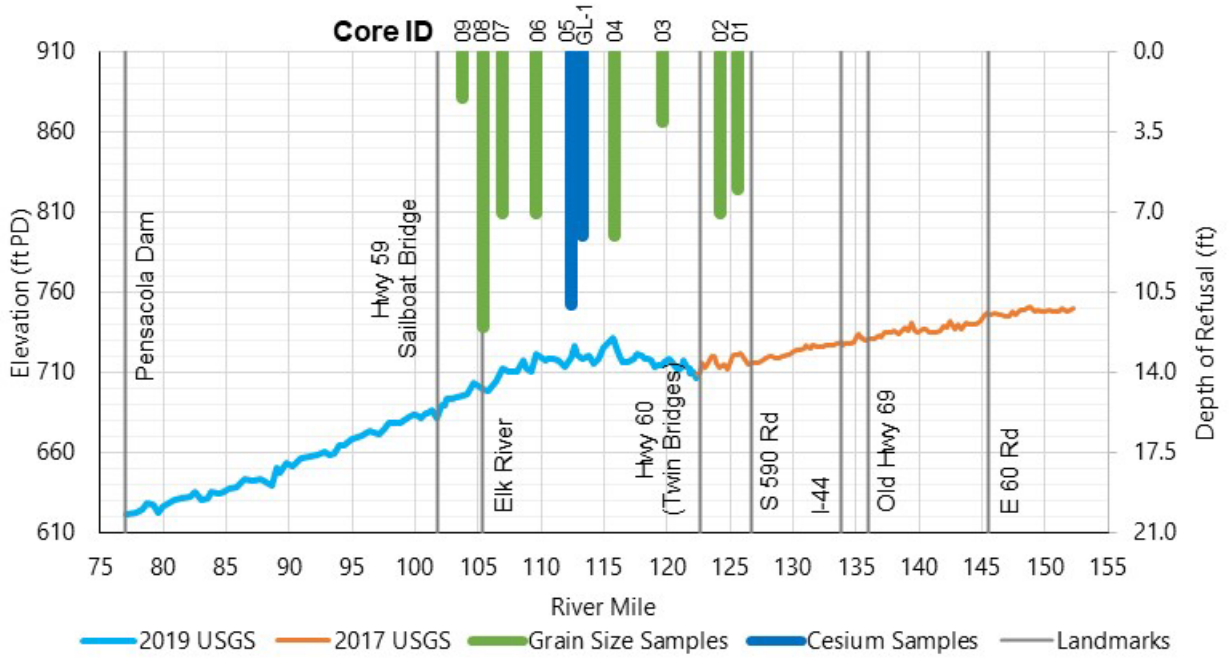

Note: GL-1 sample tested for cesium activity by USGS (Juracek and Becker 2009)

The USGS (Juracek and Becker 2009) analyzed sediment Cs-137 levels to determine the approximate age of sediment in various locations within Grand Lake. The 2008 study collected samples from five sites, with one located in the region of the delta feature, one near the confluence with the Elk River, and three others located further downstream in the reservoir (Figure 57). Where USGS data showed a clear, defined Cs-137 peak, the findings were considered settled.

Figure 57
Locations of Sediment Cores Collected for Cesium Analysis

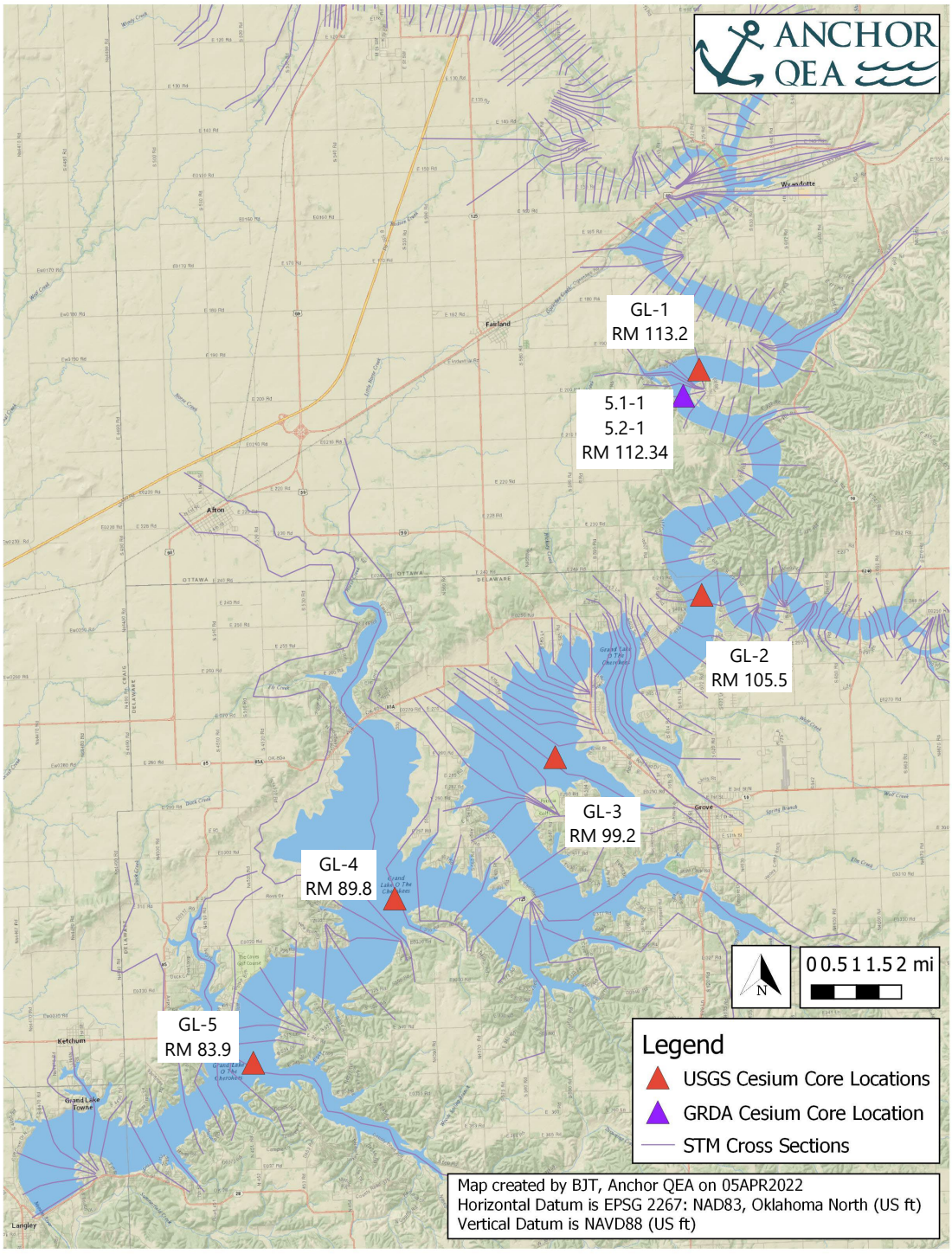

Note: Locations of USGS cores taken from Juracek and Becker (2009).

A major goal of sampling was to collect a significantly deeper sample near USGS site GL-1. The USGS sample was approximately 6 feet, and it was decided that a vibracore sample of approximately 10 feet would be sufficient to trigger re-evaluation and Cs-137 analysis. Shorter cores would not likely produce different results from the USGS study (Juracek and Becker 2009). Cores lower in the basin were not analyzed as the USGS dataset was sufficiently robust and were not of interest for delta feature analysis. The cores that met this criterion were 5.1-1 and 5.2-1 as shown in Figure 57.

The vibracore samples show a thicker sediment deposit, which suggests the SBP was not reliably capturing sediment layer thicknesses. Most likely, the penetration of the SBP signal was limited by a layer of biotic activity within the surface of the sediment; several core samples had air bubbles in the top few feet produced by decomposition or other biological activity. This produces readings indicating a softer, air-filled layer above the firmer silt and clay sediment that would register as a separate layer during SBP surveying (Aqua Survey 2004; Science Applications International 2001). As a result, further analyses relied on vibracore sampling rather than SBP results.

Vibracore sampling showed thicker layers of soft sediment deposition, and also provided opportunity to evaluate Cs-137 trends measured by a USGS study (Juracek and Becker 2009).

USGS analysis showed that Cs-137 peaks were located approximately 3 to 6 feet below the bed surface (Figure 58). Those peaks represent sediment that was deposited in approximately 1963, indicating that just 3 to 6 feet of sediment had deposited since 1963 at sites GL-2, -3, -4, and -5 (Figure 57).

Figure 58
Comparisons of Relative Cesium Activity within the USGS Core Samples

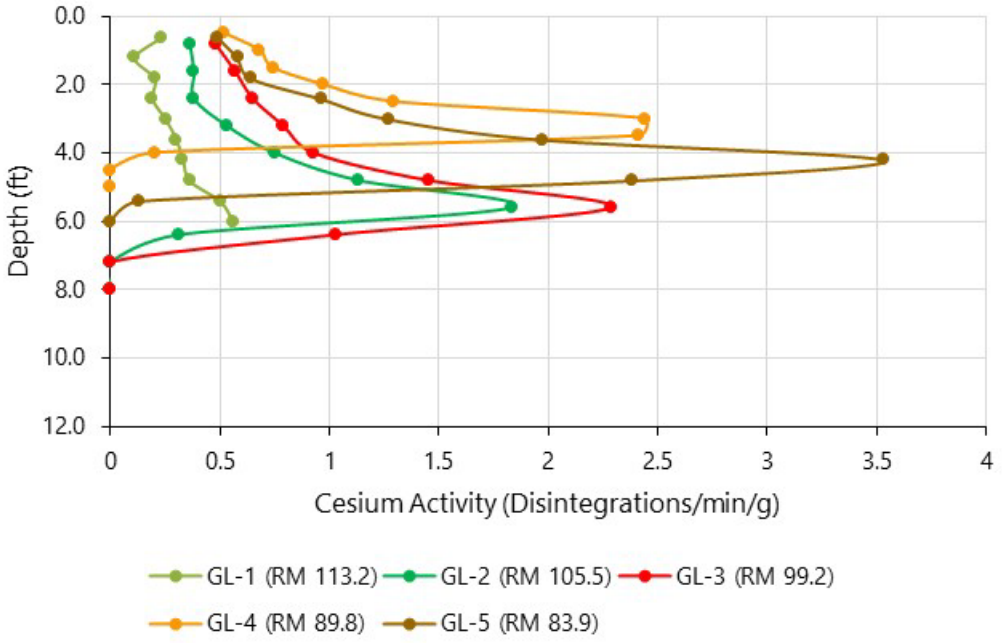

Notes: The peak cesium activity indicates the soil layer associated with deposition in approximately 1963. All material above that layer is assumed to have deposited since the nuclear testing ban.

Source: Figure adapted from Juracek and Becker (2009).

The sample in the delta feature (GL-1) showed no spike in Cs-137. Juracek and Becker (2009) concluded the sediment they collected was all deposited post-1963. The USGS interpreted this to indicate that the area was not continually depositional but washes away due to wave action or large flow events before new sediment redeposits. This follows typical reservoir delta feature evolution, with surface sediments at the top of the delta feature washing downstream and extending the delta feature further into the reservoir rather than increasing the top elevation.

During GRDA's vibracore sampling, they repeated the USGS efforts to obtain longer (deeper) cores and see if a longer sample would capture a characteristic Cs-137 spike that denotes a 1963 sediment layer. GRDA collected approximately 11-foot cores near site GL-1 (cores 5.1-1 and 5.2-1) and processed them for Cs-137 analysis. The location of cores 5.1-1 and 5.2-1 are displayed in Figure 57.

GRDA sent 10 samples at equally spaced intervals within each core for Cs-137 evaluation. The results show a similar pattern to those of the USGS study, with no apparent Cs-137 peak (Figure 59).

Figure 59
Comparisons of Relative Cesium Activity Between USGS Core Sample GL-1 and GRDA Samples 5.1-1 and 5.2-1

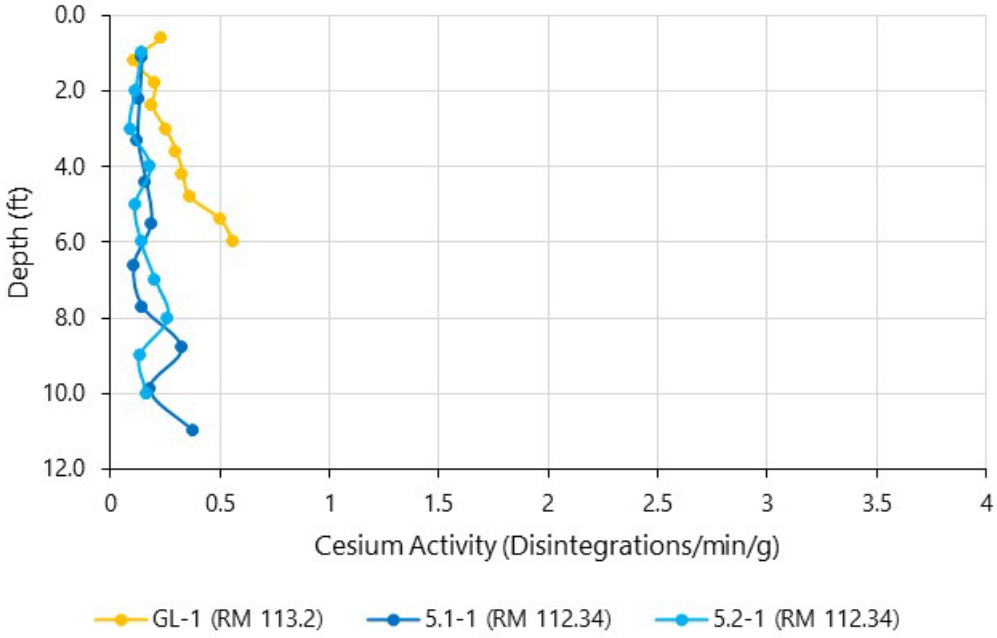

Notes: GL-1 activity levels taken from Juracek and Becker (2009)
The lack of a defined cesium activity peak indicates that all sediment collected in the core was deposited after 1963.

This further suggests that deposition in the top 10 feet of the soil column is all post-1963 and that the site is not continuously depositional, instead indicating regular mixing of the materials at the top of the delta feature. These results agree with the USGS (Juracek and Becker 2009) findings that this location sees regular disturbance and is not continually depositional and is consistent with typical delta feature evolution patterns (Vanoni 2006).

2.3.6 December 2022 Investigation Results

The bathymetric survey mapped the area around the low-head dam in Miami. Results showed that bed elevations in this reach range from approximately 732.6 to 740.6 feet PD (Figure 60).

Figure 60
Bed Elevation Map from Bathymetric Survey Results; Miami Low-Head Dam is Located at Approximately RM 135.25 on the Neosho River

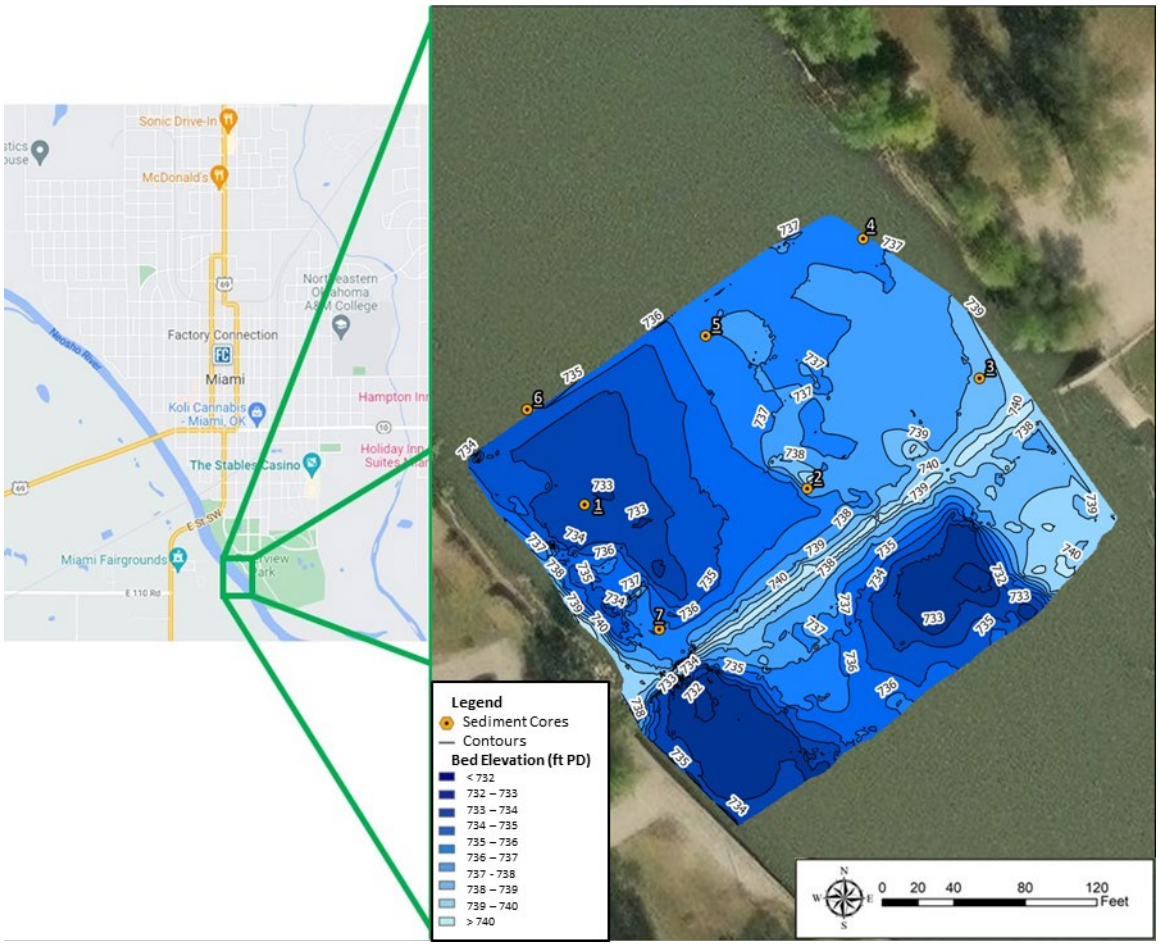

Note: Elevations shown in the figure are in feet above Pensacola Datum (PD)

As shown in Figure 60, the low-head dam base protrudes several feet out of the streambed, and an upstream pool approximately 4 feet deeper than the base of the dam is present upstream. This is an expected feature in systems where the bedload is insufficient to fill the upstream side of the structure.

The City of Miami (2022) argued that the dam was designed to pass bedload sediment and that the results of the bathymetric survey prove there is meaningful bedload sediment transport. However, in observing a significant number of small dams, sediment is nearly always deposited upstream of the structure if the river is transporting a significant quantity of bedload sediment. Designing a modern system where the bedload is consistently passed through the structure has met with limited success, and it is unlikely that a structure built 100 years ago without access to modern modeling and design

tools would be an exception. It is rare to find systems where sediment deposition is not an issue—unless bedload sediment transport is limited. Even with gates or other openings in the structures, sediment still tends to deposit upstream of dams. The only way this dam could operate for 100 years with such insignificant deposition upstream of the dam is if very little coarse sediment is moving downstream. GRDA's analysis relies on considerable experience with sediment deposition upstream of small dams and bedload data.

This is consistent with field measurements and the findings of Byerley (1995), which showed that the Neosho River has neither significant gravel material nor the capacity to move it. Byerley's research found that the chert gravel supply was cut off by the John Redmond Dam and the Neosho River has not moved significant volumes of gravel since that dam was constructed in the mid-1960s. As a result, there has been only limited movement of gravel in the Neosho River downstream of John Redmond Reservoir.

A far more likely explanation for the bathymetry findings is that a limited quantity of large, coarse-grained sediment moved downstream between the time the low-head dam was constructed and the John Redmond Reservoir was opened. As the gravel and coarser sediment moved downstream, the material encountered the low-head dam at Riverview Park, blocked the archways, and gradually accumulated upstream of the structure. When the John Redmond Reservoir opened, gravel transport essentially ceased in this reach of the Neosho River, as discussed by Byerley (1995).

The field team attempted vibracoring at seven locations, as shown in Figure 60. The rig was lowered to refusal, and two of the attempts produced no sediment (i.e., depth to refusal was 0 feet), as shown in Table 17. Coring indicated that the material upstream of the low-head dam is largely coarse material. It also indicated the presence of an armor layer—i.e., finer material below the gravel—consistent with expectations for an armored streambed with limited bedload transport (Figure 61).

Table 17
Sediment Core Descriptions

Core ID	Depth (ft)	Water Level (ft PD)	Mudline Elevation (ft PD)	Core Length (ft)
Core 1	7.6	741.94	734.34	0.00
Core 2	5.7	742.18	736.48	0.62
Core 3	4.5	743.56	739.06	0.37
Core 4	5.67	743.11	737.44	0.56
Core 5	6.25	743.12	736.87	0.50
Core 6	10.25	743.34	733.09	0.00
Core 7	7.33	743.097	735.767	0.67

Figure 61
Sample Photo of Core Sample from Near Miami Low Head Dam Showing the Natural Armoring of the Bed at This Location

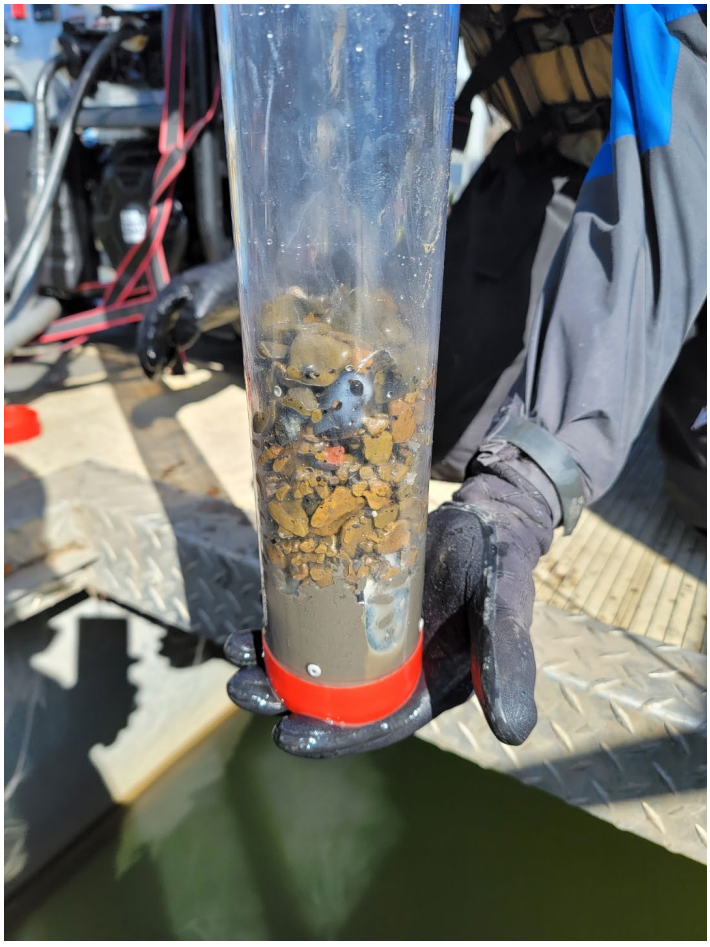

A more detailed discussion of the fieldwork is included as Exhibit 8.

2.4 Discussion

The field campaign provided valuable insights for the sediment study. Initial understanding of the reservoir indicated the system was dominated by sand and gravel sediments (Mussetter 1998; Tetra Tech 2018). Although that appears to be the case in the riverine components of the overall system, field work results have found cohesive silts and clays play a far more important role than initially anticipated.

The relative dearth of bedload sediment transport and comparatively high concentrations of fines moving in suspension through the watershed have indicated a need to focus extra resources on silt- and clay-sized sediment modeling. Because silt and clay deposits typically exhibit cohesive characteristics, along with several other complicating factors, the complexity of the overall sediment study and associated modeling tasks increases. *Modeling Sediment Movement in Reservoirs*, prepared by the U.S. Society on Dams (USSD) Committee on Hydraulics of Dams, Subcommittee on Reservoir Sedimentation (USSD 2015), presents a discussion of the issues associated with cohesive sediments. Some of the challenges are related to changing density over time through the process of consolidation; others are related to the fact that cohesive sediment particle motion is determined primarily by electrochemical surface forces rather than gravity forces, which dominate sand and gravel motion. Further complicating the development of appropriate input data and parameters is the fact that the data show a wide degree of variability from sample to sample and location to location.

To develop the necessary information, additional efforts for sediment core sampling were required beyond what was originally planned in the Sediment Study Plan. The study team selected locations for and performed sampling of the reservoir bed. The material was then subjected to erosion testing for model parameterization. SEDflume testing provided multiple valuable data points for sediment within the Grand Lake reservoir.

Critical shear stress is perhaps the most important of the SEDflume outputs. The gradual consolidation of fine, cohesive material and its effect on erosion resistance as a function of depth within the sediment column are crucial for accurately modeling sediment transport and deposition within the basin. Its use in developing the STM will allow HEC-RAS to determine whether sediment will erode from the bed or remain in place during a variety of flow conditions, and particle size and density parameters will allow the model to determine whether deposition will occur.

2.4.1 Sediment Transport

2.4.1.1 Suspended Sediment Transport

Sediment transport data, in the form of suspended sediment sampling, were collected at various USGS stations on the primary rivers of interest flowing into Grand Lake. In addition to the USGS data, suspended sediment samples were collected by Anchor QEA at these same stations. At each station, regression analyses were conducted to develop a numerical relationship between suspended sediment transport (in tons per day) and flow that forms a rating curve between sediment transport and flow. The data used for the development of the suspended sediment transport rating curves include all available data from the USGS through July 8, 2021, and the Anchor QEA data collected through July 1, 2021.

A preliminary assessment of the two sets of data reveals that they both lie within the bounds of variability typically seen in sets of suspended sediment data. The Anchor QEA data, however, generally lie in the middle to lower end of the range of the available data. It is possible that because these data were collected in recent years and the USGS data cover the entire period of record, which dates several decades back in time, there may be a trend toward lower sediment transport from these rivers over time.

Sediment transport data are only collected occasionally so no continuous, or even daily, record of sediment transport exists. With a sediment transport rating curve, the regression equation can be applied to the daily flow data to develop an estimate of the long-term historical quantity of sediment flowing past given stations on these rivers and hence sediment transport into the reservoir. Figure 62 presents an example of the available suspended sediment transport data on the Neosho River near Commerce.

Figure 62
Suspended Sediment Transport Rates and Fluvial Discharge Measured on the Neosho River near Commerce, Oklahoma

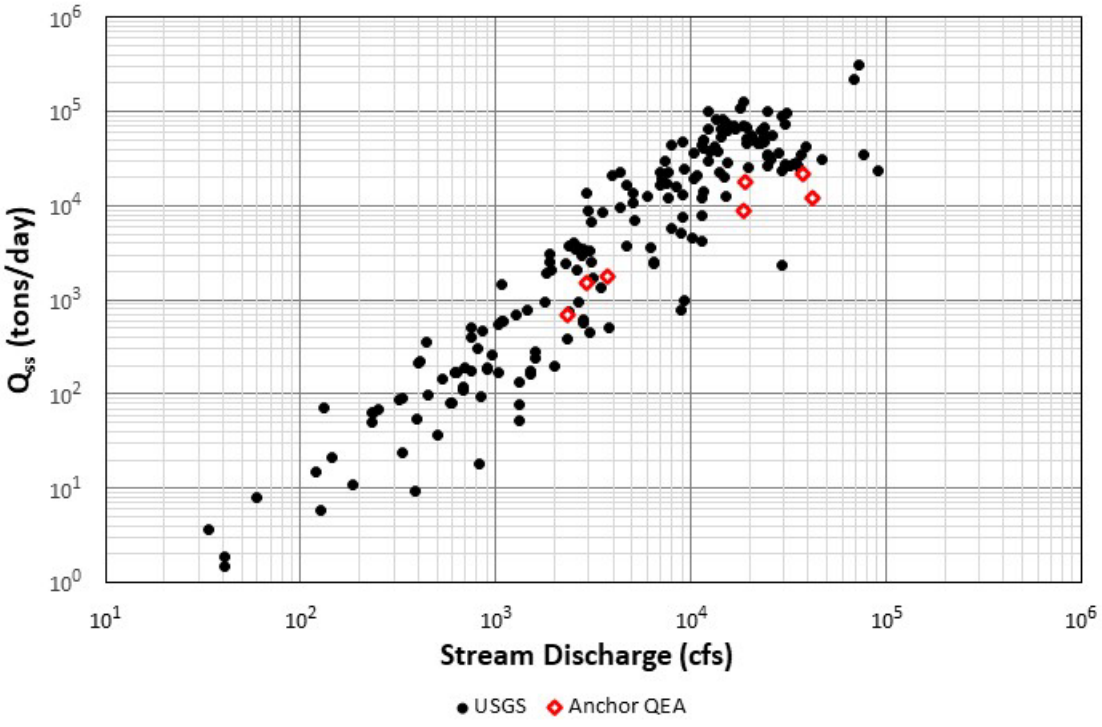

Analysis of the particle size distribution of the suspended sediment samples collected by Anchor QEA are shown in Figure 63 through Figure 66. These data show that suspended sediment is

predominantly finer than 0.0625 millimeter (mm), which is the break point between sand and silt. Consistent with the bed material in the reservoir, most of the suspended sediment consists of silt and clay-sized sediment, which is being transported into the reservoir.

Figure 63
Fine Sediment as Fraction of Total Suspended Sediment Sampled on the Neosho River near Commerce, Oklahoma

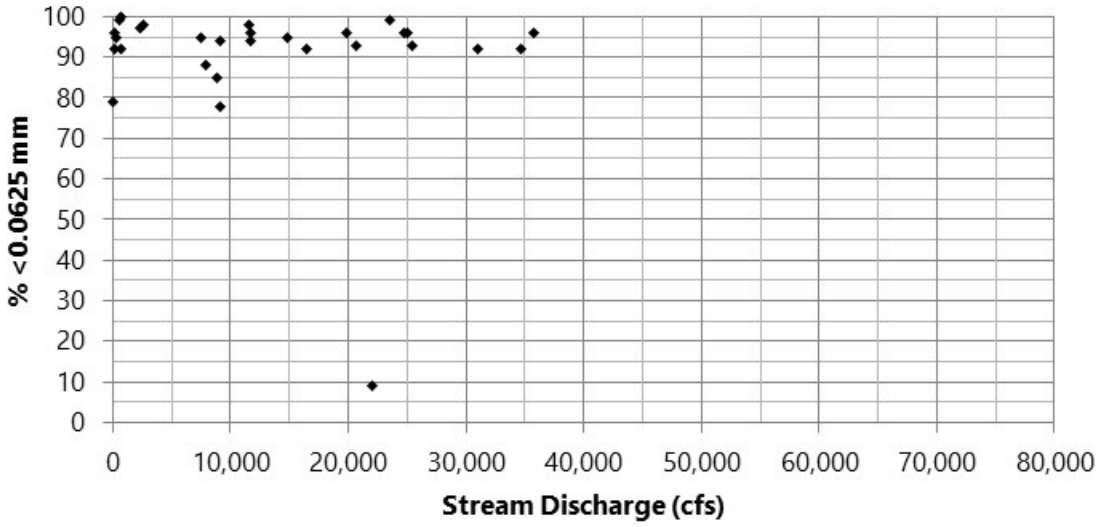

Figure 64
Fine Sediment as Fraction of Total Suspended Sediment Sampled on Tar Creek near Commerce, Oklahoma

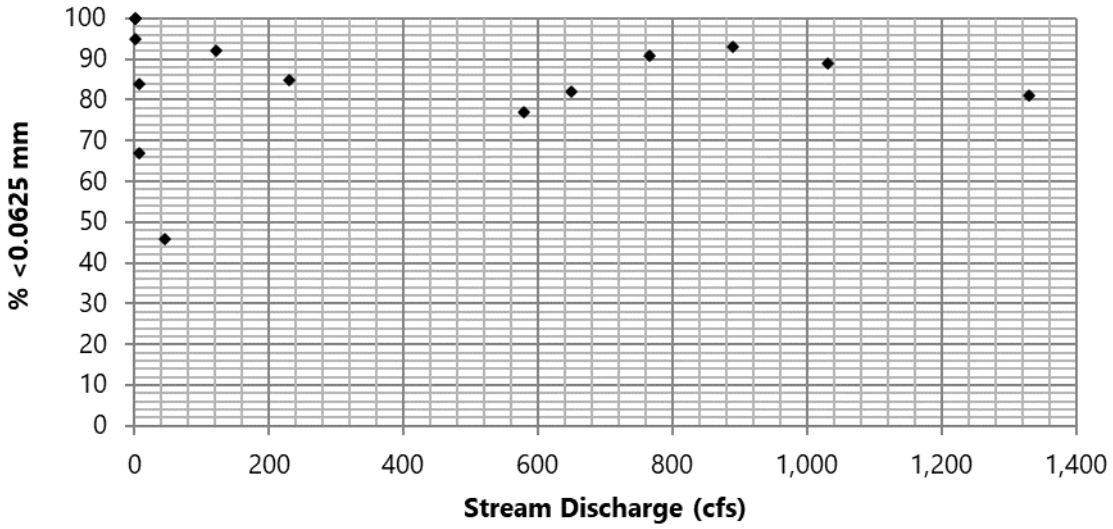

Figure 65
Fine Sediment as Fraction of Total Suspended Sediment Sampled on the Spring River near Quapaw, Oklahoma

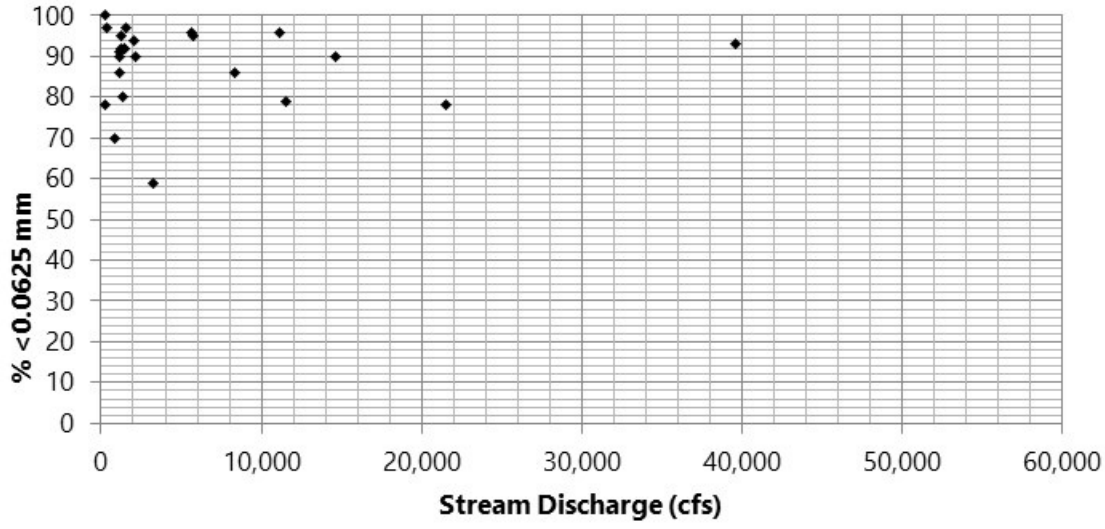

Figure 66
Fine Sediment as Fraction of Total Suspended Sediment Sampled on the Elk River near Tiff City, Missouri

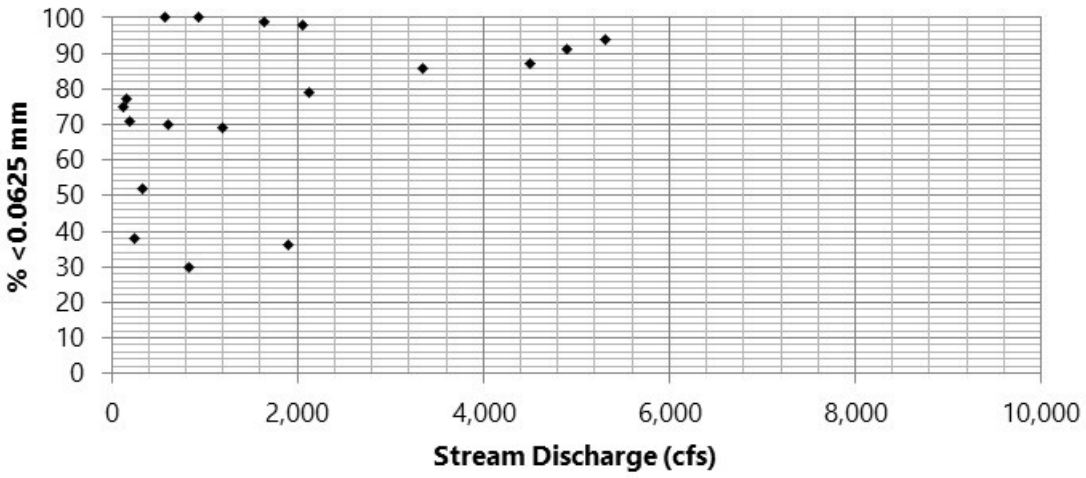

2.4.1.2 Bedload Sediment Transport

Although bedload sediment transport data have been collected, these data indicate virtually no bedload transport. This is likely because shear stresses induced by the velocity of the flowing water have not been sufficient to mobilize, erode, and transport the coarse sediment sizes (primarily gravel) in the upstream river reaches where bedload sampling was conducted. This will be further evaluated in the STM using critical shear criteria for non-cohesive sediments.

Investigations near the Miami low-head dam also indicate there is limited bedload sediment transport. The fact that the dam and its base continue to protrude several feet above the streambed upstream suggests there is very little bedload transport, otherwise the gravel would build up on the upstream face of the dam or, at least, its base until it was approximately level upstream of the dam. Core samples in the area also show an armor layer that is more resistant to transport, which is consistent with other field findings.

3 Qualitative Geomorphic Analysis

Several physical features affect the geomorphology of the rivers in the study area that either exist naturally or have been constructed. Such features include Pensacola Dam, bridges, and geologic and geomorphic features.

3.1 Pensacola Dam

Pensacola Dam is located at RM 77. With any impounded stream, water velocities decrease near the head of the reservoir, resulting in some amount of sediment deposition. This phenomenon is the expected geomorphic response as found in the scientific literature for virtually any reservoir on an alluvial river (Figure 67; Simons and Senturk 1992). Deltas are also discussed by USACE (1995), U.S. Bureau of Reclamation (Huang et al. 2006), Fan and Morris (1992), and Vanoni (2006).

Figure 67
Typical Geomorphic Response to Dam Construction

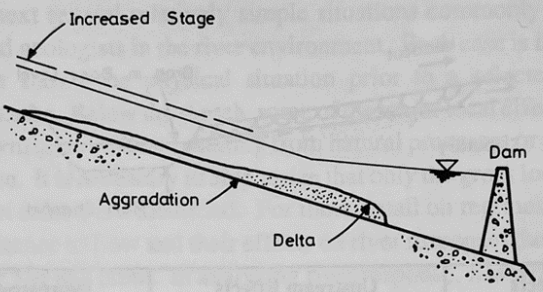

Local Effects	Upstream Effects	Downstream Effects
Aggradation of bed	See local effects	See downstream effects, Fig. 2.18
Loss of waterway capacity	Change in base level for tributaries	
Change in river geometry	Deposition in tributaries near confluences	
Increased flood stage	Aggradation causing a perched river channel to develop a change in the alignment of the main channel	

Source: Simons and Senturk (1992)

The impacts of Project pool elevations are addressed in the hydrology and hydraulics (H&H) study USR, filed concurrently with this report.

Figure 68 shows the Neosho River profile over time. Note that the upstream head of the deltaic feature starts at approximately RM 122 (near the Burlington Northern railroad bridge), which is more than 20 miles downstream of where the WSE of 745 feet PD at the top of the conservation pool intersects the river thalweg approximately 0.5 mile downstream of the USGS Commerce gage at RM 145.4 (East 60th Road Bridge). The bathymetric survey data show that sediment deposition forming the delta feature does not occur until sediment has traveled more than 20 miles downstream into the reservoir.

Figure 68
Historical Neosho River Thalweg Comparison

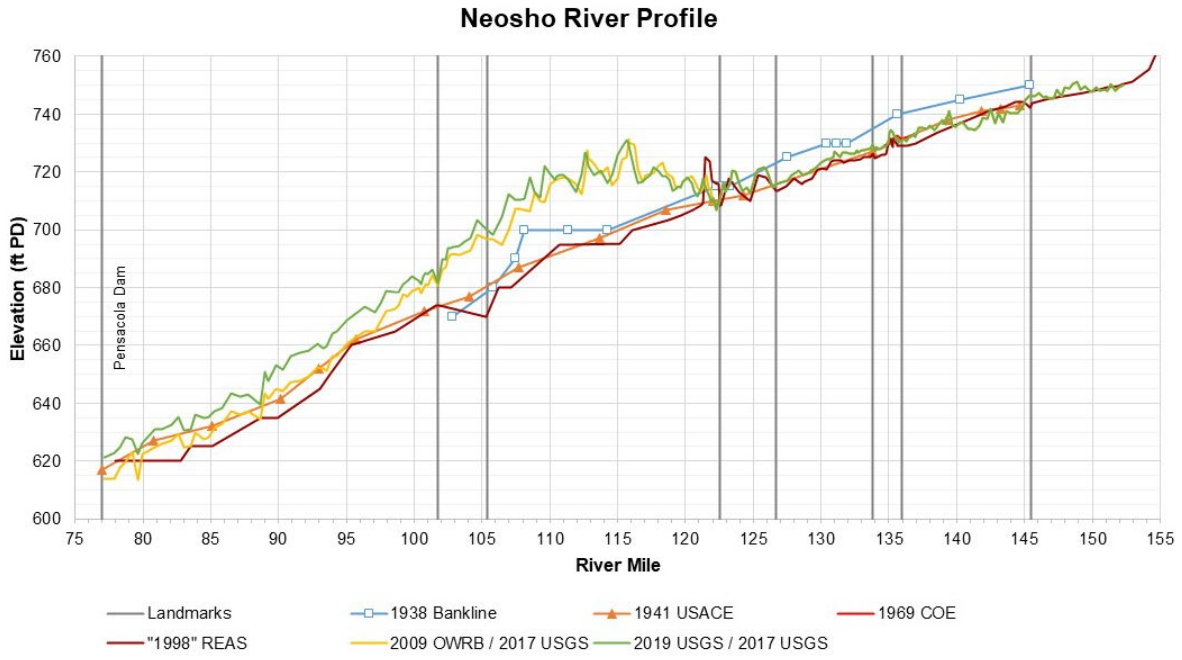

Note: This plot covers the Neosho River from RM 152.2 at the upstream end to the Pensacola Dam at RM 77.12 on the downstream end.

This clearly shows that sediment forming the delta feature is transported a considerable distance downstream into the conservation pool. Because sands and gravels tend to drop out of the water column sooner, if a significant portion of the sediment load consisted of bed material load (sand and gravel), the delta feature would have begun forming much farther upstream near the head of the reservoir. Therefore, the delta feature location further supports what field sampling showed: the feature consists primarily of fine sediment.

Figure 69 from *Modelling of Cohesive Sediment Dynamics* (Lumborg and Vested 2008) shows the various stages and characteristics of sediment as it deposits on the bed of the reservoir. Although this article focuses on coastal deltas, similar processes also occur on reservoir deltas.

Figure 69
Typical Reservoir Sedimentation Processes

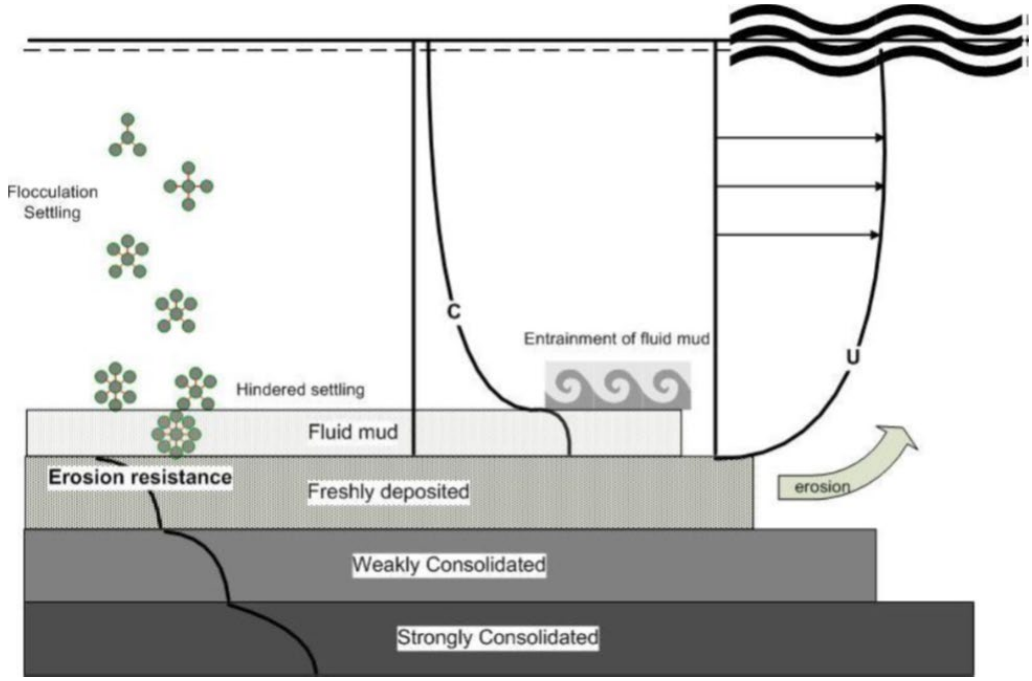

Source: Lumborg and Vested (2008)

Suspended sediment forms flocs that deposit at the bed. With increasing currents, the fluid mud layer is re-entrained. Bed shear stresses can be enhanced by short surface waves, and during spring tides or storms the lower sediment layers erode (Lumborg and Vested 2008).

Lumborg and Vested (2008) explain the various stages and characteristics of suspended sediment deposition as follows:

> Fluid mud / hyper concentrated suspensions: The concentration of suspended sediment in the water column increases towards the bed. When the flocs begin to touch each other and interact hydrodynamically the settling velocity is reduced. This phenomenon is known as hindered settling and may lead to high concentration suspensions or fluid mud layers. Fluid mud is a concentration of fine-grained material in which settling is substantially hindered. It forms when the rate of settling exceeds the capacity of dewatering. The process forms a very concentrated suspension that acts neither as a Newtonian fluid nor as a sediment bed. The lower concentration limit of naturally occurring fluid mud layers is often given as about 10 kg m^3. This concentration can often be recognized as a lutocline and it is around this concentration that the suspension transits to become framework supported and much less mobile than the suspension. Fluid mud layers are thus layers with extreme concentrations of

sediment. The layer is moveable but moves as a gel rather than as a Newtonian fluid. Fluid mud layers accomplish a significant challenge for fine-grained sediment modelling.

When the box core samples were collected for the SEDflume testing, those individuals collecting the samples observed the following (Integral Consulting 2020): "In general, sediment consisted of silt and clay with a surface layer of unconsolidated, relatively mobile sediment." They describe a layer of "fluff" of "unconsolidated sediment" on top of the sediment surface and describe the surface material eroding "in clouds" of sediment. The description of an unconsolidated layer of fluff is consistent with the layer of fluid mud as previously described in the scientific literature. These sediment samples were collected in March 2020, months after the last significant runoff (with associated high sediment loading from 2019) and prior to any significant runoff in 2020. This would tend to result in a minimal layer of fluid mud that would result from the recession limb of a high flow event at the time when samples were collected. A more prominent layer of fluid mud would likely be found during or on the recession limb of the inflow hydrograph when sediment loading would be more significant, and this fluid mud layer would likely be a seasonal or temporary feature of the bed. This layer of unconsolidated sediment or fluid mud continues flowing farther downstream into the deeper portions of the reservoir as far as the dam.

As Lumborg and Vested (2008) stated, "The combination of hydrodynamic, sediment and biological processes make it difficult to predict cohesive sediment dynamics." Given that most of the inflowing sediment consists of fine material (silt and clay), and although some of these materials are deposited in the delta feature, significant portions of the sediment load can flow into deeper portions of the reservoir toward the dam. This is indicated by the 2009 and 2019 bathymetry data, which are consistent with the Lumborg and Vested (2008) discussions in the scientific literature.

3.2 Bridges

Several bridges span the rivers of interest and the reservoir. Bridges typically constrict river flow as bridge supports and embankments encroach on the flow area. Bridges also tend to be located at relatively narrow sections of the river to minimize cost of construction.

Because bridges constrict flow, they typically cause backwater effects upstream of the bridge. The backwater effects include increased WSEs and reduction in velocity. At the bridges themselves, the reduced flow areas result in increased velocities. Bridges also potentially trap debris such as floating logs, which further constricts the flow and increases the backwater effect. The effects of hydraulic constrictions at bridges potentially cause sediment deposition upstream of the structure due to the reduced velocities.

An extreme example of bridge encroachment on the river and floodplain is the railroad bridge just downstream of the Twin Bridge area below the confluence of the Neosho and Spring rivers. Figure 70 and Figure 71 present aerial views of this area.

Figure 70
Confluence of Neosho and Spring Rivers at Twin Bridges and the Railroad Bridge

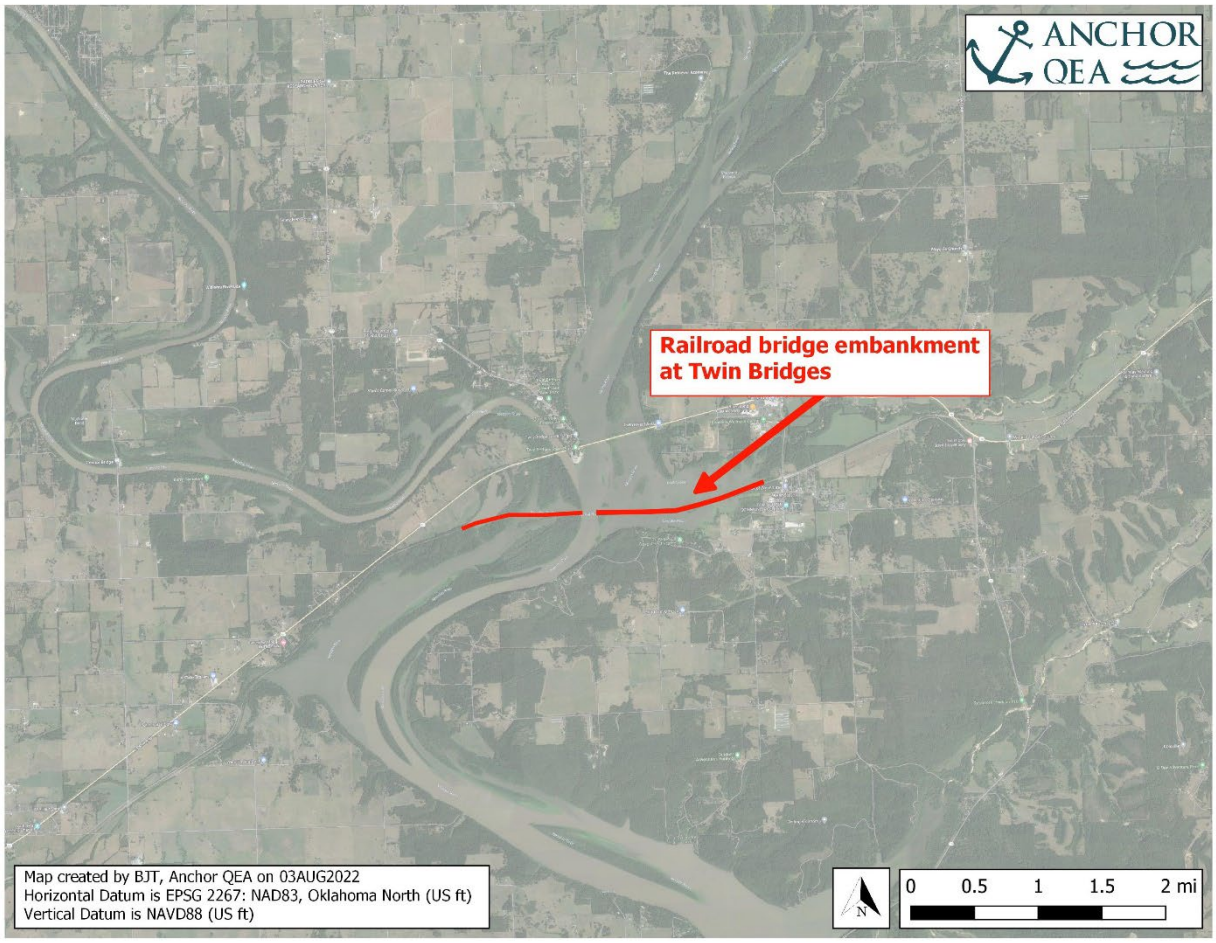

Figure 71
Burlington Northern Railroad Bridge and Embankment near Twin Bridges Photograph Looking East

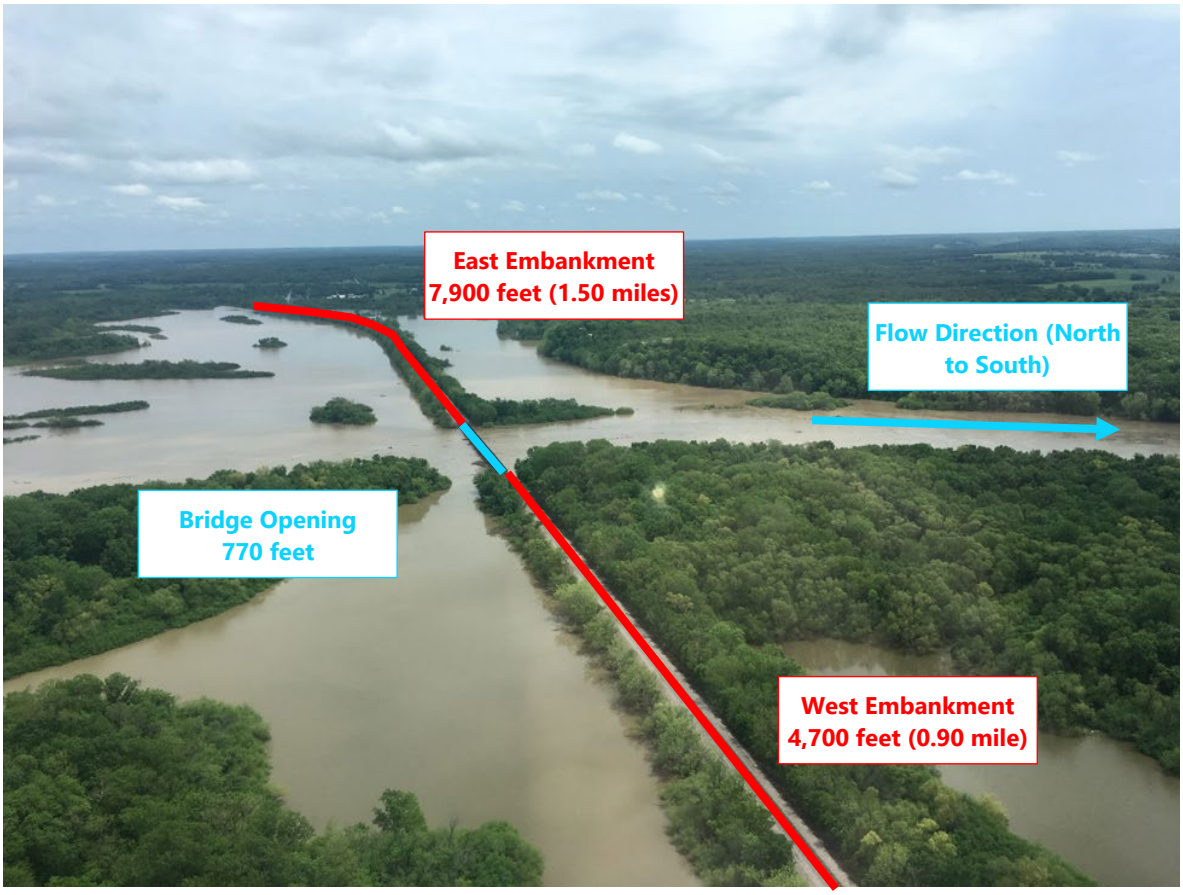

Notes: Photograph taken on May 2, 2019; USGS reported daily discharges were as follows:

- Neosho River near Commerce: 37,700 cfs (USGS 2021a)
- Tar Creek near Commerce: 192 cfs (USGS 2021c)
- Spring River near Quapaw: 48,500 cfs (USGS 2021e)

Flow direction is from left to right, and discharge must pass through the 770-foot bridge constriction.

The cross section at the Burlington Northern Railroad bridge (Figure 72) shows that the top of the embankment across the floodplain is at an average elevation of approximately 758 feet PD (note that the figure is from HEC-RAS and thus has a vertical datum of NGVD29). The width of the bridge opening is approximately 770 feet and the total embankment length is approximately 12,600 feet (2.4 miles).

Figure 72
Burlington Northern Railroad Bridge Cross Section

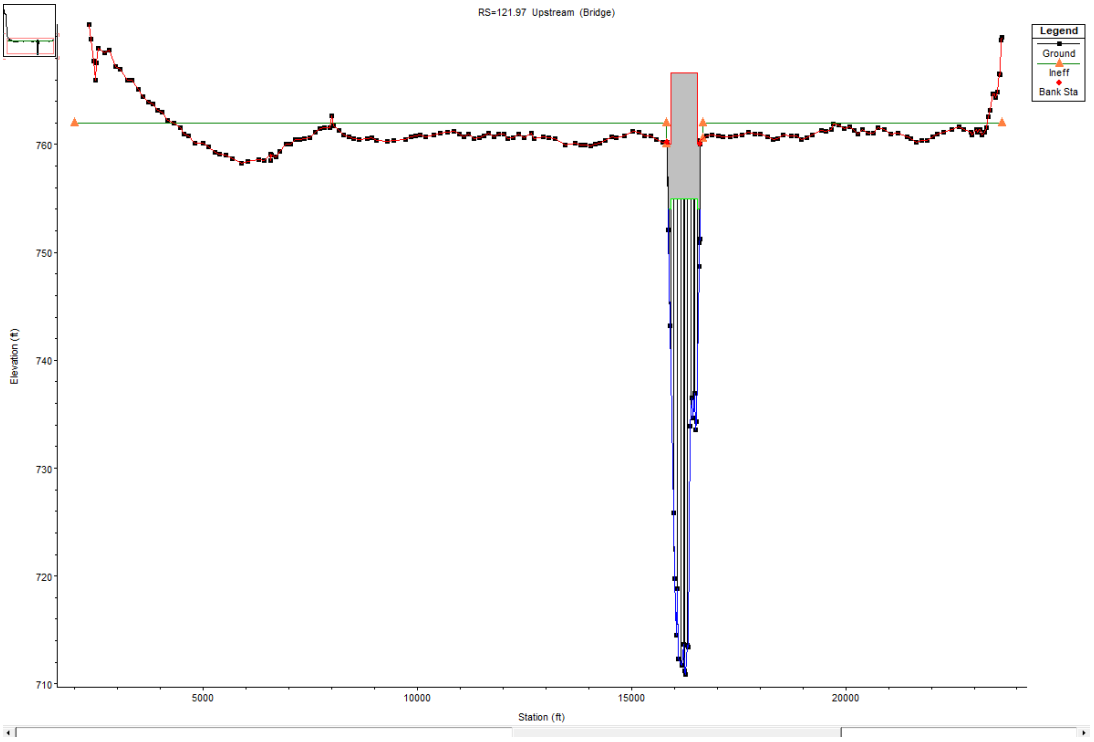

The aerial image (Figure 70) shows that the flow upstream of the railroad bridge is approximately 11,700 feet (2.22 miles) wide, whereas the width of the Neosho and Spring rivers upstream of Twin Bridges is approximately 2,250 feet wide (Neosho River is approximately 350 feet wide and Spring River is approximately 1,900 feet wide). The significant increase in water width by a factor of approximately five times shows the effect of the bridge in causing a backwater effect and blockage of the floodplain by the embankments.

Bridge piers frequently trap debris because moderate to high flow events carry floating trees and other materials. The following images show debris trapped on bridge piers during the flow event that occurred late in April through May 2019. Peak daily flow on the Neosho River was 90,100 cubic feet per second (cfs) on May 24, 2019; however, the photographs of debris were taken in early May before the flood peak (Figure 73).

Figure 73
May 2019 Photographs of Debris Trapped on Bridge Piers

Additional photographs were taken in December 2019, months after the peak flow in May 2019. The photographs show evidence of debris trapped on bridges, with some debris up on the bridge deck itself (Figure 74).

Figure 74
December 2019 Photographs of Debris Trapped on Bridge Piers

Notes: Top photographs show the abandoned railroad bridge at RM 134.60, approximately 0.6 mile upstream of the Tar Creek confluence.
Bottom photograph is from the East 60th Road Bridge (USGS Neosho River near Commerce gage) at RM 145.4.

3.3 Geologic Features

Vertical rock banks are evident in various reaches along the Neosho River. Examples of vertical rock banks are shown in Figure 75.

Figure 75
Photographs of Vertical Rocky Banks Along the Neosho River

Notes: Top photograph was taken near RM 129.07 on the Neosho River, approximately 2.4 miles upstream of Connors Bridge.
Bottom photograph was taken near RM 127.47 on the Neosho River, approximately 0.75 mile upstream of Connors Bridge.

Locations of the examples of rocky banks are shown in Figure 76, Figure 77, and Figure 78.

Reaches of river that are confined by vertical rock banks eliminate the floodplain and confine the flow to a relatively narrow cross section, which constricts the flow, potentially causing upstream backwater effects and sediment deposition.

Figure 76
Locations of Vertical Rocky Banks on Aerial Imagery

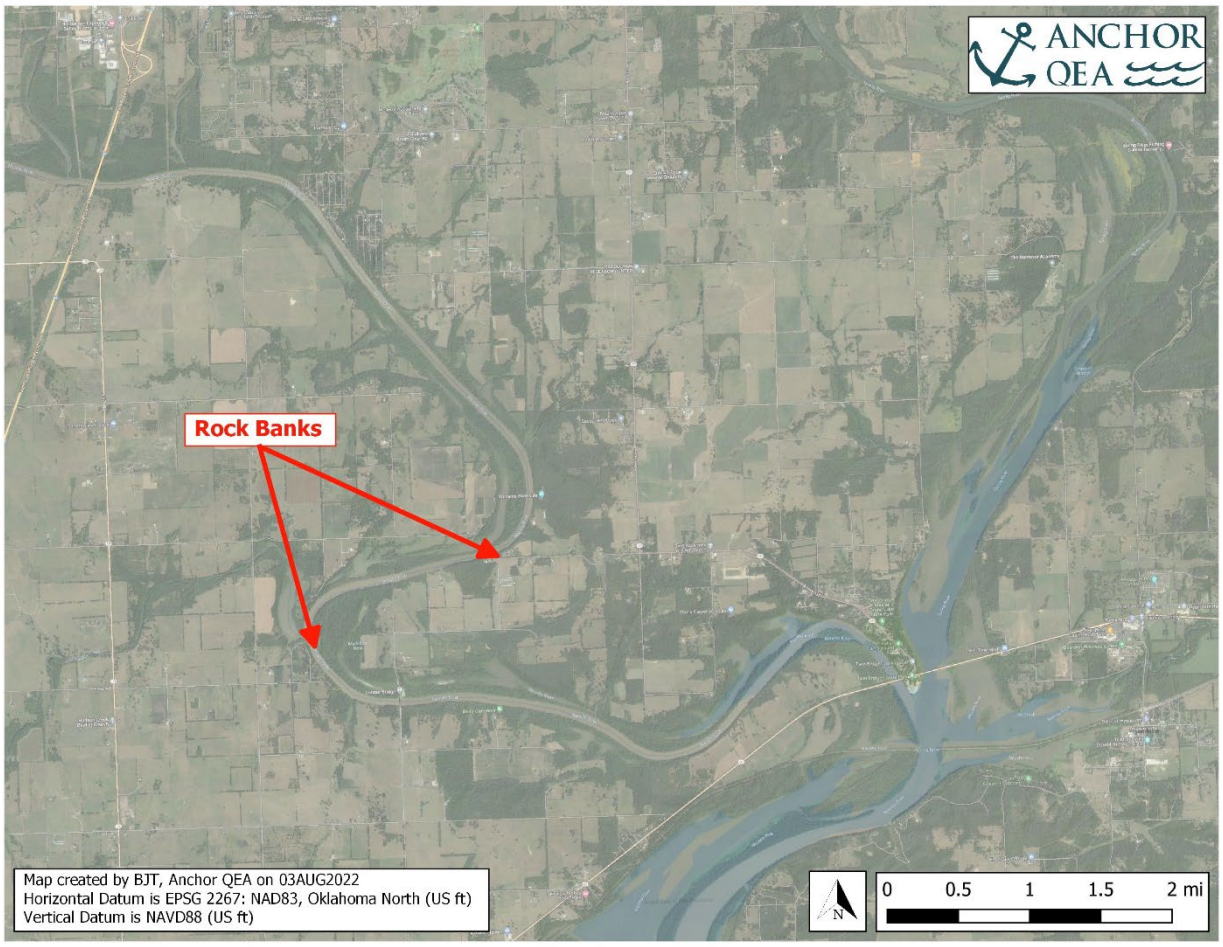

Figure 77
Locations of Vertical Rocky Banks on Topographic Map

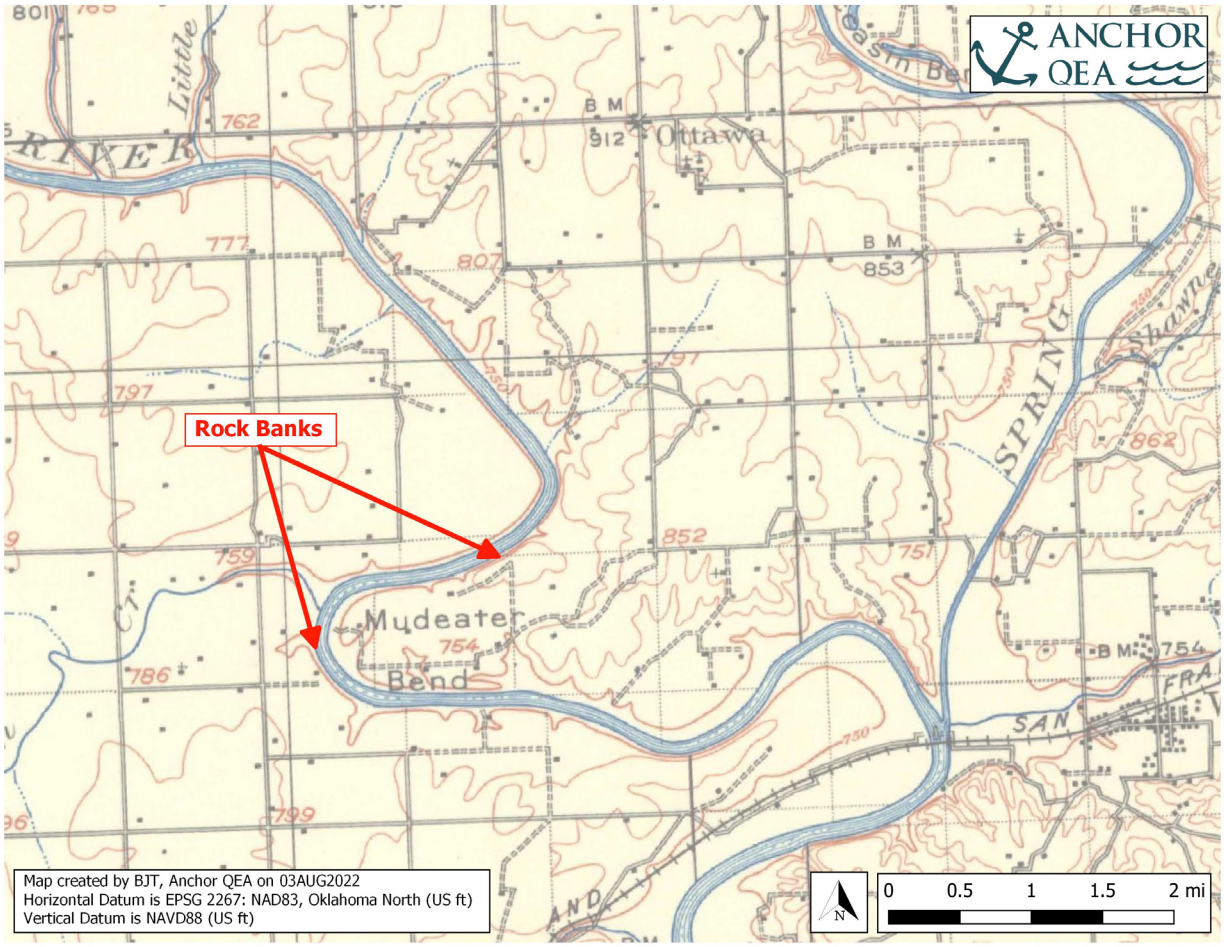

Source: Wyandotte, USGS (1907)

A now-submerged bioherm (ridge) composed of erosion-resistant limestone and chert was discussed by McKnight and Fischer (1970) and is located at RM 108. Such structures could also be submerged terraces or talus piles and are part of the southern flank of the exposed and eroding Ozark Uplift often referred to as the Ozark Plateau or Ozark Highlands, but more specifically the Springfield Plateau. They are composed of the Mississippi Boone formation (GRDA 2017) and cause narrowing in the now-submerged valley. Dendritic drainage patterns from the surrounding uplands entering the submerged valley impede the transport of sediment downstream into the lower reaches of the reservoir and cause aggradation of sediment in these sections of submerged river valley. Additional evidence of ridges composed of limestone and chert within the now-submerged valley can be observed in the grade changes of the 1938 bank line elevation profile (Figure 78). The bank line grade change begins at RM 108 and extends upstream to approximately RM 115. Note that the other

profile lines in Figure 78 display thalweg elevations. The 1938 profile is the only representation in Figure 78 of the now-submerged valley elevation.

Figure 78
Historical Neosho River Thalweg Comparison

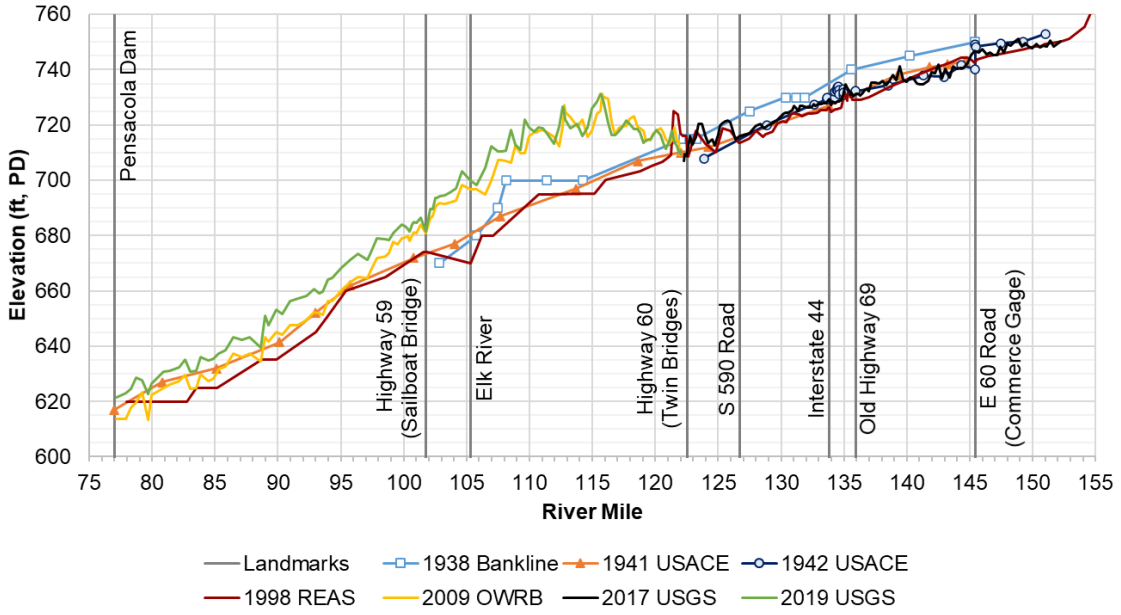

Note: This plot covers the Neosho River from RM 152.2 at the upstream end to the Pensacola Dam at RM 77.12 on the downstream end.

Submerged ridges in the now-submerged valley can act as stable points. Many of these ridges are perpendicular to downstream flow in the valley and can cause sediment to deposit between and amongst the submerged ridges. These stable points are capable of forming the delta feature that is shown in the 2019 USGS profile and the 2009 OWRB profile from RM 100 upstream to RM 122 (Figure 78).

Because McKnight and Fischer (1970) is not a complete catalogue of all erosion-resistant, submerged ridges in the original river valley, it is likely that there are other such ridges in the submerged valley where the delta feature has formed at the edge of the Ozark Uplift.

Evidence of the Ozark Uplift can also be observed on the 1907 topographic map with 50-foot contours shown in Figure 79 (USGS 1907). The entire original river valley from RM 107 to RM 122 displays convoluted and closely spaced contour lines east of the original river channel from RM 107 to RM 120 and on both the east and west sides from RM 107 to RM 110. Therefore, it can be reasonably concluded other ridges submerged in the original river valley that are part of the Ozark

Uplift impede the transport of sediment downstream into the deeper portions of the reservoir and cause the delta feature to form in this location.

Figure 79
Geologic Constrictions along Neosho River in the Region of the Delta Feature

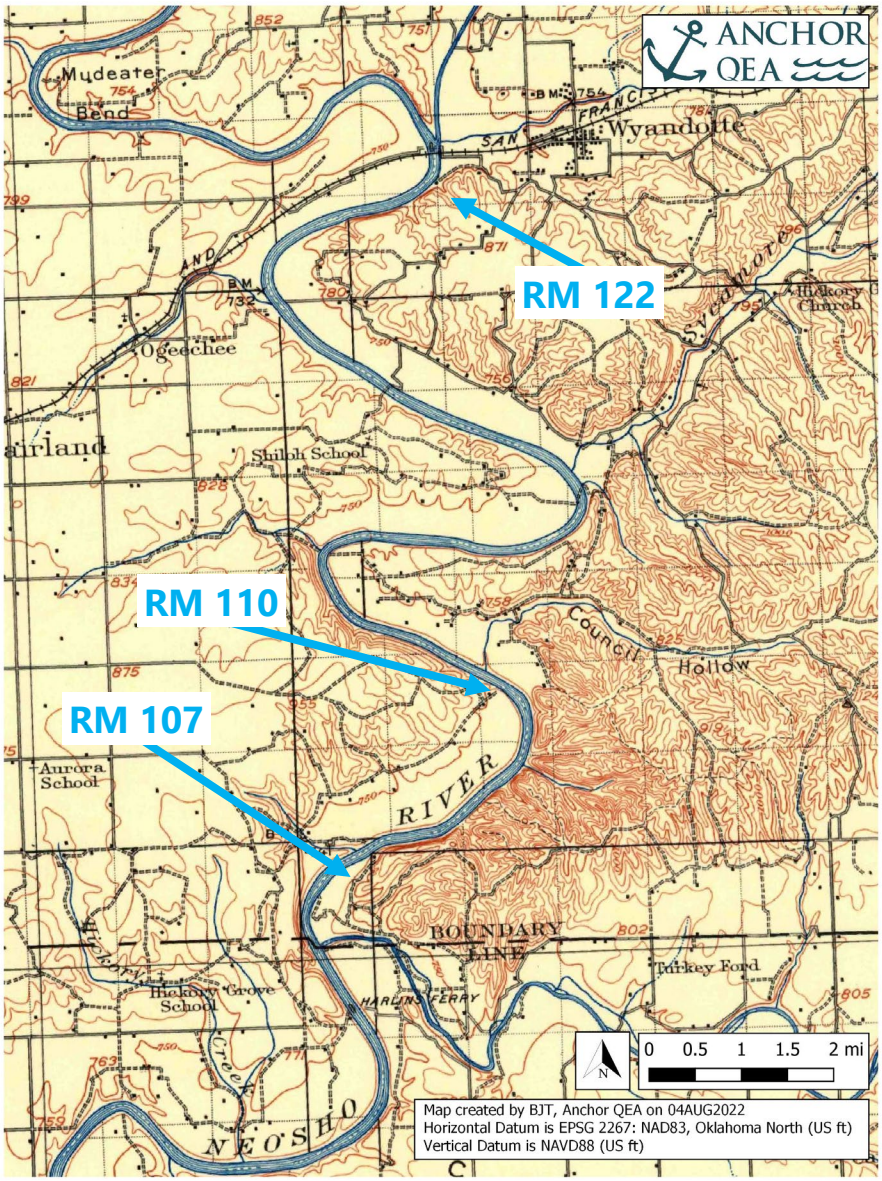

Even in areas without submerged ridges, talus piles, or terraces, the presence of the Ozark Uplift in the vicinity of the delta feature indicates the original channel bottom is likely composed of limestone and chert from the Ozark Uplift that has eroded over time.

The presence of the Ozark Uplift limestone in the area of the delta feature has likely played one of the more significant roles in forming the delta feature to its current size instead of continuous downstream transport of sediment to the location of the dam.

3.4 Riverine Features

At a confluence of a tributary, some of the sediment load from the tributary is frequently deposited, forming a tributary bar within the river (Figure 80).

Figure 80
Illustration of Types of Bars that Occur in Alluvial Channels

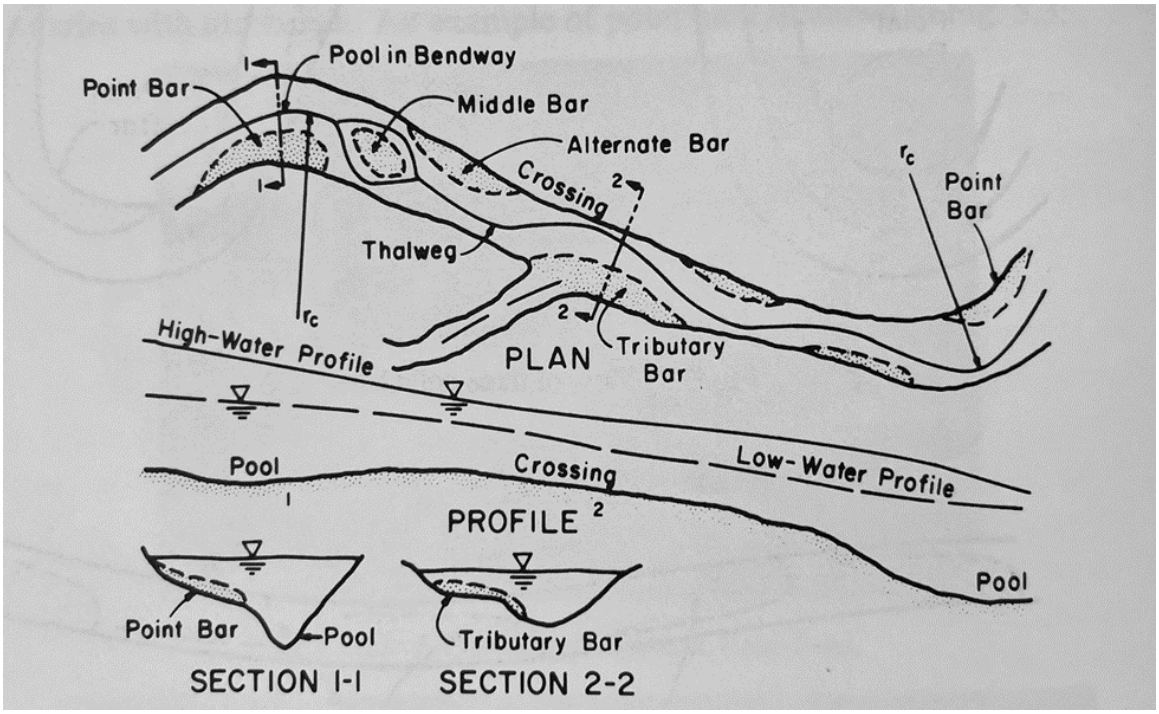

Source: Simons and Senturk (1992)

Tributary bars form because the slope of the tributary is typically steeper than the river into which it flows, so some portion of the sediment load cannot be readily transported downstream resulting in sediment deposition. This process also occurs when the tributary transports a high sediment load or a coarser sediment load than the main river.

The slope of the Neosho River bed in the vicinity of the Elk River confluence based on the 1941 USACE data is approximately 2.06 feet per mile. The slope of the Elk River bed upstream of the confluence based on the 2019 data is approximately 3.21 feet per mile, which is approximately 56% steeper than the Neosho River. This difference in riverbed slopes would tend to result in

sedimentation in the form of a tributary bar at the confluence. The slope of the Spring River bed is approximately 2.21 feet per mile, which is approximately 7% steeper than the Neosho River.

As stated previously, the Ozark Uplift composed of Mississippi Boone limestone and chert crosses the Neosho River at the confluence of the Elk River. This feature, combined with the steeper slope of the Elk River and the attendant potential for the formation of a tributary bar, suggest a natural tendency for sediment deposition at this location. Although these geomorphic features affect potential sedimentation patterns at this location, it is not possible to quantify these effects on the overall sedimentation pattern.

In addition to the geologic features of the area, there are also flood protection levees upstream that disconnect the river from the floodplains. By building up the streambanks, water is confined to the channel during large flow events, which results in increased water levels because the increased discharge cannot spread to the flat, open areas of the historical floodplains. This can increase flood risk to areas not protected by levees or protected by shorter levees.

4 Quantitative Analysis

The second level of analysis in the three-level approach is quantitative analysis of sedimentation. Beyond the original rationale for the development and application of the three-level approach, additional discussion regarding the quantitative analysis was presented in the USP.

4.1 Quantitative Sediment Transport Evaluation

In addition to the STM, GRDA used a quantitative engineering analysis of sediment transport in the study area. This fulfills the second part of the three-level approach discussed in previous proposals and will focus on the delta feature and the lower reservoir, where the deposition of cohesive materials has the largest potential impacts on the power pool. GRDA used this analysis as a means of validating the model outputs and providing additional confidence in STM results. Recent evaluations of computer modeling by the USSD Committee on Hydraulics of Dams, Subcommittee on Reservoir Sedimentation (2015) suggest that the results of a HEC-RAS model evaluating cohesive sediments may not be reliable. Regarding reservoir sedimentation models, the committee states the following:

> Sediment transport models incorporate a certain degree of simplification to be computationally feasible. Simplified models run into the risk of not obtaining a reliable solution, whereas increasing the model complexity can complicate the problem formulation and incur more input data preparation, calibration, and verification costs. Most of the commonly used numerical sediment transport models were originally developed for the analysis of movable bed rivers having coarse sediments and employ sediment transport equations developed from flume and river data where the effect of fine or wash load on fall velocity, viscosity, and relative density can be ignored. In contrast, reservoir problems may involve the analysis of grain sizes ranging from cobbles in the upstream delta area to clays near the dam. The silts and clays which normally behave as wash load in most rivers, and which are ignored in many river sedimentation models often constitute the majority of the total sediment load in a reservoir. Most 1D sediment transport models, and transport functions, are designed for noncohesive sediment transport. Models often include the addition of simple cohesive sediment computational procedures to enhance model capability. (USSD 2015)

Such is the case with HEC-RAS, where simple cohesive sediment computational procedures were added to a model developed primarily for use in analyzing non-cohesive sediment transport. Specifically, relationships of critical shear and erosion rate developed by Krone (1962) and Partheniades (1962) are the relationships used in HEC-RAS for cohesive sediment.

The USSD (2015) findings also state the following:

> In summary, the sediment transport conditions associated with reservoirs are extremely complex. Detailed analysis of many of these problems lies beyond present knowledge, and only qualitative or rough quantitative estimates can be provided. Caution should be used in the application of numerical techniques in either hand calculations or computer models.

As discussed above, the cohesive sediment modeling routines used in HEC-RAS are limited. It is necessary to have a second analysis to ensure those limitations do not produce erroneous sedimentation predictions. Density currents, mud flows, and other phenomena associated with transported sediment (Lumborg and Vested 2008; van Rijn n.d.; Zavala 2020) are almost certainly active in this system and the routines used in HEC-RAS do not account for those processes. It is expected that this will primarily be of concern lower in the reservoir, hence the decision to directly use the STM only above RM 100 and use a different technique to evaluate sedimentation in the lower reservoir.

For these reasons, GRDA also performed a quantitative engineering analysis of sediment transport within the study area. This approach relied on measured field data including sediment transport, erodibility, and grain size distributions; bathymetric surveys; and overbank topographic information.

Sediment transport equations in the STM for both non-cohesive and cohesive sediments use hydraulic shear stress as the driving force causing erosion and transport of sediment. The quantitative analysis focuses on the relationship between hydraulic shear stress caused by flowing water and the pattern of sediment movement or sedimentation as documented by the change in bathymetric surveys over time.

Some supportive analyses of the sediment transport and bathymetric data are necessary to relate the pattern of sedimentation to hydraulic shear stress. These include development of sediment rating curves and sediment density. The sediment rating curves relate sediment transport (in units of tons per day) to the flow of water. The sediment rating curves are applied to the flow data to compute the quantity of sediment being transported down the various rivers and into the reservoir. The density, or specific weight of sediment, in units of pounds per cubic foot, is utilized to convert the tonnage of sediment being transported or deposited to the volume of sediment being deposited.

4.2 Development of Sediment Transport Rating Curves for Quantitative Analysis

Initial development of sediment rating curves was conducted in the ISR. These sediment rating curves have been updated for this quantitative analysis. Significant sets of sediment transport data are available from USGS and collected specifically for this Project by Anchor QEA as discussed in

Section 2. Figure 81 shows the set of suspended sediment transport data for the Neosho River with sediment transport plotted against flow. This graph is plotted on a log-log scale, typically used in showing the relationship between sediment transport and flow. As observed, there is considerable scatter in the data, which is again typical in observations of sediment transport and flow.

Figure 81
Suspended Sediment Concentration Samples and Stream Discharges During Sampling on the Neosho River Near Commerce (USGS Gage 07185000)

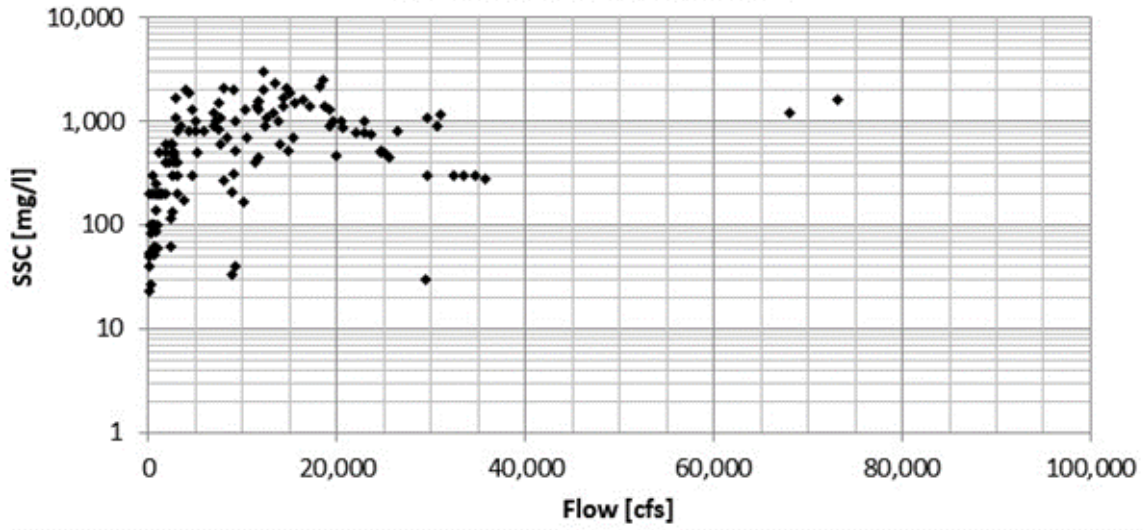

Note: Only two samples were collected at discharges above 40,000 cfs.

In analyzing sediment transport whether using a computer model or other quantitative analyses techniques, a sediment rating curve is developed from the data to quantify sediment transport as a function of flow. Typically, a power relationship is utilized because this type of relationship generally fits these data.

To aid in the development of these relationships between sediment transport and flow, a tool has been included in HEC-RAS 6.2 called the "Sediment Rating Curve Analysis Tool" (USACE 2022). Within this tool are two components: bias correction and stationarity to improve the quality of the sediment rating curve. Bias correction rectifies "bias implicit to the log-transform regression used to develop sediment rating curves." Stationarity explores "how sediment data change over time and fit rating curves to temporal sub-sets of the observations."

The following is from the HEC-RAS explanation of the Sediment Rating Curve Analysis Tool:

> Log-transforming the regression makes it relatively easy to fit a power function to log-distributed data. However, it also introduces a bias when the data are untransformed. For example, the observations in the figure below have equal and opposite residuals in the

logarithmic transformation (0.7). However, when these residuals untransform, the positive residual is larger than the negative residual. Therefore, the log-transformed linear regression ends up with larger positive residuals than negative, making the fit power function systematically low. This rating curve will under-predict sediment load for a given flow.

Applying the bias correction decreases the likelihood that the resulting regression will underpredict the sediment load when using the standard power function for the sediment transport rating curves.

The stationarity concept simply considers the extent to which trends in sediment transport may be occurring over time. This concept is explained in the Sediment Rating Curve Analysis Tool documentation (USACE 2022).

4.2.1 Stationarity Analysis

Sediment load changes over time. Agricultural impacts, land use changes, fires, mass wasting events, dam removals, and eruptions can increase sediment loads, whereas dams, pavement, and improved agricultural practices can decrease sediment loads (Walling and Fang 2003).

Because sediment load data are often scarce, modelers want to make use of all the data available. But it is important to test the load stationarity. The assumption of stationarity is simply that sediment loads do not change over time. Therefore, sediment assessments require analysts to plot and evaluate the data in time blocks, particularly before and after known system changes like a dam or gravel mining policies. If there is a big shift in the rating curve over time, consider using the most recent data to develop the future conditions rating curve.

Figure 82 is an example of a stationarity analysis of a USGS gage (USGS 2021b) as shown in the HEC-RAS stationarity analysis. This particular evaluation compares sediment loading before and after construction of the John Redmond Dam in 1964, and it shows that flows from before its completion carried more sediment than more recent flows. This indicates that the upstream reservoir is trapping sediment and decreasing the loading rates at Grand Lake.

Figure 82
Stationarity Evaluation Example from HEC-RAS

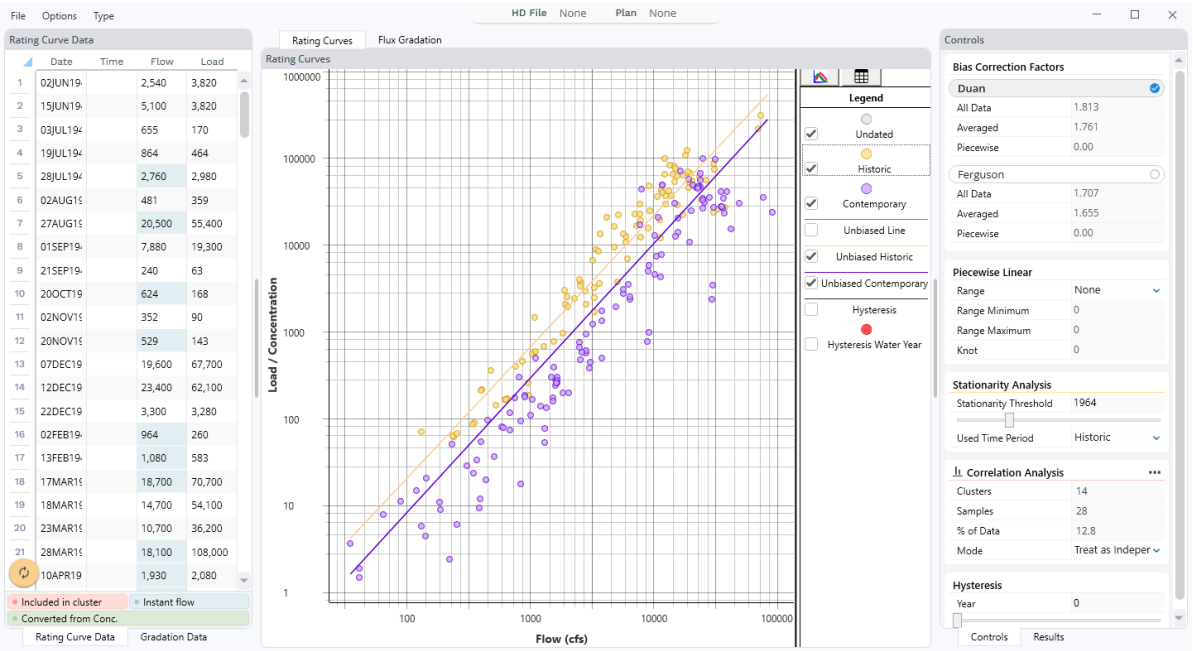

Note: HEC-RAS Sediment Rating Curve Analysis Tool showing stationarity evaluation of USGS Gage 07185000 (Neosho River near Commerce, Oklahoma) with pre-1964 samples in gold and post-1964 samples in purple. This analysis illustrates the decreasing trend in sediment loading over time.

The relationship between flow and load can change systematically over time. If you cannot assume that the relationship between flow and load is "stationary" (constant over time), it may not be appropriate to use all the data for an analysis or model. For example, when calibrating a model in a system with non-stationary sediment data, it is appropriate to use the historical rating curve that reflects the data over the calibration period. Alternately, when forecasting, it is appropriate to use a rating curve based on the most recent relationship. Scientists and modelers should always, at a minimum, evaluate their data stationarity. But if sediment data are non-stationary, they must partition their data to develop a rating curve appropriate for the time period under consideration.

Sediment loading changes over time due to a variety of factors. These include changes in agricultural practices such as the introduction of no-till methods and the use of cover crops, both of which are supported by the Natural Resources Conservation Service (NRCS). Land use changes also affect sediment loading, as forests reduce soil erosion in areas that were previously dominated by agriculture. Furthermore, recent improvements in erosion control and sediment loading practices such as natural stream borders and stormwater retention practices help remove soils from stormwater runoff, reducing sediment loads. In the case of Grand Lake and the Neosho River, the

presence of the John Redmond Dam traps significant volumes of sediment and prevents it from reaching the study area.

This study used the Sediment Rating Curve Analysis Tool to correct for bias and the concept of stationarity to account for the reduction in sediment transport over time that exists in the data.

4.3 Suspended Sediment Regression Analyses

Suspended sediment transport data in tons per day is plotted as a function of flow in Figure 83 for all available data, segregating the USGS data and Anchor QEA data. It must be noted that sediment transport data are typically plotted on a log-log graph. The reason for this is that there is considerable scatter in the data. For example, at a flow of approximately 9,000 cfs, the sediment transport data range from 991 to 48,600 tons per day, which covers a large range, with the higher data point being 49 times greater than the lower data point at the same flow. The uncertainty in fitting a single curve to measured sediment loading data is a significant challenge for sediment transport modeling.

Figure 83
Suspended Sediment Transport: Neosho River Near Commerce

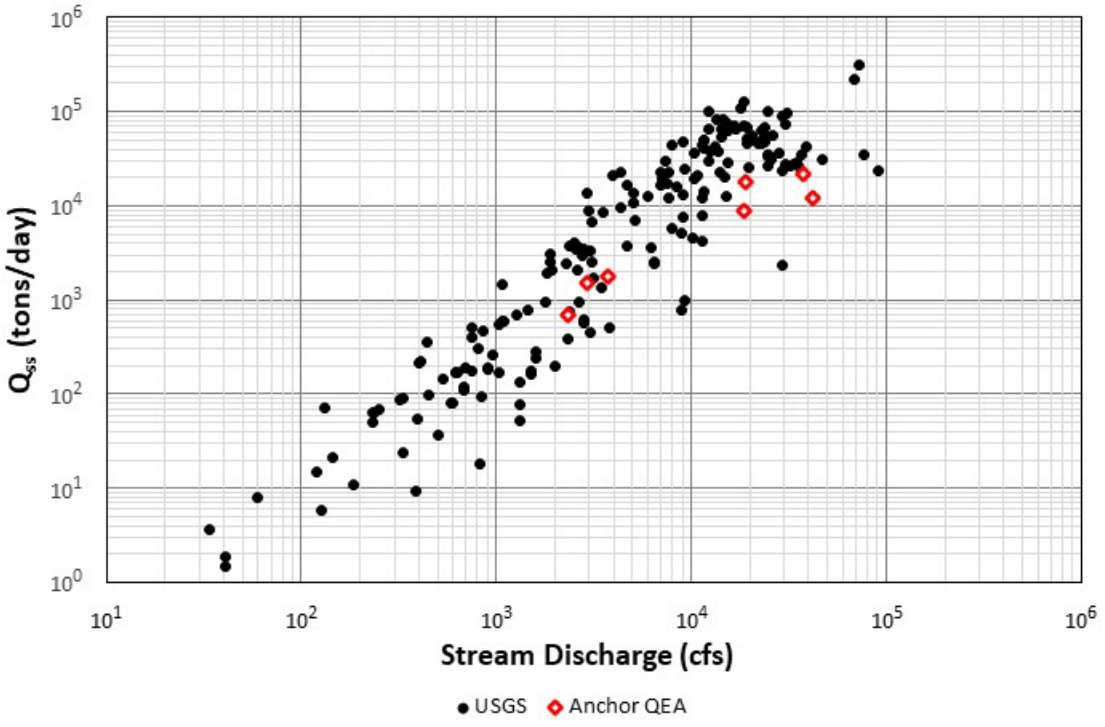

The Anchor QEA data, which were collected in recent years from 2019 to 2021, tended to be on the lower range of the scatter plot typically found in plotting sediment transport data. This prompted an evaluation of whether there were any trends in the relationship between sediment transport and flow as indicated by the data. The Neosho River sediment transport data were collected from 1944 through the present (data for this report extend through summer 2021). Figure 84 presents the same data segregated into various time periods or sets of data over time. As can be seen in the stationarity evaluation, the data show a temporal trend of generally reduced sediment loads with the highest sediment loads occurring in earlier decades and lower sediment loads occurring in recent decades.

Figure 84
Suspended Sediment Transport (Segregated Over Time): Neosho River Near Commerce

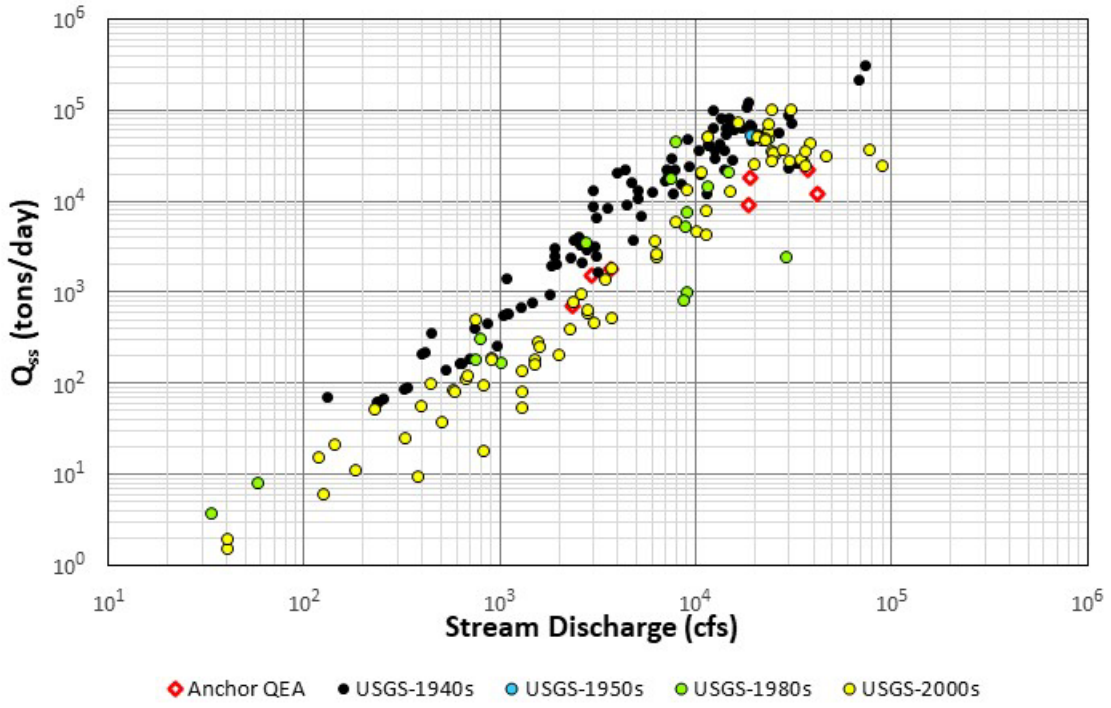

Regression analyses were conducted on the data segregated into two sets: 1940 through 2008 and 2009 to 2021 (Figure 85), corresponding to the availability of bathymetric data.

Figure 85
Suspended Sediment Transport Regression Analyses (1940–2008 and 2009–2021): Neosho River Near Commerce

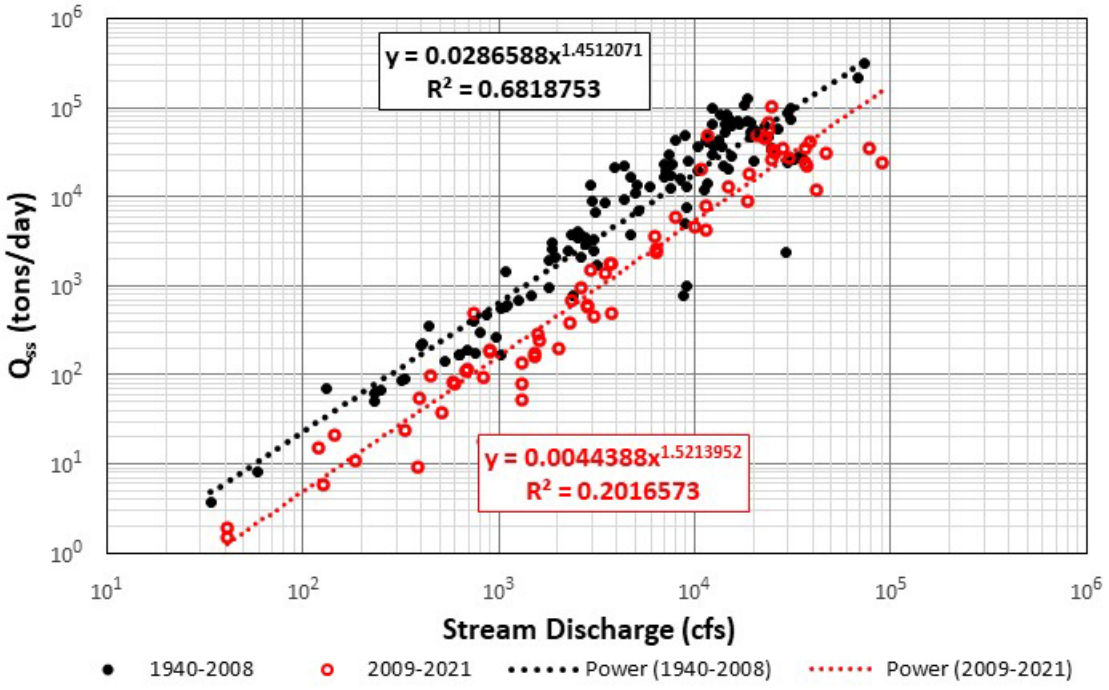

The regression analyses show two distinct relationships with the 1940 to 2008 curve being significantly higher than the 2009 to 2021 curve (again noting that the data and regressions are plotted on a log-log graph). Based on these regression analyses, the suspended sediment transport ranges from approximately 4 times greater at lower flows to approximately 2.9 times greater at higher flows, comparing the 1940 to 2008 curve to the 2009 to 2021 curve. In other words, the data indicate that suspended sediment transport was between approximately 3 to 4 times greater for the earlier time period than the most recent time period. This is a significant decrease in sediment supply over time to consider in the analysis and modeling of sediment transport. One reason there has been a decrease in suspended sediment transport in the Neosho River is the fact that the John Redmond Reservoir on the Neosho River has been trapping sediment since its completion in 1964. Other factors may also have contributed to the trend in decreasing sediment loads over time such as erosion-reduction measures along upstream river channels, land-use changes, and changes in vegetation along the key tributaries; but the effect of sediment trapping in John Redmond Reservoir is a known and significant factor.

Regression analysis was also conducted for the pre- and post-John Redmond Reservoir era as shown in Figure 86. This analysis shows similar results to the pre- and post-2009 because most of the data collected prior to 2009 were collected prior to 1964.

Figure 86
Neosho River Pre- and Post-John Redmond Reservoir Suspended Sediment Relationships with Flow

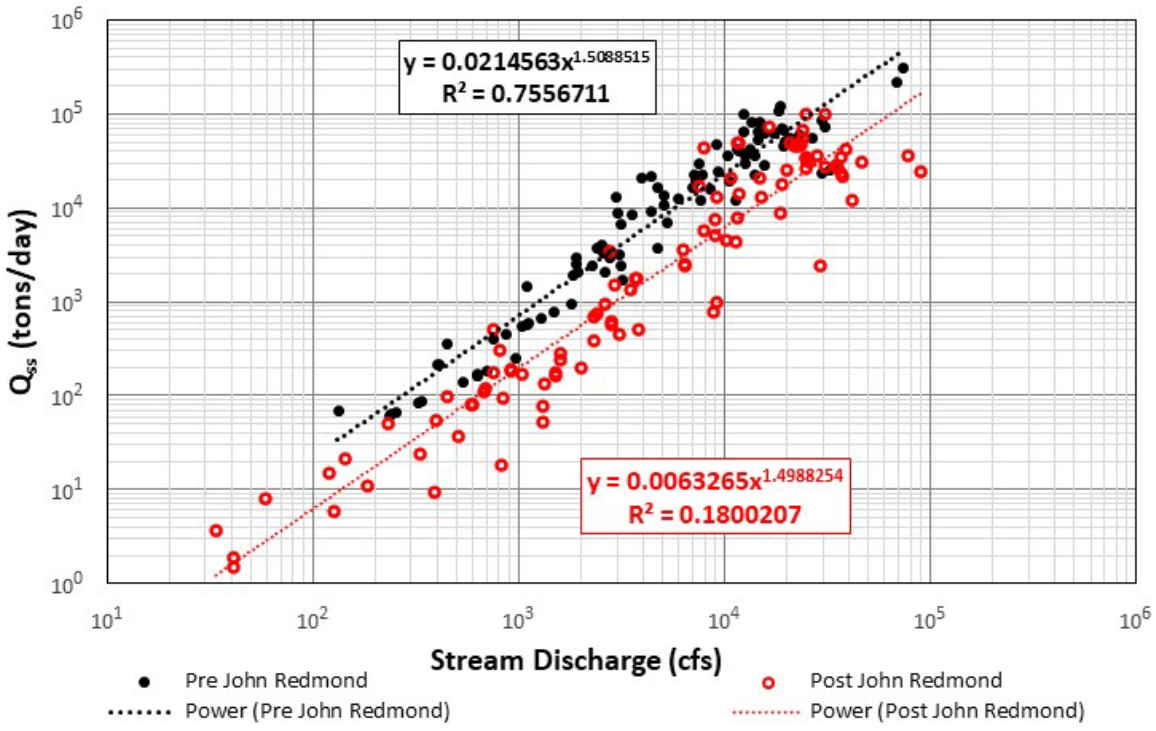

The final sediment rating curves for the quantitative analysis used the unbiased approach from HEC-RAS and pre- and post-2009 for all rivers. The 2009 break point was chosen because the OWRB survey was completed at that time, making it convenient for comparison of pre- and post-survey sediment loading. The Neosho River was an exception; it uses 1964 as the break point, which coincides with completion of the John Redmond Reservoir and the subsequent reduction in sediment loading to Grand Lake. These rating curves are shown in Figure 87 through Figure 94.

Figure 87 shows the pre-1964 data on the Neosho River in red (along with the associated regression curve and equation), and the equation using output from the unbiased sediment rating curve analysis is shown in black (along with the associated equation). The unbiased equations are the sediment rating curves used in the quantitative analysis for each respective time period.

Figure 87
Neosho River Comparisons of Pre-1964 Biased and Unbiased Sediment Curves

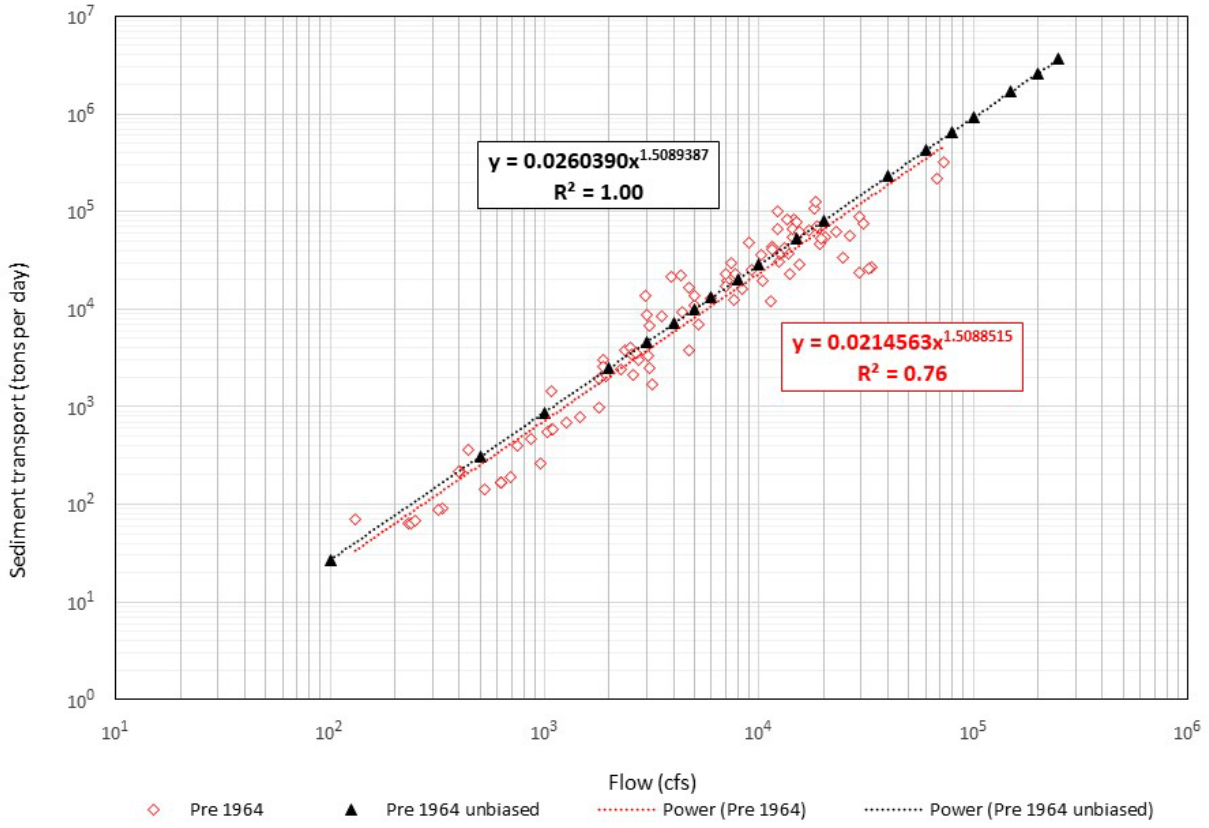

Figure 88 presents the same information for the post-1964 time period, again with the data points shown in red and the unbiased equation shown in black.

Figure 88
Neosho River Comparisons of Post-1964 Biased and Unbiased Sediment Curves

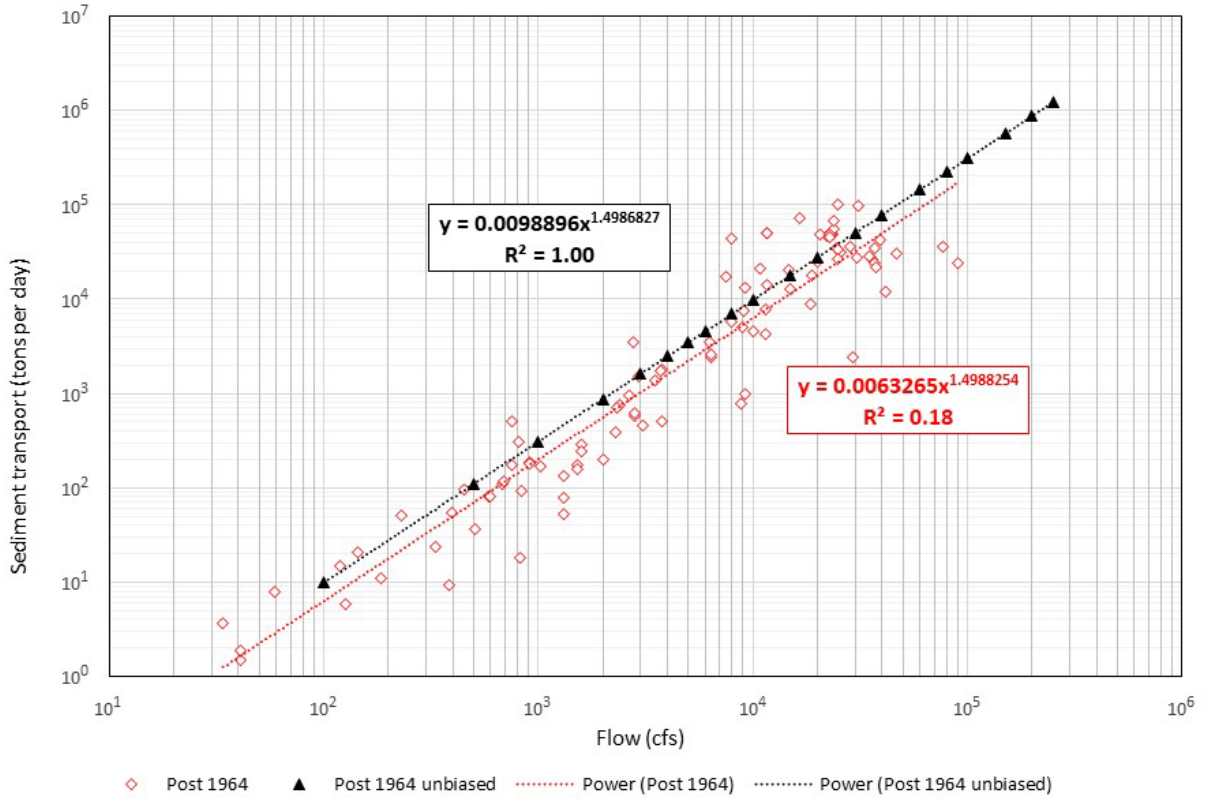

Figure 89 and Figure 90 present the datasets for pre- and post-2009 time periods on the Spring River with the unbiased regressions from the unbiased analysis from HEC-RAS shown in black.

Figure 89
Spring River Comparisons of Pre-2009 Biased and Unbiased Sediment Curves

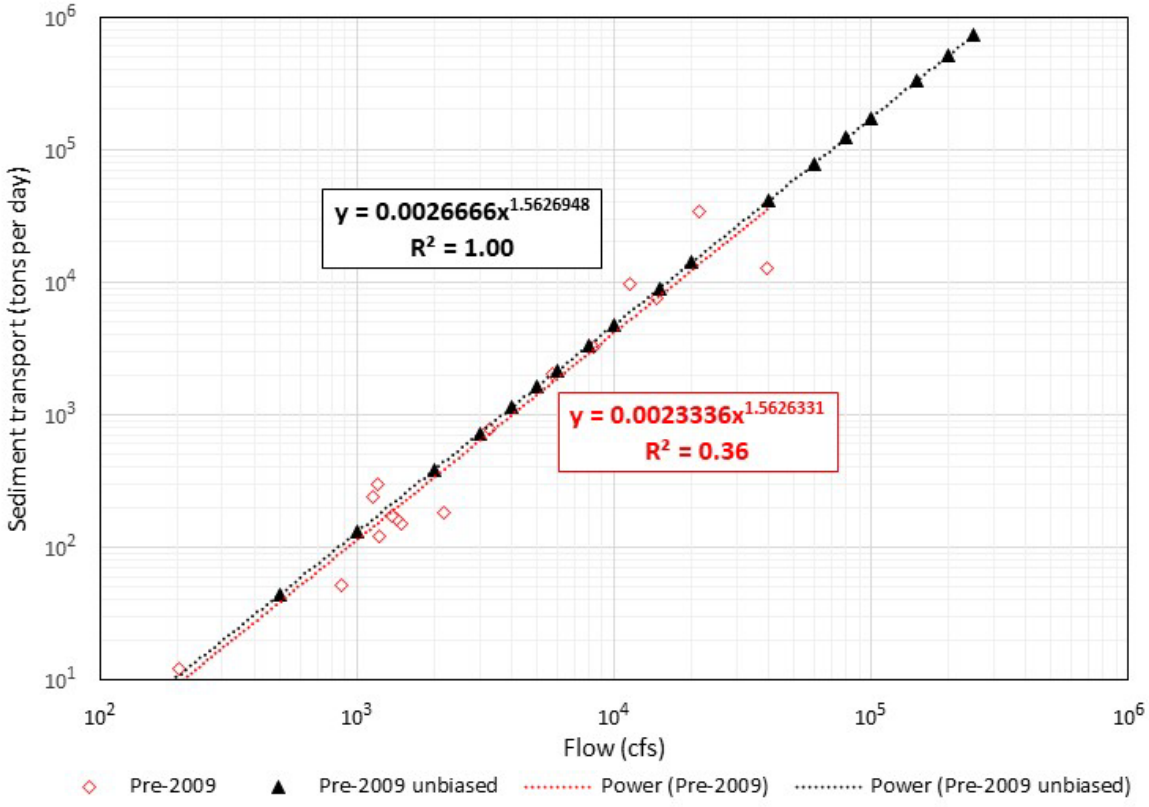

Figure 90
Spring River Comparisons of Post-2009 Biased and Unbiased Sediment Curves

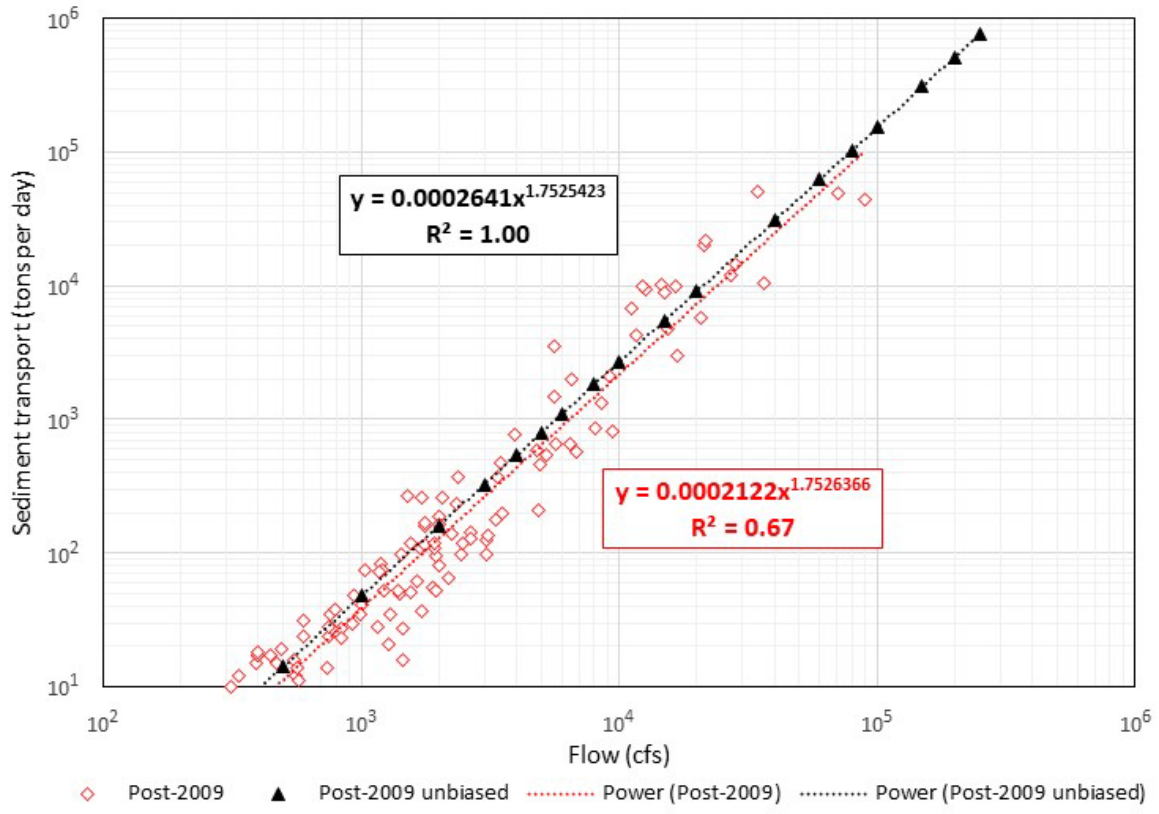

Figure 91 and Figure 92 present the Elk River data for pre- and post-2009 time periods in red and the corresponding unbiased equations for the respective time periods in black.

Figure 91
Elk River Comparisons of Pre-2009 Biased and Unbiased Sediment Curves

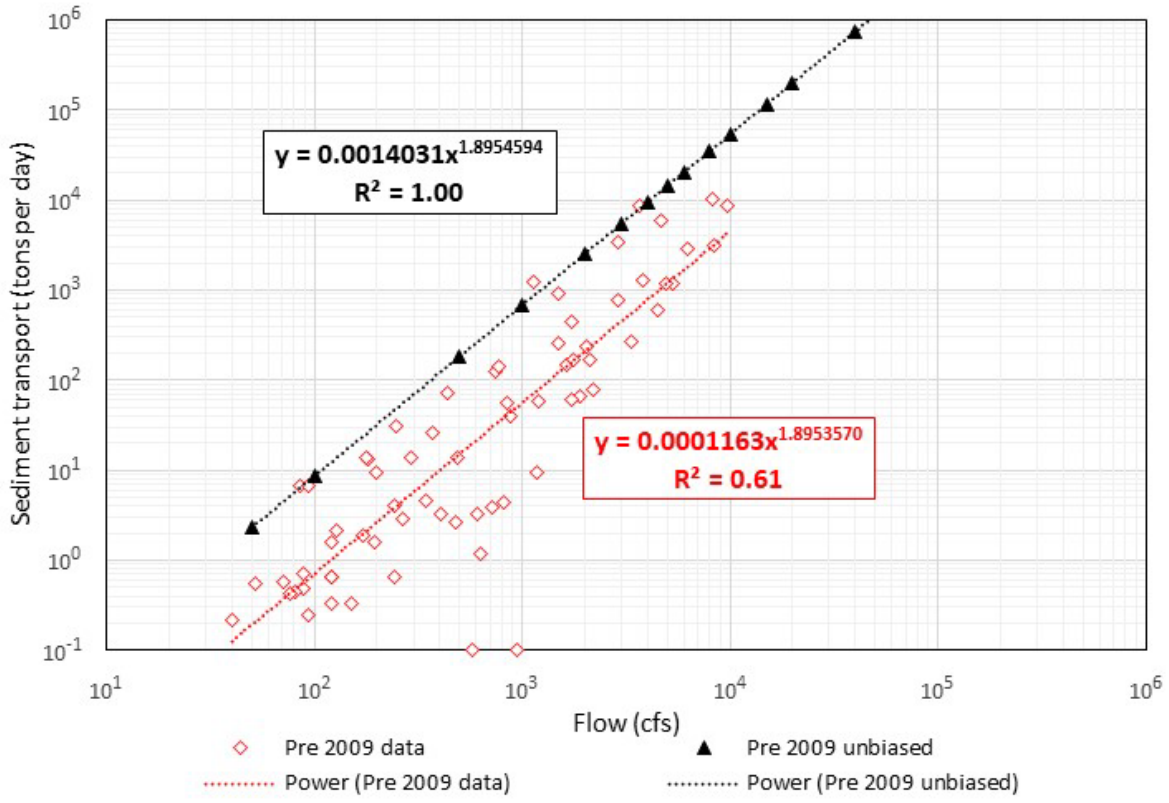

Figure 92
Elk River Comparisons of Post-2009 Biased and Unbiased Sediment Curves

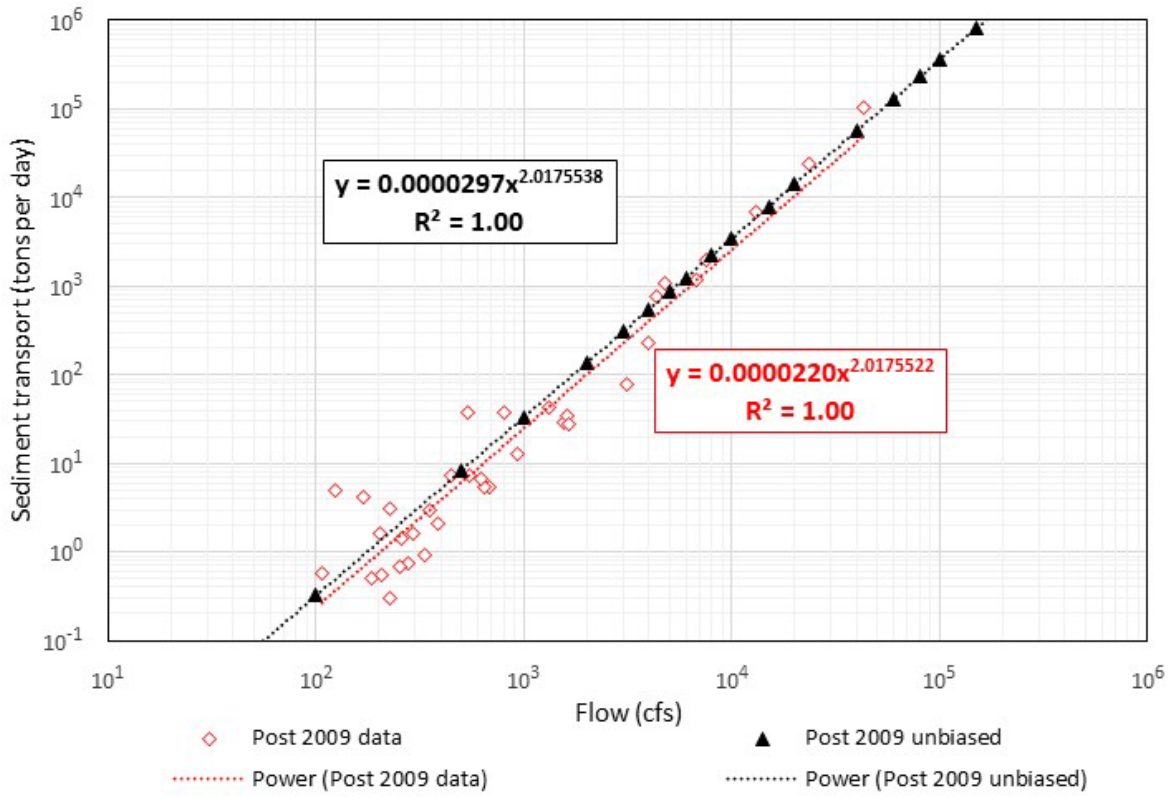

Figure 93 and Figure 94 present the Tar Creek data for pre- and post-2009 time periods in red and the corresponding unbiased equations for the respective time periods in black.

Figure 93
Tar Creek Comparisons of Pre-2009 Biased and Unbiased Sediment Curves

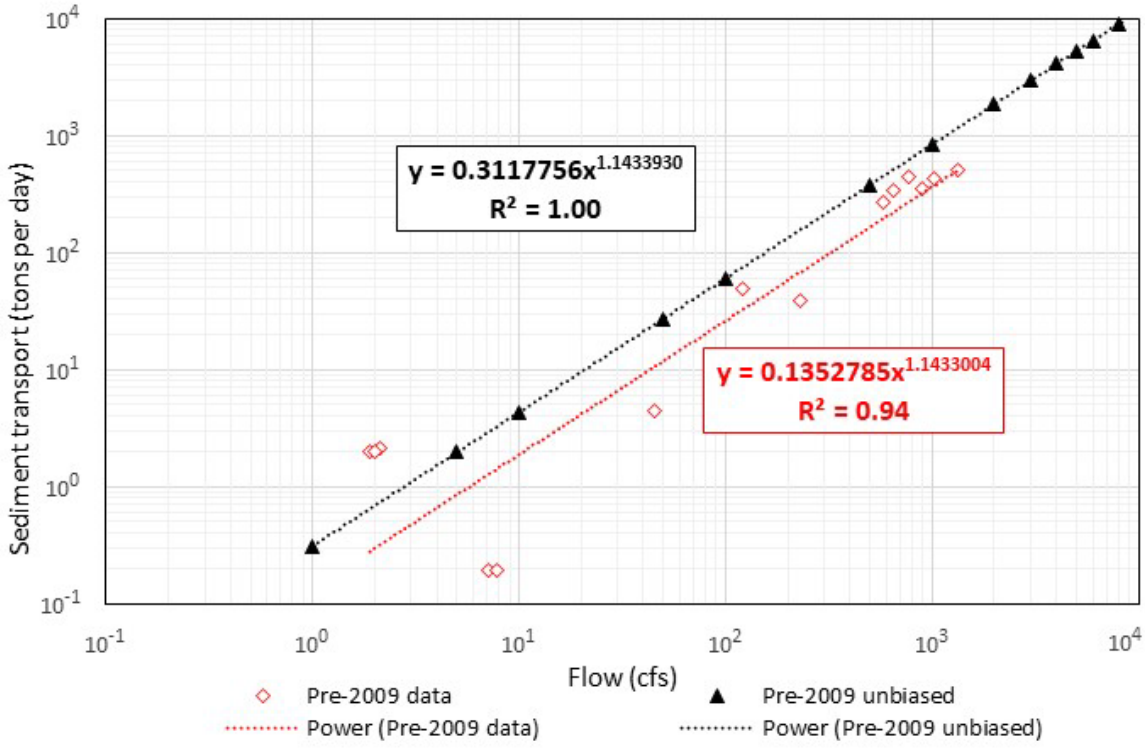

Figure 94
Tar Creek Comparisons of Post-2009 Biased and Unbiased Sediment Curves

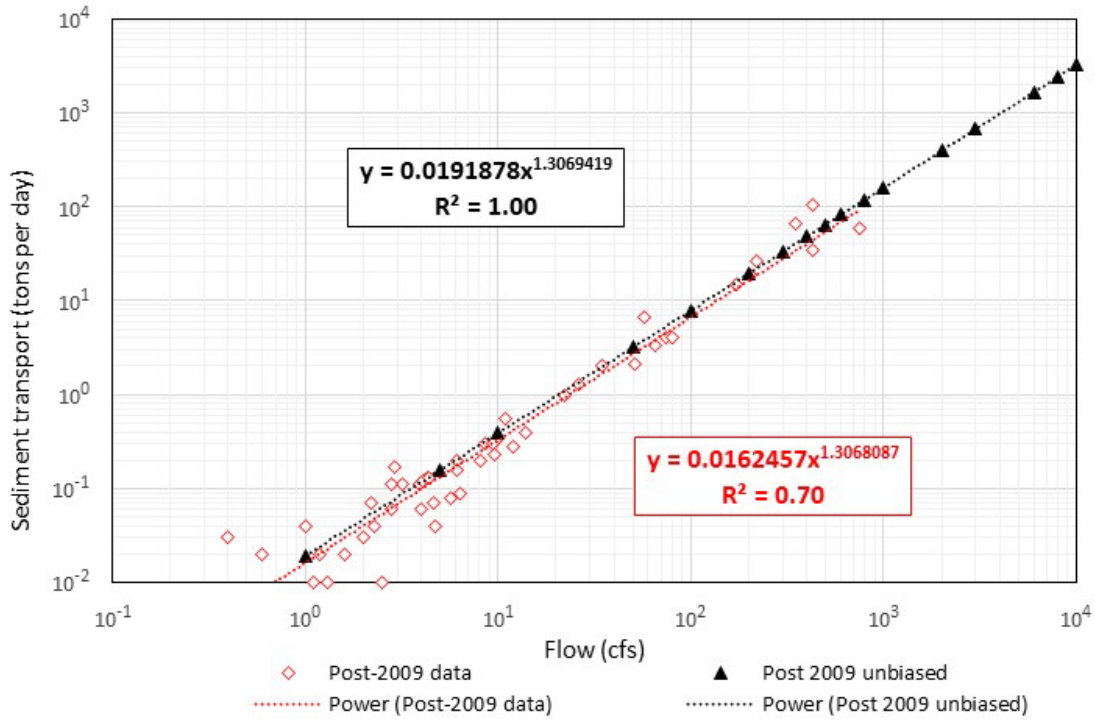

A summary of the sediment rating curves is presented in Table 18.

Table 18
Sediment Transport Rating Curve Equations (Unbiased, Considering Stationarity)

River	Pre-2009	Post-2009
Neosho*	$Q_{ss} = 0.0260390\ Q^{1.5089387}$	$Q_{ss} = 0.0098896\ Q^{1.4986827}$
Tar	$Q_{ss} = 0.3117756\ Q^{1.1433930}$	$Q_{ss} = 0.0191878\ Q^{1.3069419}$
Spring	$Q_{ss} = 0.0026666\ Q^{1.5626948}$	$Q_{ss} = 0.0002641\ Q^{1.7525423}$
Elk	$Q_{ss} = 0.0014031\ Q^{1.8954594}$	$Q_{ss} = 0.0000297\ Q^{2.0175538}$

Note: *Neosho values are pre- and post-1964.

These sediment rating curves were applied to the historical flow data to compute the tonnage of sediment flowing down the rivers and into Grand Lake. They were also applied to the future hydrology to compute the tonnage of sediment for the future scenario.

Summaries of basic flow and water level statistics have been developed, along with corresponding quantities of sediment transported for various time periods of interest using the bias-corrected rating curves considering stationarity. These time periods include 1940 to the beginning of 2009, 2009 through 2019, and future scenarios from 2020 through 2069. For the future scenarios (2020 through 2069), flow and water levels are presented for both anticipated operations and baseline operations (see Section 7 for discussion of anticipated/baseline operations). These summaries provide perspective and comparisons of these key variables between the various time periods.

A summary of flow and WSE averages is presented in Table 19.

Table 19
Summary of Flow and Water Levels

Tributary	1940–2009	2009–2019	2020–2069 Anticipated Operation	2020–2069 Baseline Operation
Neosho River (cfs)	3,818	4,312	4,183	4,183
Tar Creek (cfs)	48	40	55	55
Spring River (cfs)	2,212	2,664	2,526	2,526
Elk River (cfs)	822	953	887	887
Grand Lake Average WSE (feet)	740.95	743.49	742.57	741.65

The tonnage of sediment transported during these various time periods was also computed using the unbiased sediment rating curves and either historical or projected hydrology (Table 20).

Table 20
Summary of Sediment Transport

Tributary	Total Sediment Transport (tons) 1940–2009	Total Sediment Transport (tons) 2009–2019	Total Sediment Transport (tons) 2020–2069
Neosho River	214,264,051	21,144,118	89,616,776
Tar Creek	864,297	19,702	122,593
Spring River	27,464,343	4,088,037	15,866,424
Elk River	57,766,979	1,432,848	3,535,827
Total	**300,359,670**	**26,684,705**	**109,141,619**
No. of years	**69**	**11**	**50**

Table 21 summarizes basic information comparing annual sediment transport for the various time periods of interest.

Table 21
Summary of Annual Sediment Transport

Tributary	Annual Sediment Load (tons/year) 1940–2009	Annual Sediment Load (tons/year) 2009–2019	Annual Sediment Load (tons/year) 2020–2069
Neosho River	3,105,276	1,922,076	1,792,336
Tar Creek	12,526	1,791	2,452
Spring River	398,034	371,640	317,328
Elk River	837,203	1,302,259	70,717
Total	**4,353,039**	**2,425,882**	**2,182,832**

Pursuant to federal law, including the Flood Control Act of 1944 and Section 7612 of the National Defense Authorization Act for 2020, flood control operations at the Project are regulated exclusively by USACE when the reservoir elevation is above 745 feet PD or expected to rise beyond that level.

An analysis of historical data from October 1, 1942 (the first time reservoir elevation data are available), through December 31, 2019, shows that Grand Lake reaches or exceeds elevation 745 feet PD 19.8% of the time. Historical flow data for these periods with a reservoir elevation at or greater than 745 feet PD were segregated, and the sediment rating curves (unbiased, pre/post 1964 for the Neosho River and pre/post 2009 for the Spring River, Elk River, and Tar Creek) were applied to these segregated flow data. The resulting tonnage of sediment delivered to the reservoir when the reservoir was at or above 745 feet PD was compared to the total tonnage of sediment delivered for the entire time period. Table 22 presents the results of this analysis for each stream and for the overall total sediment percentage.

Table 22
Percentage of Sediment Delivered to Grand Lake: Above and Below Water Level 745 feet PD

River	Percentage of sediment delivered >745 feet PD	Percentage of sediment delivered < 745 feet PD
Neosho River	75.1	24.9
Tar Creek	63.2	36.8
Spring River	80.0	20.0
Elk River	75.4	24.6
Total	75.6	24.4

When the reservoir elevation is greater than 745 feet, which only occurs 19.8% of the time, 75.6% of the sediment load is delivered to the reservoir. Under normal operating conditions, which occurs 80.2% of the time, 24.4% of the total sediment load is delivered to the reservoir.

4.4 Sediment Density

Generally, the density of sediment is lower for fine material such as silt and clay and higher for the coarser sand and gravel. In Lane and Koelzer (1943), data were presented regarding the density of sediment deposits in reservoirs. Vanoni (2006) also discusses reservoir sediment density. This study compiled data from a wide variety of sources in the United States as well as Europe and Asia. For reservoirs in Texas, the data showed that for finer silt at the head of reservoirs, the density averaged 82 pcf. In the middle reach of reservoirs, the density was 55 pcf, and for finer material farther downstream that was continually submerged the density was 31 pcf. Deposited sediment in the Missouri River basin ranged from 25.2 to 116 pcf, with a corresponding sand content ranging from 4.9% to 93.5%. The sediment density in a European reservoir ranged from 21.6 to 87.2 pcf, depending on the depth of the sample, which ranged from 1 to 20 meters. Sediment traps in this reservoir showed surface layer deposits ranged from 13.7 to 29.4 pcf. The Soil Conservation Service reported 318 samples of sediment density with a sediment density range of 20.1 to 101.7 pcf. The average density for submerged deposits of fine material for 210 samples was 44 pcf. Vanoni (2006) states the following:

> A determination of unit weight which should be used for reservoir sediment in any case is a complicated problem involving a number of variables. Among them are the manner in which the reservoir will be operated, the size of the sediment particles, the rate of compaction of the sediment, and perhaps other factors.

Lane and Koelzer (1943) presents a figure relating the unit weight of sediment to the percent of sand in the deposit (Figure 95).

Figure 95
Relation of Unit Weight of Deposited Sediments to Percent of Sand

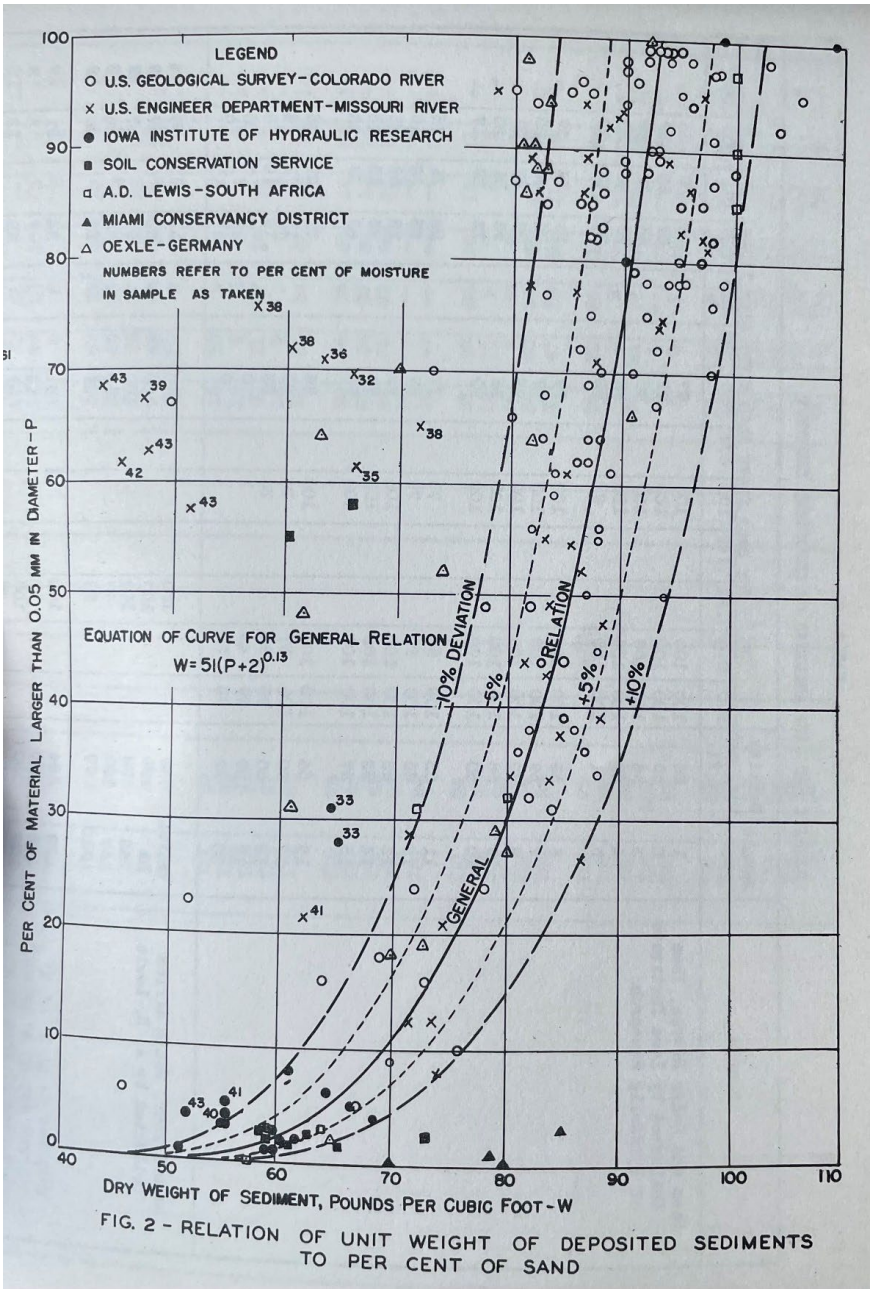

Source: Lane and Koelzer (1943)

The particle size distribution data from the recent core samples collected in 2022 are summarized in Exhibit 6.

The laboratory that conducted the particle size distribution analysis uses the U.S. Department of Agriculture (USDA) soil classification and size classification. The size breakdown between clay, silt, and sand is shown in Figure 96 from the *Engineering Field Manual* (USDA 1990).

Figure 96
Relationship between Particle Size and the USDA Textural Soil Classes, the Unified Soil Classification System, and the AASHTO Soil Classes

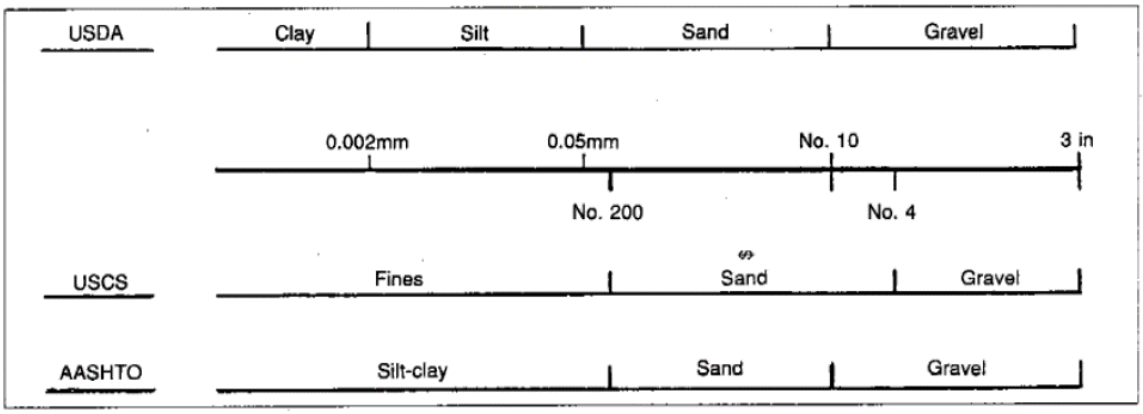

Table 23 presents the breakdown between clay, silt, and sand based on USDA classification.

Table 23
Sediment Type and Size Range

Sediment Type	Sediment Size (mm)
Clay	<0.002
Silt	0.002–0.05
Sand	0.05–2

4.5 Quantitative Analysis of Bathymetric Change Related to Hydraulic Shear Stress

The quantitative analysis of sediment transport consists of using the basic data and quantitative tools to analyze the hydrology, hydraulics, and resulting effect on sedimentation in Grand Lake. This analysis uses the historical bathymetric data combined with the hydraulic analysis of historical flows and reservoir operation to develop a relationship between hydraulic shear stress and sedimentation pattern. Hydraulic shear stress is the driving force behind the transport and deposition of sediment. Hydraulic shear stress is the basic variable used in many sediment transport equations for both

cohesive and non-cohesive sediments to determine whether sediment is eroded or deposited, and the rate at which sediment is transported.

There are two steps in developing a relationship between sediment transport (and associated sedimentation patterns) and hydraulic shear stress. The first step is to run HEC-RAS to calculate hydraulic shear stresses. This step uses the hydraulically calibrated HEC-RAS model over the historical periods of available channel geometry/bathymetric data and hydrologic data of streamflow and historical water levels in the reservoir. The geometry remains fixed based on the surveyed geometry over the time periods utilized. The second step is to determine the pattern of sedimentation based on historical bathymetric surveys. The actual sets of data utilized to compute volume change and pattern of sedimentation are the HEC-RAS input data in the same hydraulic model for the available surveys. Using these two sets of information, the relationship between hydraulic shear stress and sedimentation can then be developed.

It should be noted that the STM itself uses the same data but attempts to simulate the interaction between hydrology, hydraulics, and sedimentation by using upstream sediment input (based on regression analyses of suspended sediment transport data and associated sediment rating curves), bed material particle size distribution data, a standard sediment transport equation (for non-cohesive sediment) available in HEC-RAS, and erosion characteristics of the cohesive sediment (which is the dominant sediment being transported to Grand Lake through the tributaries). The model is run for a given time period starting with the circa-1940 geometry to calibrate parameters in the model such that the computed channel geometry and bathymetry reasonably match the surveyed channel geometry and bathymetry in 2009 at the end of the calibration period. The model is then extended to evaluate whether the results reasonably reproduce the 2019 geometry as a validation process. If the model can be reasonably calibrated and validated, then it can be utilized to predict the future sedimentation patterns for a range of operation and hydrologic scenarios. As noted in the ISR, this is an extremely complicated process given the complex relationship between hydraulic shear stress and the wide variations (five orders of magnitude) in erosion parameters and considerable variability of sediment density, both of which vary with depth below the surface of the sediment column and with time because cohesive sediments consolidate and strengthen with time.

An advantage of the quantitative analysis is that the approach directly utilizes the change in bathymetric data as input to develop relationships between hydraulic shear and sedimentation pattern. In contrast, the STM calibration/verification process attempts to simulate the sedimentation pattern by judicious selection of erosion and related sedimentation parameters in the model (i.e., engineering judgment), with the objective of reasonably matching the change in bathymetric data. In other words, the quantitative analysis process uses the change in bathymetric data as input and the hydraulic shear stresses computed from the fixed-bed model, whereas the STM uses a range of parameters to attempt to match the change in bathymetric data using the hydraulic shear stresses

computed from the movable bed model. If the STM could perfectly simulate the complex interaction between erosion parameters and hydraulic shear, it would achieve essentially the same results as the quantitative analysis approach. This is because successful calibration of the STM means that the model reasonably matches the change in bathymetry. The quantitative analysis directly uses this change in bathymetry to develop a relationship between hydraulic shear and sedimentation.

The first step in the quantitative analysis is to determine the hydraulic shear stresses through hydraulic modeling. The STM was modified for the quantitative analysis by setting pass-through nodes (which pass sediment through each cross section without allowing any sediment deposition) at all cross sections as well as not allowing any erosion of the bed, thereby keeping the 2009 channel geometry the same through the entire run to compute the hydraulic conditions from 2009 to 2019. As described in Section 2.6 of the USP, at a number of cross sections (spaced approximately 5 miles apart except more closely spaced over the delta feature), the hydraulic results were analyzed statistically and summarized. These data (maximum and average hydraulic shear stress) were plotted (Figure 97) as a function of longitudinal location (RM).

Figure 97
Hydraulic Shear Stress Profile of Neosho River, 2009 Geometry, 2009–2019 Historical Flows and Operation

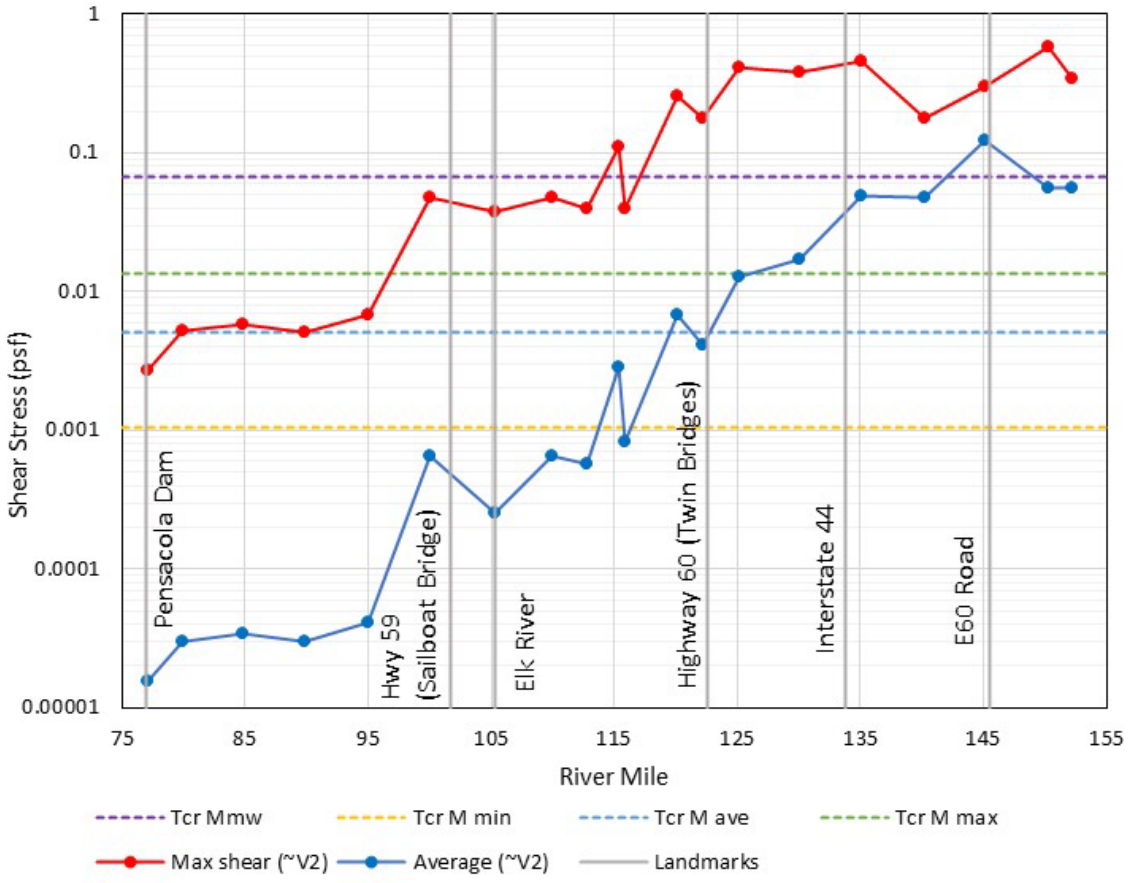

Notes:

Tcr Mmw	Critical shear stress for mass wasting
Tcr M min	Minimum critical shear stress for particle erosion across all samples
Tcr M ave	Average critical shear stress for particle erosion across all samples
Tcr M max	Maximum critical shear stress for particle erosion across all samples
Max shear (~V2)	Maximum modeled bed shear stress, proportional to velocity^2
Average (~V2)	Average modeled bed shear stress, proportional to velocity^2

HEC-RAS (USACE 2016) utilizes a default relationship to compute shear stress for the sediment transport equations as shown in Equation 2.

Equation 2

$\tau = \gamma dS$

where:

τ	=	bed shear stress
γ	=	specific weight of water
d	=	water depth
S	=	energy grade slope

Where depths are large, such as in the case of a reservoir, this can overestimate shear stress. Another way of computing shear stress is shown in Equation 3:

Equation 3

$\tau = \frac{1}{8}\rho f V^2$

where:

τ	=	bed shear stress
ϱ	=	specific weight of water/acceleration of gravity
f	=	Darcy-Weisbach friction factor
V	=	water velocity

The shear stress computed by Y d S was compared to 1/8 ϱ f V^2. This analysis showed that in the lower part of the reservoir, the shear stress using Y d S is significantly different than shear stress using 1/8 ϱ f V^2. For purposes of this analysis, the approach for computing hydraulic shear stress is the velocity method.

The shear stress generally decreases in the downstream direction as depths and cross-sectional area of the flow increases as it flows into the reservoir. As a point of reference (although not used in this component of the analysis), Figure 97 includes the values of critical shear stress at the surface of the sediment column developed from the SEDflume data and laboratory analysis.

The next component of the analysis is to use the sedimentation pattern that historically occurred based on the change in bathymetric data. Figure 98 presents the percentage of sediment by volume passing each cross section. The volumes were computed directly from the HEC-RAS geometry data

using the average end area method from one cross section to the next and the distance by RM between sections.

Figure 98
Cumulative Percentage Sediment Passing by Volume 2009–2019

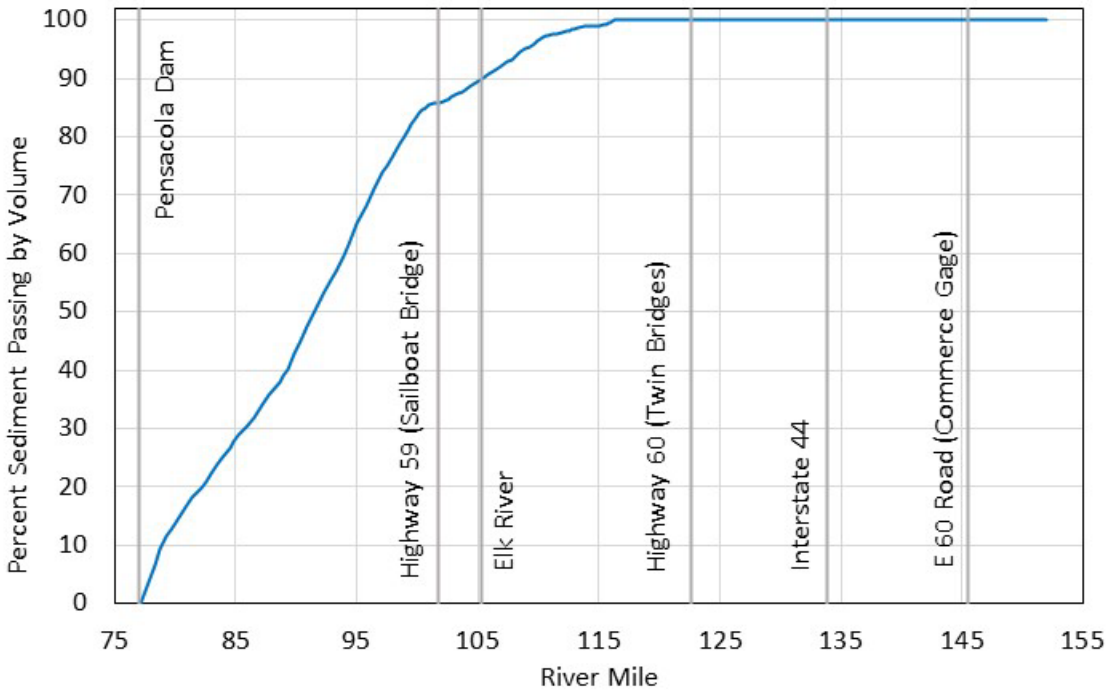

Note that the location where the percentage of sediment passing begins to drop below 100% is at approximately RM 116. At this location, the average hydraulic shear stress is approximately equal to the minimum critical shear stress for the surface layer of cohesive sediment from the SEDflume laboratory analysis.

These two sets of information were then combined to develop a relationship between hydraulic shear stress and the percentage of sediment passing downstream with the 2009 geometry (Figure 99).

Figure 99
Percentage of Volume Passing vs. Shear Stress on Neosho River, 2009 Geometry

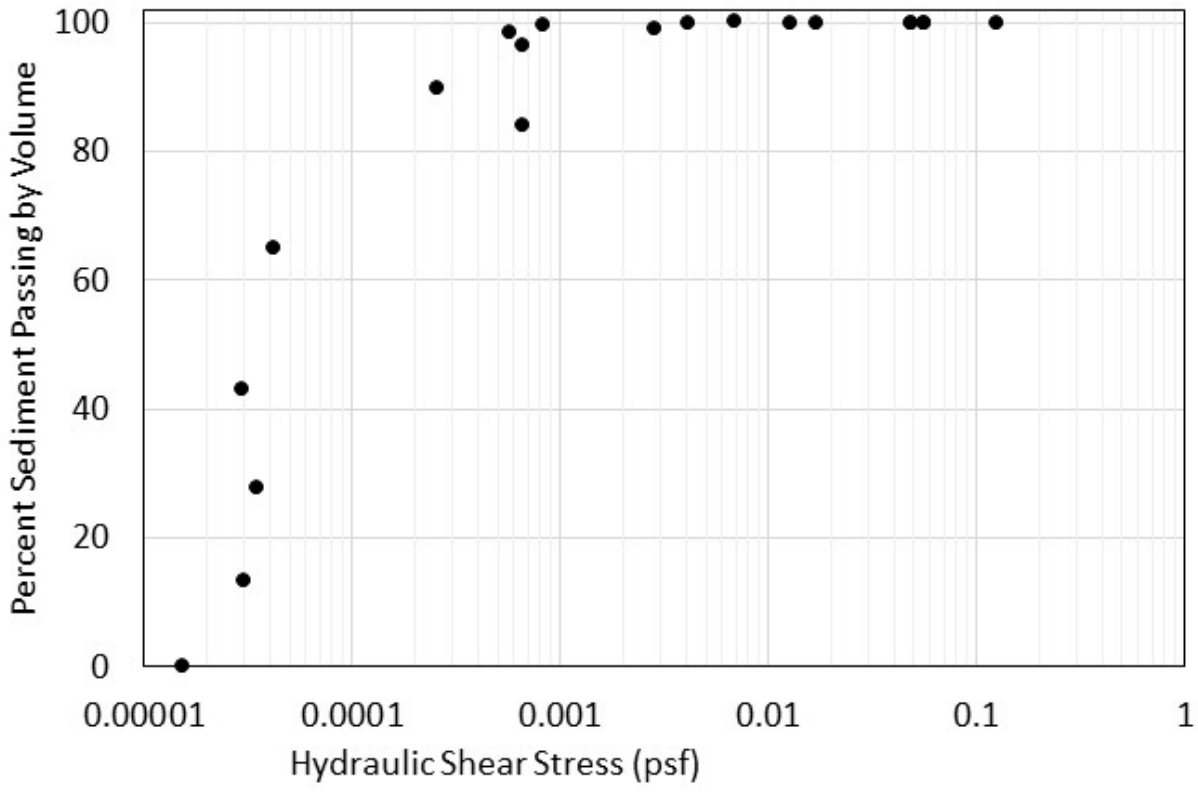

Figure 99 clearly demonstrates that there is a relationship between hydraulic shear stress and sedimentation pattern. To bracket this relationship developed between hydraulic shear stress and sedimentation that occurred between 2009 and 2019, the same information was developed based on applying HEC-RAS using 2019 geometry and the sedimentation that occurred during this time period (Figure 100).

Figure 100
Percentage of Volume Passing vs. Shear Stress on Neosho River, Comparison of 2009 Geometry and 2019 Geometry

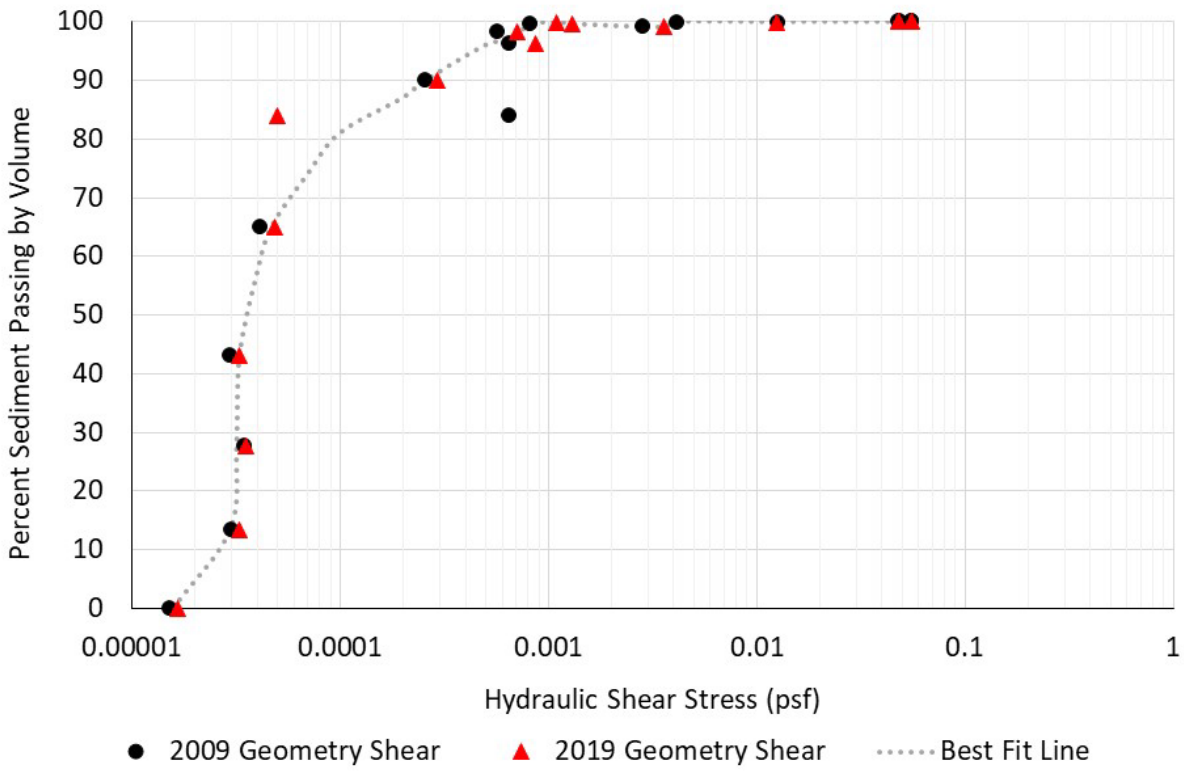

The best fit line above correlates to the values shown in Table 24.

Table 24
Relationship between Shear Stress and Percent Sediment Passing by Volume

Shear Stress (lb/ft^2)	Percent Volume Passing (%)
1.59E-05	1.64E-06
2.99E-05	13.48
3.20E-05	27.71
3.30E-05	43.00
4.00E-05	57.00
4.70E-05	65.03
7.00E-05	74.00
1.00E-04	81.00

Shear Stress (lb/ft^2)	Percent Volume Passing (%)
2.00E-04	87.00
2.56E-04	89.93
5.00E-04	96.00
6.54E-04	97.00
8.22E-04	99.50
1.10E-03	99.96
1.31E-03	99.61
2.84E-03	99.12
3.58E-03	99.12
4.14E-03	99.96
6.63E-03	100.04
6.87E-03	100.04
1.24E-02	99.96
1.67E-02	100.00
4.88E-02	100.00
5.55E-02	100.00
5.56E-02	100.00

Using the 2009 or 2019 hydraulics that bracket the 2009 to 2019 change in sedimentation pattern produces essentially the same resulting relationship between hydraulic shear and sedimentation. This lends some confidence in using this relationship to predict future patterns of sedimentation, based on different scenarios of flow and reservoir operations by computing the hydraulics through fixed-bed HEC-RAS simulation for alternative scenarios and then applying the relationship to develop alternative future sedimentation patterns. This is similar to considering the reservoir as a full-scale physical model and developing relationships from the data and analysis to make predictions.

With this relationship based on data and hydraulic analysis (using the hydraulically calibrated HEC-RAS model), the fixed-bed HEC-RAS model was then run using the anticipated reservoir operation and future flow scenario (see Section 7). HEC-RAS produces the longitudinal hydraulic shear distribution under the anticipated operation and future flow scenario. This hydraulic shear distribution is then applied to the above relationship between hydraulic shear and the percentage of sediment passing. From this, the percentage of sediment passing based on hydraulic shear is then related back to location along the profile because the locations where the various hydraulic shear stresses are known are from the output of HEC-RAS.

4.5.1 Future Scenarios

To quantify the effect of future flow and operation scenarios on sedimentation, the hydraulic shear stresses were calculated using the fixed-bed HEC-RAS model for anticipated and baseline operation scenarios using a 50-year period of flow as described in Section 7.1.1. The basic statistics of average flow and water level for these flow and operation scenarios are summarized in Table 25, along with the 1940 to 2009 and 2009 to 2019 historical data for comparison.

Table 25
Average Discharge and WSE at Pensacola Dam for Future Scenario

Tributary	1940–2009	2009–2019	2020–2069 Anticipated	2020–2069 Baseline
Neosho River (cfs)	3818	4312	4183	4183
Tar Creek (cfs)	48	40	55	55
Spring River (cfs)	2212	2664	2526	2526
Elk River (cfs)	822	953	887	887
WSE (feet PD)	740.95	743.49	742.57	741.65

The average hydraulic shear stress for the anticipated operation and baseline operation 50-year scenarios is shown in Figure 101 (also compared to the run using 2019 geometry and 2009 to 2019 historical flows and operation). Note that all three scenarios produce similar results with the future flows, with "baseline operation" resulting in slightly higher shear stresses (by 13%) than the "anticipated operation" due to the lower average water level.

Figure 101
Average Hydraulic Shear Stress Profile on Neosho River during Future Scenario

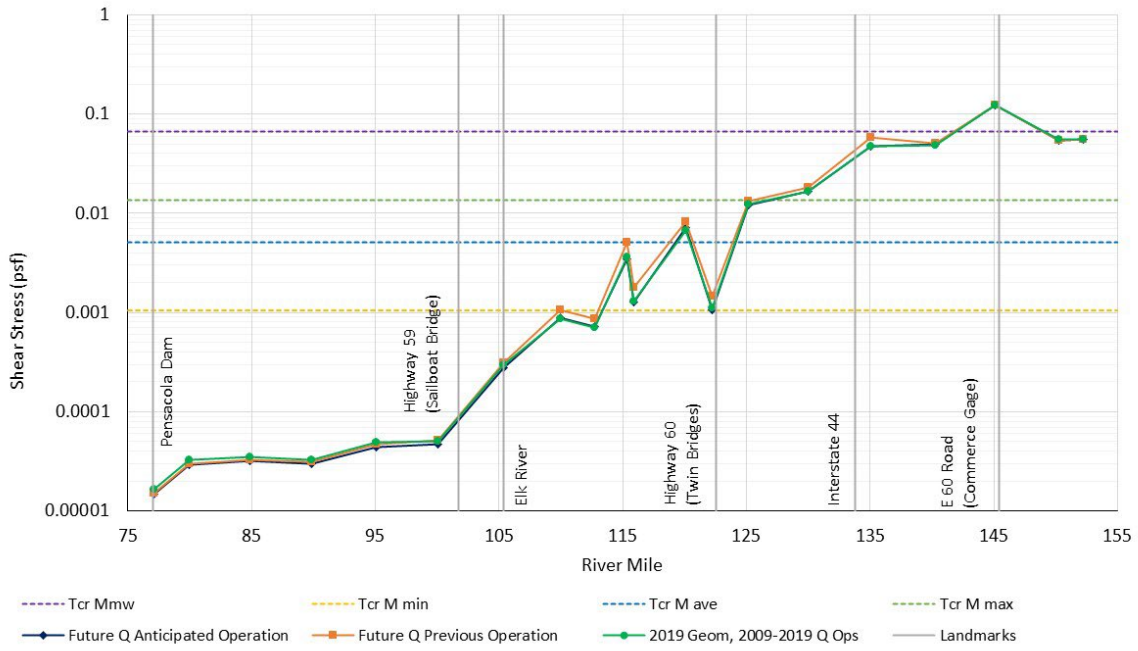

Notes:	Tcr Mmw	Critical shear stress for mass wasting
	Tcr M min	Minimum critical shear stress for particle erosion across all samples
	Tcr M ave	Average critical shear stress for particle erosion across all samples
	Tcr M max	Maximum critical shear stress for particle erosion across all samples
	Future Q Anticipated Operation	Future flows under *Anticipated Operations*
	Future Q Baseline Operation	Future flows under *Baseline Operations*
	2019 Geom, 2009-2019 Q Ops	2009-2019 historical flows and reservoir operations

The hydraulic shear stress from the 2020 to 2069 hydrology with the anticipated and baseline operations were then utilized to develop the percent sediment passing graph. These values were then correlated back to the location along the river profile. This results in the graph shown in Figure 102 (with the previously developed relationship based on change in bathymetric data for comparison).

Figure 102
Cumulative Percentage of Sediment Passing by Volume for Future Scenario

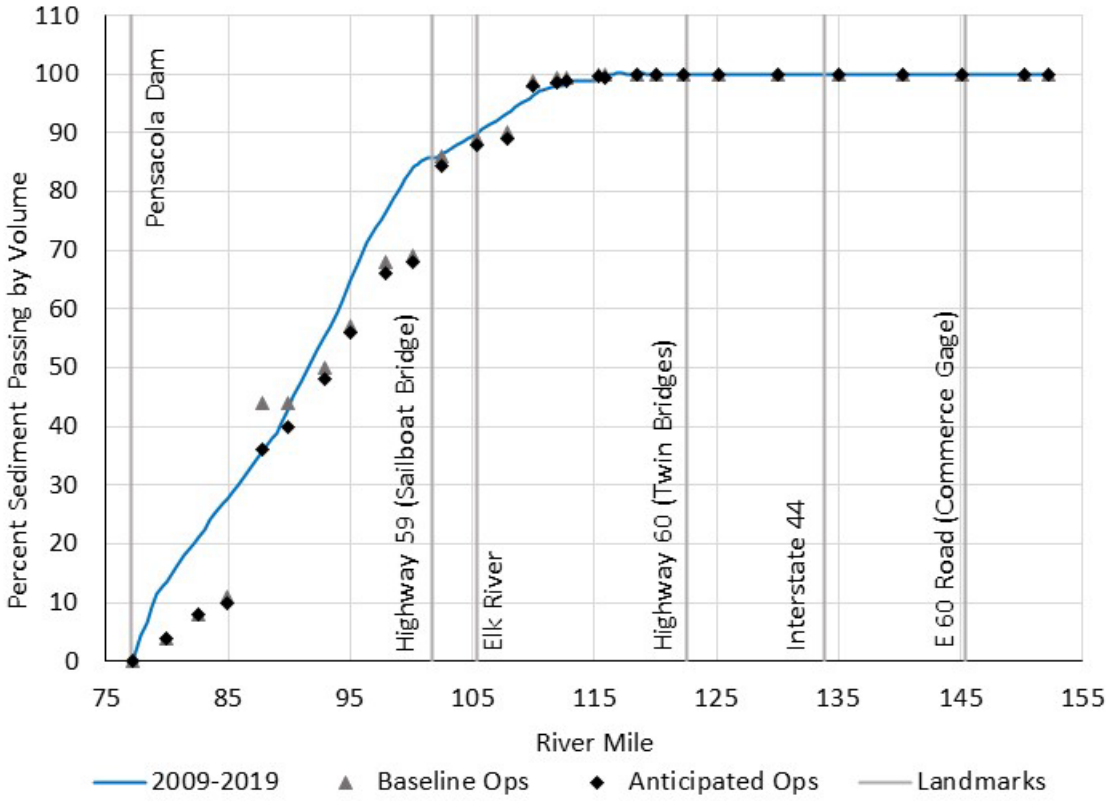

Based on these computed points of percent passing along the profile through the reservoir and the surface area between the cross sections, coupled with the density of sediment, the corresponding vertical deposition of sediment was estimated for the future 50-year scenarios.

Based on the longitudinal distribution of the percentage of sediment passing cross sections along the river/reservoir profile, the average change in bed elevation due to sediment deposition was calculated along this profile. The tonnage of the incoming sediment load was calculated using the 2020 to 2069 hydrology and the sediment rating curves (unbiased post-1964 for the Neosho River and unbiased post-2009 for the Spring and Elk rivers and Tar Creek). To compute the depth of deposition requires conversion of the tonnage of sediment to volume and then to depth of sediment deposition. Sediment tonnage was then converted to volume using the density or specific weight of the sediment deposit as discussed in the next paragraph. The depth of sediment deposition was then computed by dividing the volume by the surface area over which the sediment is deposited.

Some specific weight data were collected in the upper layers of the sediment deposit as part of the SEDflume data collection program. These data showed that the upper layer (approximately 1 foot) of the sediment deposit ranged from 21.2 to 103 pcf and averaged 52.7 pcf. Although no actual data exist to quantify the specific weight below the surface layer, sediment size distribution data from the core sample dataset show that the sediment deposition in the delta feature region consists primarily of silt and clay (89%) and an average of 11% sand (using the USDA definition of sand being <0.05 mm). This information, combined with the relationship developed by Lane and Koelzer (1943), results in a range of specific weights ranging from 63 to 78 pcf and averaging 70 pcf. The specific weight utilized in the STM (Section 6.2.2) was 58 pcf. Both values are plausible and generally fit within the range of values either found in the sampling of Grand Lake (see Section 2.3.3) or from the analysis of other reservoirs as shown by Lane and Koelzer (1943).

The first level of analysis is to use the tonnage of sediment coming into the reservoir based on the 2020 to 2069 hydrology and sediment rating curves spread uniformly over the surface area of the reservoir (45,000 acres) at an average density of 70 pcf. This results in an average depth of sediment deposition of 1.59 feet over this 50-year time period. Although this basic calculation provides some perspective on the quantity of sediment in terms of depth of deposition, the next step is to distribute this sediment based on the information generated from the longitudinal distribution of hydraulic shear for this 50-year time period and the relationship between hydraulic shear and percentage of sediment passing cross sections along the river/reservoir. Results of this analysis using the percentage passing each location and the surface area of the reservoir, coupled with average density of 70 (58) pcf, and incoming sediment load over the 50-year time period of 109,141,619 tons were plotted along the longitudinal profile from RM 122.25 to RM 77.12 for both future scenarios (Figure 103) showing average bed elevation change and Figure 104 showing volume change). The analysis assumes sediment from the various tributaries comes into the Neosho River rather than subtracting the Elk River component and only including this sediment at the confluence. This compensates to some degree for the fact that approximately 10% of the drainage area is not accounted for in terms of flow and sediment input which, in turn, is counteracted by the fact that the sediment trapping efficiency is somewhat less than 100%. These relatively small percent differences being on the order of 10% or less is well within the scatter exhibited by the sediment transport data and the measurement errors in the flow data.

The quantitative analysis shows very little sediment deposition, with even some scour, down to approximately RM 115. The analysis shows approximately 2 feet (2.6 feet at 58 pcf) of deposition between RM 115 and RM 112.75. This is in an area of relatively lower bed profile between the two higher points at RM 115 and RM 112.75 shown on the thalweg profile. Between RM 112.75 and RM 110, the analysis shows some scour. The quantitative analysis shows no significant rise of the existing high point of the delta as indicated in the 2009 and 2019 bathymetric surveys. Downstream of RM 110, more significant sediment deposition occurs, but the analysis shows some oscillations

between sedimentation and scour. This analysis shows minimal sedimentation on the top surface of the delta feature (with some deposition being indicated in the low area between the two existing high points on the thalweg profile). The bulk of the sediment delivered to the reservoir deposits on the lower face of the delta downstream of RM 110. This is consistent with the progression of delta formation in the scientific literature (Figure 105 and Figure 106), where the downstream face of the delta progressively builds in the downstream direction on the foreset slope.

Figure 103
Average Bed Elevation Change 2020–2069 (70 pcf Sediment Density)

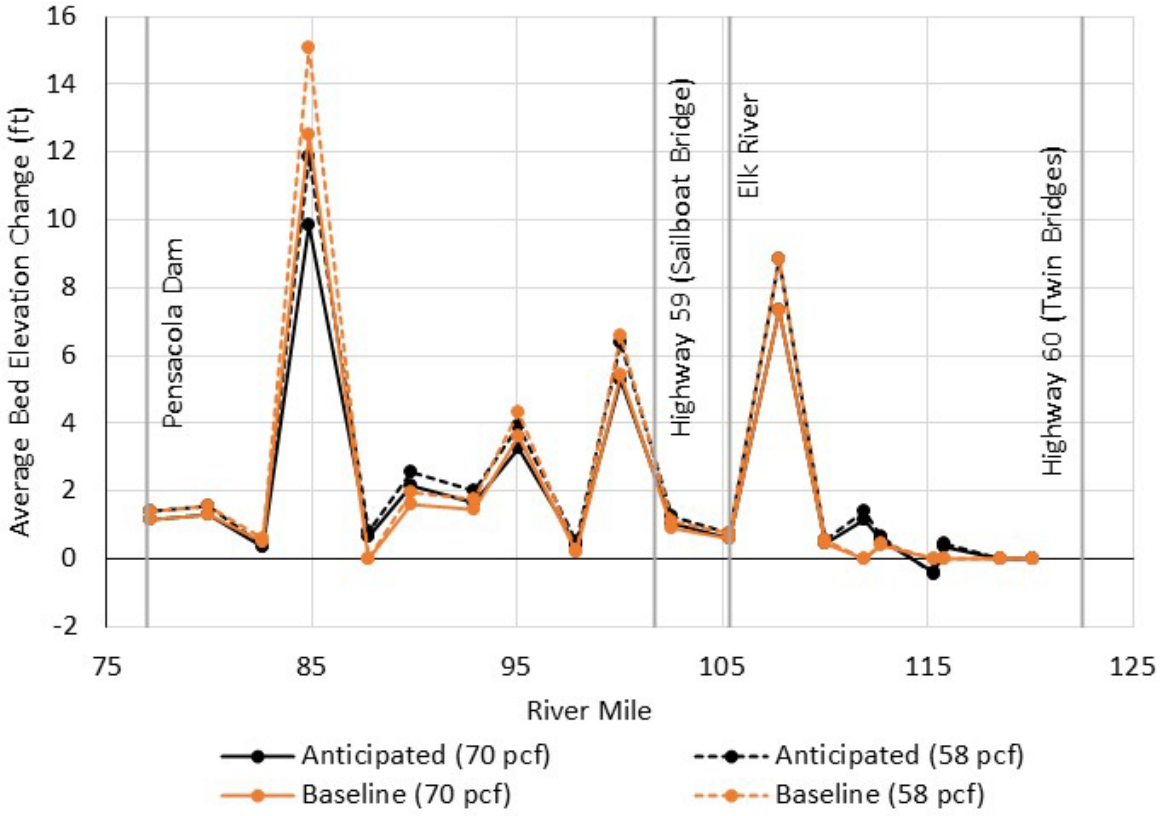

Notes: RM 85 is approximately 1.1 miles upstream of the Drowning Creek confluence.

Figure 104
Average Bed Volume Change 2020–2069

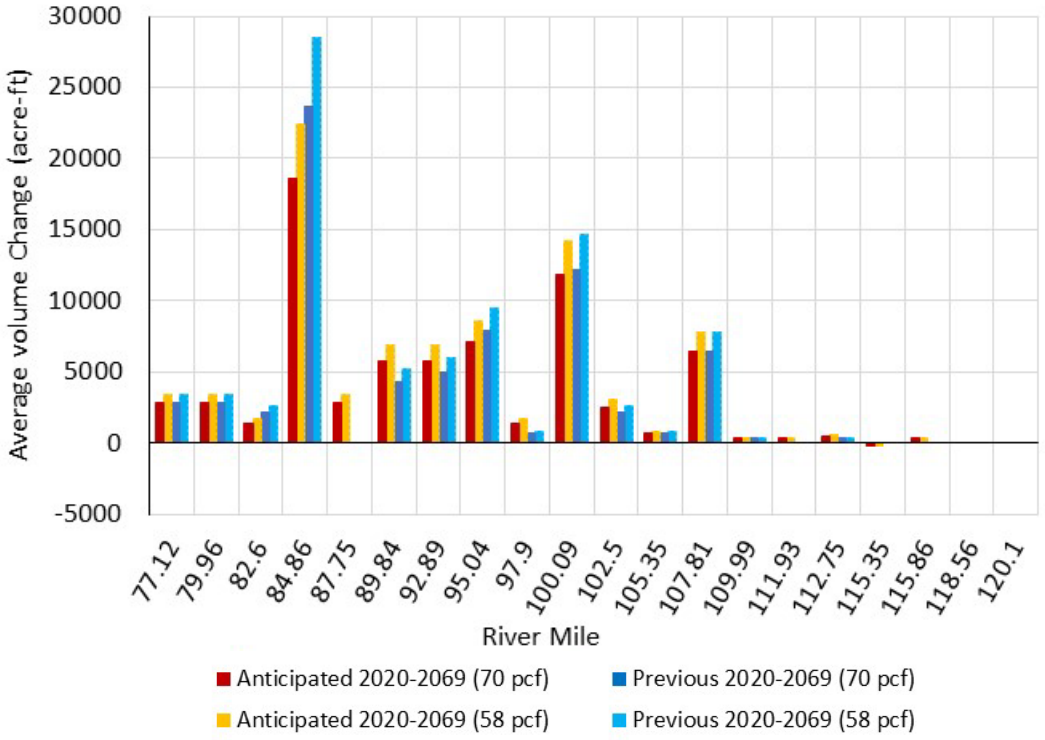

Figure 105
Profile of Typical Reservoir Delta

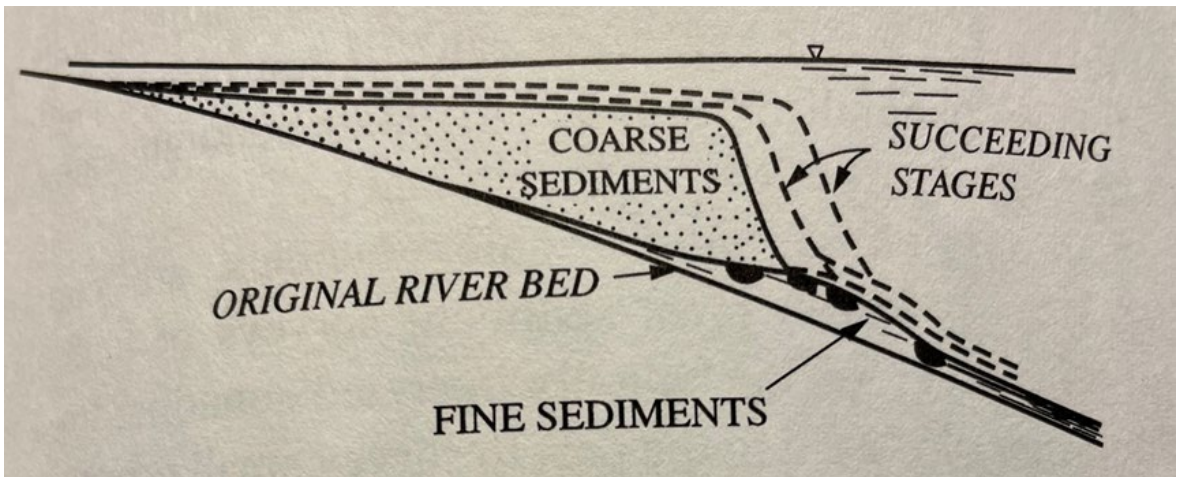

Source: Figure 3.30, Vanoni (2006)

Figure 106
Reservoir Delta Form

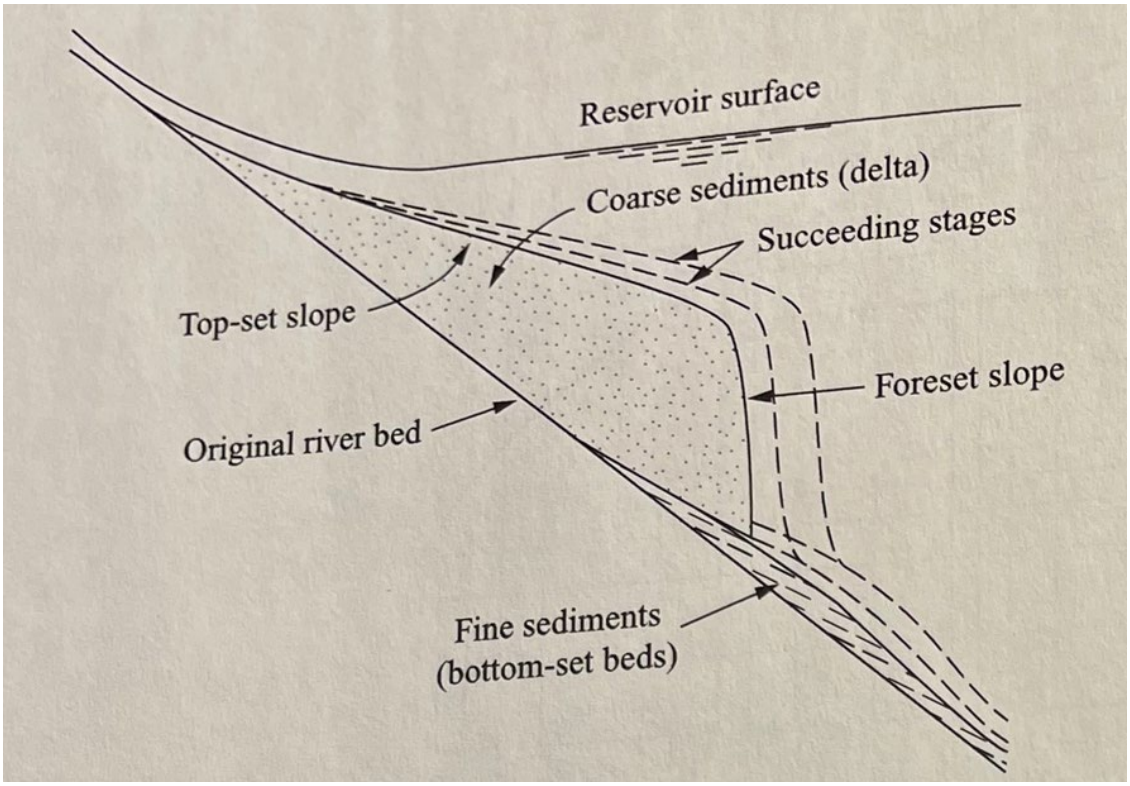

Source: Figure 5.44, Vanoni (2006)

Again, one of the key conclusions is that because the vast majority of the sediment being transported down these rivers and into the reservoir consists of silt- and clay-sized materials (with very little sand or coarser material), this sediment is primarily depositing 35 miles downstream from the upper end of the reservoir (most sedimentation in the future flow and operation scenarios is quantified to be occurring downstream of RM 110).

As discussed in Section 3, there are multiple factors contributing to the delta feature and its location within the study area. The Ozark Uplift formation, confluence of the Spring River, and the confined upstream channels all play a role in the location and elevation of the delta feature.

Furthermore, the delta feature is currently in dynamic equilibrium, with all available evidence suggesting that deposition on the crest during low flows is washed further downstream during high flows. Dynamic equilibrium, in engineering terms regarding sedimentation, occurs when the bed experiences relatively minor fluctuations about a mean bed elevation with no significant long-term trend.

The long-term growth of the feature is expected to be on the downstream face, where it will affect storage volume. Its presence and predicted future evolution do not provide evidence that future upstream water levels will significantly increase due to sedimentation.

Regardless of that fact, it is also relevant to note that the USACE dictates Project operations whenever WSE at the dam is above 745 feet PD or expected to rise above that level. GRDA has no control over the incoming streamflow, nor do they even control dam operations during the largest events. As shown in the analysis of sediment inflow at or above 745 feet PD, which only occurs 19.8% of the time, delivers 75.6% of the incoming sediment load to the reservoir. This sediment inflow is a result of upstream erosion and sediment transport over which the Project has no control and most of the sediment is delivered to the reservoir when USACE is in operational control of Grand Lake.

4.6 Trapping Efficiency

Several methods have been developed to estimate the sediment trapping efficiency, which are typically based on such factors as the inflow rate compared to storage capacity and residence time of water in the reservoir. These relationships were developed based on data from several reservoirs for which such data exist.

A significant set of data exists on sediment trapping efficiency of a major reservoir on the Neosho River, the John Redmond Reservoir located upstream of Grand Lake. Data have been collected for a considerable time that include the volume of sediment deposited as well as the incoming sediment load and release of sediment downstream of the dam. This set of data is more extensive and complete than most datasets used in the development of the typical sediment trapping efficiency relationship. It is also noteworthy that these data were collected on the river with the greatest sediment load (Neosho River) that contributes to Grand Lake.

John Redmond Reservoir is primarily a flood control reservoir with a relatively small conservation pool and a large flood control pool above the conservation pool. The conservation pool provides 50,501 acre-feet of storage and the flood control pool provides 524,417 acre-feet of storage (Engineering-Environmental Management, Inc. 2013).

The top of the conservation pool is at elevation 1,039 feet above the National Geodetic Vertical Datum of 1929 (NGVD29) and the top of the flood control pool is at elevation 1,068 feet NGVD29. The reservoir covers 29,800 acres and the length of the reservoir is approximately 4.5 miles from where water enters the reservoir to the dam. A source of information on the studies of reservoir sedimentation in John Redmond Reservoir is found in a 2021 USGS report (Kramer et al. 2021). The following information is summarized from this report.

The drainage area contributing to John Redmond Reservoir is 3,015 square miles and has a storage capacity of 816,795 acre-feet.

During years with a complete data record at Neosho Rapids and Burlington (2010, 2014 to 2019), the trapping efficiency of the reservoir ranged from 82% to 94% (mean: 89%).

Different reservoir outflow management strategies, including operating near normal capacity as opposed to higher flood pool levels, could reduce the total reservoir storage lost by 3% (approximately 261 acre-feet).

Grand Lake is significantly larger than John Redmond Reservoir. Grand Lake is approximately 68 miles long and the storage capacity is approximately 1.44 million acre-feet (at elevation 745 feet PD). Being significantly longer and with a larger storage capacity, it is likely that the sediment trapping efficiency of Grand Lake is greater than that of John Redmond Reservoir. Because the sediment trapping efficiency of John Redmond Reservoir averages 89% (with a range of 82% to 94% over recent years), the sediment trapping efficiency of Grand Lake is well into the 90%-plus range, if not approaching the high 90% range. A review of aerial images shows some clear water released from Pensacola Dam at relatively high flows (with quite turbid water flowing into the reservoir), but on other images some turbid water is being released through the dam. This suggests that under some circumstances the sediment trapping efficiency is not 100%. Based on the comparison with John Redmond Reservoir, which recently averaged 89%, again it is likely that the sediment trapping efficiency of Grand Lake is in the high 90% range based on these comparisons and observations.

Regarding the effect of operations on flushing sediment through John Redmond Reservoir, the USGS study found that operating John Redmond Reservoir at an elevation of 1,039 feet NGVD29 (which is the top of the conservation pool) was 3% more effective in reducing storage loss than operating the reservoir "to higher flood pool" levels (top of flood pool is 1,068 feet NGVD29). So, a reduction in water level of up to 29 feet only produced a 3% reduction in sediment trapping. This was determined by continuous water quality monitoring coupled with a two-dimensional (2D) hydrodynamic model (CE-QUAL-W2) to evaluate sediment trapping reduction by altering reservoir operations. The specific study (Lee and Foster 2013) as summarized in Kramer et al. (2021) concluded that "The idealized alternative outflow management scenario was projected to reduce sediment trapping in the reservoir by about 3 percent."

Given that Grand Lake is significantly larger and operates the conservation pool at a range of 3 feet, lowering the water level only a few feet will not produce significant benefits in terms of sediment trapping.

Based on the quantity of sediment computed using the sediment transport rating curves over the 50-year future scenario, approximately 109 million tons of sediment are delivered to Grand Lake. This converts to a volume of 71,587 acre-feet at 70 pcf and 86,398 acre-feet at 58 pcf (assuming a 100% sediment trapping efficiency). This volume of sediment resulting in storage loss to the reservoir would be distributed according to the results of the hydraulic shear stress analysis for the anticipated

(or baseline) operations as shown in Figure 95. This figure shows that no sediment is deposited upstream of RM 116, approximately 10% of the sediment is deposited between RM 116 and RM 105 (Elk River confluence), approximately 22% is deposited between RM 105 and RM 100, and the remaining 68% is deposited between RM 100 and the dam.

4.7 Summary and Conclusions of Quantitative Analysis

The quantitative analysis developed a relationship between hydraulic shear stress and the pattern of sedimentation specifically in terms of the percent of sediment passing each cross section based on the change in historical bathymetry using historical flows and operation.

The quantitative analysis of the future 50 years of hydrology and operation shows no significant sediment deposition on top of the delta feature that would adversely affect existing hydraulic control in upstream reaches. Most of the sediment delivered to the reservoir is transported past the top of the delta feature, farther downstream to the downstream face of the feature. Approximately 98% to 99% of the incoming sediment load is transported past RM 110. The future flows with baseline operations cause slightly reduced deposition on the downstream face of the delta feature and shift the deposition slightly downstream compared to the anticipated operation. This comparison of computed sediment deposition pattern demonstrates the very small effect on sedimentation of operating the reservoir according to baseline operations.

The average hydraulic shear stress for future flow conditions remains greater than the minimum critical shear stress determined by the SEDFlume analysis down to approximately RM 110. Sedimentation downstream of RM 110 is in the reach of the reservoir that is several feet below the highest elevation of the delta feature, which occurs farther upstream at approximately RM 116. For example, the predicted elevation of the delta feature with an average of 3 to 4 feet of deposition after 50 years reaches an elevation of approximately 724 feet PD. The highest elevation in the delta feature based on the 2019 data, which occurs at approximately RM 116 (approximately elevation 729 feet PD), remains without significant aggradation at that location after 50 years. The quantitative analysis demonstrates that the top surface of the delta feature is in a state of dynamic equilibrium. This state of dynamic equilibrium is consistent with the fact that the average shear stress over the top of the delta feature is generally equal to or greater than the minimum critical shear from the SEDflume analysis. In addition, considering that much of the sediment passing through this area continues farther downstream being in a state of fluid mud, rather than actual stationary deposition as discussed in the scientific literature, this further suggests a state of dynamic equilibrium of the top of the delta feature.

With this pattern of predicted sediment deposition, located downstream of the high point on the delta feature and at an elevation several feet below this high point, it cannot reasonably be expected to adversely affect upstream hydraulics and flooding. Based on the relatively small change in

effectiveness of moving sediment downstream with the comparison between the future flows with anticipated operation and baseline operation, as well as the USGS analysis of the effect of significant changes in water level resulting in very limited changes in sediment storage in John Redmond Reservoir, there is no basis to conclude that there would be any significant benefit in continuing to operate Grand Lake as it has been under baseline conditions or at lower levels.

Bathymetric data from 1940 to 2009 show the development of the delta feature. Again, as discussed in Section 3, there are multiple factors contributing to the location and size of the delta feature. It is located on the Ozark Uplift, which slows water and increases deposition. The steeper Spring River contributes additional sediment loading that is likely to deposit near the confluence as flow velocities decrease. Additionally, the rocky cliffs and levees confining the Neosho River channel upstream of the confluence result in raised velocities and sediment carrying capacity. As flow reaches the site of the delta feature, flows can spread, velocities and corresponding bed shear stresses decrease, and sediment drops out of the water column.

The average water level at Pensacola Dam between 1942 (at the start of the earliest reliable records) and 2009 was 740.95 feet PD. From 2009 to 2019, there was no significant rise of the top of the delta surface on what is called the top-set slope, yet the average water level was 743.49 feet PD. The data show delta formation and growth on the top-set slope from 1940 to 2009 when the average water level was 2.49 feet lower than the 2009 to 2019 time period when virtually no upward growth on top of the top-set slope occurred. Figure 107 shows the delta feature evolution. As discussed previously, there is no indication that the crest elevation of the delta feature is expected to increase over the next 50 years either in literature (Vanoni 2006) or in this analysis. The data contradict the theory that operating at a lower level would keep the level of the top of the top-set slope lower. Although this could be considered contradictory to the approach suggested by the City to keep the delta surface low, it emphasizes the complexities of interaction between flow, sediment transport, critical shear, and water level to eventuate equilibrium.

Figure 107
Comparison of Historical Thalweg Profiles on the Neosho River

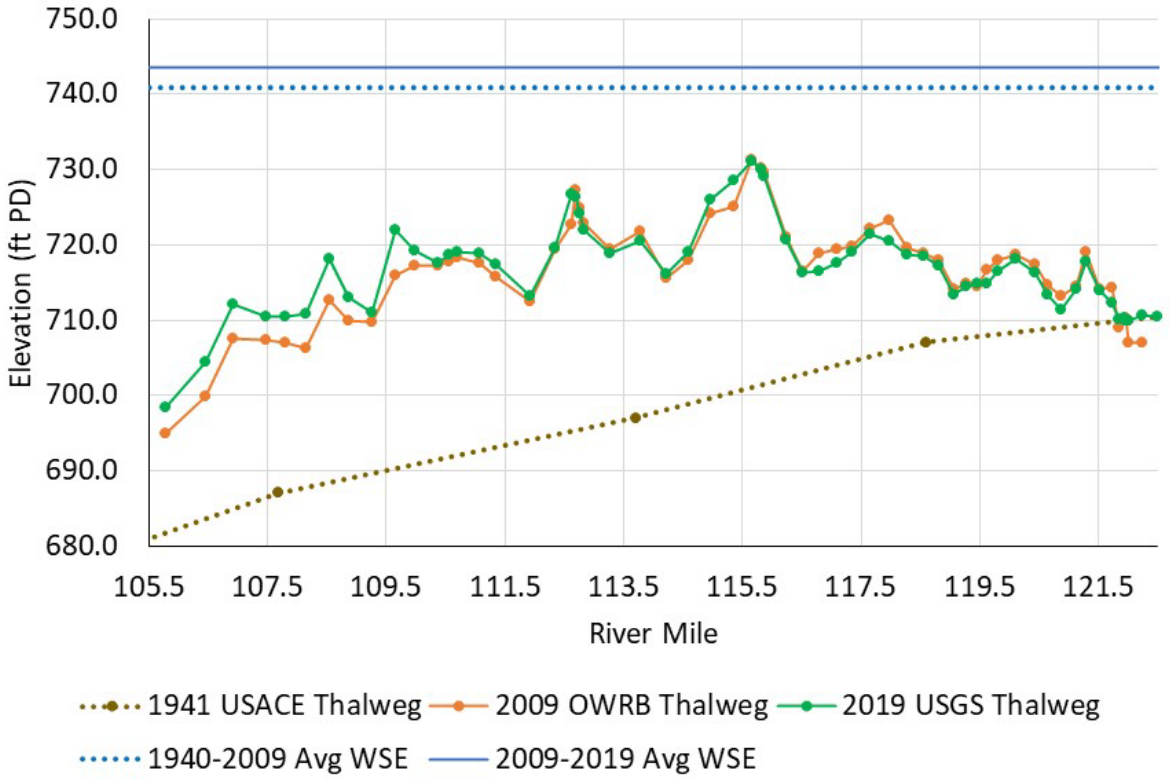

Note that the delta feature accumulation occurred primarily during the lower water levels from 1940 to 2009, and vertical growth was essentially stopped from 2009 to 2019 when average water levels were higher despite the City's claims that increased water levels will create a higher delta feature. By 2019, further deposition is only expected to occur on the downstream face of the delta feature rather than on the crest as predicted by scientific literature (Vanoni 2006).

Once the top of the top-set slope reached the level where the hydraulic shear equals or exceeds the critical shear of the sediment surface over a sufficient portion of time, then no significant sediment deposition occurs on this key portion of the delta feature, and a state of dynamic equilibrium has developed. This is consistent with the findings of the studies on John Redmond Reservoir, where operating the reservoir at a significantly lower water level only improved sediment transport through the reservoir by 3%.

Based on the quantity of sediment computed using the sediment transport rating curves over the 50-year future scenario, approximately 109 million tons of sediment are delivered to Grand Lake. This converts to a volume of 71,587 acre-feet at 70 pcf and 86,398 acre-feet at 58 pcf (assuming a 100% trapping efficiency). This volume of sediment (storage loss from the reservoir) would be distributed according to the results of the hydraulic shear stress analysis for the anticipated (or baseline) operations. The analysis shows that virtually no sediment is deposited upstream of RM 116,

approximately 10% of the sediment is deposited between RM 116 and RM 105 (Elk River confluence), approximately 22% is deposited between RM 105 and RM 100, and the remaining 68% is deposited between RM 100 and the *dam*.

It is logical to conclude the delta feature is currently in dynamic equilibrium because the quantitative analysis relating shear to percentage of sediment being transported farther downstream indicates no significant sediment deposition on the top surface of the delta feature (topset slope). A riverine-like system such as the upper reservoir, which includes the delta feature, moves sediment according to the shear stress created by inflows. As inflows increase, shear stress increases proportionately. In other words, the upper reservoir's ability to move sediment increases proportionally with inflow. Therefore, if there is a significant inflow event, rather than creating a significant backwater effect, the finer sediments composing the delta feature will be moved farther downstream and out of the way because they will not have the ability to hold back the water and create a backwater effect (Figure 108). As shown by the hydraulic analysis, the average shear stress is generally greater than the critical shear stress on the topset portion of the delta feature. The quantitative analysis shows that most of the sediment deposition occurs downstream of the topset slope where hydraulic shears progressively decrease below critical shear for the cohesive sediment. To believe the delta feature has the ability to hold back a significant inflow event and create a backwater effect when it is composed primarily of fine sediments as the City asserts is contradictory to the fundamental scientific principles of shear stress and dynamic equilibrium.

Figure 108
Conceptual Delta Formation under Low and High Flow Conditions

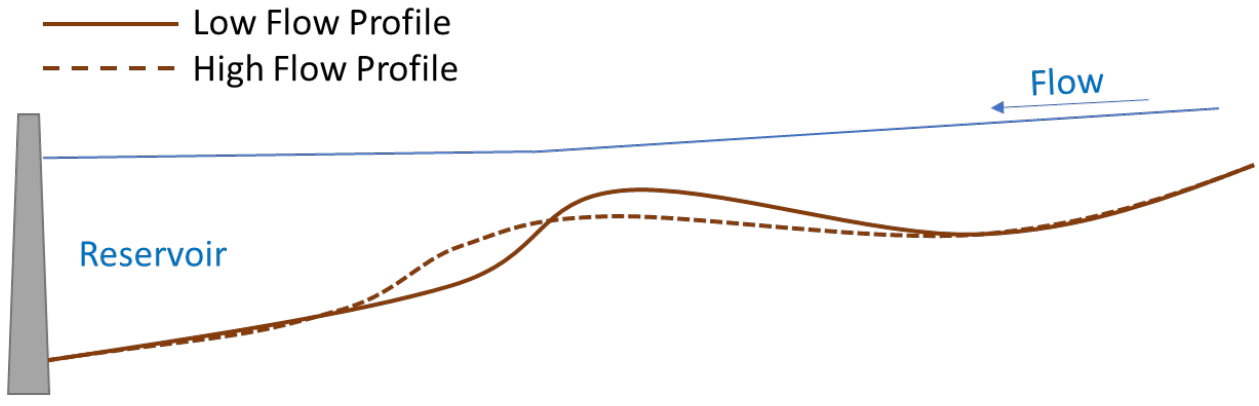

It is important to remember that Grand Lake is under operational control of USACE when the water level approaches or exceeds elevation 745 feet PD and that under these conditions, which only occur 19.8% of the time, delivers 75.6% of the incoming sediment load to the reservoir. Neither the upstream sediment load nor operational control of Grand Lake is controlled by GRDA at that time.

5 Sediment Transport Model Development

Following the data-gathering phase of the project, the team developed the STM. Terrain files, USGS gaging station records, sediment transport rates, and sediment sampling information were used as inputs for the model.

The STM was developed using HEC-RAS v. 6.2 as available from USACE. The software is one of the leading fluvial system modeling packages and is frequently used for flood evaluations, hydrologic and hydraulic studies, and sediment transport estimates. The original version of the STM as submitted in December 2021 was built in HEC-RAS v. 5.0.7. This decision to use the newer software was made to take advantage of more robust sediment transport code that was included with the software updates.

The STM directly models the system above RM 100 as requested in FERC's May 27, 2022 SMD (page B-6). This modification to the original plan allows more accurate modeling of sediment deposition patterns by focusing primarily on the non-cohesive portion of sediment loading (and cohesive sedimentation not defined by density currents) and its impacts on water levels, which HEC-RAS was developed to evaluate. HEC-RAS is less well-suited to model the cohesive sediment that is found lower in the reservoir.

As discussed in the USP and subsequent SMD, the results of the STM were exported to a one-dimensional (1D) UHM for hydraulic evaluation. The 1D UHM was based on the STM and was developed in HEC-RAS v. 6.2 to maintain consistency with the STM. The 1D UHM is distinct from the STM and was run in fully unsteady hydraulic-only mode. More detailed discussion of this model is included in Section 7.4 of this report.

5.1 Terrain Information

Terrain files were developed to provide input geometries for the STM. These files were compilations from a range of surveys performed between approximately 1940 and 2019. A full description of the available datasets can be found in Section 2.1.1 of this report. All elevations are reported in reference to the PD unless otherwise noted.

5.1.1 Circa-1940 Terrain

The circa-1940 terrain was built from digitized 1938 USACE topographic maps and surveyed channel information from 1941 and 1942. Topographic maps were georeferenced using Geographic Information System (GIS) software and contour lines were traced and assigned elevations.

These topographic data came from several sets of contour maps. One was a relatively high-resolution set of 1:10,000 maps with labeled contours. Another was a 1:31,680 maps that did not contain legible contours. Where the 1:10,000 maps were available, they were used to develop the

topographic surface; the 1:31,680 maps were only used where the others could not be used (Figure 109).

Figure 109
Graphic Showing Map Coverage of the Study Area

Note: The maps on white background are the 1:10,000 scale contour maps with legible, labeled contour elevations; maps with a brown background are the 1:31,680 scale with no legible contour elevation labels.
Source: USACE (1938)

Once all contours had been compiled, GIS software was used to create a three-dimensional (3D) surface, which provided a basis for the overbank portions of the system.

Channel surveys completed by USACE in 1941 and 1942 were then used to cut stream channels into the topography. As discussed in Section 2.1.1.1 of this report, there were no station/elevation data available for the Neosho River below the Neosho River/Spring River confluence. Instead, that data were estimated from elevation/area and elevation/width relationships.

The USACE reports mention plates that present the geographic location of surveyed cross sections, but the plates were not included in the files retrieved from USACE archives. Therefore, exact locations of surveyed cross sections were unknown. The USACE reports did include downstream reach lengths between cross sections. Given the changing stream meanders, uncertainty of circa-1940 survey measurements, and imprecise definition of reference points provided in the 1941 and 1942 USACE reports, there is uncertainty in the georeferenced location of many of these cross sections.

To address this shortcoming, known landmarks such as bridges were used to estimate the geographic location of surveyed cross sections. Between these landmarks, cross sections were placed according to documented downstream reach lengths. Linear scaling factors were applied to downstream reach lengths when the sum of documented reach lengths between landmarks did not match the physical distance between landmarks. This process was effective for portions of the Neosho River near the City of Miami where multiple, closely spaced bridges could be used as landmarks but was less effective along the Elk River where bridge locations were not documented in the circa-1940 cross-sectional surveys.

Several of the cross-section surveys included bridge geometries, which allowed for accurate placement of those cross sections. One example is shown in Figure 110, which is taken from the USACE (1942) revised envelope curve document and shows cross section GN-R-21 at the U.S. Highway 66 Bridge near Miami. Between known reference points, the distances were adjusted with a linear scaling factor to place cross sections more accurately.

Figure 110
Published Cross-Section Information for GN-R-21 Showing U.S. Highway 66 Bridge

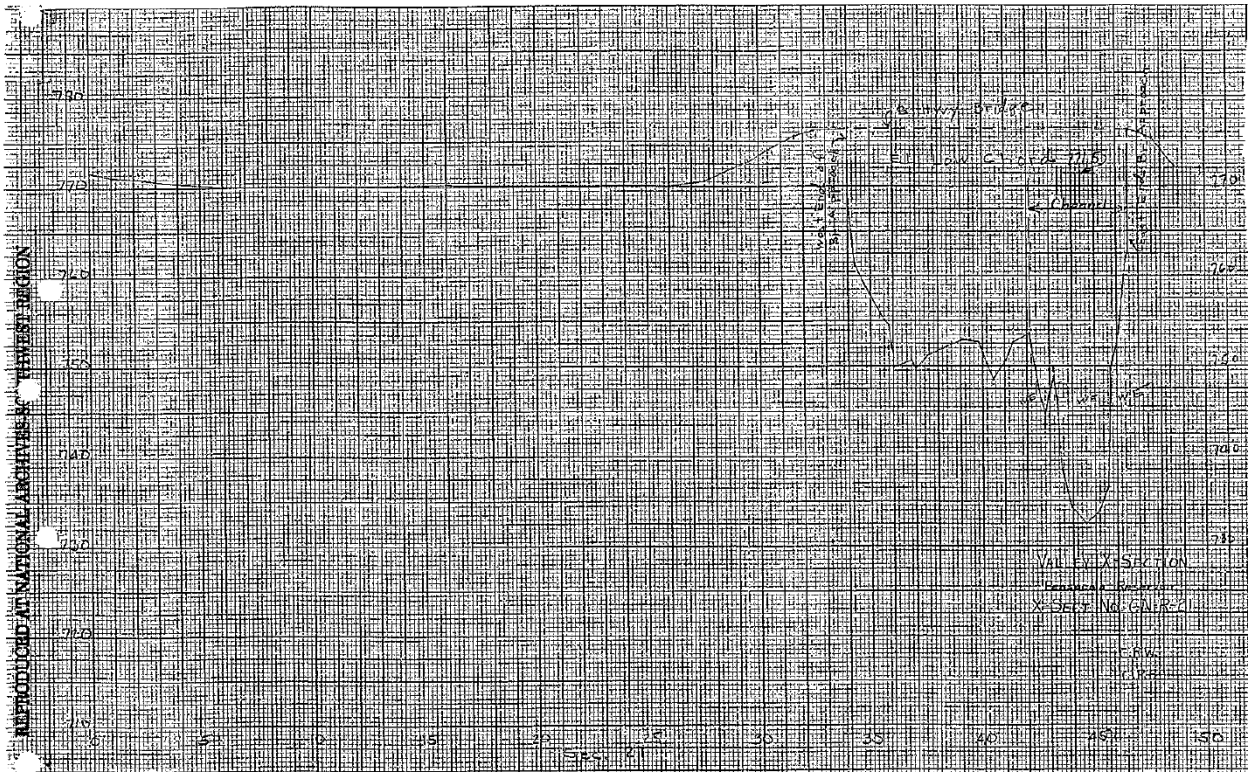

Source: USACE (1942)

This figure is a typical image of the cross-sectional surveys and was chosen to illustrate the difficulty of using the circa-1940 survey data; it is difficult to read, horizontal scales are not explicitly stated, and hand-written notes are occasionally illegible. Regardless, this also represents the most complete dataset of site conditions at the time of Project construction.

On the Elk River, no bridges were included in the surveys (USACE 1941). Downstream reach lengths listed in the report were initially used to locate the surveyed cross sections. However, using these initial locations, the cross sections were approximately 20 feet above the topographic data. To better locate these cross sections, bank elevations were extracted from the reported surveys compared to streambank elevations in the 1938 USACE topographic maps. Correlation between surveyed cross-section bank elevations and topographic bank elevations were used to georeference the cross sections. The documented downstream reach lengths between the surveyed cross sections were maintained in the georeferenced set of cross sections to maintain the surveyed bed slope.

Once the locations of the channel cross-section surveys were defined, the channels were cut into the topographic surface along the stream thalwegs to produce a full circa-1940 terrain file. This was imported to HEC-RAS and model cross sections were cut from the terrain.

Model quality is sensitive to the quality of data available for model development. The terrain data represent one of the largest sources of uncertainty in this study. Data from circa 1940 is limited by the resolution of digital maps, lateral accuracy of original measurements, vertical accuracy of the available equipment, and legibility of contour labels on the available maps. There is also uncertainty regarding the georeferencing of the contour mapping and the exact locations of many of the surveyed cross sections, and there are no longer records available of the station-elevation data from many of the circa-1940 surveys.

These are imperfect datasets, but they also represent the *best available data for this time period*. These shortcomings in data quality were discussed in detail in both the USP submitted by GRDA in April 2022 and in Section 2.1.1 of this report. To address this, the STM was used to simulate bounding scenarios of high and low sedimentation as a means of accounting for the potential range of outcomes as discussed in Section 7.1.2 of this report.

5.1.1.1 Manning's *n* Values

Manning's *n* values were assigned based on aerial imagery collected by the USDA (USDA 1938, 1939a, 1939b, 1940). The land use was visually identified and roughness parameters were developed according to Arcement and Schneider (1989). The parameters were assigned based on the composite roughness values shown in Table 26 and Figure 111.

Table 26
Composite Manning's *n* Values for Circa-1940 Land Use

Land Use Classification	Composite Manning's *n*
Stream Channel[1]	0.03
Ponded Water	0.04
Urban	0.07
Farmland	0.08
Light Vegetation	0.10
Thick Vegetation	0.15

Notes:
Composite values based on Arcement and Schneider (1989).
1. Stream channel roughness assigned based on typical bed channels.

Figure 111
Land Use Classifications of the Grand Lake Study Area as Determined from Circa-1940 Soil Conservation Service Aerial Imagery

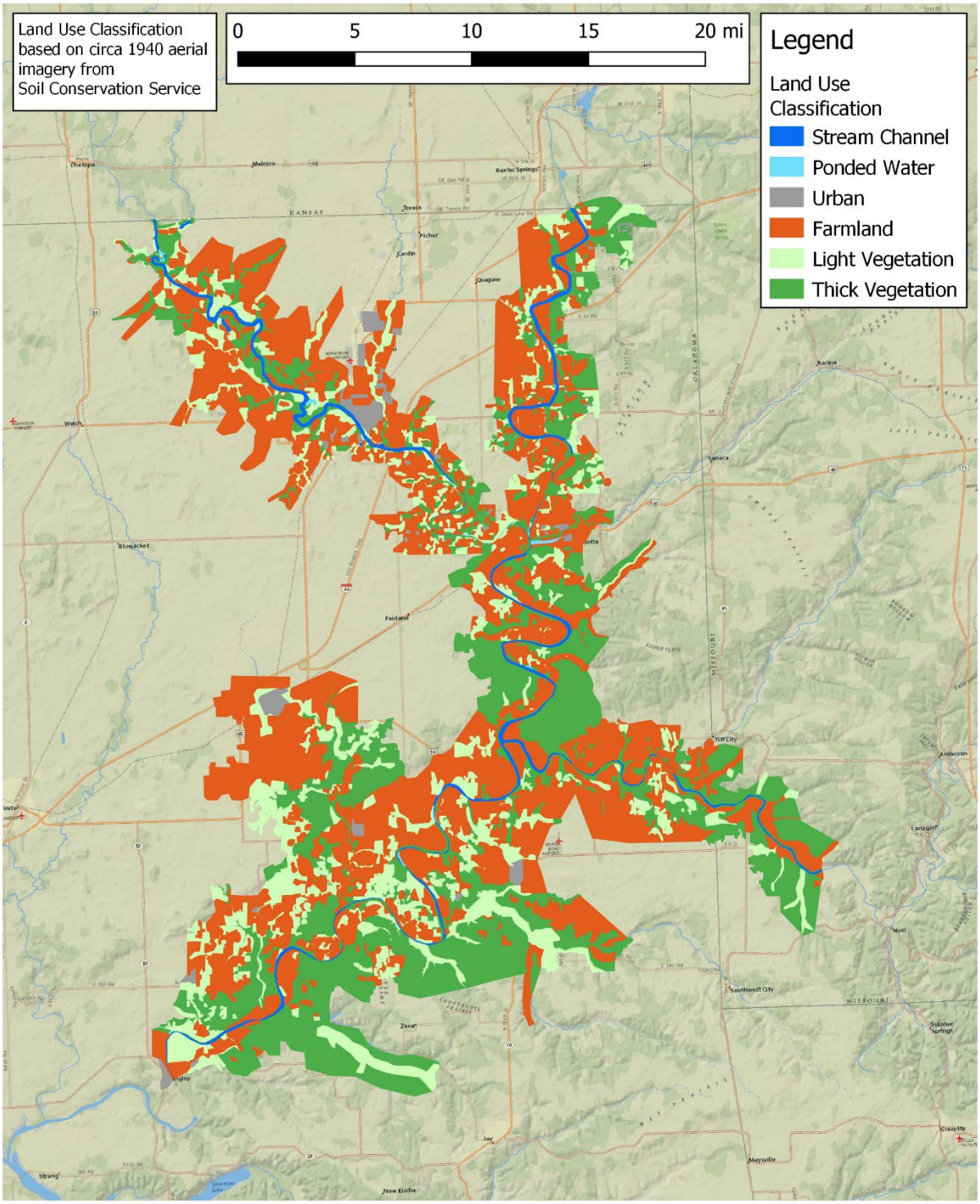

5.1.2 Modern Terrain

The UHM's 2D flow areas were converted to 1D cross sections. These were cut from the relevant model terrain using built-in features of the HEC-RAS geometry editor. Cross-section stations were then filtered to limit station-elevation points at each cross section to a maximum of 500 individual values in accordance with HEC-RAS modeling requirements. Filtering was also performed using standard HEC-RAS features; data were filtered using the program's "Minimize Area Change" option.

Land use patterns were used to determine the base Manning's *n* values for the model. Where cross sections were copied from the UHM to the STM, these were left unchanged. Where 2D flow areas had been converted to 1D cross sections, river stations were used to define the Manning's *n* values to match the UHM values at those locations.

Bridge geometry information was gathered from the Oklahoma Department of Transportation, Missouri Department of Transportation, local and county road commissions, and measurements provided by GRDA. Bridge geometries in HEC-RAS typically are input as separate structures, with bridge deck geometry, support piles, and abutments entered into the program along with widths and cross sections immediately upstream and downstream of the structure.

5.2 Streams

The STM consisted of four streams: the Neosho, Spring, and Elk rivers, as well as Tar Creek.

5.2.1 Neosho River

The Neosho River was modeled from RM 152.25 to RM 99.82, approximately 22 miles upstream of Pensacola Dam (USGS gage 07190000). It was divided into three reaches with junctions at the confluence with the Spring and Elk rivers (upstream of RM 122.25 and 105.35, respectively).

5.2.2 Spring River

The Spring River was modeled from RM 21 to its confluence with the Neosho River at RM 0.

5.2.3 Elk River

The Elk River was modeled from RM 19.59 to the confluence with the Neosho River and Grand Lake at RM 0.

5.2.4 Tar Creek

Tar Creek was modeled from RM 7.6 to the confluence with the Neosho River. The downstream end of Tar Creek was modeled with normal depth, as discussed in Section 5.3. Geometry of the lateral structure was cut from the terrain and filtered to 500 data points to comply with model

requirements. The STM therefore does not contain cross sections below Tar Creek RM 1.6; the rest of the creek was included in the lateral extent of Neosho River cross sections.

5.3 Boundary Conditions

Boundary conditions (BCs) define parameters at the model limits. HEC-RAS offers several options for BC types, including WSE, discharge, and normal depths. WSE and discharge can be set as a specified time series, and normal depths can be calculated based on the friction slope. For the STM, upstream BCs (at the upstream extents of the Neosho, Spring, and Elk rivers, as well as Tar Creek) were defined by USGS discharge measurements stepped at intervals ranging from 15 to 60 minutes. The downstream BC was set as normal depth with a friction slope of 0.0033 vertical feet per horizontal feet [ft/ft] (for Tar Creek) and recorded WSE at Pensacola Dam (Neosho River). WSE measurements taken at Pensacola Dam were used to set the downstream water levels in the model. These data points are provided at 1-hour intervals. These inputs were used to run the model in Quasi-Unsteady Mode.

Water temperature can also be defined in *Quasi-Unsteady* models and is an important component of STMs. Water viscosity is related to temperature, with higher temperatures producing lower viscosity values. The decreased viscosity reduces sediment transport capacity and is therefore a necessary input parameter. Because this affects sedimentation, it was included in the sensitivity analysis discussed in Section 7.4.2.2 of this document.

5.4 Sediment Data

Input data for the STM includes the sediment supply for the upstream boundary for each stream, the sediment characterizing the bed of each stream through the various reaches, and the erosion parameters defining the cohesive sediment where it is found in the river or lake beds. Data from field work was adapted to create the inputs. Specific parameters are described in the following subsections.

5.4.1 Upstream Sediment Supply

The upstream sediment supply applies the suspended sediment regression curves to develop a sediment rating curve (table of suspended sediment transport rate in tons per day with flow). This table is input into the HEC-RAS model for each stream: Neosho River, Tar Creek, Spring River, and Elk River. These tables can be seen as input files for the STM. The model then computes suspended sediment inflow at the upstream boundary of each stream for each time step of the model using the flow data for the calibration time period (1942 through 2019). The upstream sediment supply for these rivers and creek are tabulated versions of the regression equations developed in Section 4.3.

5.4.2 Bed Material

For each cross section and for each stream, a bed material size distribution was developed as input into the STM. These data are based on the particle size distributions for the bed material and core sampling analysis and can be seen as input tables of the particle size distribution for each cross section.

As previously shown (see Section 2.3.2), the bed of these streams and the reservoir consist of a wide range of sediment sizes resulting in a bi-modal distribution of sediment, one of which is fine, cohesive material (primarily silt and clay), and the other distribution being non-cohesive material (primarily gravel with some sand and finer material as well as cobble-sized material). Further complicating the bi-modal distributions, samples of primarily non-cohesive gravel exist near samples of predominantly cohesive silt and clay. In addition, samples do not show any clear longitudinal trend of sediment characteristics where an upstream sample may be fine, cohesive sediment and the next sample farther downstream may be coarse, non-cohesive sediment. This range of longitudinal distributions of sediment in close proximity complicates development of input data that describe the characteristics of the bed of these streams. The following examples demonstrate this complexity.

Figure 112 and Figure 113 show the wide range of bed material sizes along the Neosho River. Locations of the sediment samples are included in Exhibit 2.

Figure 112
Neosho River Sediment Size Gradation Results Comparison

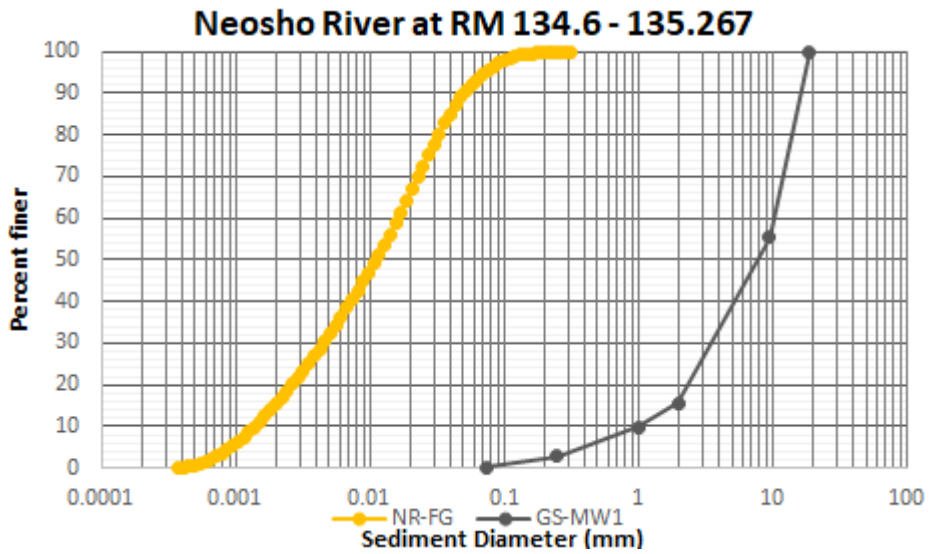

Figure 113
Neosho River Sediment Size Gradation Results Comparison

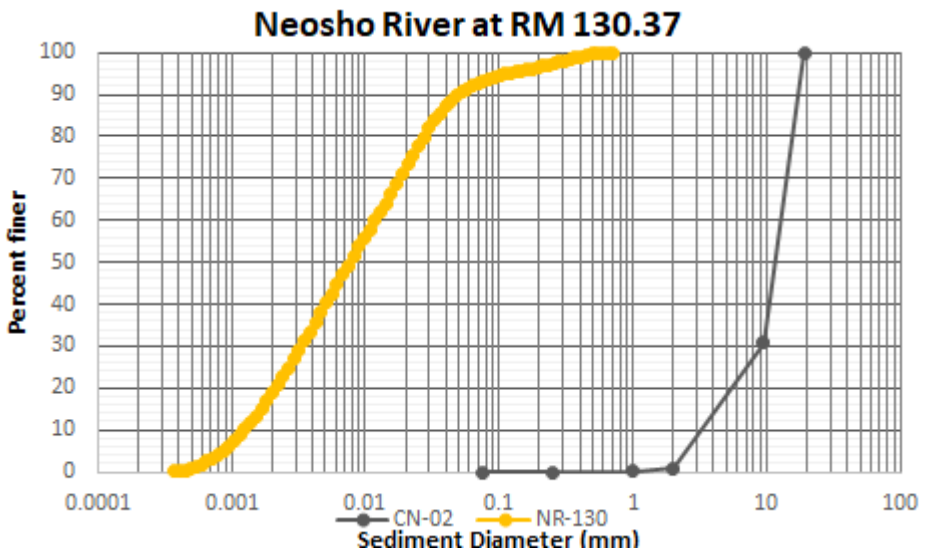

Farther downstream in the upper reservoir, this same wide range in bed material size distributions continue in close proximity to these separate samples (Figure 114 and Figure 115).

Figure 114
Upper Grand Lake Sediment Size Gradation Results Comparison

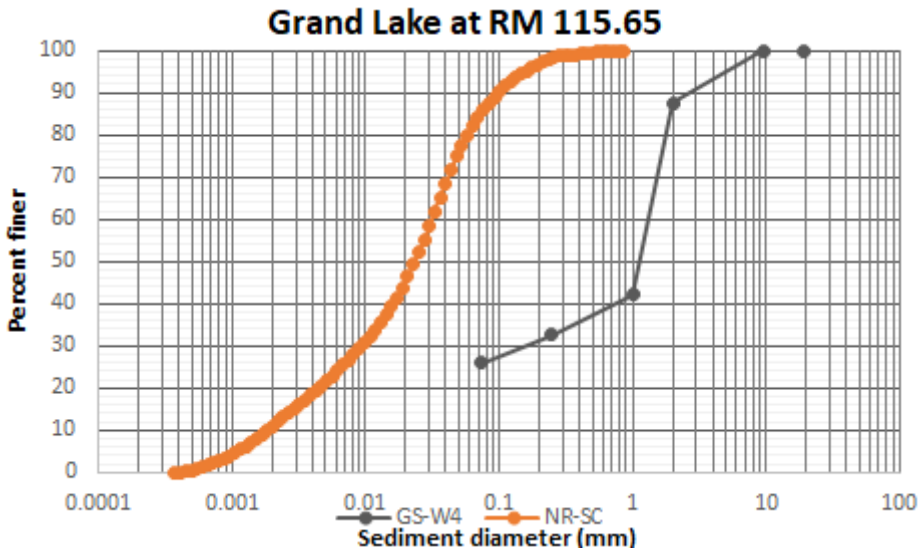

Figure 115
Upper Grand Lake Sediment Size Gradation Results Comparison

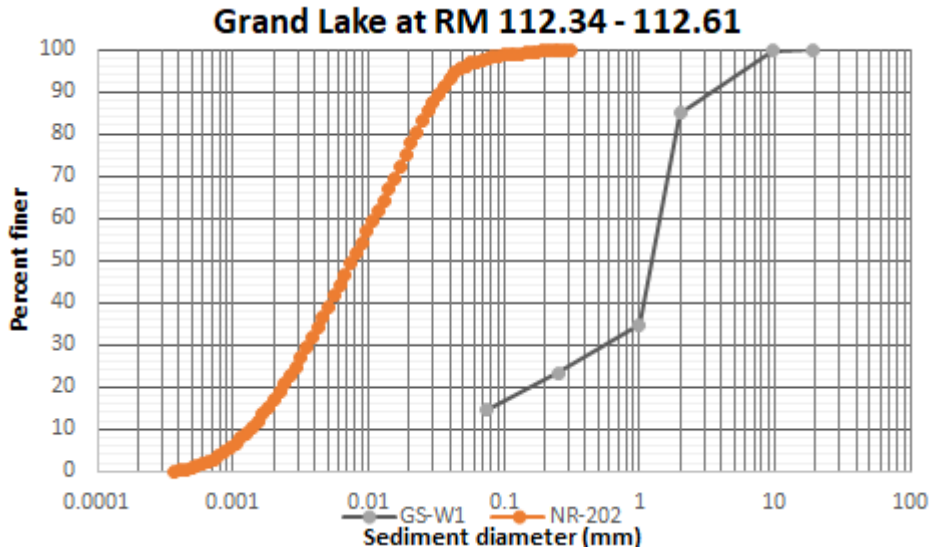

This same disparity in adjacent samples continues on the tributaries as well (Figure 116 through Figure 121).

Figure 116
Tar Creek Sediment Size Gradation Results Comparison

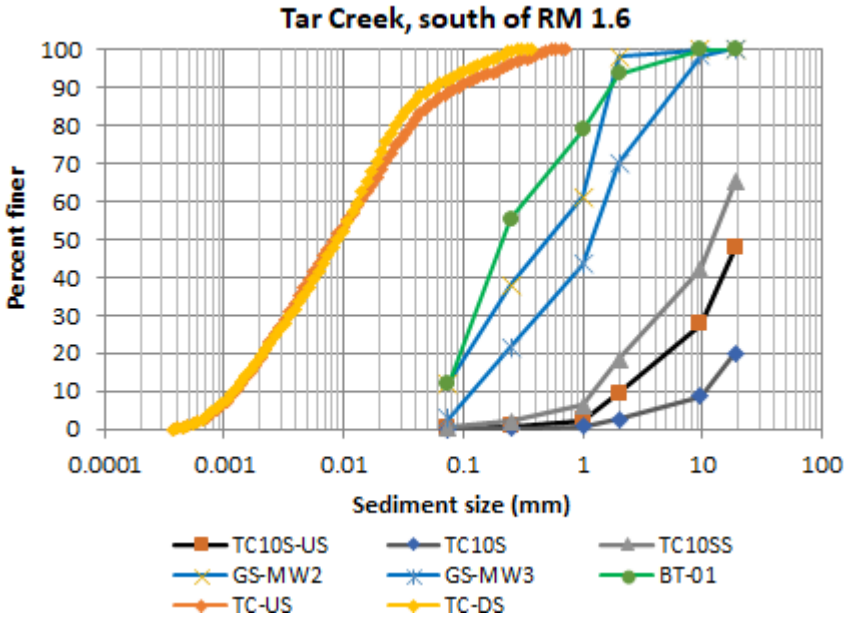

Figure 117
Spring River Sediment Size Gradation Results Comparison

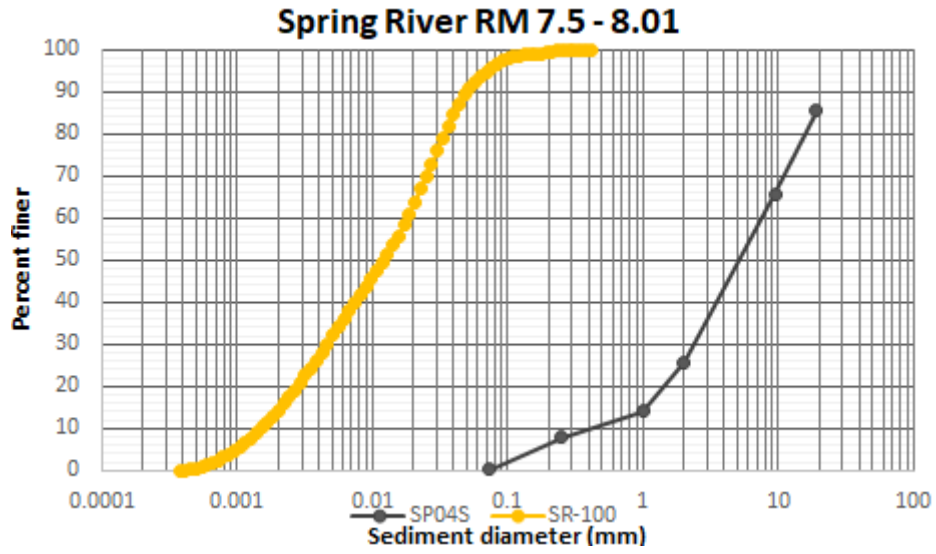

Figure 118
Spring River Sediment Size Gradation Results Comparison

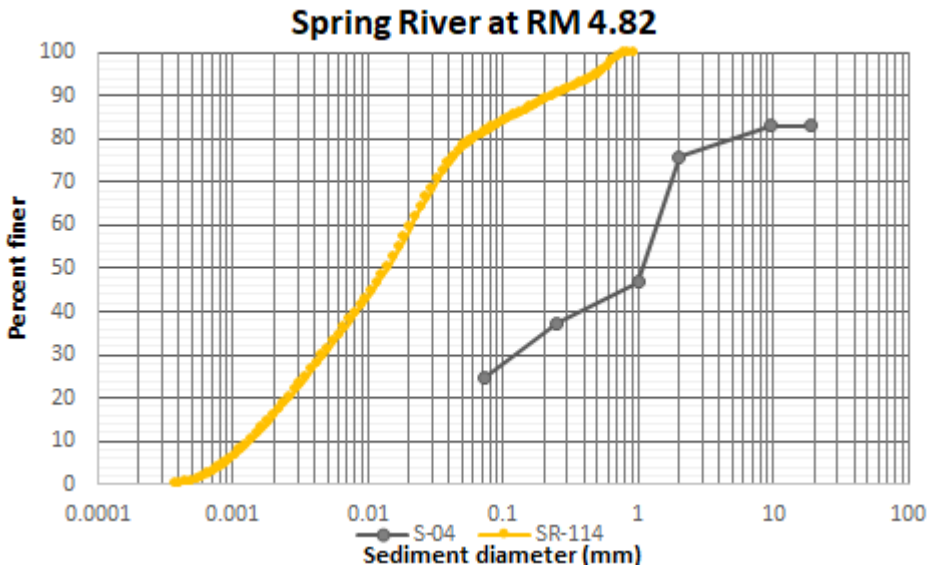

Figure 119
Spring River Sediment Size Gradation Results Comparison

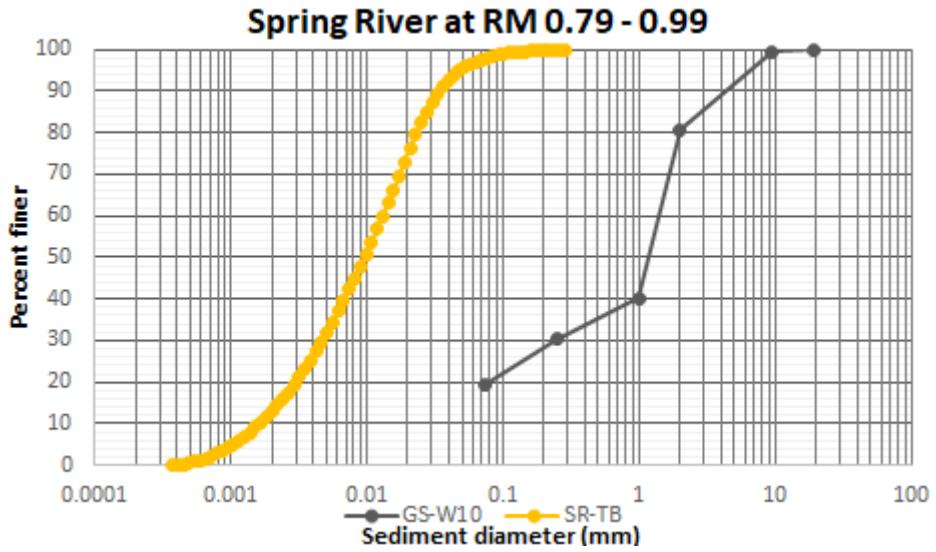

Figure 120
Elk River Sediment Size Gradation Results Comparison

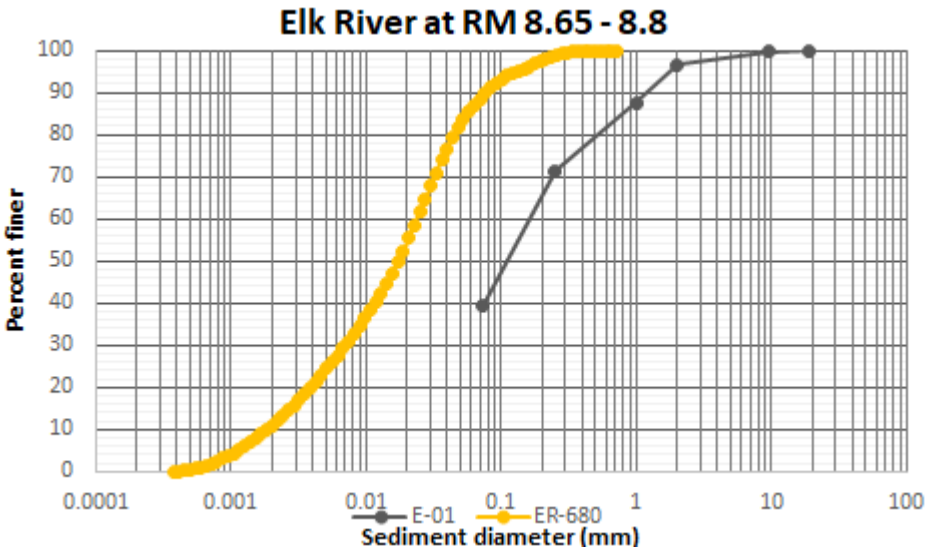

Figure 121
Elk River Sediment Size Gradation Results Comparison

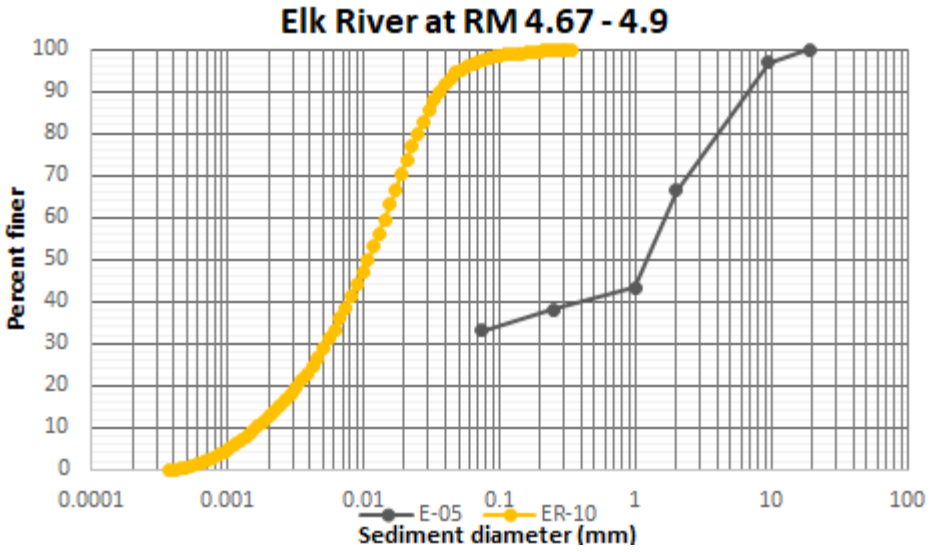

The above plots show that samples taken along the Neosho, Spring, and Elk rivers, as well as Tar Creek, include both fine cohesive sediment (primarily silt and clay) near non-cohesive sediment (primarily gravel along with some finer sediment and coarser sediment). These bi-modal distributions cover six log cycles of sediment size in samples collected in relatively close proximity (but different times: December 2019 and March 2020). This wide range of sediment types and sizes is due to fine sediment being transported down river and deposited in the reservoir during certain events or seasons and then flushed farther downstream under other flow and reservoir conditions.

As discussed in Section 2.1.3.1, under some conditions, the bed consists of fine-sized sediment (silt and clay), and under other conditions, in close proximity to the fine samples, the bed consists primarily of coarser, non-cohesive sediment (gravel and sand). The data and observations indicate that the fine sediment transported down river into the upstream reaches of the reservoir as suspended load tends to deposit temporarily under some hydrologic and hydraulic conditions and then is flushed farther downstream under other hydrologic and hydraulic conditions as suggested previously by Mussetter (1998).

Tetra Tech's discussion from both the 2015 and 2016 reports, *Hydraulic Analysis to Evaluate the Impacts of the Rule Curve Change at Pensacola Dam on Neosho River Flooding in the Vicinity of Miami, Oklahoma* (Tetra Tech 2015, 2016), make comparisons between 1940, 1998, and 2015 survey data and basic hydraulic and sediment transport concepts to conclude that:

> Because the amount of sediment that can be carried by the river is controlled by the local hydraulic energy, and the required amount of energy increases with increasing particle size, the coarser-grained portion of the sediment load (i.e., sands and gravels) will typically deposit on the river bed near the head of the reservoir and the finer grained sediment will be carried progressively farther downstream into the reservoir. (Tetra Tech 2016)

And regarding the quantities of deposition:

> Based on the bank elevations, there has been approximately 15 feet of overbank deposition in the vicinity of Twin Bridges between 1940 and 2015.
>
> Comparison of the thalweg (i.e., minimum bed elevation) profiles from the 2015 bathymetry with thalweg elevations measured in 1940 indicates that the bed has aggraded by an average of about 5 feet, with over 10 feet of aggradation in some locations in the 6- to 7-mile reach upstream from Twin Bridges/U.S. Highway 60. (Tetra Tech 2016)

Although Tetra Tech presents a logical position that the coarser-grained portion of the sediment load (sands and gravels) would tend to deposit in the upper reach of the reservoir, recent collection of bedload transport data showed virtually no transport of those grain sizes in the rivers. The sediment team used equipment specifically designed to capture sands and gravels and found no evidence of coarse material transport even at the highest flows sampled in 2019 and 2020, which represents more than 90% of the recorded flow regime. It is difficult to conclude significant deposition of these sizes of sediment is occurring on the bed when no movement of such materials has been measured.

Sediment transport sampling shows that virtually all sediment transport consists of fine silts and clays, and that bed samples at a given location alternate between stationary coarse materials and more mobile fines. Therefore, it is clear the earlier observation of Mussetter and current observations of the transitory nature of fine sediment deposition are valid and most of the fine sediment load is eventually moved farther down into the reservoir without permanent or ongoing deposition in the more riverine sections of the river. These are the complexities of the sediment transport analysis, which were addressed through the data collection, analysis, and modeling process. Any previous quantification and conclusions regarding the sediment transport and deposition process must be evaluated considering these complexities, significantly increased data, and further analysis including the modeling process.

Several factors contribute to a complicated analysis and model development effort, as follows:

- Sediment sizes and types are quite different, even when collected near other samples representing entirely different sediments.
- There is a wide range in sediment density from sample to sample and depth below sediment surface.
- Non-cohesive sediments are expected to follow standard transport equations and parameters and are found in certain bed samples but not in the bulk of the incoming sediment load.
- Incoming sediment load consists primarily of fine sediment that will deposit under some conditions and exhibit a wide range of erosion and transport parameters that vary location to location and depth below sediment surface.

Further complicating the physical characteristics of the diversity of sediment types, sizes, and characteristics is the fact that the bulk of data collected to develop the sediment characteristics were collected in 2019 and 2020, whereas the model calibration period starts in 2009. If these types of data were collected in 2009, they were collected before this study began and the findings have not been available to the STM development team. As a result, although channel and reservoir geometry were surveyed in 2009, the river and lakebed sediment characteristics for 2009 are based on data collected a decade later, which may or may not represent conditions at the beginning of the calibration period. STM setup and calibration present a very complicated and challenging task.

6 Sediment Transport Model Calibration

STM calibration was performed in two components. As with any model calibration procedure, it is easiest to start with the simplest format available, ensure accuracy, then increase complexity. For the STM, that meant beginning with hydraulic calibration and neglecting sediment movement, erosion, and deposition. Once the hydraulics were well-calibrated, sediment transport was added to the STM, and the sediment model parameters were finalized.

Sediment calibration and validation simulations ran from 1942 to 2019. Results were then compared against measured data from 1998 REAS surveys, the 2009 OWRB survey, and USGS surveys performed in 2017 and 2019 as discussed in Section 6.2.2.

The overall goal of this step was to create a baseline geometry using the 2019 terrain dataset that could be used to predict future sediment transport, erosion, and deposition patterns.

6.1 Hydraulic Calibration

6.1.1 Circa-1940 Geometry

Hydraulic data for calibrating the circa-1940 model is not available in the upper reaches of the study area. WSE data are not available for the circa-1940 model, so calibration was performed by assigning Manning's *n* roughness parameters based on land use as described in Section 5.1.1.1.

6.1.2 Modern Geometry

Hydraulic calibration for the modern geometry focused on matching peak WSE records. WSE information was provided by a collection of USGS gages, WSE monitoring stations placed by the project team, and high water mark information provided by Tetra Tech.

6.1.2.1 Model Inputs

Model input parameters were developed specifically for the hydraulic calibration components. Sediment modeling was not included in this part of the calibration procedure.

6.1.2.1.1 Sediment Information

The process started with hydraulic calibration. To remove any sediment influence, an empty sediment dataset was created for the entire model domain. This dataset included an arbitrary bed gradation and set maximum erodible depths to 0 feet throughout the model. The BCs were set to clear water inflow conditions, and all cross sections were defined as pass-through nodes (meaning sediment would not deposit and instead be transported downstream).

6.1.2.1.2 Modeled Events

Hydraulic calibration involved using known parameters from USGS data. BCs were defined as described in Section 5.3 for several flow events. The modeling team selected six events for calibration; these were also used for UHM calibration procedures. The timing of specific events and peak stream discharges used for hydraulic calibration are listed in Table 27.

Table 27
Modeled Flow Events and Stream Discharges

Event Date	Peak Stream Discharge (cfs)			
	Elk River at Highway 43	Neosho River at East 60th Road	Tar Creek at East 50th Road	Spring River at East 57th Road
July 2007	4,830	141,000	2,490	105,000
October 2009	39,300	46,100	5,150	66,200
December 2015	107,000	45,400	3,320	151,000
January 2017	1,140	10,200	672	15,900
April 2017	107,000	58,200	2,980	114,000
May 2019	66,500	91,400	6,410	109,000

The downstream WSE at Pensacola Dam was defined by USGS gage records, and the downstream BC for Tar Creek at its confluence with the Neosho River was set at normal depth with a friction slope of 0.0033 ft/ft.

6.1.2.2 Roughness Parameters

Calibration of hydraulic models in HEC-RAS relies primarily on hydraulic roughness parameters. These are typically reported as Manning's *n* values and are usually defined within a set range by land cover type (Table 28). The STM values were based on UHM roughness parameters throughout the model domain. Generally, higher *n* values produce slower flows and raise WSE, whereas lower *n* values decrease WSE.

Table 28
Typical Overland Manning's *n* Values by Land Cover

Land Cover	*n* Value
Field crops	0.040
Pasture	0.080
Urban	0.070
Urban, dense	0.090
Water	0.040

Land Cover	*n* Value
Woody vegetation	0.100
Woody vegetation, dense	0.150

In-channel Manning's *n* values were adjusted iteratively until simulated WSE results showed reasonable agreement with recorded measurements. Table 29 lists in-channel roughness values developed during the calibration process.

Table 29
Base Manning's *n* Roughness Parameters for Streams in the Sediment Transport Model

Reach	*n* Value
Grand Lake (reservoir, up to RM 121.29)	0.020
Neosho River (RM 121.51 up to RM 122.33)	0.025
Neosho River (RM 122.46 up to RM 130.87)	0.024
Neosho River (RM 131.01 up to RM 133.99)	0.035
Neosho River (RM 134.09 up to RM 135.37)	0.015
Neosho River (RM 135.46 up to RM 152.2)	0.030
Elk River	0.015–0.053
Spring River (full reach)	0.0332
Tar Creek	0.027–0.100

These base roughness values were then modified based on changes in stream discharge values. River bedforms have a significant influence on hydraulic roughness. As stated by Mussetter (1998), the bedforms are affected by flow volumes, generating different bed roughness values as a function of total discharge. In HEC-RAS, "Flow Roughness Factors" were used to tune the model to account for changes in bed roughness at higher or lower flow rates. These parameters are shown in Table 30 and Table 31.

Table 30
Flow Roughness Parameters for Elk and Spring Rivers and Tar Creek in the Sediment Transport Model

Elk River		Spring River		Tar Creek	
Discharge (cfs)	Flow Roughness	Discharge (cfs)	Flow Roughness	Discharge (cfs)	Flow Roughness
0	1.30	0	0.90	0	0.80
40,000	1.25	50,000	1.00	4,600	0.95
66,500	0.85	110,000	1.00	4,700	0.90

Elk River		Spring River		Tar Creek	
Discharge (cfs)	**Flow Roughness**	**Discharge (cfs)**	**Flow Roughness**	**Discharge (cfs)**	**Flow Roughness**
75,000	0.80	120,000	1.20	4,800	1.00
105,000	0.80	151,000	1.20	5,500	1.00
110,000	1.00	152,000	1.00	6,400	0.90
				6,500	1.00

Table 31
Flow Roughness Parameters for the Neosho River in the Sediment Transport Model

RM 130.54–135.267		RM 135.37–152.25	
Discharge (cfs)	**Flow Roughness**	**Discharge (cfs)**	**Flow Roughness**
0	0.80	0	0.80
45,000	0.80	45,000	1.10
60,000	1.30	60,000	1.20
65,000	1.30	91,000	1.10
91,000	1.30	92,000	1.00
92,000	1.00		

6.1.2.3 Results

Model calibration results showed good agreement with measured WSEs, as discussed herein.

Model calibration results as compared to USGS gages are shown in Figure 122. The average difference between simulated maximum WSE and measured maximum USGS gage WSEs is 0.06 foot; the model slightly overpredicts WSE at the USGS gages for the calibration events.

Figure 122
Overprediction and Underprediction of Simulated WSE at USGS Gages

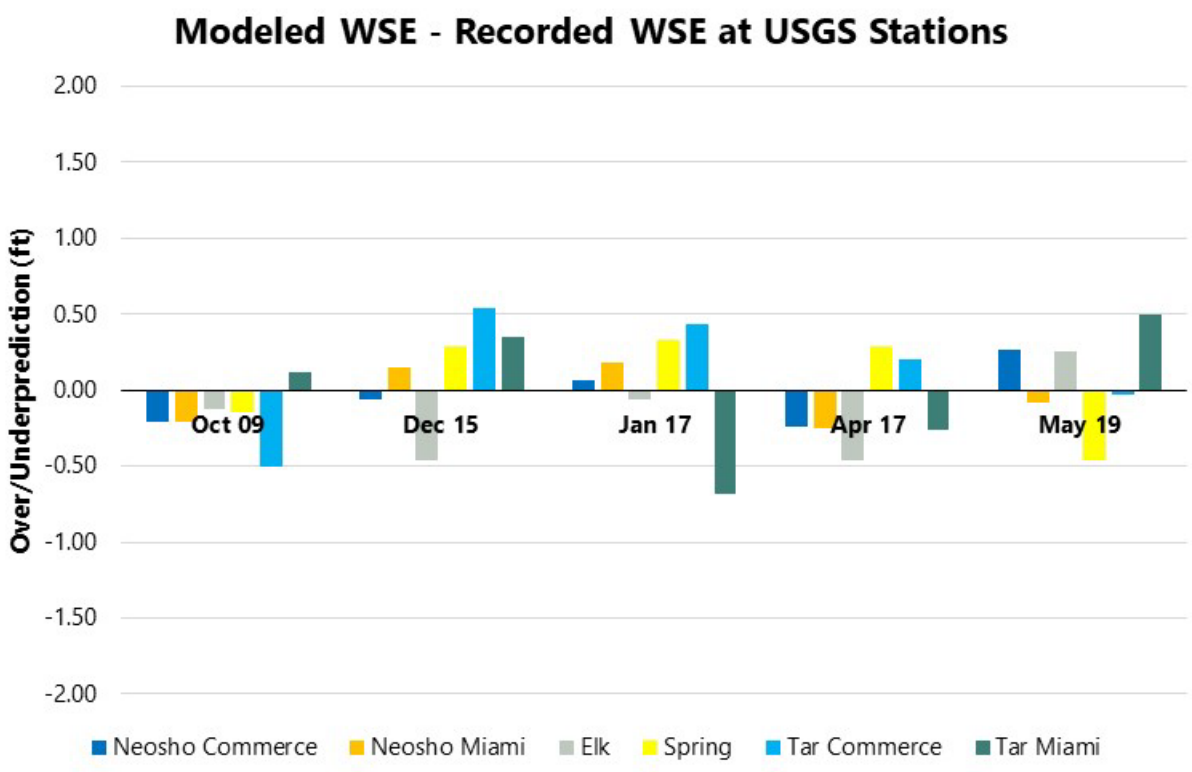

STM calibration results were also compared to high water marks as compiled by Tetra Tech (2016). Model results from the July 2007, October 2009, and December 2015 calibration run are shown in Figure 123 through Figure 125. Average model difference is 0.29 feet for July 2007, -0.59 feet for October 2009, and -0.66 feet for December 2015; the model overpredicted WSEs during the July 2007 event and underpredicted for the October 2009 and December 2015 events when compared to measured high water marks.

Quasi-unsteady modeling presents difficulties when evaluating WSE measurements downstream of tributaries. WSE is heavily influenced by the arrival times of peak flow pulses from contributing streams. Because quasi-unsteady models change the relative arrival times downstream of confluences, it is difficult to accurately model maximum WSE at those locations. For STMs, it is impractical to model with fully unsteady flows; for WSE evaluations, the UHM is a more fitting tool.

Figure 123
Comparison of STM WSE Results and Measured High Water Marks during the July 2007 Event

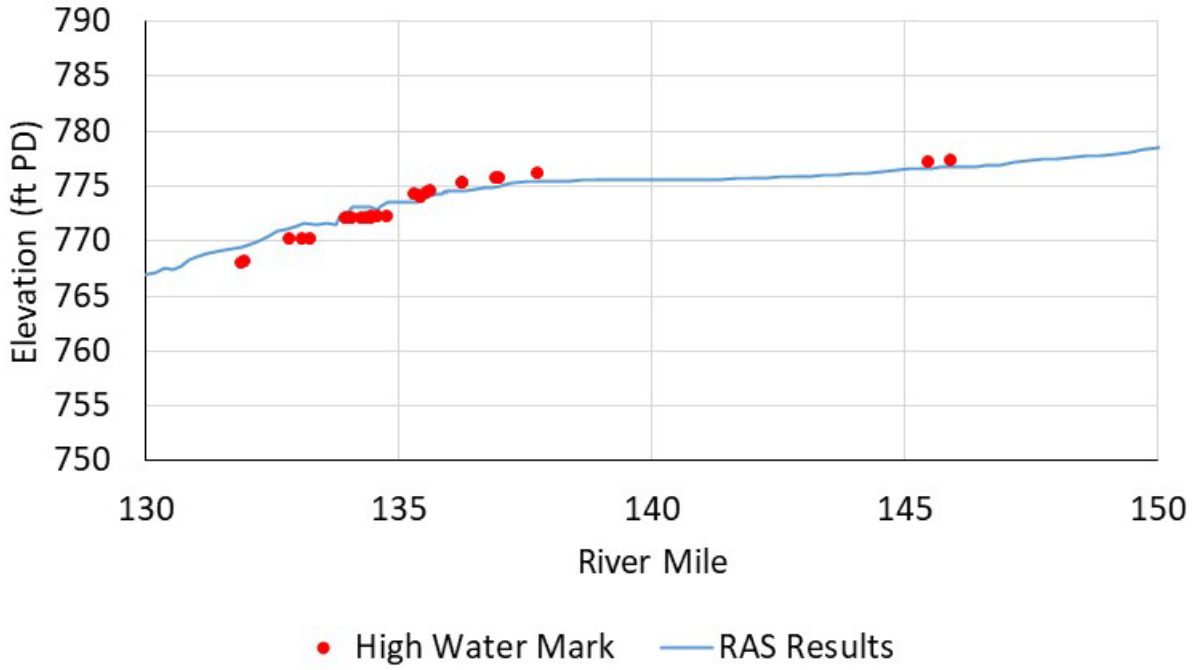

Figure 124
Comparison of STM WSE Results and Measured High Water Marks during the October 2009 Event

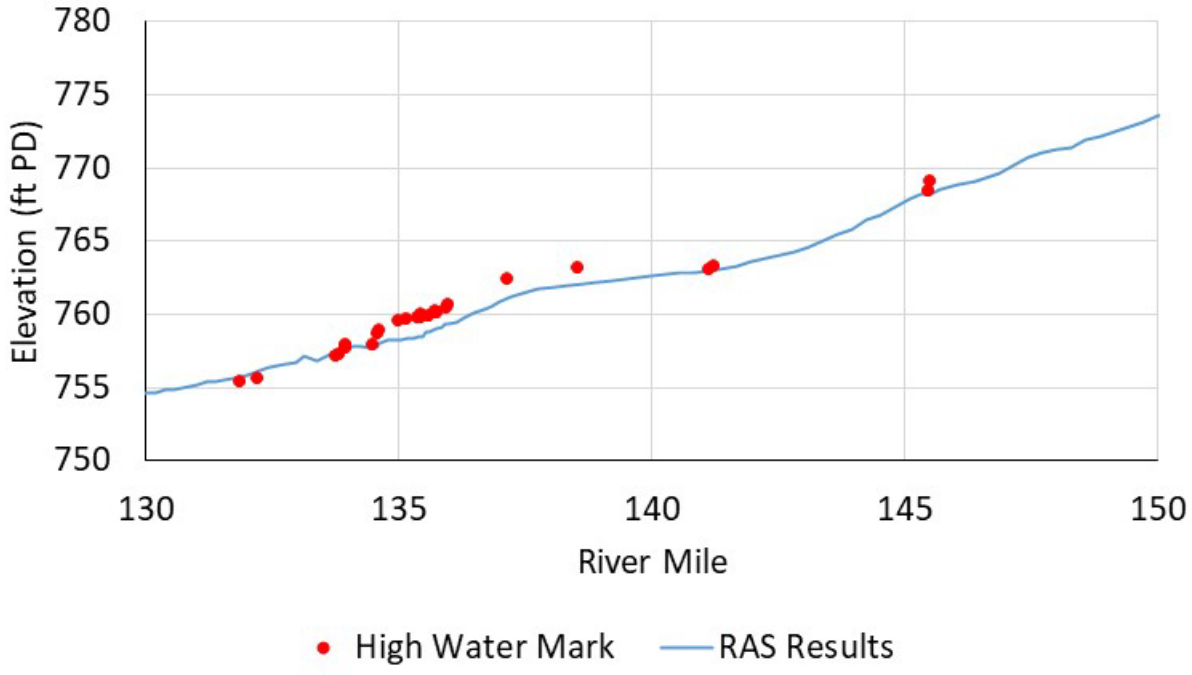

Figure 125
Comparison of STM WSE Results and Measured High Water Marks during the December 2015 Event

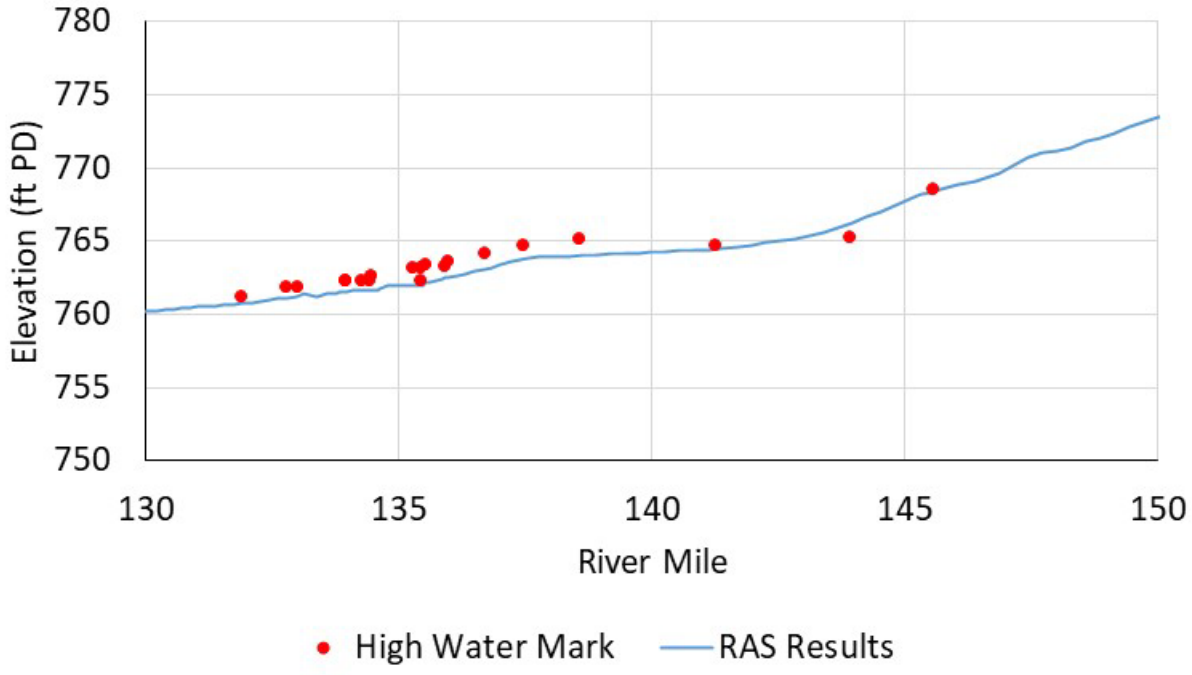

A third source of calibration WSEs was the field monitoring data collected during the study. The WSE loggers were in place for three of the calibration events: January 2017, April 2017, and May 2019. Not all logger locations have data for a given event; some were washed away or vandalized when attempts were made to retrieve data. Logger 9 was missing for both events, and data from loggers 7 and 8 were not included in calibration because they were located in areas where incoming, ungaged streams affected WSE reporting. These were initially placed before model parameters had been fully defined. Loggers 13, 14, 15, and 16 were located downstream of model extents. Figure 126 shows the location of loggers used in the calibration process.

Figure 126
Locations of Anchor QEA Loggers

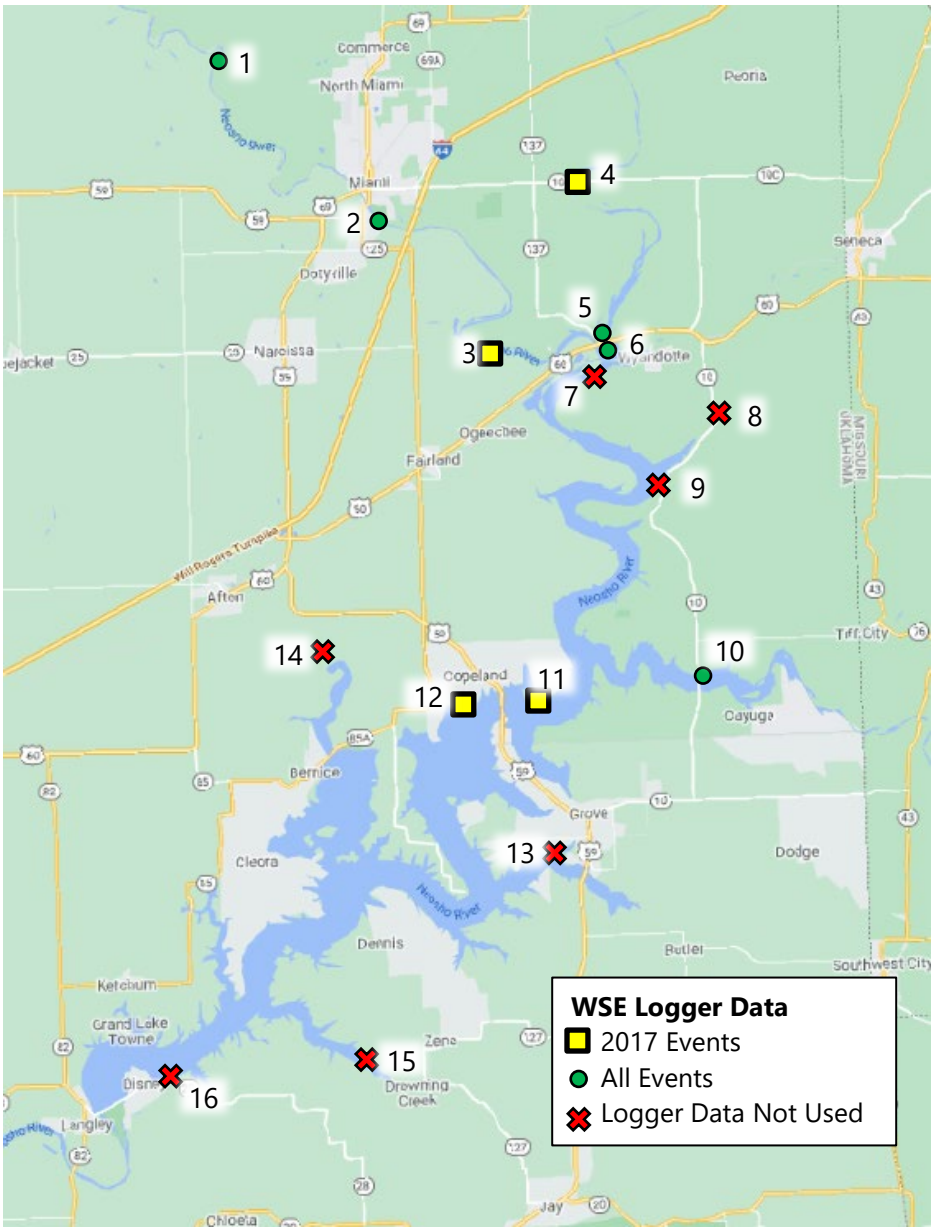

Note: Data from loggers 7, 8, 9, 13, 14, 15, and 16 were not used in the analysis as discussed above.

Figure 127 shows the overprediction and underprediction of peak WSE at the logger locations for those loggers used as calibration points. During the January 2017 event, the model averaged an overprediction of WSE by 0.23 foot. During the April 2017 event, the model averaged an underprediction of 0.15 foot. For the May 2019 event, the model averaged an underprediction of 0.47 foot.

Figure 127
Comparison of STM WSE Results and Measured Values from Anchor QEA Loggers

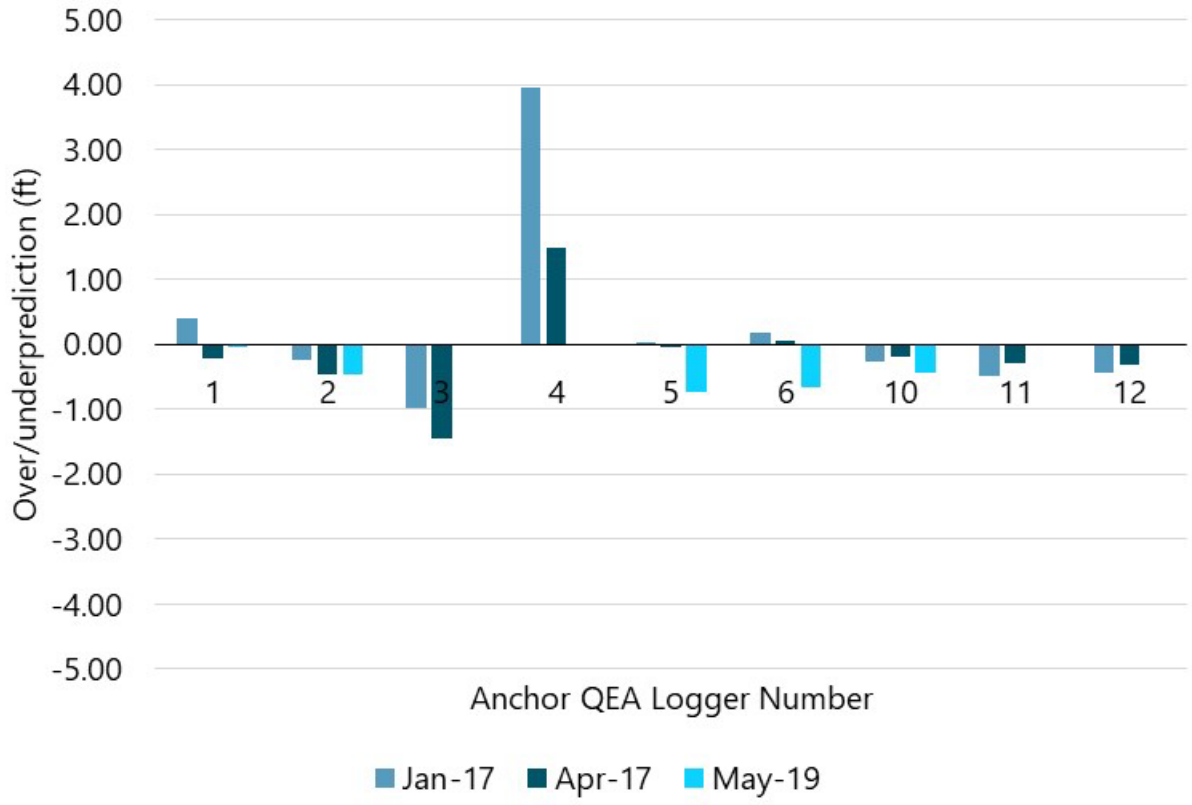

The STM hydraulic results were also compared to UHM simulations. The comparisons shown in the WEST ITR (2022) indicated significant differences between the models. By using the HEC-RAS bridge routines instead of lidded cross sections, the STM showed improved agreement with the UHM as presented in Figure 128 and Figure 129.

Figure 128
Neosho River WSE at RM 122.75, Upstream of Highway 60 near Twin Bridges State Park with STM Bridge Routines

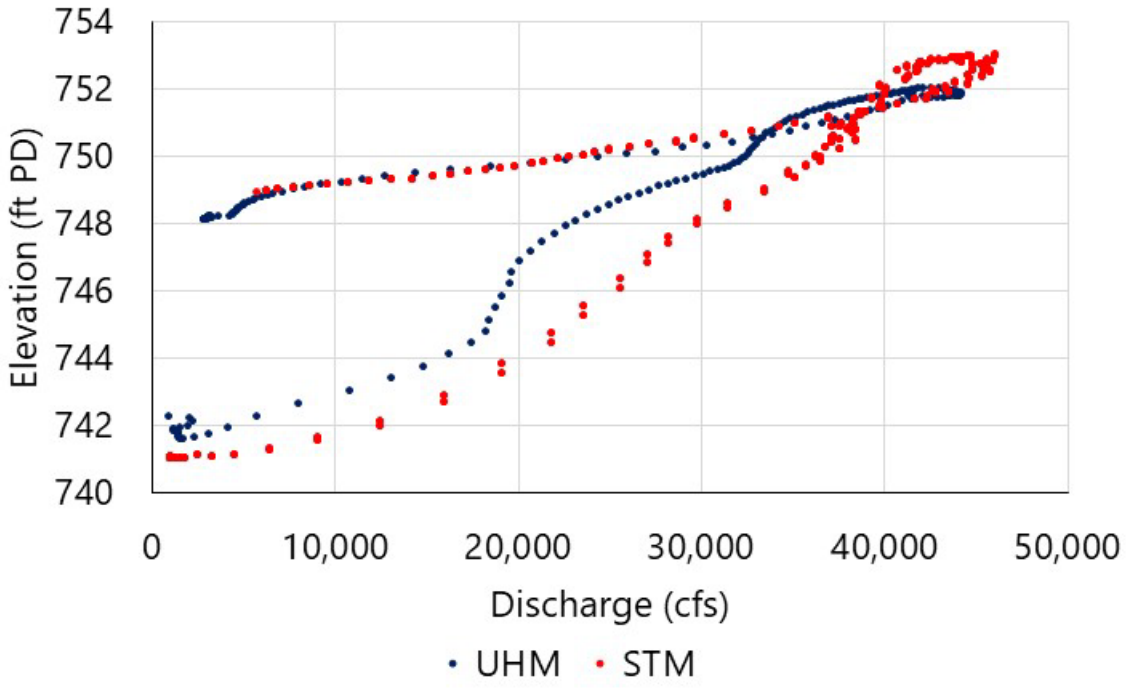

Similar results were found at RM 122, which is between the Highway 60 and Burlington Northern railroad bridges.

Figure 129
Neosho River WSE at RM 122, Between US-60 and Burlington Northern Railroad Bridges near Twin Bridges State Park with STM Bridge Routines

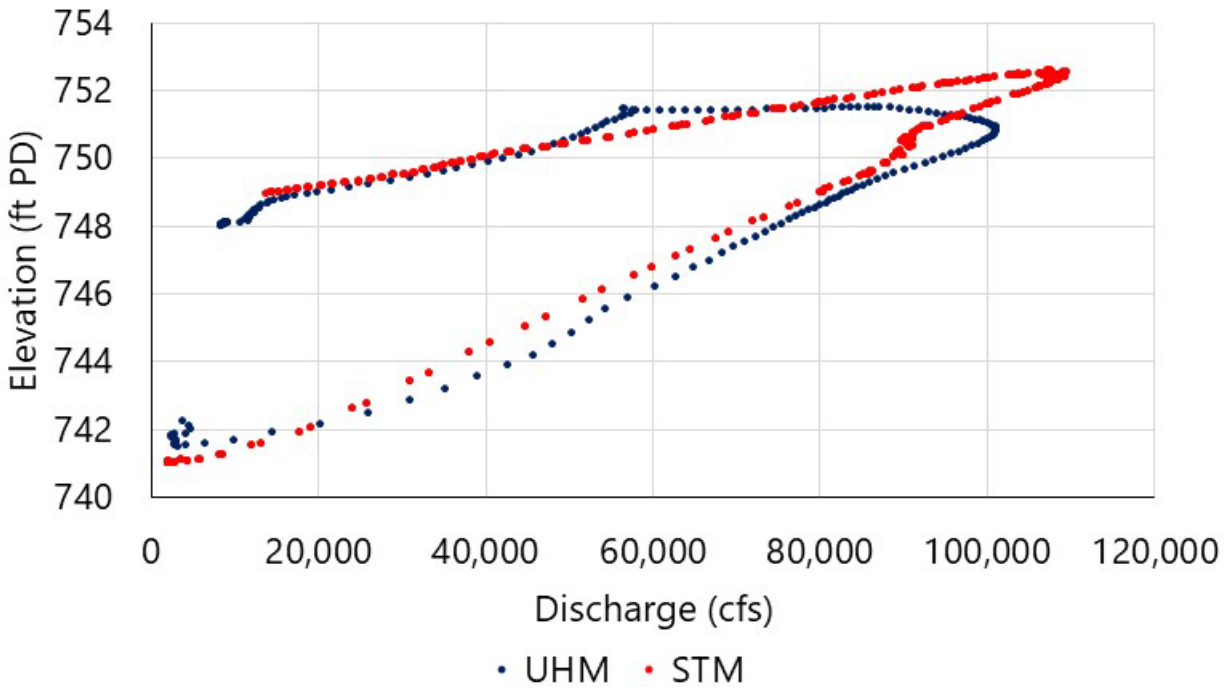

Figure 130 shows the Burlington Northern Railroad bridge and embankment backing up high flows in May 2019.

Figure 130
Burlington Northern Railroad Bridge and Embankment Viewed from Twin Bridges Boat Launch in May 2019

Source: GRDA, May 2019

6.2 Sediment Calibration

6.2.1 Model Inputs

6.2.1.1 Hydraulic Parameters

Sediment transport calibration was performed between 1942 and 2019. This was a function of available hydraulic information; continuous USGS (2021g) reservoir storage records at Pensacola Dam date to October 1942. The original WSE data are unavailable, but the USGS provided the historical stage-storage curves and dates of use (Strong 2022). Storage volumes were converted to elevations with those curves and used to set downstream WSEs in the calibration runs.

Historical flow data available from USGS gages (USGS 2021a, 2021b, 2021f) provided inflow volumes dating back to 1940 on the Neosho, Elk, and Spring rivers. Inflow volumes were recorded from 1984 to 1990 and 2004 to present on Tar Creek (USGS 2021e).

Due to the lack of available data for Tar Creek from 1940 to 1984, a synthetic hydrograph was generated using the Spring River as a reference hydrograph. The available flow data for Tar Creek (1984 to 2022) were compared to the same date range for Spring River. Spring River was chosen based on similarities in location and geographical extent of the watershed, despite the fact that Spring River is a significantly larger system than Tar Creek.

Linear regression comparing all peak daily discharges of Spring River and Tar Creek for the available data record resulted in a relatively poor correlation (R^2 = 0.29). Visual comparison of typical event hydrographs showed Tar Creek to recede more quickly to baseflow after precipitation events as would be expected of a smaller watershed. To account for this, relative peaks in the daily discharge were used for the comparison between the two watersheds. Relative peaks above the 10% daily exceedance flow for Tar Creek (110 cfs) were identified using Hydrologic Engineering Center Statistical Software Package (HEC-SSP) data filtering. The timing of Tar Creek peaks was compared to relative peaks of the Spring River daily discharge data and found that a Spring River daily discharge peak occurred within ±2 days of the Tar Creek peak discharge for 87% of the events. The linear relationship between these two peaks was much higher than when using all flows (R^2 = 0.65, Figure 131), and this linear relationship was used to determine Tar Creek peak flows during the missing period of record (1940 to 1984).

The majority of Tar Creek peak flows occurred 1 day before the peak flow of Spring River, and therefore the estimated peaks for Tar Creek throughout the missing period of record were assumed to occur 1 day before the Spring River peaks of that same time period. Based on visual examination, Tar Creek event hydrographs typically rose to the peak in a single day and then receded to pre-event levels in 2 to 3 days. Therefore, in the synthetic hydrograph for Tar Creek, event discharges were reduced to 50% of the peak for the following day, and to 25% of the peak the second day following the event. For all other daily flows in the synthetic hydrograph, the daily percent exceedance flow of Spring River was matched to the daily percent exceedance flow of Tar Creek to develop the background flow data. The same relationship was used to fill the data gap in Tar Creek daily discharge between 1994 and 2004.

Figure 131
Comparison of Tar Creek and Spring Creek Peak Events Over the 10% Daily Exceedance Flow (1984–2022)

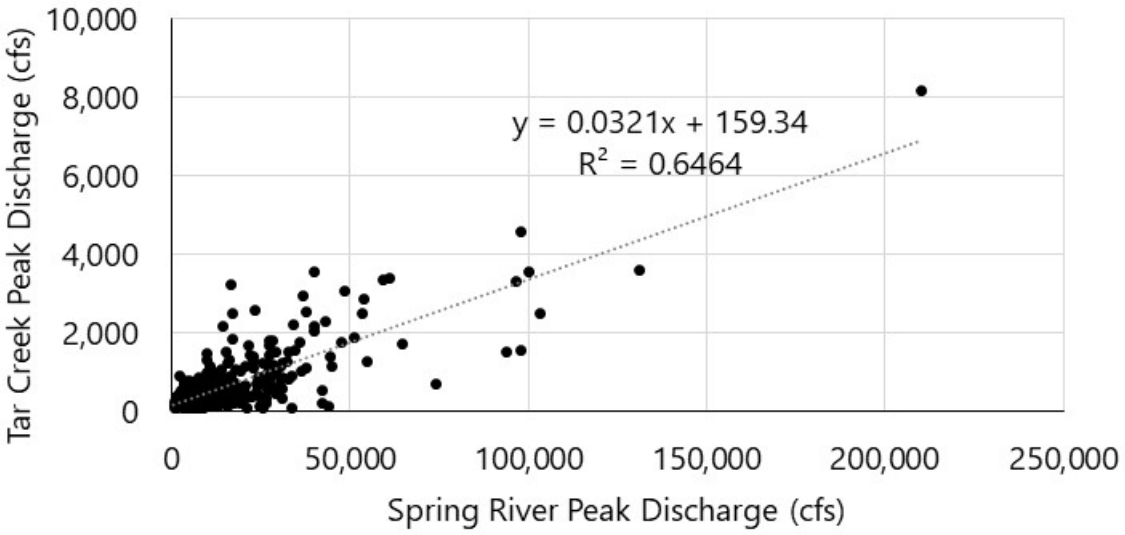

Another important part of the hydraulic inputs for STMs is the water temperature in the system. These data were derived from water level logger measurements collected from December 2016. Daily average temperatures of the Neosho River from East 60th Road were used as an approximation of temperatures throughout the year and applied for the period of evaluation (Figure 132).

Figure 132
Temperature Time Series for 1 Year of STM Simulation

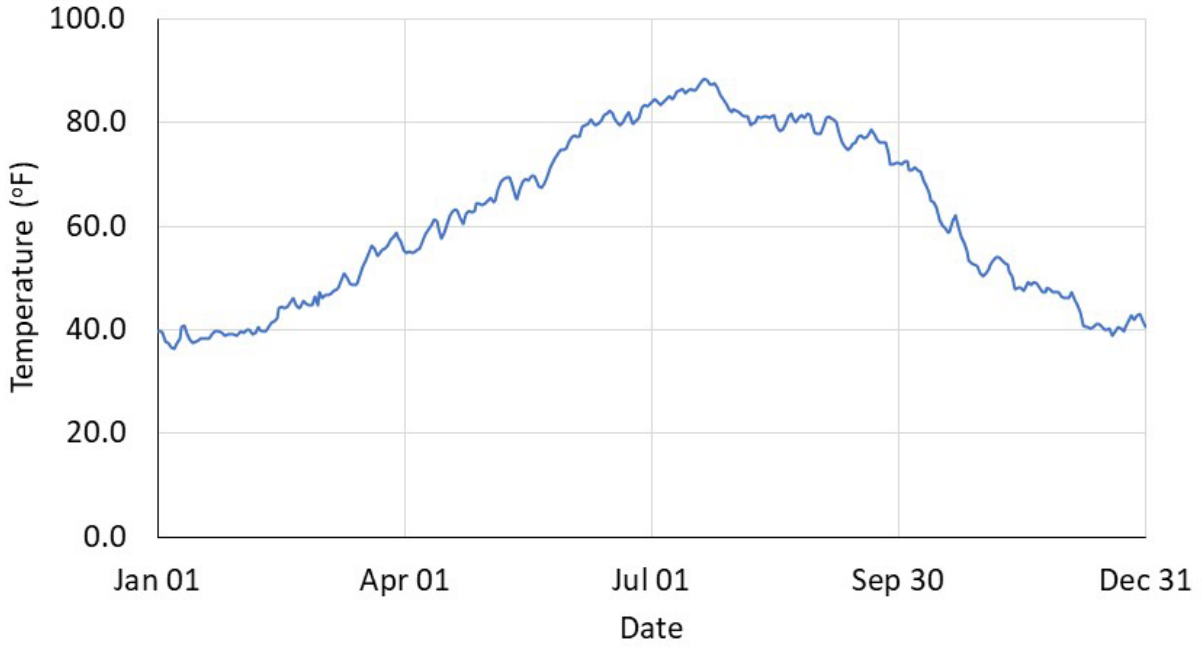

Note: Temperature data were repeated for each year throughout the duration of each simulation

6.2.1.2 Sediment Parameters

6.2.1.2.1 Bed Sediment

There are no known sediment data from pre-Project conditions in the modeled tributaries. Sediment properties were therefore assumed to have been similar to present-day sediment at the upstream extents of the reaches. Sediment grab samples collected during this study were used to define starting bed sediments as shown in Table 32 and their locations are highlighted in Figure 133.

Mobile bed limits were set to bank stations with a maximum erodible depth of 5 feet, and the Rubey falling velocity was used.

Table 32
Sediment Samples Used to Define Circa-1940 Bed Material

Stream	Sample	Cohesive Sediment Parameters			
Stream	Sample	Critical Shear Stress (lb/ft^2)	Erosion Rate, M ($lb/ft^2/hr$)	Critical Mass Wasting Shear Stress (lb/ft^2)	Mass Wasting Erosion Rate, M_{MW} ($lb/ft^2/hr$)
Neosho River	NR-60S	0.008352	0.00062	0.066816	0.08700
Spring River	S-02	0.002297	0.05053	0.066816	34.75437
Elk River	ER-76S	0.002506	0.06772	0.066816	9.04153
Tar Creek	TC60S	0.003550	0.03483	0.006816	22.70010

Note:
Detailed sediment information is included in Exhibit 2 of this report.

The cohesive parameters of the samples were also used for model development and played an important role in determining the erosive characteristics of the bed sediments. HEC-RAS uses the Krone-Partheniades relationship to parameterize the sediments (USACE 2016). The SEDflume (Integral Consulting 2020) results informed selection of the parameters presented in Table 32.

Figure 133
Location of Sediment Grab Sampling Efforts within the Grand Lake Watershed

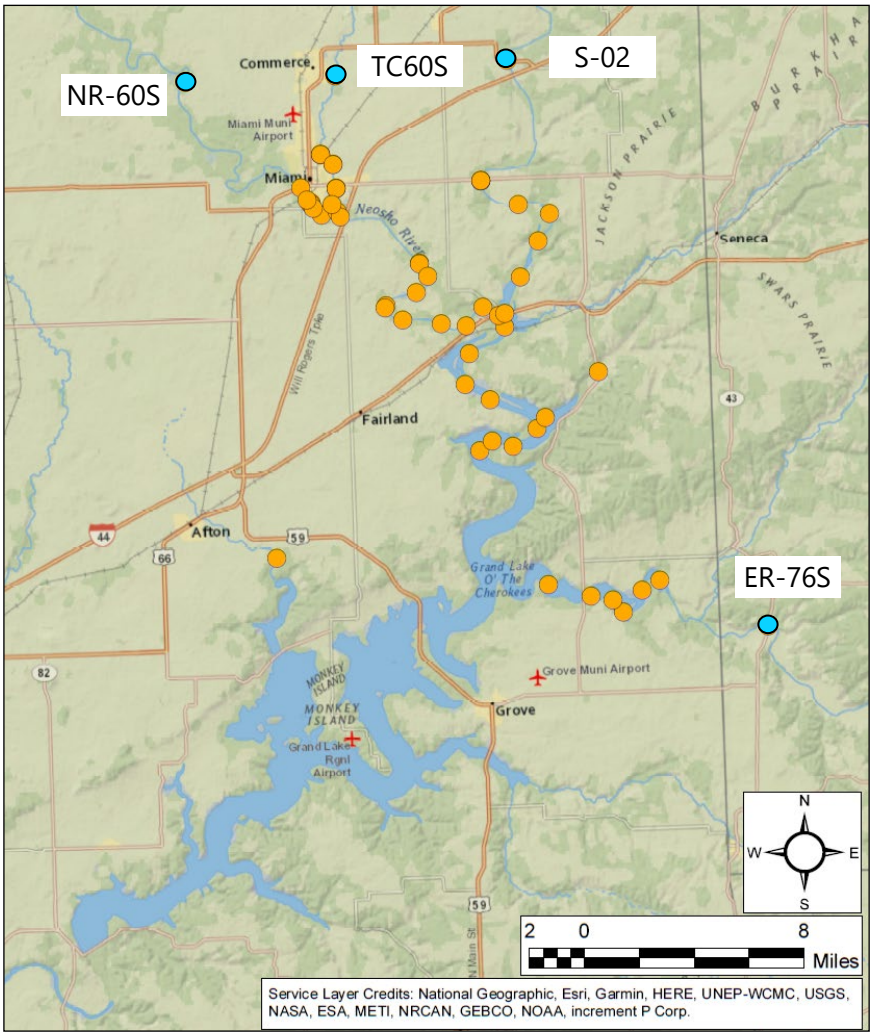

Notes:
Samples shown in teal (NR-60S, TC60S, S-02, and ER-76S) mark the most upstream locations of grab samples collected during this phase of the study. They were used to define circa-1940 bed conditions.
Samples shown in orange were used to define the bed conditions for future-looking sediment simulation runs.

6.2.1.2.2 Sediment Inflows

Sediment inflow information is sparse during the period of record as discussed in Section 2.1.3.2. The data were supplemented with measurements collected during this study (see Section 2.2.4).

The sediment inflow rating curves were developed from USGS measurements and supplemented with those discussed in Section 2.2.4. The Sediment Rating Curve Analysis Tool in HEC-RAS v. 6.2 was used to develop sediment rating curves for upstream boundaries of the model. This tool downloads

SSC information from user-selected USGS gages and allows importation of user data to create rating curves.

Sediment rating curves are often presented in the form of Equation 4.

Equation 4

$Q_{ss} = aQ^b$

where:

Q_{ss}	=	sediment load
a and b	=	constants
Q	=	stream discharge

When fitting this power function, most systems use the Least Mean Squares Error method, introducing implicit bias and resulting in an underprediction of incoming sediment loads. It is important to correct this bias when developing sediment rating curves for models. A more detailed discussion of this issue is presented in the HEC-RAS User's Manual (USACE 2016).

The Sediment Rating Curve Analysis Tool has built-in methods to remove that bias and present a more accurate sediment rating curve as explained in Section 1 of this report.

The rating curves shown in Table 33 were selected for this study.

Table 33
Sediment Rating Curves for STM Inflow Boundaries

Stream	Equation
Neosho River	$2.6039 \cdot 10^{-2} Q^{1.5089387}$
Spring River	$8.239 \cdot 10^{-3} Q^{1.5043}$
Elk River	$1.4031 \cdot 10^{-3} Q^{1.895494}$
Tar Creek	$3.117756 \cdot 10^{-1} Q^{1.143393}$

Note:
Rating curve equations were developed from a combination of data collected as part of this study and USGS gaging station information. Equations were then developed using the Duan method (Duan 1983) in the HEC-RAS Sediment Rating Curve Analysis Tool.

The sediment gradation data were taken from the measurements performed as part of this study. The information in Table 34 shows the distribution of grain sizes selected for incoming flow data.

Table 34
Grain Size Distributions of the Incoming Sediment Load

Stream	% Clay (< 0.004 mm)	% Very Fine Silt (0.004–0.008 mm)	% Fine Silt (0.008–0.016 mm)	% Medium Silt (0.016–0.032 mm)	% Coarse Silt (0.032–0.0625 mm)	% Very Fine Sand (0.0625–0.125 mm)
Neosho River	50	11	12	12	13	2
Spring River	40	10	11	15	20	4
Elk River	50	10	11	11	10	8
Tar Creek	50	10	11	11	10	8

Inflowing sediment erosive parameters are shown in Table 35. This was based on evaluation of sediment in the system and was also used for calibration parameters during model development.

Table 35
Incoming Sediment Erosive Parameters

Critical Shear Stress (lb/ft^2)	Erosion Rate, M ($lb/ft^2/hr$)	Critical Mass Wasting Shear Stress (lb/ft^2)	Mass Wasting Erosion Rate, M_{MW} ($lb/ft^2/hr$)
0.002506	0.06772	0.066816	9.04153

6.2.2 Calibration Evaluation

The primary metric used for model evaluation was sediment deposition volumes. This information was extracted from model runs by comparing the mass of sediment deposited between the start of the simulation and the next available bathymetry survey according to Figure 134 and Table 36.

Figure 134
Modeled Reaches Used for Calibration and Validation by Available Survey Data (All Starting Geometry was Based on Circa-1940 Data)

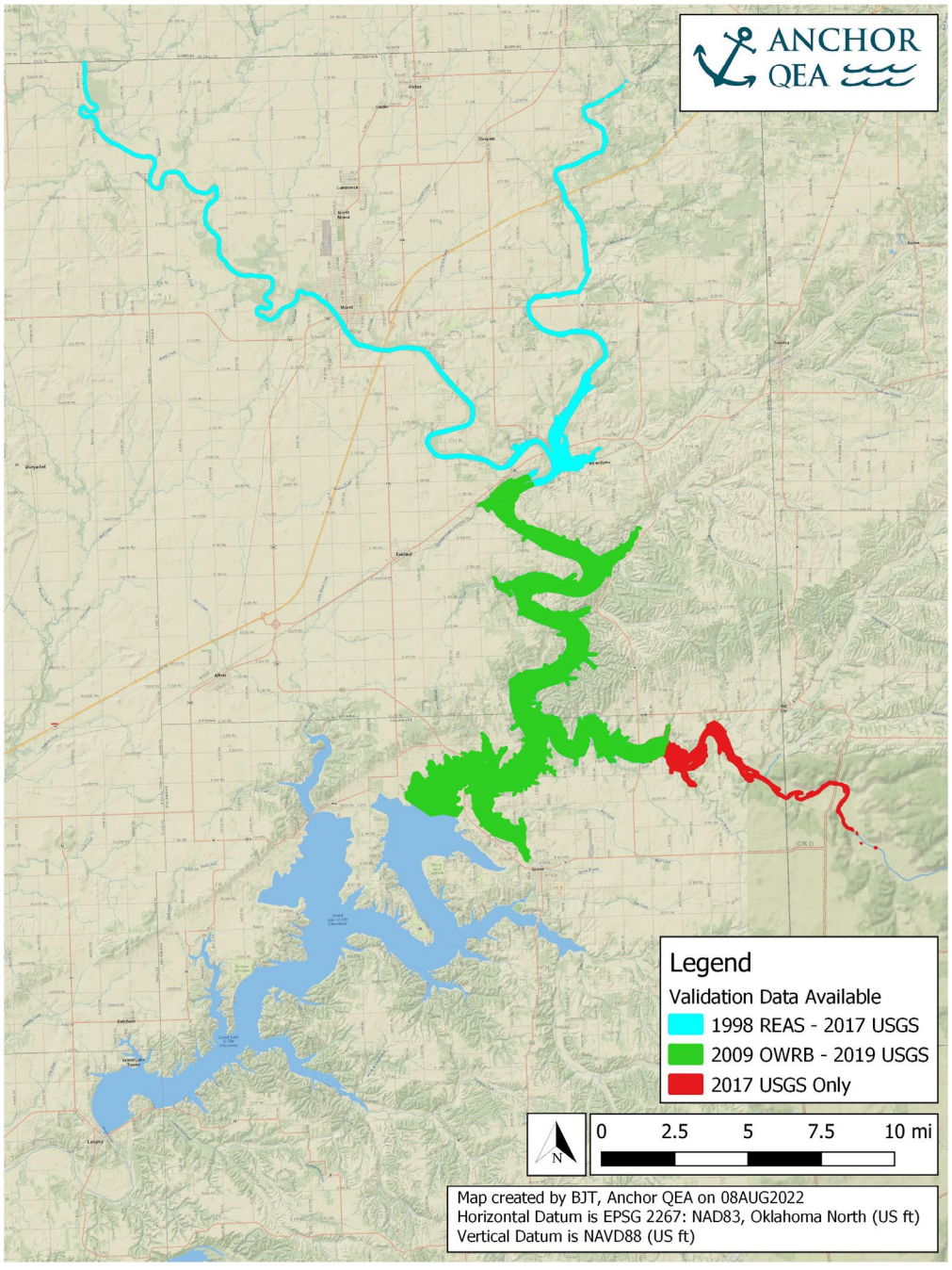

Table 316
Model Reaches and Available Survey Data for STM Development

Reach	Starting Survey	Calibration Survey	Validation Survey
Upper (Above RM 120.1)	Circa-1940 USACE	Circa-1998 REAS	2017 USGS
Lower (RM 120.1–RM 100)	Circa-1940 USACE	2009 OWRB	2019 USGS
Elk River (Above RM 5.47)	Circa-1940 USACE	2017 USGS	N/A
Reservoir (Below RM 100)	Circa-1940 USACE	2009 OWRB*	2019 USGS

Note:
*2009 OWRB data were not used for long-term analysis downstream of RM 100 (Section 2.1.1.5.1). Sedimentation rates from 1940 to 2009 were implausibly different than 2009 to 2019, so an assessment of deposition from 1940 to 2019 was used instead.

Sediment calibration runs simulated flow from October 1942 through October 2019. Evaluation of the results was based on the available survey information for the Neosho River, Spring River, and Elk River. Cross-sectional data from 1941 were digitized from survey data obtained from USACE surveys (1941). For the Neosho River below the Spring River and the Elk River, the current dataset was obtained from the 2019 bathymetric survey data. For the Spring River and the Neosho River upstream of the Spring River, the 2017 bathymetric survey data were used since the 2019 data extents did not include these areas.

River mile stations of the cross sections from the 1941 data were used to identify the most comparable cross sections in the contemporary datasets. Not all the 1941 cross sections had an exact river mile station match in the current data, so the nearest possible cross section was used—with most comparisons being within 0.05 river mile. The river mile stations of each river are shown in Table 37 through Table 40. Horizontal stationing differed between 1941 and 2017/2019 due to a lack of precise geographical information on where the 1941 cross sections are located. To match the horizontal position of 1941 and 2017/2019 cross sections, the horizontal stationing for the 1941 data were shifted based on visual comparison with the contemporary datasets.

Cross-sectional channel area was calculated based on a reference elevation set at the approximate high water level for each cross section, with the same elevation being used between each set of 1941 cross sections and 2017/2019 cross sections. The area under this elevation and above the cross-section elevation was considered the cross-sectional area and these were differenced to find the cross-sectional change in channel capacity. Figure 135 through Figure 138 provide examples for each river, showing the 1941 cross sections, 2017/2019 cross sections, and the reference elevation. Finally, the volume change was calculated using the same approach used by HEC-RAS in defining the representative bed sediment volume for a cross section, which multiplies cross-sectional change in area by the average of upstream and downstream reach lengths. Table 37 through Table 40 show the reference elevation, cross-section areas for 2017 and 2019, change in cross-sectional areas, and the volumetric change in channel cross sections in millions of cubic feet for each river.

Table 37
Elk River 1941 to 2017 Cross-Section Comparison

1941 Cross Section (RM)	2017 Cross Section (RM)	Reference Elevation (feet PD)	1941 Area (ft^2)	2017 Area (ft^2)	Change In Area (ft^2)	Change In Volume ($ft^3 \times 10^6$)
0.76	0.8	758.93	118,092	105,556	12,536	107
3.22	2.96	758.93	132,363	114,771	17,592	220
5.50	5.18	758.93	98,125	77,321	20,804	218
7.20	6.44	758.93	109,768	77,994	31,773	318
9.28	8.41	763.93	118,092	110,807	7,285	74
11.03	10.08	763.93	55,118	44,891	10,227	91
12.64	11.68	763.93	22,140	18,833	3,308	34
13.77	12.8	763.93	18,459	19,849	-1,390	-4
					Reach Total	**617**

Figure 135
Example Elk River Cross Section RM 9.28

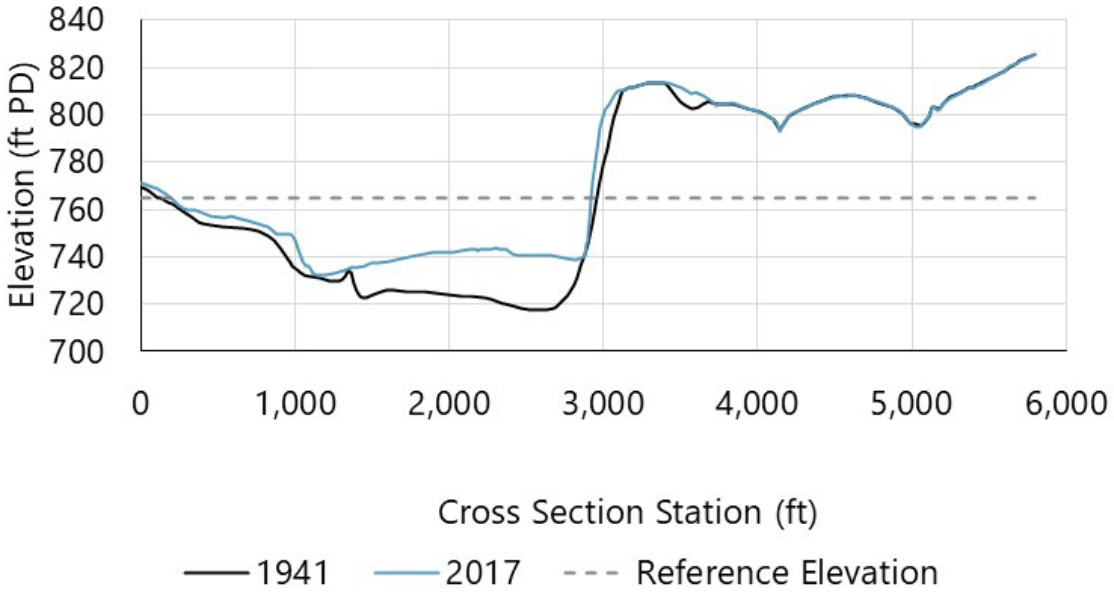

Table 38
Neosho – Below Spring River 1941 to 2019 Cross-Section Comparison

1941 Cross Section (RM)	2019 Cross Section (RM)	Reference Elevation (feet PD)	1941 Area (ft^2)	2019 Area (ft^2)	Change In Area (ft^2)	Change In Volume ($ft^3 \times 10^6$)
100.78	100.82	758.93	347,839	308,627	39,212	555
104.07	104.18	758.93	260,683	212,408	48,275	874
107.68	107.81	758.93	156,905	109,099	47,806	1,000
113.70	113.79	758.93	97,942	61,154	36,788	1,060
118.60	118.56	758.93	72,891	52,126	20,765	268
					Reach Total	**3,757**

Figure 136
Example Neosho River – Below Spring River Cross Section RM 118.60

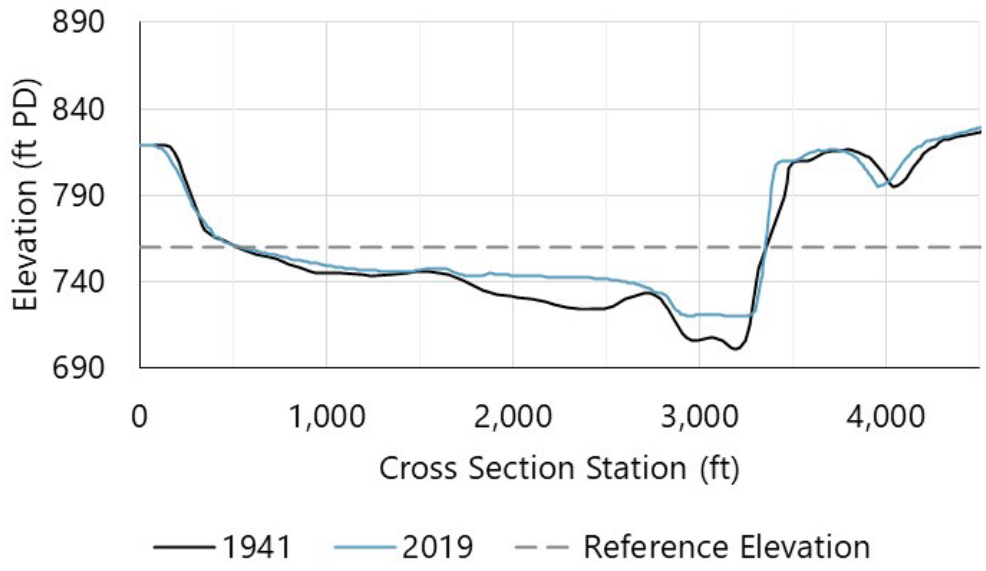

Table 39
Neosho – Above Spring River 1941 to 2017 Cross-Section Comparison

1941 Cross Section (RM)	2017 Cross Section (RM)	Reference Elevation (feet PD)	1941 Area (ft^2)	2017 Area (ft^2)	Change In Area (ft^2)	Change In Volume ($ft^3 \times 10^6$)
124.25	124.20	748.93	16,177	12,082	4,095	70
129.98	130.01	753.93	41,877	26,911	14,967	377
133.79	133.80	753.93	13,037	8,500	4,537	85

1941 Cross Section (RM)	2017 Cross Section (RM)	Reference Elevation (feet PD)	1941 Area (ft^2)	2017 Area (ft^2)	Change In Area (ft^2)	Change In Volume ($ft^3 \times 10^6$)
137.07	136.98	753.93	7,849	6,655	1,193	17
139.26	139.19	758.93	8,807	7,902	905	11
141.80	141.67	763.93	17,090	12,737	4,353	46
143.23	143.38	763.93	7,442	6,520	922	10
144.64	144.52	763.93	6,865	5,340	1,526	70
					Reach Total	**617**

Figure 137
Example Neosho River – Above Spring River Cross Section RM 124.25

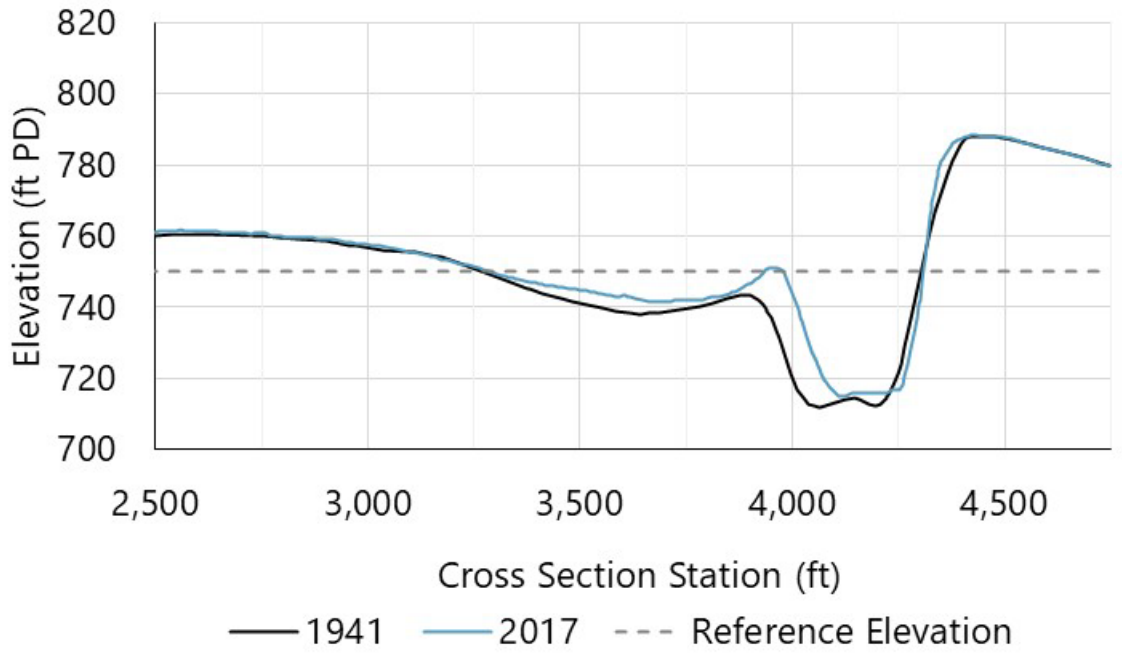

Table 40
Spring River 1941 to 2017 Cross-Section Comparison

1941 Cross Section (RM)	2017 Cross Section (RM)	Reference Elevation (feet PD)	1941 Area (ft^2)	2017 Area (ft^2)	Change In Area (ft^2)	Change In Volume ($ft^3 \times 10^6$)
0.78	0.79	748.93	24,892	19,476	5,415	74
5.19	5.1	748.93	9,721	6,945	2,776	43
6.63	6.64	753.93	8,897	8,388	508	7

1941 Cross Section (RM)	2017 Cross Section (RM)	Reference Elevation (feet PD)	1941 Area (ft^2)	2017 Area (ft^2)	Change In Area (ft^2)	Change In Volume ($ft^3 \times 10^6$)
10.49	10.51	753.93	7,846	4,440	3,406	51
12.35	12.43	768.93	11,400	12,884	-1,484	-21
15.89	15.93	768.93	8,187	6,074	2,113	25
16.84	16.88	768.93	9,240	4,784	4,456	11
					Reach Total	**191**

Figure 138
Example Spring River Cross Section RM 15.89

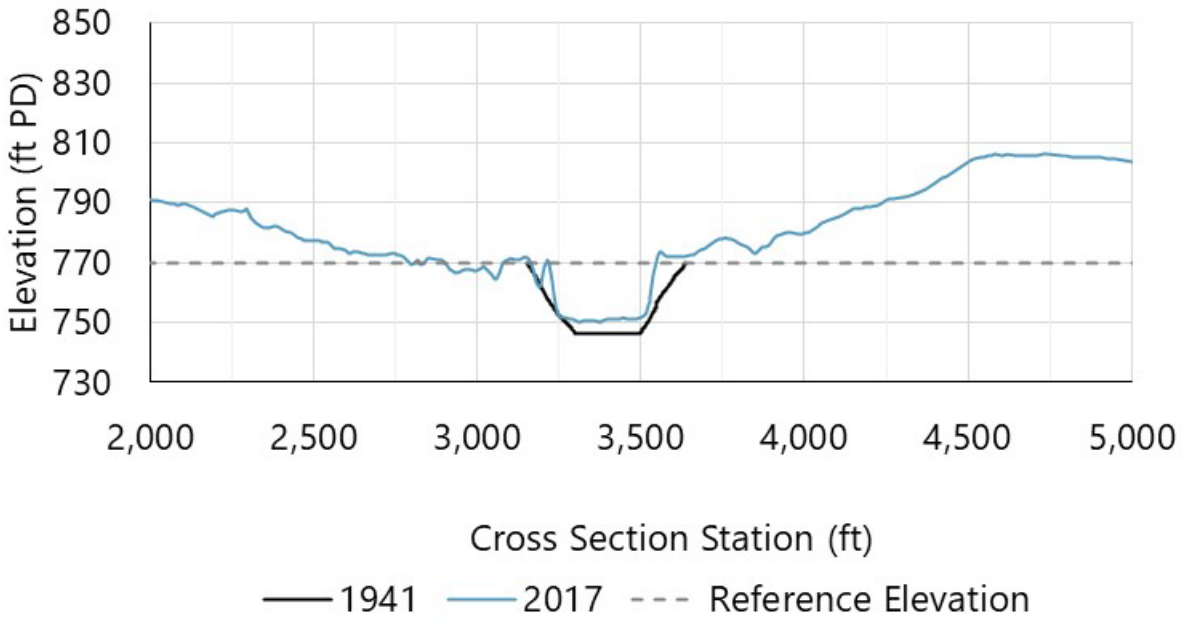

The simulation data were then compared to measured data using metrics defined by Moriasi et al. (2007). Specifically, the Nash-Sutcliffe Efficiency (NSE), which evaluates the ratio of noise to measured data variance (Nash and Sutcliffe 1970) as defined in Equation 5.

Equation 5

$$NSE = 1 - \left[\frac{\sum_{i=1}^{n}\left(Y_i^{obs} - Y_i^{sim}\right)^2}{\sum_{i=1}^{n}\left(Y_i^{obs} - Y^{mean}\right)^2}\right]$$

where:

Y_i^{obs}	=	the *i*th observation for the constituent being evaluated
Y_i^{sim}	=	the *i*th simulated value for said constituent
Y^{mean}	=	the mean of observed data
n	=	the total number of observations

Another metric used was the Percent Bias (PBIAS) as defined by Gupta et al. (1999). This is used as a measure of the tendency for the simulation to overpredict or underpredict the constituent of interest and is defined in Equation 6.

Equation 6

$$PBIAS = \left[\frac{\sum_{i=1}^{n}\left(Y_i^{obs} - Y_i^{sim}\right) \cdot (100)}{\sum_{i=1}^{n}\left(Y_i^{obs}\right)}\right]$$

where:

$PBIAS$	=	percent bias

Where *PBIAS* is expressed as a percentage, and it is consistent with percent difference in volume.

The third metric from Moriasi et al. (2007) used in this study was the RMSE-Observations Standard Deviation Ratio (RSR) as defined by Singh et al. (2004). This measure is a reformulation of the RMSE that normalizes results so an ideal model will produce an RSR of 0. It is defined as shown in Equation 7.

Equation 7

$$RSR = \frac{RMSE}{STDEV_{obs}} = \frac{\left[\sqrt{\sum_{i=1}^{n}\left(Y_i^{obs} - Y_i^{sim}\right)^2}\right]}{\left[\sqrt{\sum_{i=1}^{n}\left(Y_i^{obs} - Y^{mean}\right)^2}\right]}$$

where:

RMSE = root mean square error

$STDEV_{obs}$ = standard deviation of the observed values

Table 41 shows typical criteria adopted by Moriasi et al. (2007) for sediment modeling.

Table 41
Statistical Criteria for Sediment Model Performance

Model Performance	NSE	PBIAS	RSR
Very Good	0.75 < NSE ≤ 1.00	|PBIAS| < 15	0.00 ≤ NSE ≤ 0.50
Good	0.65 < NSE ≤ 0.75	15 ≤ |PBIAS| < 30	0.50 ≤ NSE ≤ 0.60
Satisfactory	0.50 < NSE ≤ 0.65	30 ≤ |PBIAS| < 55	0.60 ≤ NSE ≤ 0.70
Unsatisfactory	NSE ≤ 0.50	|PBIAS| ≥ 55	RSR > 0.70

Note: Adapted from Moriasi et al. (2007)

6.2.2.1 Results

The model performed well in most areas of the Neosho River (Figure 139). The model agrees with measured data in most of the reach upstream of RM 120.1, with the exception of RM 130.01, and it also agrees on the upstream face of the delta feature (RM 120.1 to RM 105), where GRDA asserted in the April 2022 USP the model was able to reasonably predict sediment deposition. Below that point, lacustrine dynamics and the prevalence of cohesive sediments decrease HEC-RAS's suitability for modeling deposition.

Figure 139
Neosho River Volume Change from Circa 1940

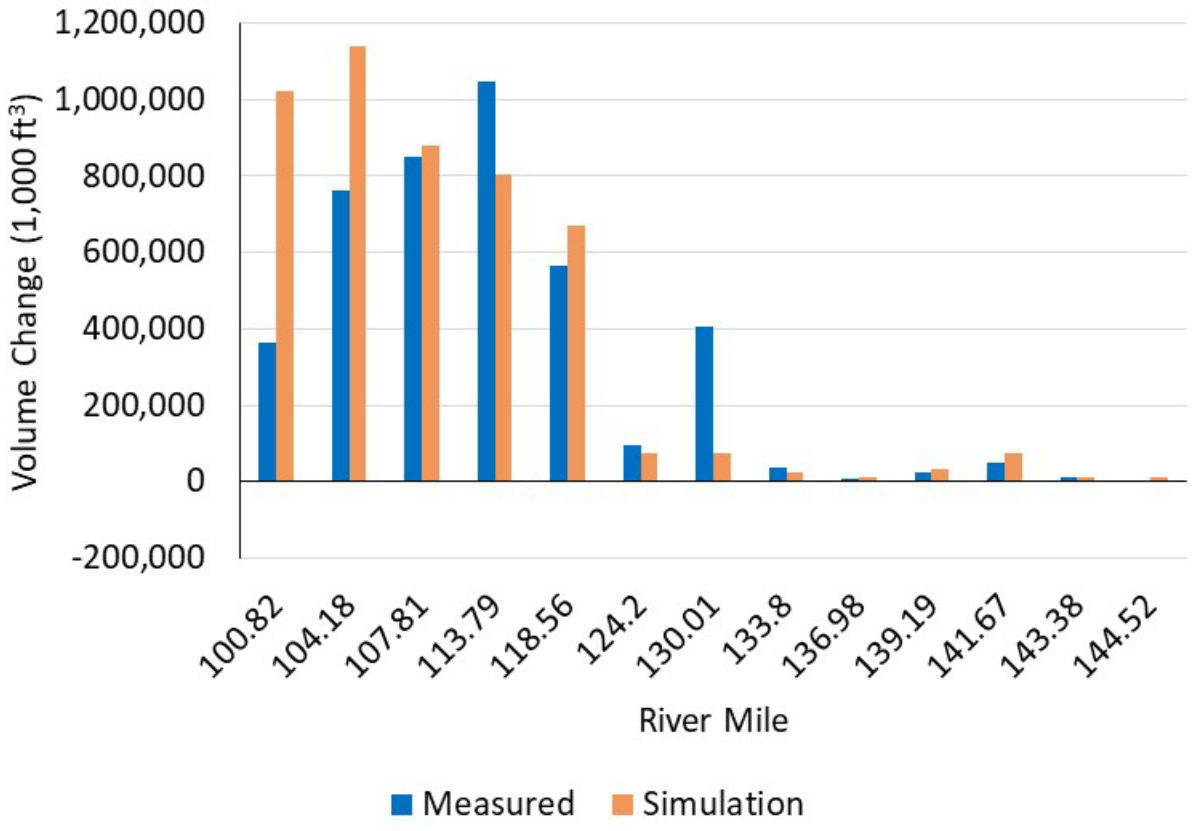

Notes: Model results above RM 120.1 are compared to 1998 REAS data.
Model results below RM 120.1 are compared to 2009 OWRB data.

There are two locations where the modeled results match poorly with the measured datasets. It underpredicts deposition on the Neosho River near RM 130.01 and overpredicts deposition on the downstream face of the delta feature (RM 104.18 and 100.82). Removing those locations from the analysis result in a much-improved calibration. The statistical analysis of calibration results with and without those cross sections are shown in Table 42.

Table 42
Statistical Calibration Evaluation Parameters of STM on the Neosho River

Reach	NSE (Target: > 0.5)	PBIAS (|Target|: < 0.55)	RSR (Target: < 0.70)
All Locations	-0.94	0.19	0.69
Excluding RM 130.01, 104.18, 100.82	0.95	0.01	0.22

Note:
Calibration of the model showed significant underprediction at RM 130.01 and overprediction on the downstream face of the delta feature (RM 104.18, 100.82).

Results on the Spring and Elk rivers were less accurate due to poor historical data quality. As discussed in Sections 2.1.1 and 6.1.1 of this report, the limitations of the data reduce the ability to perfectly simulate sediment transport. As discussed previously, the exact locations of the circa-1940 cross-sectional surveys were estimated based on reported stream distances (USACE 1941, 1942) and placed on the 1938 topographic maps (USACE 1938). Uncertainty of the placement of the cross-section survey data contributes to reduced model calibration results.

Spring River results are presented in Figure 140 and Elk River results are shown in Figure 141.

Figure 140
Spring River Volume Change from Circa 1940

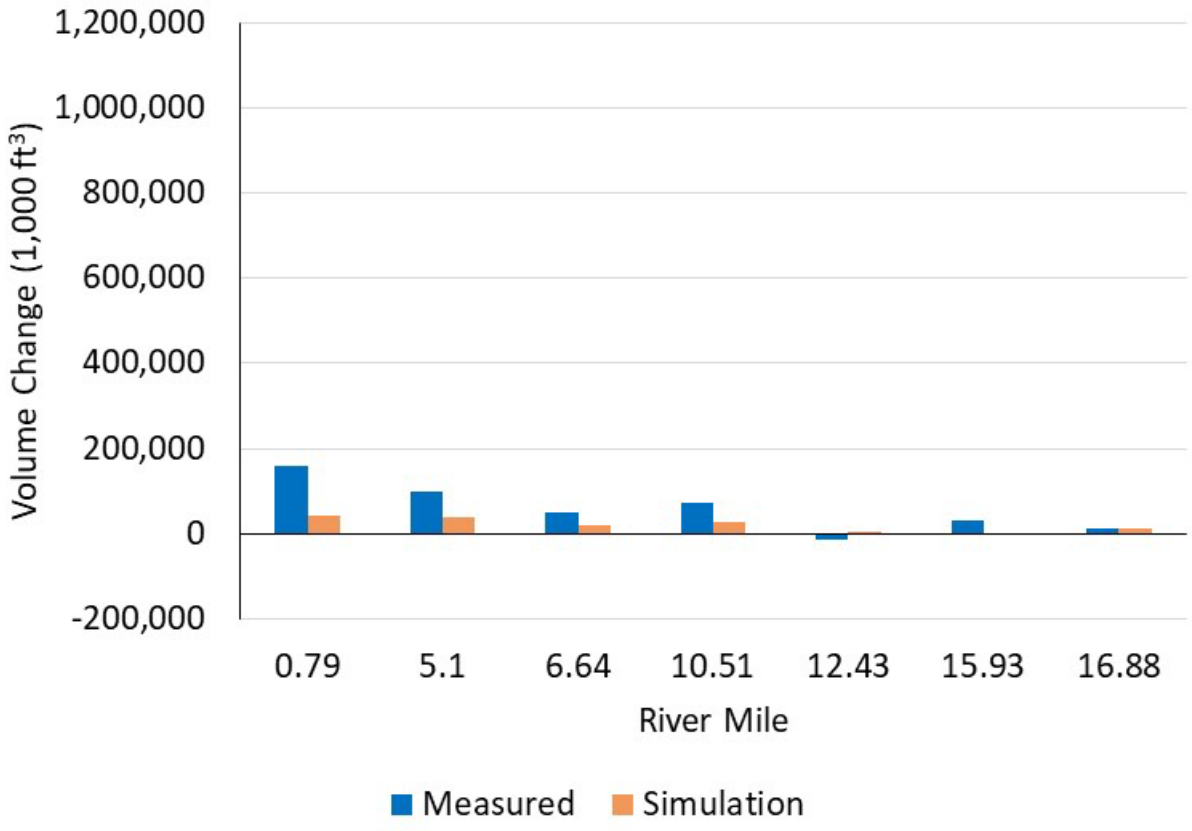

Note: Model results are compared to 1998 REAS data.

Figure 141
Elk River Volume Change from Circa 1940

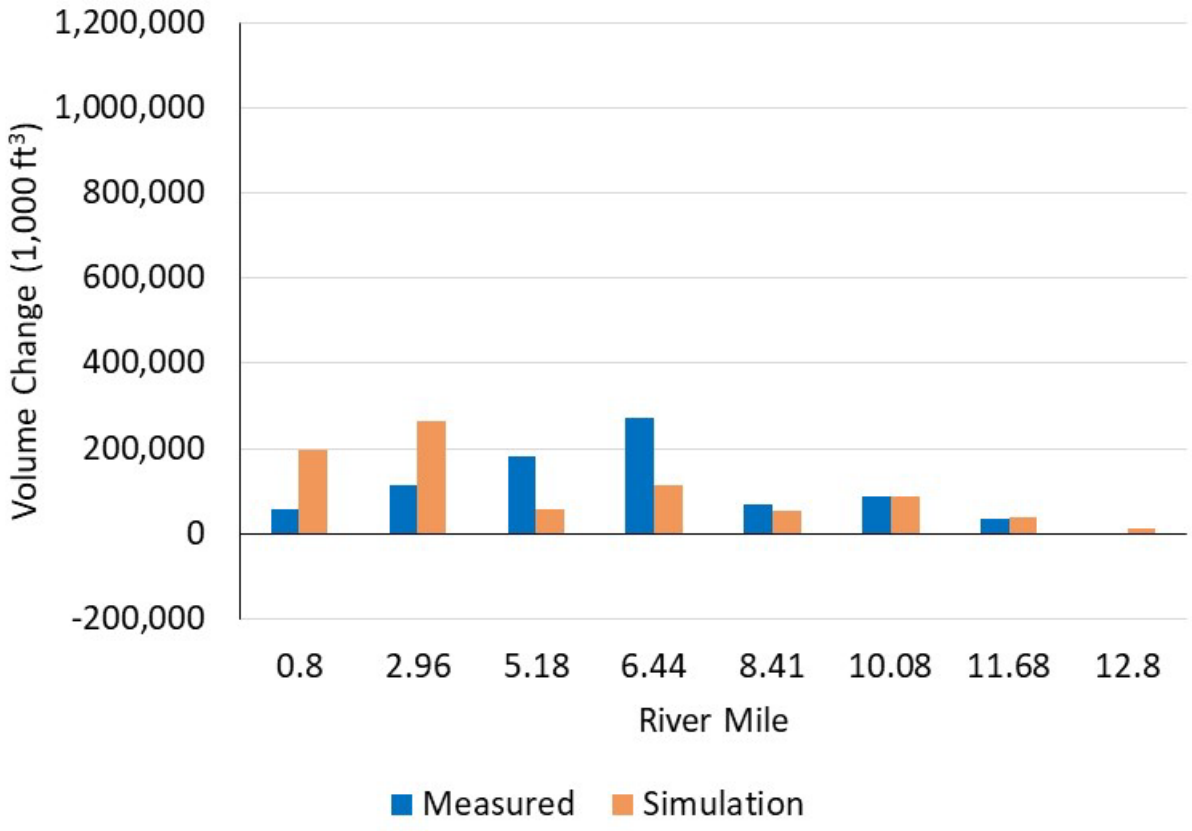

Notes: Model results above RM 5.47 are compared to 2017 USGS data.
Model results below RM 5.47 are compared to 2009 OWRB data.

The statistical analysis of the Spring River and Elk River model results is presented in Table 43.

Table 43
Statistical Calibration Evaluation Parameters of STM on the Spring and Elk Rivers

Reach	NSE (Target: > 0.5)	PBIAS (|Target|: < 0.55)	RSR (Target: < 0.70)
Spring River	0.04	-0.62	0.98
Elk River	-0.55	0.03	1.24

The model tends to underpredict sediment deposition on the Spring River and overpredict deposition on the Elk River. These rivers have the least reliable cross-sectional survey placements, with no bridges to reference for cross-section locations.

Another method of comparing the model results to measured data is to compare predicted and measured geometry. Two of the more useful means of evaluating channel evolution with HEC-RAS models are average channel and average section elevations. These metrics contain far more geometry information than a simple thalweg plot; a thalweg plot looks only at the lowest point of the cross section, whereas the other metrics incorporate the trends across the entire stream channel and submerged portion of the model. These are more closely related to hydraulic flow areas and are in many cases a better means of condensing channel geometry into a simple profile.

6.2.2.2 Calibration Validation

After calibration, the model performance was compared to the latest available modern surveys as shown in Figure 142. The results are presented below.

Figure 142
Neosho River Volume Change Validation

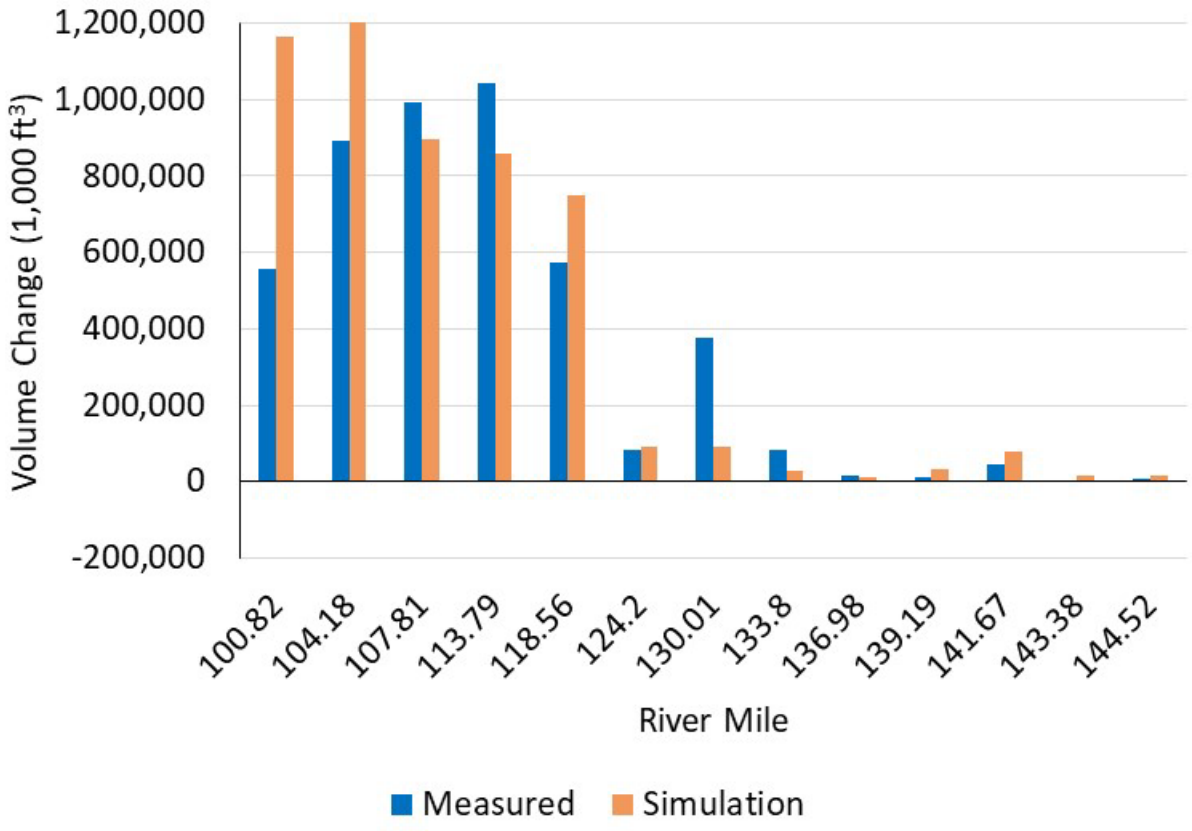

Notes: Model results above RM 120.1 are compared to 2017 USGS data.
Model results below RM 120.1 are compared to 2019 USGS data.

The validation results on the Neosho River showed similar patterns to those in the calibration; deposition was significantly overpredicted on the downstream face of the delta feature (below RM 105) and underpredicted near RM 130.01. Statistical evaluations are shown in Table 44.

Table 44
Statistical Validation Evaluation Parameters of STM on the Neosho River

Reach	NSE (Target: > 0.5)	PBIAS (|Target|: < 0.55)	RSR (Target: < 0.70)
All Locations	-0.64	0.25	0.69
Excluding RM 130.01, 104.18, 100.82	0.80	0.13	0.44

Notes:
Calibration of the model showed significant underprediction at RM 130.01 and overprediction on the downstream face of the delta feature (RM 104.18, 100.82)

Validation on the Elk and Spring rivers was less precise than on the Neosho River, similar to the calibration results (Figure 143 and Figure 144).

Figure 143
Spring River Volume Change Validation

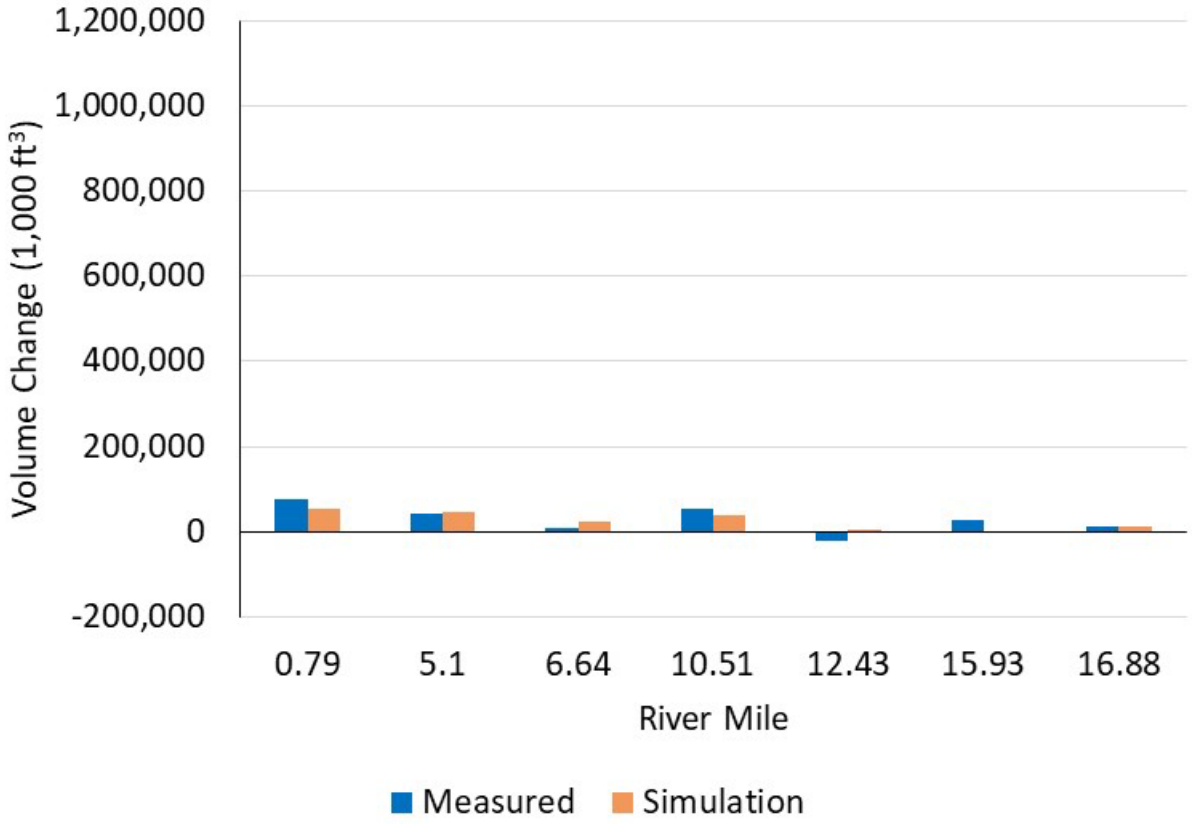

Figure 144
Elk River Volume Change Validation

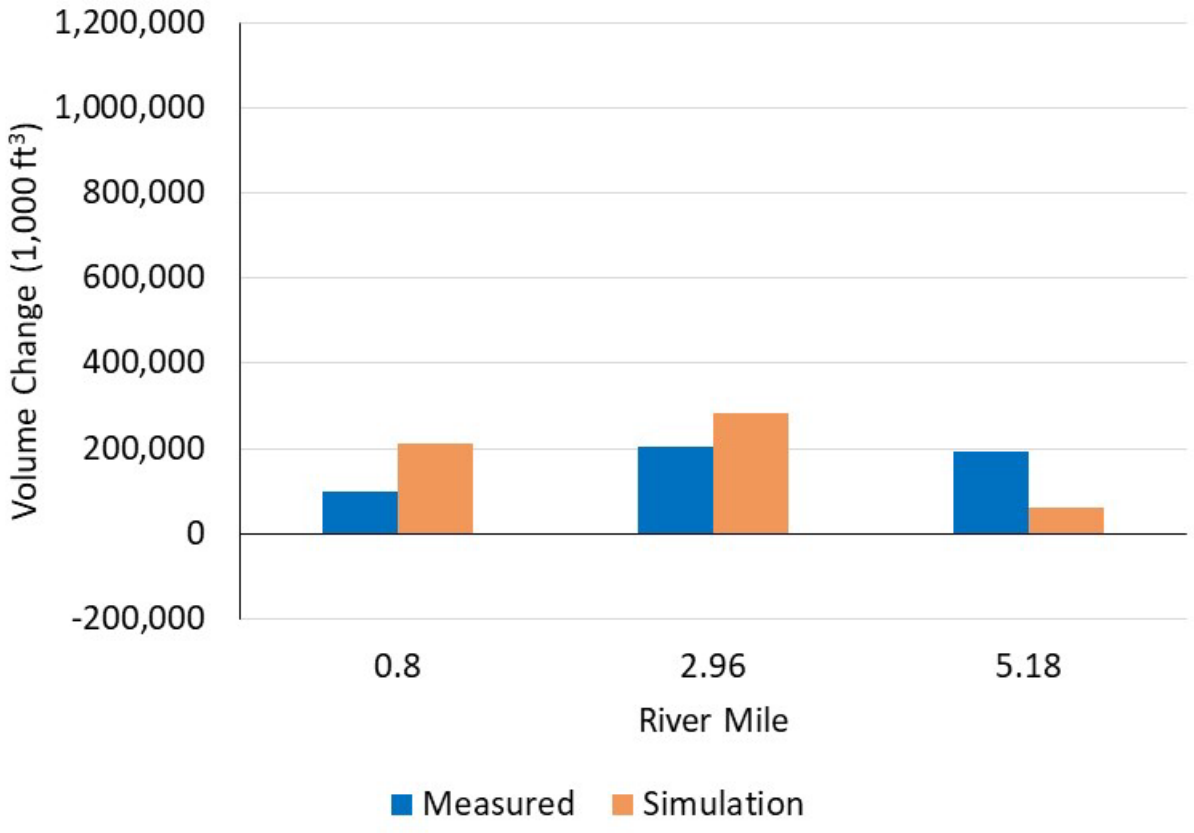

Note: There is no available validation data on the Elk River above RM 5.46 as shown in Table 36.

The statistical analysis of the validation fits for the Elk River and Spring River is shown in Table 45.

Table 45
Statistical Validation Evaluation Parameters of STM on the Spring and Elk Rivers

Reach	NSE (Target: > 0.5)	PBIAS (|Target|: < 0.55)	RSR (Target: < 0.70)
Spring River	0.62	-0.09	0.62
Elk River	0.08	-0.04	0.98

As during calibration, the model performance in validation runs is limited by the quality of available datasets. This was a known issue during model development and was discussed in the USP. To address this issue, the model was run using several input conditions for sedimentation as a means of bounding the expected sediment deposition and transport within the study area.

Another method to evaluate STMs is comparing average channel and average section profiles. This was discussed by WEST in their ITR (2022) in detail, but a brief summary of the measurement is provided here. The average channel and average section profiles are a more effective means of showing stream geometry than a simple thalweg profile. The thalweg *only* uses one point per cross section to show a stream profile; average section and average channel take the entire channel or entire cross section into consideration, condensing for more information into the profile plot. This also provides a more representative method of evaluating hydraulic characteristics, because it accounts for the cross-section geometry as well as the thalweg.

The Neosho River average channel and average section profiles are shown in Figure 145 and Figure 146. Mean error in channel elevation on the river compared to measured modern geometry data is -1.1 feet, meaning the model underpredicts bed elevations as compared to measured values. Mean error in average section elevations was -1.8 feet.

Figure 145
Neosho River Comparison of Measured and Modeled Average Channel Profiles

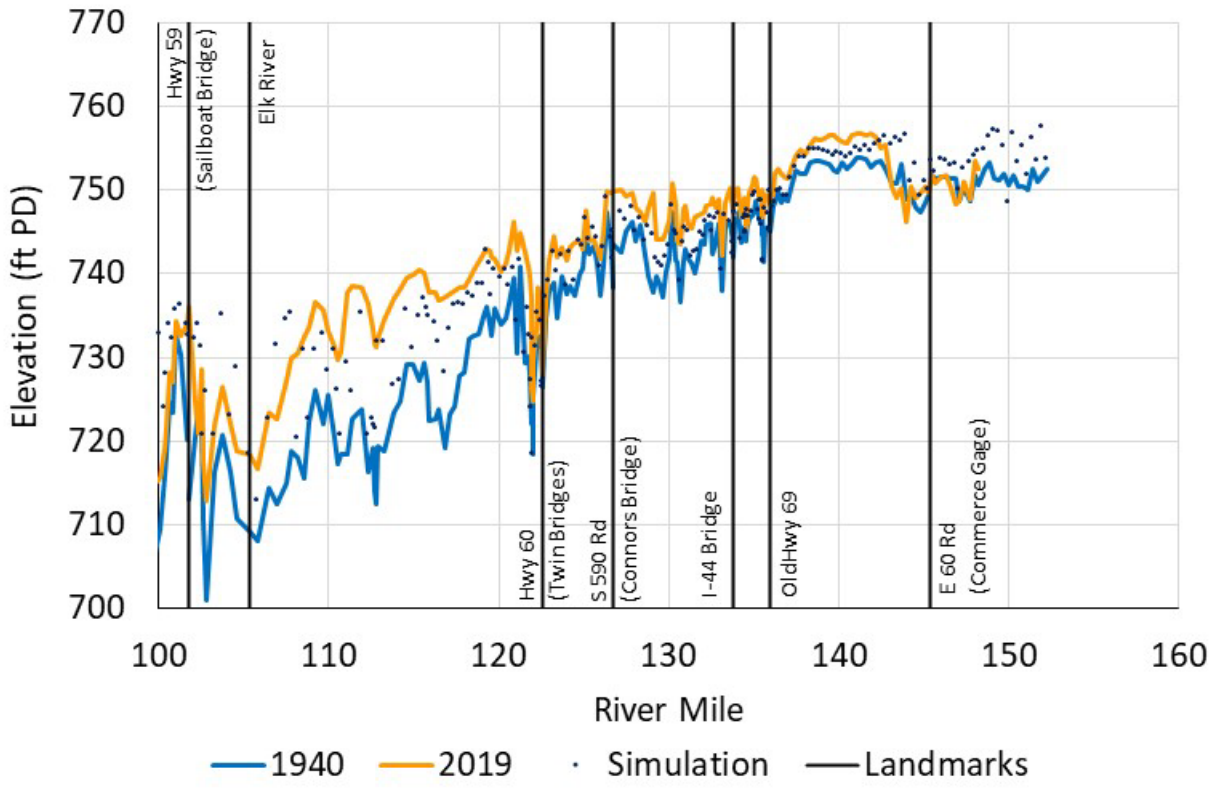

Figure 146
Neosho River Comparison of Measured and Modeled Average Section Profiles

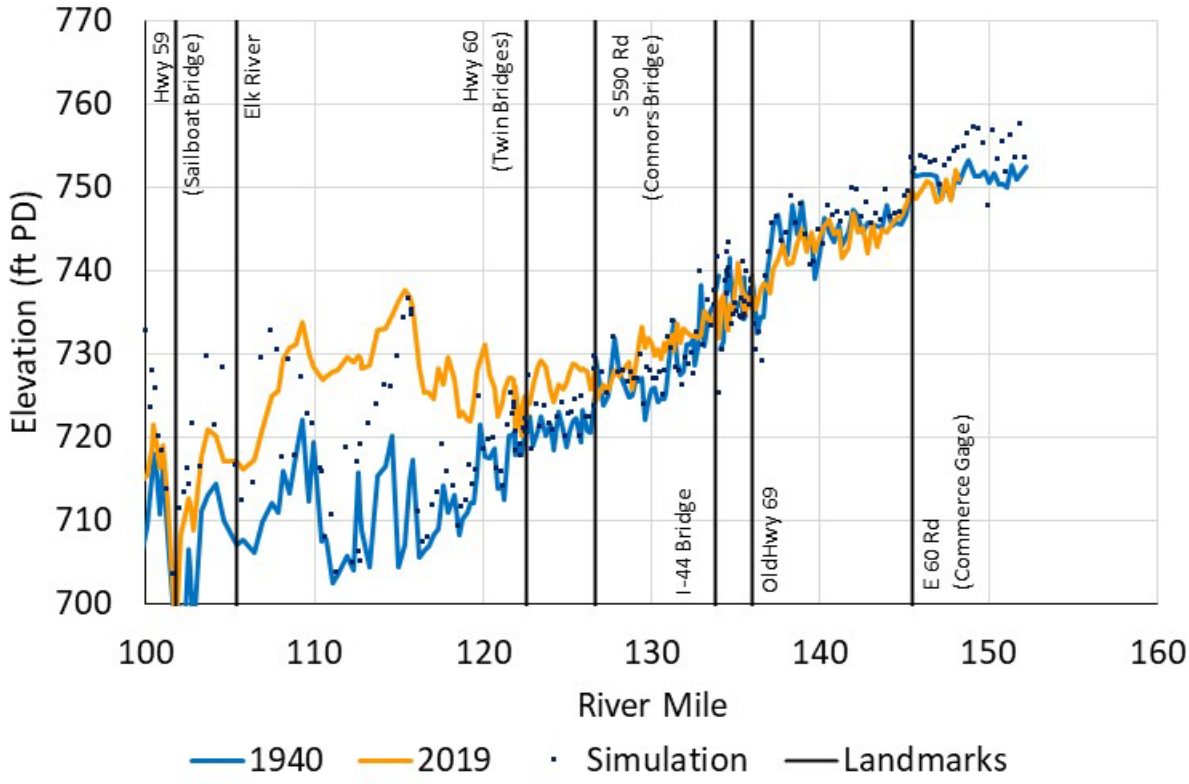

The differences in average channel and average section are largely explained by the poor quality of the circa-1940 geometry. The circa-1940 geometry relies on far fewer measured cross sections that were then interpolated to produce the circa-1940 geometry. Overbank areas are based on poorly scanned topographic maps, resulting in uncertainty when digitizing contour lines. These resulted in several areas of relatively wide channels between measured cross sections.

In contrast, the 2019 geometry is based on high-resolution data. The channels are far narrower in this geometry. As a result, the circa 1940 channel is often wider than its 2019 counterpart and would require significantly more deposition to match total volume changes between measured portions of the river.

HEC-RAS provides outputs showing cumulative volume in a river reach. This calculation finds the volume at every cross section in the model. For the reach between RM 145.4 (East 60th Road, USGS Commerce gage) and the confluence with the Spring River, HEC-RAS reports a volume difference of

53,700 acre-feet between the digitized and interpolated 1940 geometry and the measured 2019 geometry.

Where historical channel cross-section information is available, the model shows good correlation with sediment deposition volumes as shown in the above results. Using only the measured cross sections as shown above results in expected deposition of just 18,500 acre-feet. This matches well with the reported model deposition of approximately 15,300 acre-feet.

In contrast, the large change reported by HEC-RAS cumulative volume outputs from 1940 to 2019 reinforces the conclusion that unsurveyed, interpolated, circa 1940 cross sections are too wide. By including all model cross sections instead of only using those with known survey data, the amount of deposition needed to match the 2019 terrain is approximately three times what is shown when using *only* surveyed locations. This significant discrepancy could only occur if the unsurveyed portions of the circa 1940 terrain had much wider channels than existed in reality. Because the data for these unsurveyed sections are based on poorly scanned contour maps, they are far less reliable than the more accurate survey information used in the above analyses.

7 Predictive Simulations

After model calibration, predictive simulations were performed to evaluate future conditions within the study area and evaluate the impact of sedimentation on upstream water levels and the power pool.

7.1 Model Inputs

Model inputs for the predictive simulations included synthetic hydrographs, bed characteristics recorded from field measurements, and sediment rating curves.

There were four separate predictive simulations to address the uncertainties associated with the available terrain information discussed earlier in this report. These included expected loading simulations under both *Baseline* and *Anticipated* operations, a *High Sedimentation* simulation with adjusted parameters to increase sediment deposition in the study area, and a *Low Sedimentation* scenario with adjusted parameters to place a lower bound on the predicted sedimentation. These will be discussed in more detail in the following sections.

7.1.1 Hydraulic Parameters

To run future sediment simulations, synthetic future hydrographs for the 50-year period of January 1, 2020, to December 31, 2069 (2020 to 2070), were generated for each of the USGS gage locations (USGS 2021a, 2021c, 2021e, 2021f) and the corresponding synthetic Tar Creek hydrograph discussed in Section 5.2.1.1 of this report. Peak annual maximum flows were examined for each of the hydrographs to identity any trends in the peak flows. No significant trends were observed at any of the locations and introduction of a scaling factor to artificially increase or decrease the severity or duration of inflow events was not warranted. Therefore, the yearly hydrographs for 2020 to 2070 were assumed to approximately repeat the set of flows from January 1, 1970, to December 31, 2019 (1970 to 2020). To create some variability in the data, the order in which the flow years occurred was randomized when applied to the future hydrographs. This created a set of randomized hydrographs that would preserve the subannual patterns of individual water years and keep the statistical peak flow events the same between past and future hydrographs. Water years were separated into leap years and non-leap years and a separate randomization was applied, such that historical leap years would only be transposed to future predicted leap years. Because there are more leap years in the projected period of record, one non-leap year was projected to a future leap year and the February 28 flow data were projected to February 29. The same generated randomization of years was applied to each gage location so that peak flows would match between locations.

The downstream BC for Tar Creek was set as a stage hydrograph during predictive simulations using an iterative process. The first iteration used a normal depth at a friction slope of 6.7×10^{-5} ft/ft. This value was near the high end of the range provided in FERC's March 2023 Study Modification

Determination. When Neosho River flows are out of their banks, this slope results in good agreement between the Neosho River and Tar Creek WSEs at the confluence, so it was selected as a reasonable estimate for the first iteration.

After the first simulation was complete, the modeling team evaluated WSEs at the downstream extent of Tar Creek and at the nearest cross section of the Neosho River. The higher of the two values at each time step was used to create a stage hydrograph that set the downstream BC on Tar Creek. A final iteration then produced another comparison point for WSEs at the Tar Creek and Neosho River confluence to confirm the stage hydrograph produced reasonable water level results at the confluence.

Downstream WSE BCs in Grand Lake were set based on Operations Model (OM) outputs. The OM results were then imported to the STM for future simulations.

7.1.1.1 Stream Temperature

Sediment transport is affected by water temperatures. Water temperature is related to water viscosity, which can increase or decrease the potential for sediment entrainment and transport or deposition.

To bound the potential sediment deposition range, temperature was adjusted for the various future scenarios. In the *Baseline* and *Anticipated* scenarios, temperatures were set to match the measured values as discussed in Section 6.2.1.1 of this report. The *High Sedimentation* and *Low Sedimentation* scenarios (bounding scenarios) used water temperatures increased by 5°F and decreased by 5°F, respectively.

7.1.2 Sediment Parameters

7.1.2.1 Bed Sediment

Bed sediment conditions were selected based on the measured grain size distributions and bed shear stresses measured in the field as part of this study. The properties were assigned to the corresponding locations on the relevant tributaries, and HEC-RAS interpolation functions were used to gradually transition bed materials between locations.

7.1.2.2 Sediment Inflows

Rating curves were adjusted for bounding scenarios, but no changes were made to incoming sediment gradations. The *Anticipated* and *Baseline* operations scenarios used the same incoming sediment rating curves as the calibration run. The *High Sedimentation* scenario increased sediment discharge by 20%, and the *Low Sedimentation* scenario decreased sediment discharge by 20%. This was applied by a simple multiplication factor applied to the rating curves and imported into the HEC-RAS sediment input file.

7.1.2.3 Fall Velocity Method

The other parameter adjusted for the bounding scenarios was the fall velocity method. The *Baseline* and *Anticipated* scenarios used the Rubey method. Analysis of the various methods available in HEC-RAS indicated that van Rijn would increase fall velocity and thus deposition, so it was used in the *High Sedimentation* run, and Dietrich was used for the *Low Sedimentation* simulation.

7.2 Data Processing

The predictive STM simulation required an iterative process to account for potential changes in OM due to future reservoir sedimentation. To evaluate predictive STM simulations, it was necessary to iteratively adjust stage-storage curves within the study area. This iterative process is described as follows:

1. The initial stage-storage curve was extracted from the 2019 HEC-RAS terrain.
2. This initial curve with the synthetic hydrographs was run in the OM to determine the downstream WSE hydrograph. The STM was then run with the downstream WSE boundary computed by the OM.
3. Upon completion of the HEC-RAS sediment simulation, the resulting geometry was processed and stage-storage upstream of RM 100 was extracted from the model. This method does not provide information about the impacts on storage downstream of the model domain. Adjustments to account for the loss of storage below RM 100 are provided below.
4. The OM was re-run with a dynamic stage-storage curve, based on a temporal linear interpolation between the starting 2019 curve and the curve output from Step 3.
5. The STM was then re-run with the downstream WSE boundary computed by the second storage-interpolated iteration of the OM. The stage-storage output from this second STM run was compared to the initial output to determine if storage values changed significantly, which would indicate the need for another iteration.

To estimate stage-storage impacts on the downstream portion of the study area, the measured historical vertical accumulation rate at the dam was projected forward in time to estimate the minimum storage elevation at the dam. Table 46 provides the estimated minimum storage elevation at the dam and total change in storage estimated from measured stage-storage curves (USACE 1941; USGS 2020) for the various future conditions.

Table 46
Historical Stage-Storage Information Used to Develop Future Stage-Storage Curves Downstream of RM 100

Stage-Storage Curve	Lowest Storage Elevation (feet PD)	Total Change in Storage (acre-feet)
1940 USACE	610.93	--

Stage-Storage Curve	Lowest Storage Elevation (feet PD)	Total Change in Storage (acre-feet)
2019 USGS	621.04	319,473
2069 (Baseline Ops)	627.44	224,400
2069 (Anticipated Ops)	627.44	224,400
2069 (High Sedimentation)	627.44	269,276
2069 (Low Sedimentation)	627.44	179,517

Based on the change in storage between 1940 and 2019, the long-term sediment deposition at the base of Pensacola Dam is approximately 0.13 foot per year. Projecting that rate into the future provides an estimated low point of approximately 627.44 feet. Because dam operations depend on storage changes, but not the specific location of sediment deposition near the dam, the low point is relatively unimportant to overall storage volume change and was therefore held constant for all predictive simulations.

To determine approximate storage volume change downstream of RM 100, the thalweg elevation at RM 100 was used as a reference point (Figure 147). This elevation was 684.01 feet at the time of the 2019 USGS survey.

Figure 147
Schematic Representation of Neosho River Thalweg for Illustration Purposes

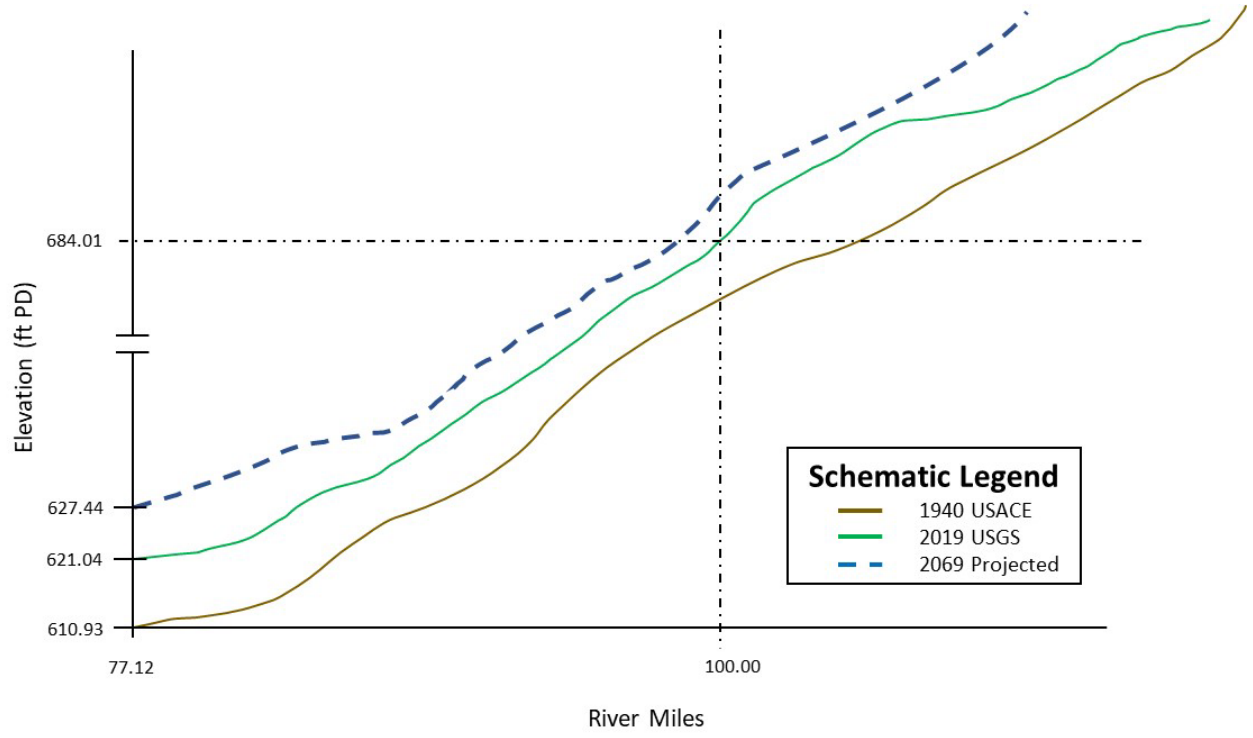

All material deposited below an elevation of 684.01 feet was therefore necessarily deposited downstream of RM 100. Material deposited upstream of RM 100 is modeled directly in the STM simulations. The remaining volume was accounted for through the use of trap efficiencies and relative sediment loading.

The volume of sediment entering, depositing in, and leaving the model domain in each simulation is summarized in Table 47.

Table 47
Modeled Sediment Loading

Simulation	Modeled Incoming Load (acre-feet)	Modeled Outgoing Load (acre-feet)	Deposited in Modeled Reach (acre-feet)	Deposited Below RM 100 (acre-feet)	Total Storage Volume Change (acre-feet)
1942–2019	402,733	236,242	166,491	152,982	319,473 (measured)
2020–2069 (Baseline Ops)	280,499	170,166	75,289	149,110	224,400
2020–2069 (Anticipated Ops)	280,499	163,302	83,466	140,933	224,400

Simulation	Modeled Incoming Load (acre-feet)	Modeled Outgoing Load (acre-feet)	Deposited in Modeled Reach (acre-feet)	Deposited Below RM 100 (acre-feet)	Total Storage Volume Change (acre-feet)
2020–2069 (High Sediment)	336,595	206,904	101,634	167,642	269,276
2020–2069 (Low Sediment)	224,397	128,804	69,369	110,148	179,517

Note: *Values are approximated by converting to volume using a sediment density of 58 pcf.

Total change in storage within the reservoir between 1940 and 2019 can be evaluated based on published stage-storage curves from USACE and USGS. For this period, the total sediment inflow as modeled was approximately 402,733 acre-feet, and total measured storage volume change was approximately 319,473 acre-feet. This corresponds to a trap efficiency of approximately 0.8.

Trap efficiency of the entire system is not expected to change drastically from one simulation to the next, so the same study-area-wide trap efficiency of 0.8 was used for all analyses. It should be noted that this may differ from trap efficiencies calculated by other methods; it relies on measured data and model results to ensure consistency through the analysis. It is not the trap efficiency for the unmodeled area alone; it includes deposition and erosion upstream of RM 100.

For the *Baseline Operations* and *Anticipated Operations* simulations, the total inflow volume of sediment was identical, and the expected trapping efficiency is the same. Therefore, the total expected change in storage volume is also expected to match (Table 47).

Relative sediment loading rates were used to calculate the storage volume change in the lower left quadrant of the schematic in Figure 147. The volume lost in that quadrant between 1940 and 2019 was measured to be 69,926 acre-feet. Storage volume change was assumed to scale with inflow volumes and adjusted accordingly (Table 48).

Table 48
Sediment Loading Compared to Storage Volume Change Below Elevation 684.01 feet PD and Storage Total Volume Change Downstream of RM 100

Simulation	Modeled Incoming Load (acre-feet)	Total Storage Change Below 684.01 feet PD (acre-feet)	Total Storage Change Downstream of RM 100 (acre-feet)
1942–2019	402,733	69,926 (measured)	--
2020–2069 (Baseline Ops)	280,499	48,702	149,110
2020–2069 (Anticipated Ops)	280,499	48,702	140,933
2020–2069 (High Sediment)	336,595	58,442	167,642
2020–2069 (Low Sediment)	224,397	38,961	110,148

Note: *Loss downstream of RM includes both the upper and lower quadrants of Figure 147 and cannot be precisely determined through available rating curves.

This storage volume change was applied to elevations below 684.01 feet at a rate proportional to the additional storage volume increment at each elevation step.

Accounting for additional storage changes in the upper left quadrant of Figure 147 used a similar approach. The difference between modeled deposition and calculated by the method above was assumed to have been in the upper left quadrant. It was assumed to also apply at a rate proportional to the incremental change in storage volume at each elevation step.

The change in total storage below 684.01 feet PD was assumed to be identical under *Baseline Operations* and *Anticipated Operations* scenarios. There is no information to determine the exact location of deposition downstream of RM 99.82, but the expected total change in volume is identical between the scenarios as discussed above. No changes were made to storage change below 684.01 feet PD, but the expected storage change was accounted for when calculating deposition in the upper left quadrant of Figure 147.

This resulted in the stage-storage curves for projected future bathymetry discussed below.

7.3 Deposition Patterns

Typical sediment deposition patterns in reservoirs follow a standard process (Vanoni 2006) illustrated in Figure 148. Sediment being carried by streamflow moves to the reservoir headwaters. As it reaches the headwaters and flow velocities decrease, sediment drops out of suspension and deposits, gradually forming a delta. Inflowing tributaries, stream geometry, bridges, and other features can also influence this process.

Figure 148
Typical Reservoir Delta Formation and Evolution—Progressive Bathymetric Surveys of the Cochiti Reservoir Delta, Rio Grande River, New Mexico

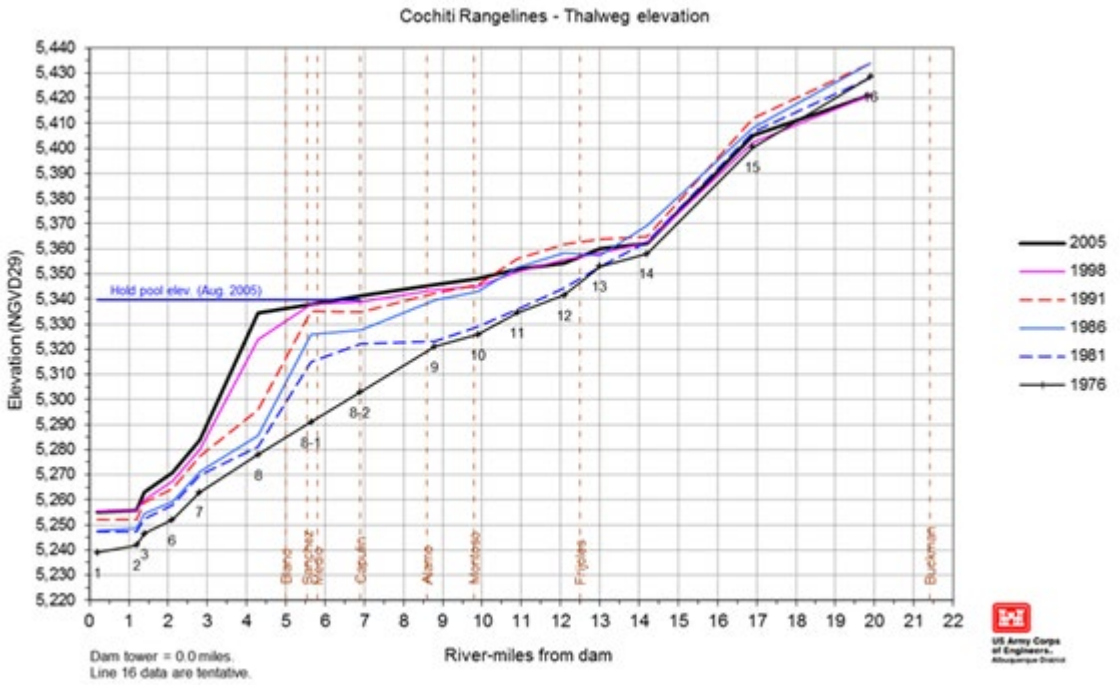

Source: WEST (2012)

Over time, the delta feature grows in height and decreases flow area within the channel. This results in raised stream velocities and associated bed shear stresses, which are the hydraulic drag forces on bed sediment. As the bed shear increases, it eventually reaches a dynamic equilibrium with the sediment critical shear stress (the bed shear stress at which sediment begins moving). The peak elevation of the delta feature stays relatively constant, gradually growing during normal and low flow events and eroding during large flow events.

As additional sediment moves into the system, it deposits further into the reservoir, adding to the downstream face of the delta feature (Vanoni 2006). Reviewing the results of the STM for future conditions shows that this typical pattern is followed in the Grand Lake reservoir.

As discussed in Section 6.2.2.1 of this document, the average channel profile provides a summary review of the final geometry that incorporates significantly more information than a simple thalweg profile. The results from the future simulations on the Neosho River are presented in Figure 149 and Figure 150.

Figure 149
Neosho River Average Channel Showing Predicted Effects of Operations

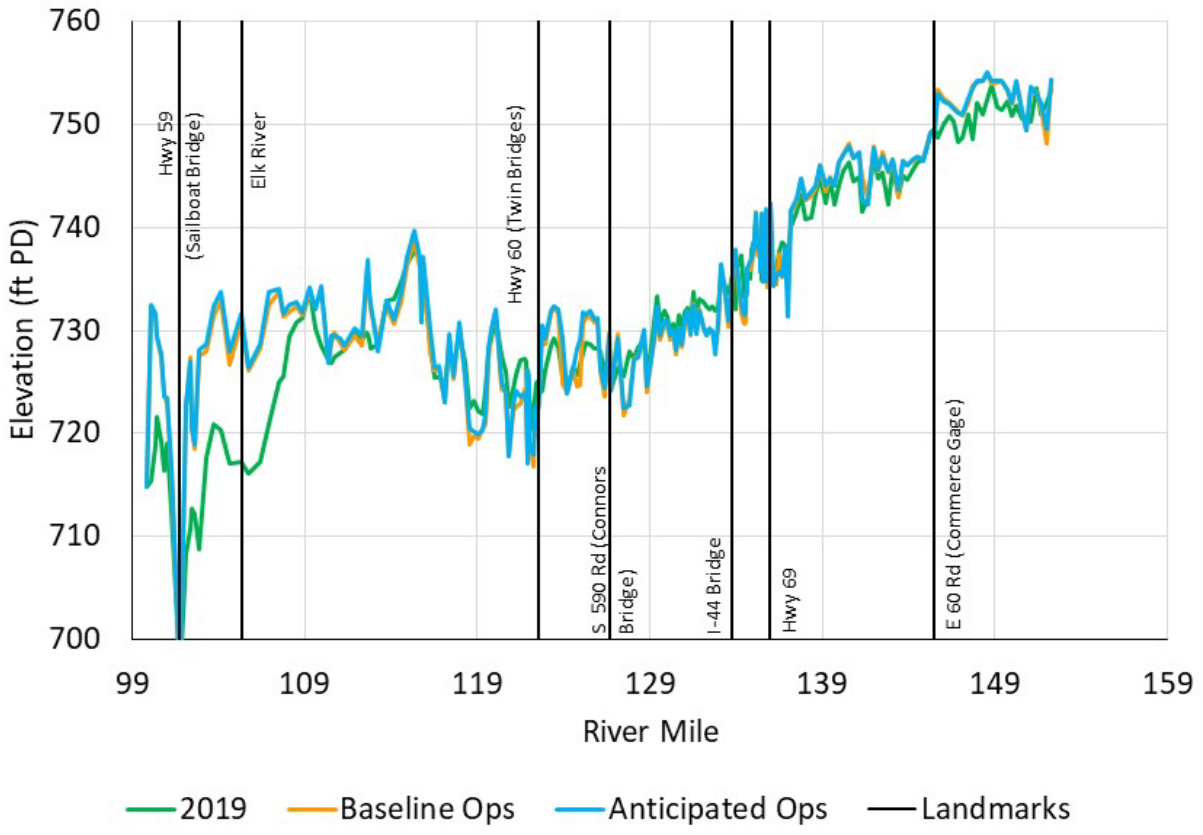

As shown above, project operations have a limited impact on sediment deposition patterns. Most of the sediment is expected to deposit on the downstream face of the delta feature (below approximately RM 109) and wash further into the reservoir.

The mean difference is just 0.29 foot of increased bed elevation under the *Anticipated* operations as compared to *Baseline* operations, and the mean absolute difference is 0.45 foot.

Figure 150
Neosho River Average Channel Showing Predicted Effects of Sediment Loading

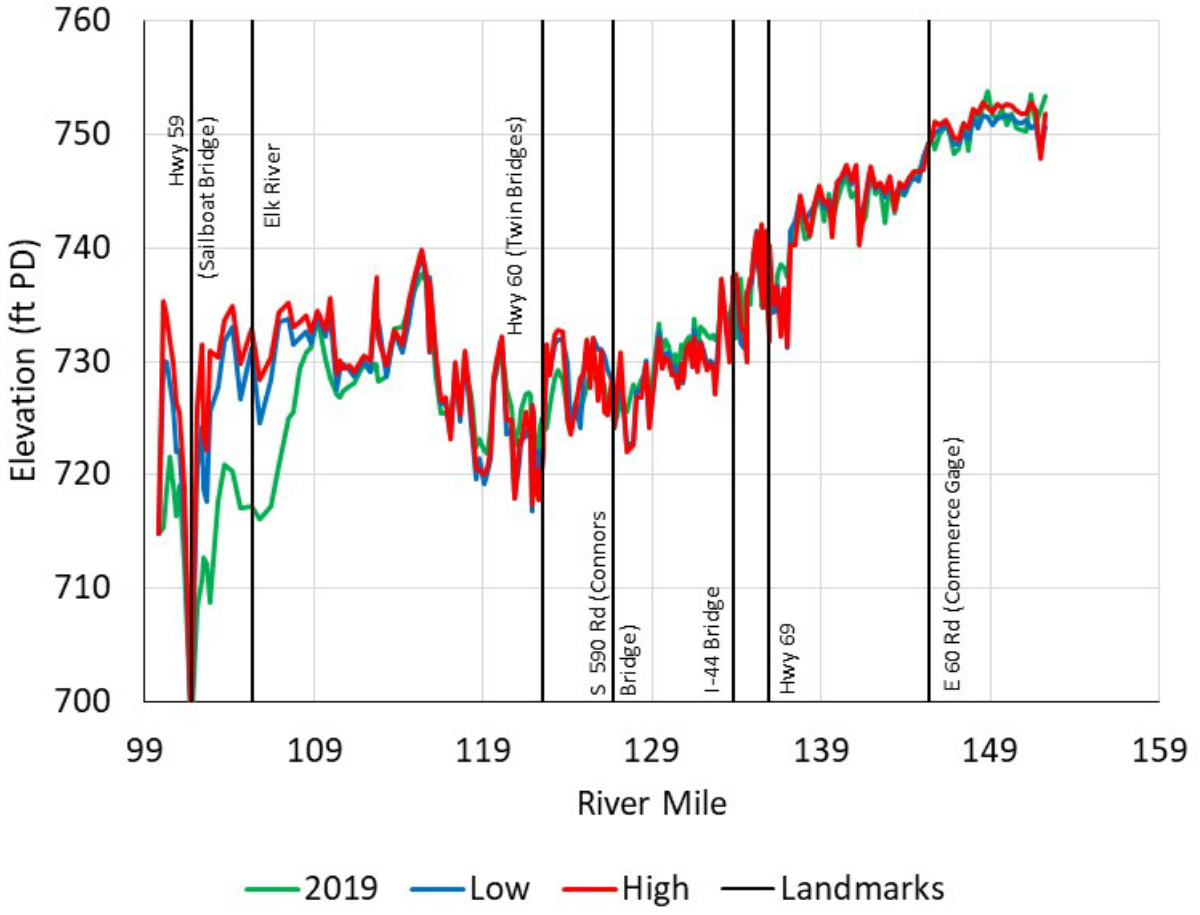

The differences between the bounding scenarios for potential sediment loading conditions are more significant than between operations parameters as shown in Table 49. The table shows a global change in average channel elevations as well as changes covering the entire delta feature and changes on the downstream face of the delta feature.

Table 49
Comparison of Average Channel Changes between Sediment Loading and Operations Scenarios

Comparison	Mean Change in Average Channel (feet)	Mean Change in Average Channel Below RM 122 (feet)	Mean Change in Average Channel Below RM 115.35 (feet)
High Sediment – Low Sediment	0.45	1.30	1.88
Anticipated Ops – Baseline Ops	0.29	0.41	0.42

As shown above, the sediment loading would account for approximately 1.55 times the deposition depth in the full modeled portion of the Neosho River. Deposition from the delta feature to the downstream extent of the model at RM 100 shows sediment loading results in 3.17 times the deposition depth as compared to Project operations. From the downstream face of the delta feature to the model limit, deposition due to sedimentation accounts for 4.48 times the volume due to Project operations. Project operations, therefore, do not drive most of the future sediment deposition in the reservoir.

Model results indicate that sediment loading to the system plays a larger role than Project operations. This is an important point to note because future sediment loading is projected to be lower than the long-term historical dataset indicates. This is attributable to a range of factors including the presence and operation of John Redmond Dam, which serves as a sediment barrier upstream of Grand Lake. Other changes include land use patterns, which show increased vegetation density since Project construction and a change from agriculture to woodland as well as changes to agricultural practices including no-till and cover crop programs that are incentivized by the NRCS. This change also decreases the amount of sediment entering the system from stormwater runoff, lowering future sediment deposition volumes. The model was run using the historical sediment inflow rating curves, which means predicted deposition is *higher* than anticipated future sediment deposition, and therefore represents a conservative estimate of future sedimentation and its impacts.

For all modeled scenarios, the sediment deposition follows typical reservoir deposition patterns, with sedimentation largely occurring downstream of the existing delta feature rather than continuing to increase the delta elevation. To evaluate the impacts of sediment deposition on upstream water levels, the final model geometries were used to create 1D UHMs.

7.4 1D Upstream Hydraulic Model Simulations

7.4.1 Background

The geometry files from the long-term STM simulations were imported to the 1D UHM for hydraulic analysis. Mead & Hunt developed the UHM to analyze the flooding impacts of modeled sedimentation. The 1D UHM was based on the STM and was developed in HEC-RAS v. 6.2 to maintain consistency with the STM. This model is distinct from the STM because it is run in hydraulic-only simulations using the fully unsteady mode. It is also distinct from the 1D/2D UHM discussed in the H&H study report. Figure 151 displays the 1D UHM model cross sections and extent.

Figure 151
1D UHM Model Cross Sections and Extent

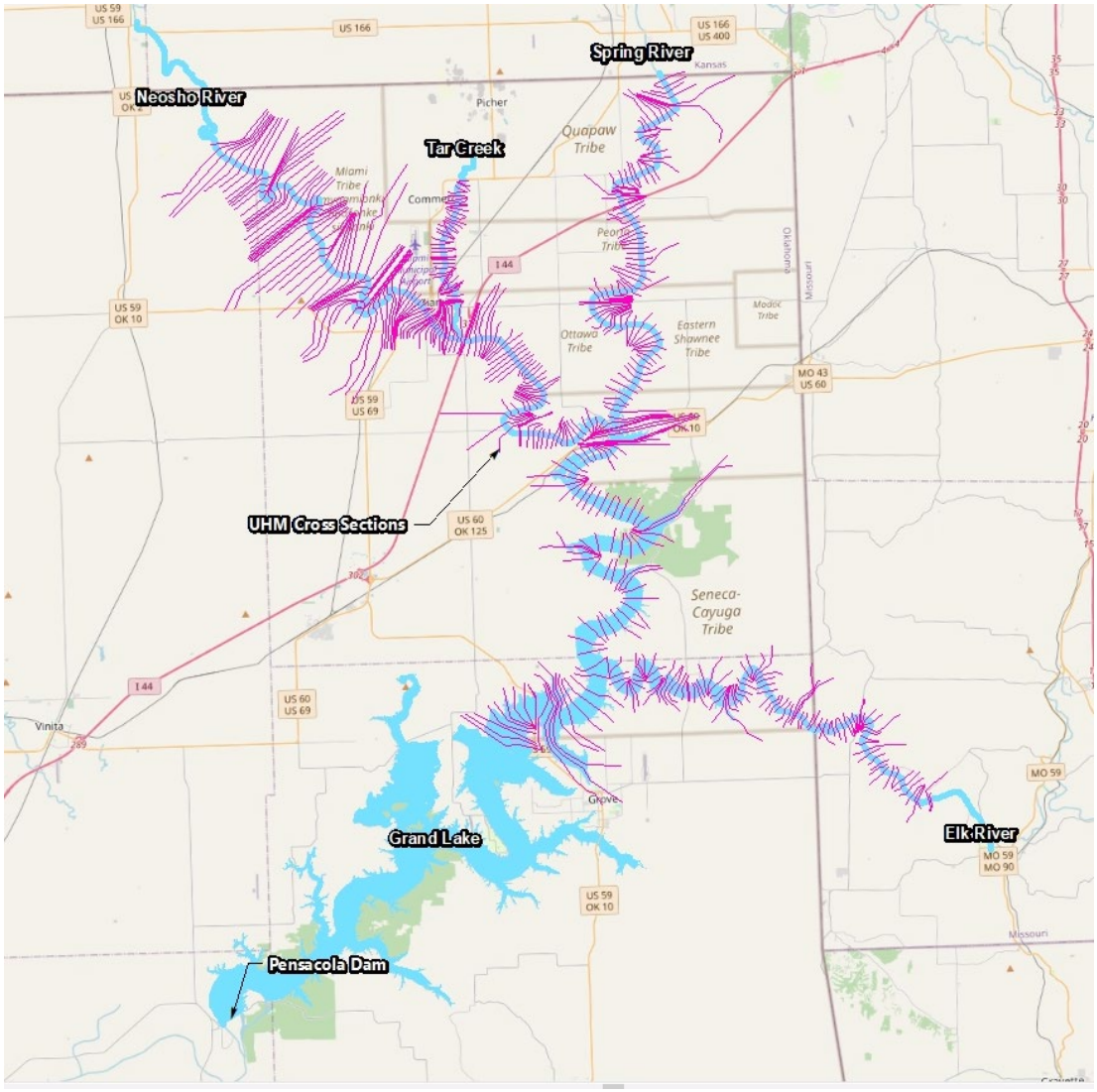

The calibrated 1D UHM was used to assess the hydraulic impact of sediment transport from 2019 to 2069 as estimated by the STM. Mead & Hunt performed hydraulic simulations of the 2069 geometry using a variety of sedimentation scenarios and dam operations in combination with the starting pool elevations and inflow events specified by FERC in its May 27, 2022, SMD (Table 50).

Table 50
1D UHM Simulation Runs Completed

Inflow Event and Starting WSE (feet PD)	Existing Stage-Storage	Future Stage-Storage			
		Anticipated Ops			***Baseline Ops***
	Sediment Rate N/A	**Expected Sediment**	**Low Sediment**	**High Sediment**	**Expected Sediment**
July 2007, 740	✔	✔	✔	✔	✔
July 2007, 745	✔	✔	✔	✔	✔
July 2007, 750	✔	✔	✔	✔	✔
July 2007, 755	✔	✔	✔	✔	✔
100-Year, 740	✔	✔	✔	✔	✔
100-Year, 745	✔	✔	✔	✔	✔
100-Year, 750	✔	✔	✔	✔	✔
100-Year, 755	✔	✔	✔	✔	✔

As shown in the table, the evaluations considered four starting WSEs, three sediment loading rates, and two operational scenarios, and compared them against existing conditions.

The 2069 STM geometry represents the predicted topo-bathymetric surface after 50 years of simulated sediment transport. The impact of dam operations on sediment transport diminishes with distance from the dam. Sediment transport is a natural process and significant geomorphic changes would occur in the study area regardless of the dam operation. The changes in WSE shown in the 1D UHM results are based on changes in bathymetry.

With any model results, boundary effects can skew data at the edges of the domain. This is apparent in the STM where coarser sediments dropped out of suspension near the upstream ends; based on measured changes in these portions of the river, it is clear that this is a numerical artifact rather than a real result. Therefore, the analyses have considered *only* the portions of the model not impacted by these BCs. The following analyses cover the river reaches shown in Table 51.

Table 51
River Reaches Considered in WSE Analyses

Stream	Analyzed Region
Neosho River	99.82–145.40
Tar Creek	1.60–7.00
Spring River	0.00–17.00
Elk River	0.00–15.00

7.4.2 Results and Discussion

The results demonstrate that future sediment inflow volumes play the primary role in determining upstream water levels during large flow events. Project operations are less important than the total volume of sediment entering the system. The following sections detail the findings on the Neosho River. Spring River, Elk River, and Tar Creek figures and tables are presented in Exhibit 6.

7.4.2.1 Future *Anticipated Operations* versus Existing Conditions

The first comparisons were made between the STM-generated 2069 geometry and existing 2019 geometry. Both sets of simulations were performed using anticipated operations, so differences shown in Table 52 are purely the result of the different geometries.

Table 52
WSE Changes from Future Geometry Compared to Existing Conditions under *Anticipated Operations* during Two Flow Events

Starting Stage (feet PD)	July 2007 (4-Year) Event				100-Year Event			
	Neosho River	Spring River	Elk River	Tar Creek	Neosho River	Spring River	Elk River	Tar Creek
Maximum Increase in WSE								
740	1.27	0.33	1.42	0.05	1.78	0.95	1.68	0.08
745	1.22	0.20	1.36	0.05	1.80	0.95	1.68	0.07
750	0.59	0.12	1.31	-0.04	1.42	1.23	1.68	0.07
755	1.03	0.22	1.32	0.03	1.48	1.29	1.68	0.07
Max	**1.27**	**0.33**	**1.42**	**0.05**	**1.80**	**1.29**	**1.68**	**0.08**
Maximum Decrease in WSE								
740	-0.06	-2.15	-0.56	-0.92	-0.01	-1.75	-0.65	-0.26
745	-0.05	-2.15	-0.15	-0.92	-0.01	-1.74	-0.65	-0.26
750	-0.67	-2.14	-0.35	-0.92	-0.02	-1.74	-0.64	-0.26
755	-0.09	-2.14	-0.25	-0.92	0.00	-1.73	-0.64	-0.26
Min	**-0.67**	**-2.15**	**-0.56**	**-0.92**	**-0.02**	**-1.75**	**-0.65**	**-0.26**
Average Change in WSE (feet)								
740	0.22	-0.26	-0.04	-0.19	0.43	0.05	0.16	0.03
745	0.23	-0.28	0.08	-0.20	0.43	0.05	0.17	0.03
750	-0.03	-0.54	-0.05	-0.24	0.44	0.16	0.20	0.03
755	0.18	-0.28	0.02	-0.20	0.44	0.19	0.20	0.02

Notes: Positive values indicate increased WSE under 2069 geometry as compared to 2019 geometry.
"Max" provides the largest increase in WSE across all starting pool elevations and locations within a stream.
"Min" provides the largest decrease (or smallest increase) in WSE across all starting pool elevations and locations within a stream.

The level of impact generally increases as starting pool elevation decreases for both the July 2007 and 100-year events.

Figure 152 shows the changes in WSE from RM 130 to RM 140 on the Neosho River for the July 2007 event. It indicates that the changes in WSE near the City of Miami are generally negligible during the July 2007 event simulation, meaning future geometry under *Anticipated Operations* predicts a *similar* WSE to existing conditions. The largest positive change between RM 133 and RM 137 occurs with starting pool elevations of 740 feet PD and 745 feet PD; the future geometry resulted in water levels 0.10 foot higher at approximately RM 135.95 near the Highway 69 bridge for both starting pool elevations.

Figure 152
Changes in July 2007 Event WSE Due to 50 Years of Expected Sedimentation under *Anticipated Operations* Compared to Existing Conditions from RM 130 to RM 140

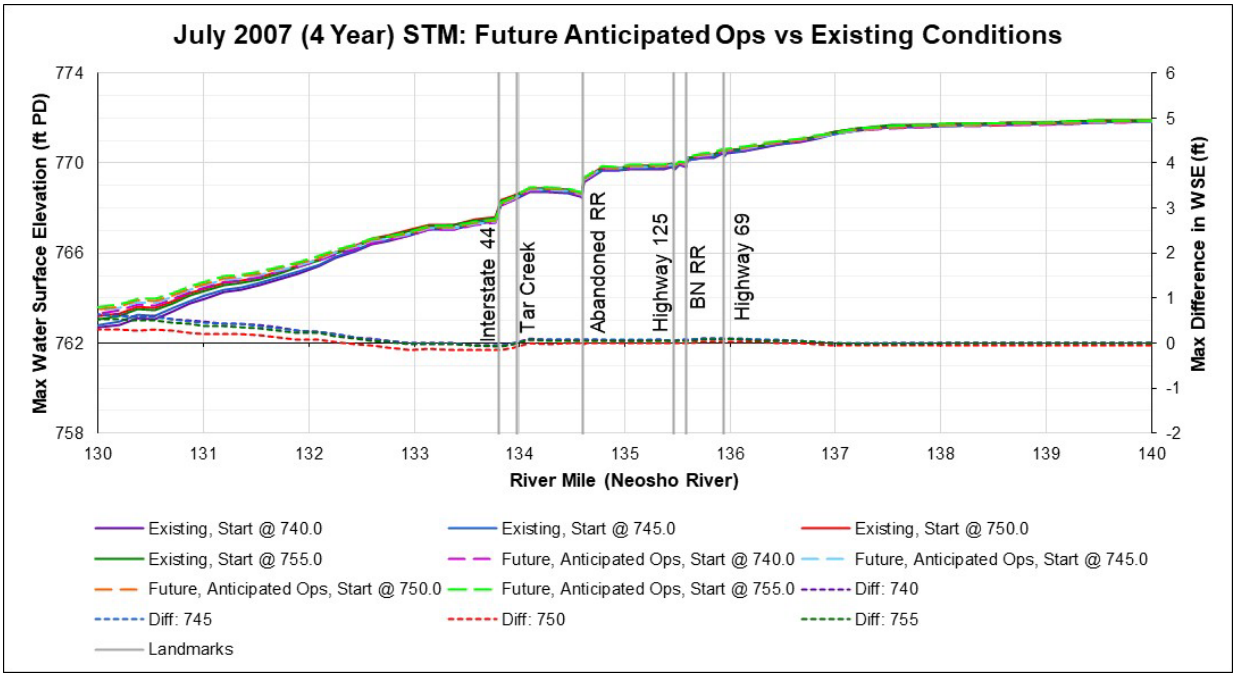

Figure 153 shows the changes in WSE from RM 130 to RM 140 on the Neosho River for the 100-year event. It indicates that the changes in WSE near the City of Miami are generally negligible during the 100-year event simulation, meaning future geometry under *Anticipated Operations* predicts a *similar* WSE to existing conditions. The largest positive change between RM 133 and RM 137 occurs with starting pool elevations of 740 feet, 750 feet, and 755 feet PD; the future geometry resulted in water levels 0.10 foot higher at RM 133.37 near the I-44 bridge.

Figure 153
Changes in 100-Year Event WSE Due to 50 Years of Expected Sedimentation under *Anticipated Operations* Compared to Existing Conditions from RM 130 to RM 140

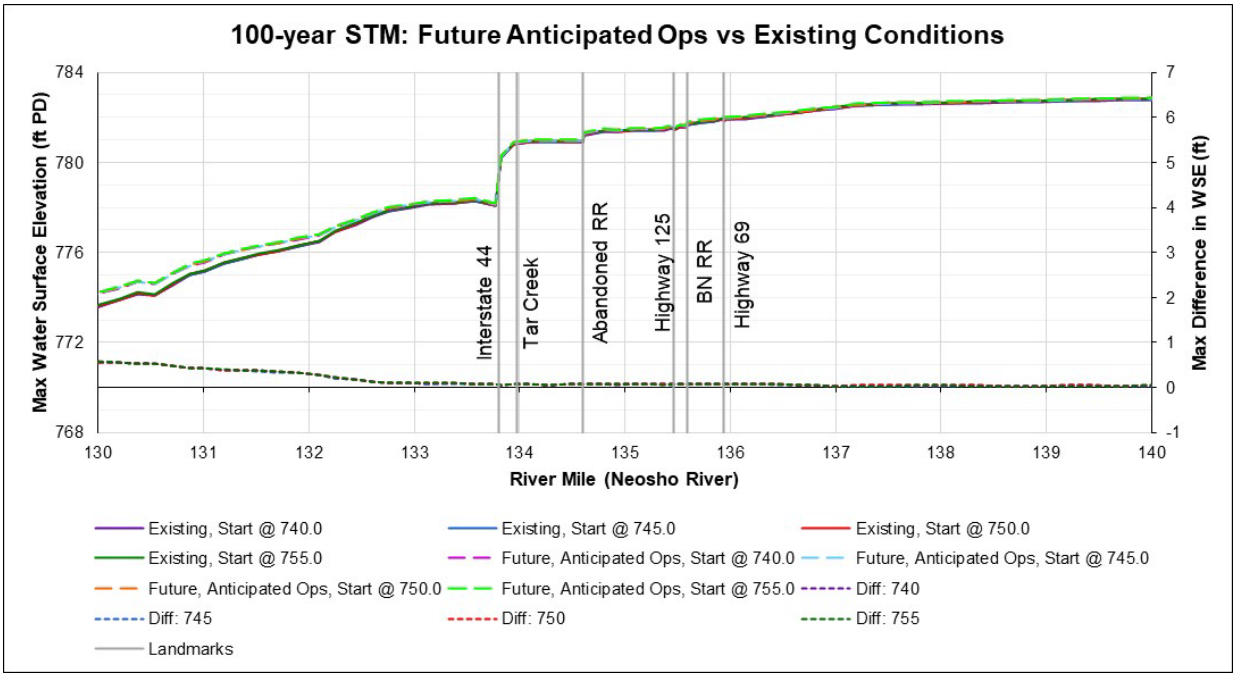

These results indicate that under both the July 2007 and 100-year flow events, water levels near Miami are expected to remain virtually unchanged despite 50 years of future sediment deposition under the anticipated operations.

Figure 154 shows the changes in WSE farther downstream, from RM 120 to RM 130 on the Neosho River for the July 2007 event. It indicates that the changes in WSE during the July 2007 event simulation are largest downstream of Miami, peaking near South 590 Road (Connors Bridge). The largest positive change between RM 120 and RM 130 occurs with a starting pool elevation of 740 feet PD; the future geometry resulted in water levels 1.27 feet higher at RM 126.39, with an average WSE impact of 0.65 foot or less.

Figure 154
Changes in July 2007 Event WSE Due to 50 Years of Expected Sedimentation under *Anticipated Operations* Compared to Existing Conditions from RM 120 to RM 130

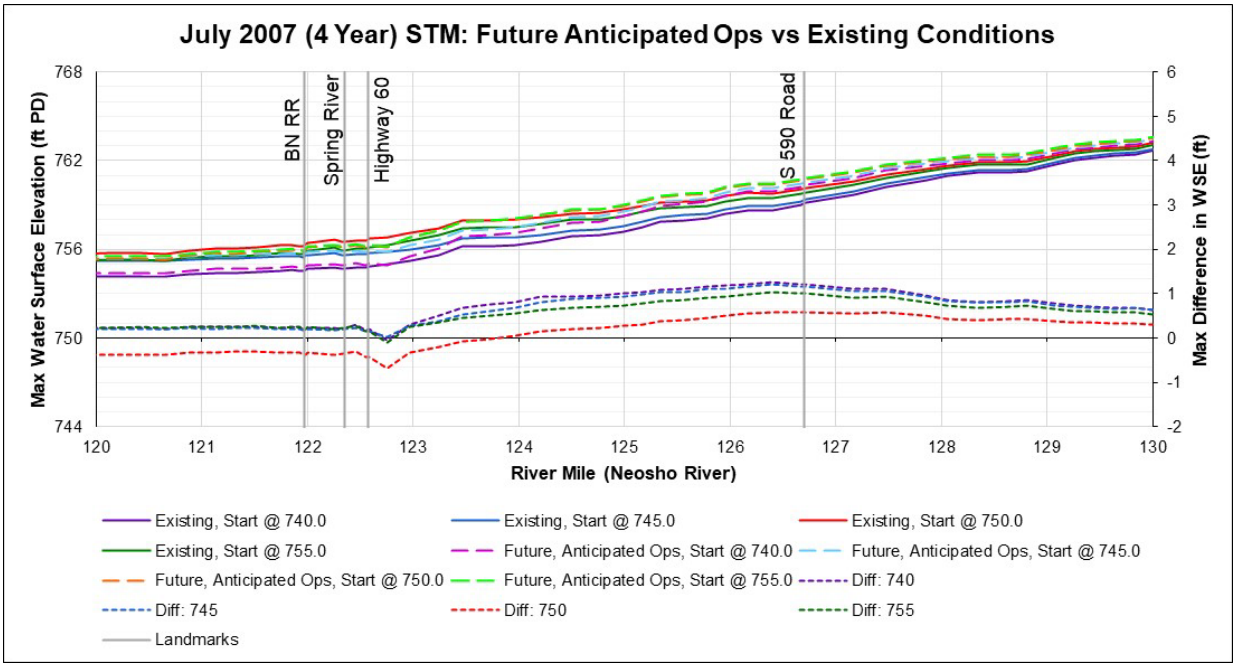

Figure 155 shows the changes in WSE from RM 120 to RM 130 on the Neosho River for the 100-year event. It indicates that the changes in WSE during the 100-year event simulation are largest downstream of Miami, peaking below Twin Bridges. The largest positive change between RM 120 and RM 130 occurs with a starting pool elevation of 740 feet PD; the future geometry resulted in water levels 1.80 feet higher at RM 122.33 upstream of the Burlington Northern railroad bridge, with an average WSE impact of 0.85 foot or less.

Figure 155
Changes in 100-Year Event WSE Due to 50 Years of Expected Sedimentation under *Anticipated Operations* Compared to Existing Conditions from RM 120 to RM 130

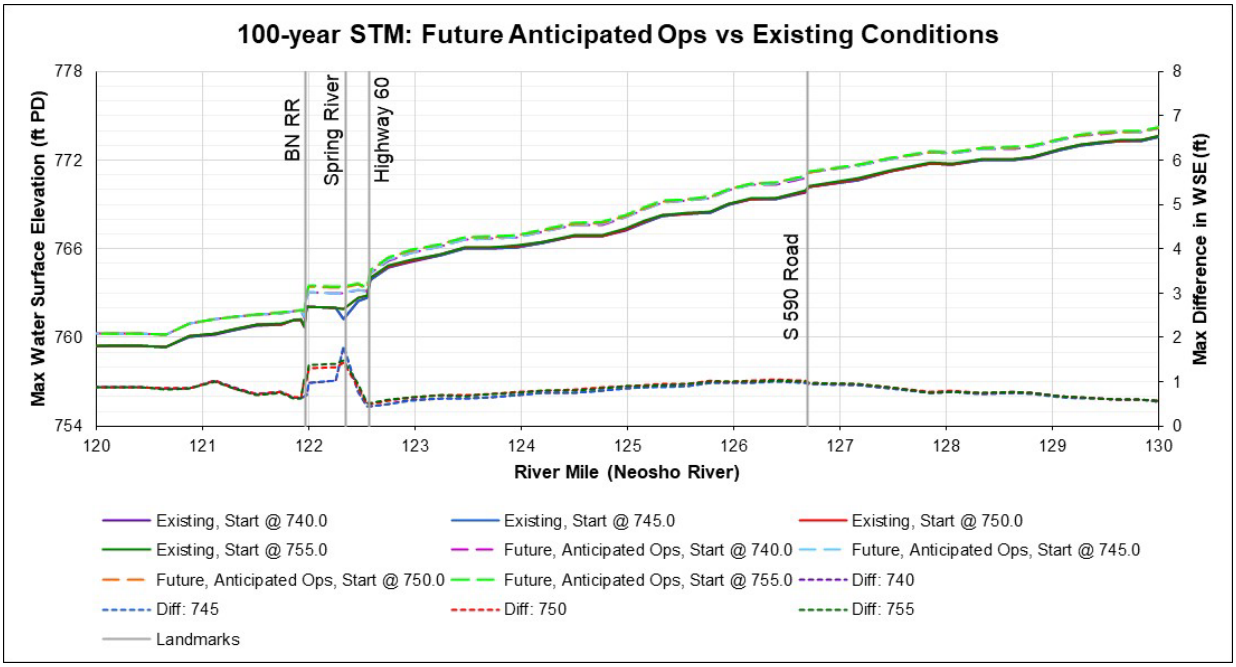

These results indicate that under both the July 2007 and 100-year flow events, water levels on the Neosho River are expected to remain similar despite 50 years of future sediment deposition under the anticipated operations. The largest impacts to WSE occur downstream of the urbanized area of Miami and are no more than 1.80 feet anywhere on the Neosho River. There is no indication that the expected future sedimentation will significantly impact inundation near heavily populated areas of Miami.

7.4.2.2 Sedimentation Rate Sensitivity

The next comparisons were performed to evaluate the impact of sediment loading on upstream WSEs. The following figures compare simulated WSE profiles for *High Sedimentation* rates and *Low Sedimentation* rates. These simulations used anticipated operations and results are shown in Table 53.

Table 53
WSE Changes between *High Sedimentation* and *Low Sedimentation* Scenarios during Two Flow Events

Starting Stage (feet PD)	July 2007 (4-Year) Event				100-Year Event			
	Neosho River	Spring River	Elk River	Tar Creek	Neosho River	Spring River	Elk River	Tar Creek
Maximum Increase in WSE								
740	0.37	0.27	0.44	0.09	0.81	0.70	0.25	0.03
745	1.29	1.18	0.20	0.09	0.82	0.71	0.25	0.03
750	0.26	0.19	0.21	0.09	0.83	0.72	0.25	0.03
755	0.36	0.28	0.22	0.09	0.84	0.73	0.25	0.03
Max	**1.29**	**1.18**	**0.44**	**0.09**	**0.84**	**0.73**	**0.25**	**0.03**
Maximum Decrease in WSE								
740	-0.05	-0.04	-0.09	-0.04	-0.03	-0.05	-0.05	-0.08
745	0.00	-0.04	-0.07	-0.04	-0.03	-0.06	-0.05	-0.08
750	-0.05	-0.04	-0.06	-0.04	-0.03	-0.05	-0.05	-0.08
755	-0.03	-0.04	-0.04	-0.04	-0.03	-0.05	-0.05	-0.08
Min	**-0.05**	**-0.04**	**-0.09**	**-0.04**	**-0.03**	**-0.06**	**-0.05**	**-0.08**
Average Change in WSE (feet)								
740	0.11	0.14	0.21	0.00	0.15	0.34	0.14	-0.01
745	0.34	0.57	0.15	0.04	0.15	0.34	0.14	-0.01
750	0.05	0.13	0.01	0.00	0.16	0.35	0.16	0.00
755	0.07	0.17	0.01	0.01	0.16	0.36	0.16	-0.01

Notes: Positive values indicate increased WSE under *High Sedimentation* loads compared to *Low Sedimentation* loads.
"Max" provides the largest increase in WSE across all starting pool elevations and locations within a stream.
"Min" provides the largest decrease (or smallest increase) in WSE across all starting pool elevations and locations within a stream.

Figure 156 shows the changes in WSE from RM 130 to RM 140 on the Neosho River for the July 2007 event. It indicates that the changes in WSE near the City of Miami are 0.12 foot or less during the July 2007 event simulation, meaning future geometry under high sediment loading predicts slightly higher WSE as compared to low sediment loading under anticipated operations. The largest positive change between RM 133 and RM 137 occurs with a starting pool elevation of 745 feet PD; the *High Sedimentation* geometry resulted in water levels 0.12 foot higher at RM 134.46 near the abandoned railroad bridge.

Figure 156
Changes in July 2007 Event WSE Due to 50 Years of Sedimentation under *High* and *Low Sedimentation* Conditions from RM 130 to RM 140

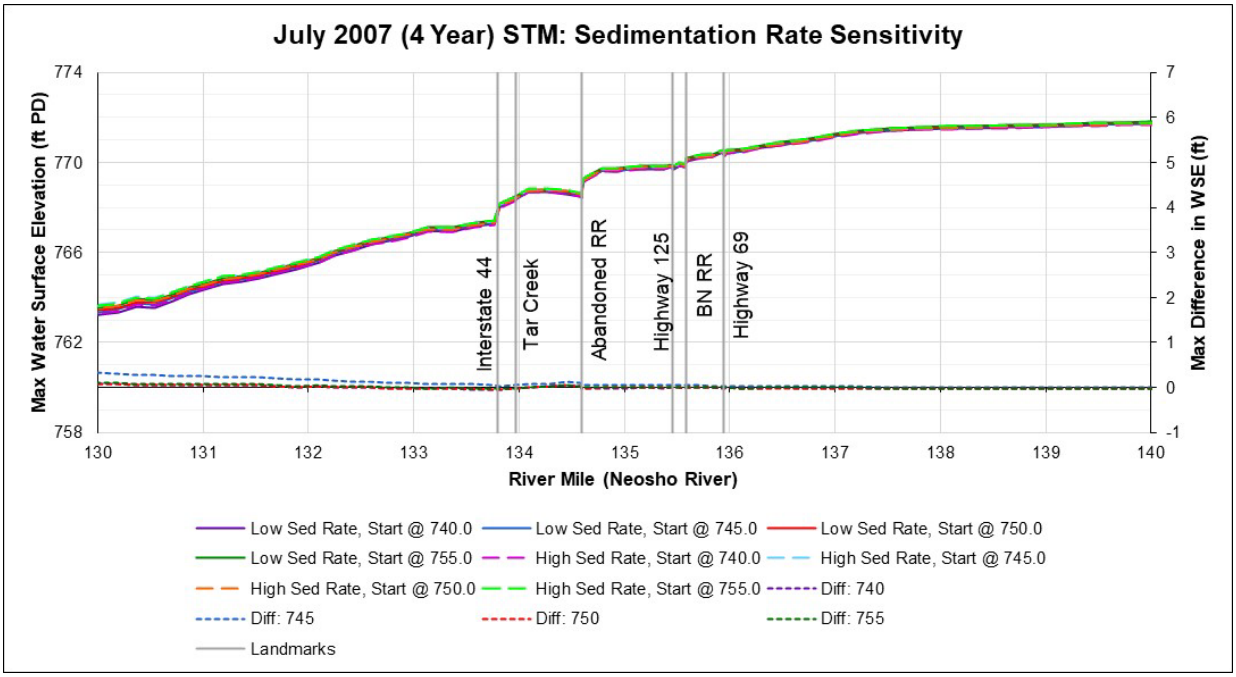

Figure 157 shows the changes in WSE from RM 130 to RM 140 on the Neosho River for the 100-year event. It indicates that the changes in WSE near the City of Miami are 0.00 foot or less during the 100-year-event simulation, meaning future geometry under high sediment loading predicts similar or lower WSE as compared to low sediment loading under anticipated operations. With starting pool elevations of 750 feet and 755 feet PD, the *High Sedimentation* geometry resulted in water levels 0.00 foot higher at RM 133.13 downstream of the I-44 bridge; other locations showed decreases in WSEs.

Figure 157
Changes in 100-Year Event WSE Due to 50 Years of Sedimentation under *High* and *Low Sedimentation* Conditions from RM 130 to RM 140

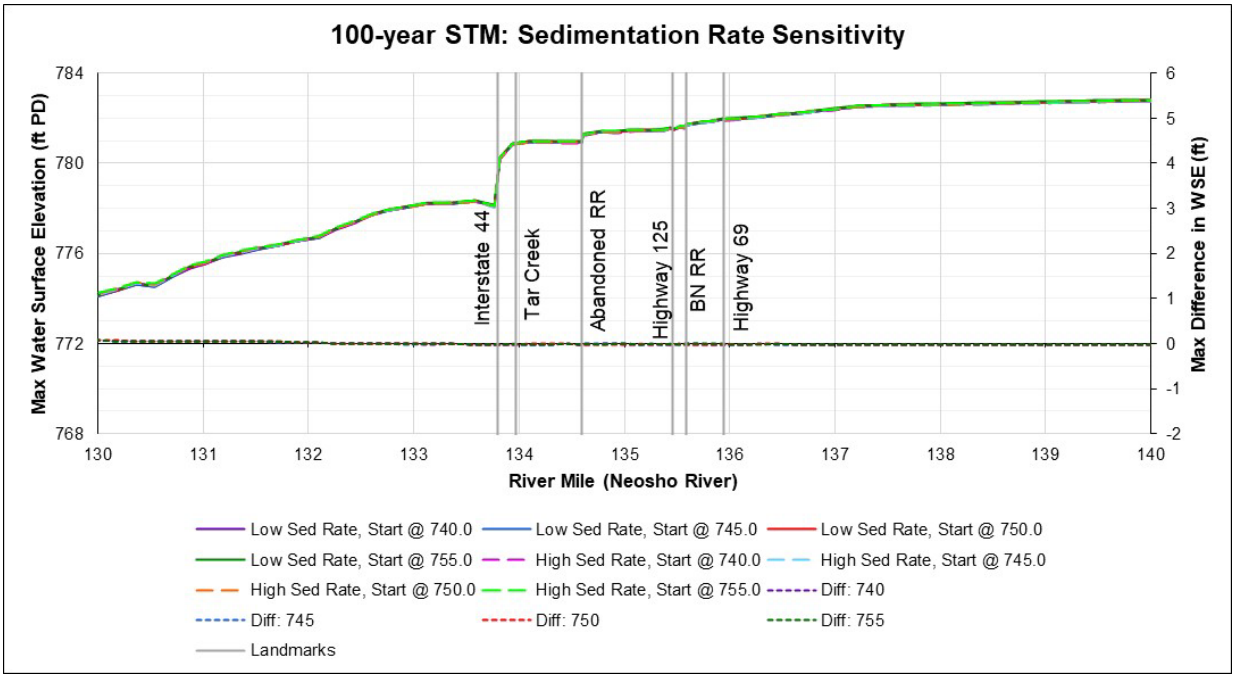

These results indicate that under both the July 2007 and 100-year flow events, water levels near Miami are expected to remain nearly constant regardless of sediment loading to the study area despite 50 years of future sediment deposition under the anticipated operations.

Figure 158 shows the changes in WSE from RM 120 to RM 130 on the Neosho River for the July 2007 event. It indicates that the changes in WSE during the July 2007 event simulation are largest downstream of Miami, peaking approximately 1.5 miles upstream of Twin Bridges. The largest positive change between RM 120 and RM 130 occurs with a starting pool elevation of 745 feet PD; the future geometry resulted in water levels 1.29 feet higher at RM 123.96 upstream of Twin Bridges.

Figure 158
Changes in July 2007 Event WSE Due to 50 Years of Sedimentation under *High* and *Low Sedimentation* Conditions from RM 120 to RM 130

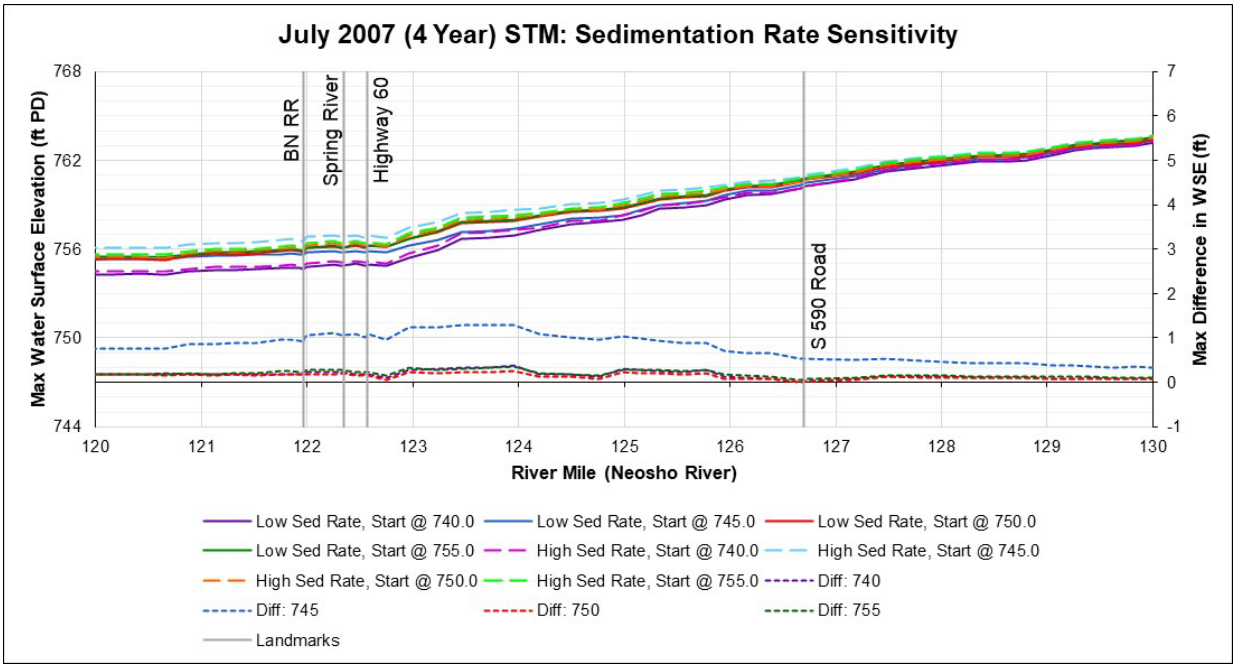

Figure 159 shows the changes in WSE from RM 120 to RM 130 on the Neosho River for the 100-year event. It indicates that the changes in WSE during the 100-year event simulation are largest downstream of Miami, peaking near the Spring River confluence. The largest positive change between RM 120 and RM 130 occurs with a starting pool elevation of 755 feet PD; the future geometry resulted in water levels 0.84 feet higher at RM 121.96 near Twin Bridges.

Figure 159
Changes in 100-Year Event WSE Due to 50 Years of Sedimentation under *High* and *Low Sedimentation* Conditions from RM 120 to RM 130

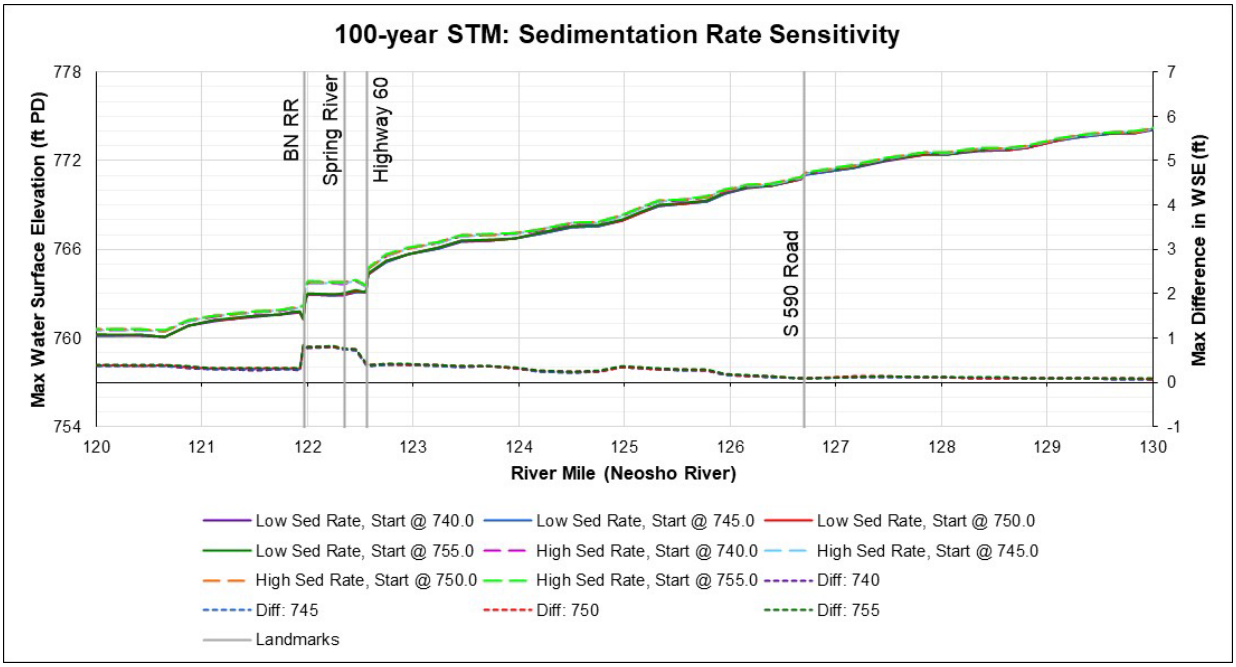

These results indicate that under both the July 2007 and 100-year flow events, water levels on the Neosho River are expected to change by as much as 1.29 feet due to the variability of sediment loading. The largest impacts to WSE occur downstream of the urbanized area of Miami near Twin Bridges. There is no indication that the future sedimentation will significantly impact inundation near heavily populated areas of Miami.

The impacts of sediment loading rates on upstream water levels are similar to those found between current and future conditions. The impacts occur primarily downstream of the City of Miami. The results show that the predicted range of inflowing sediment quantity, which is not controlled by GRDA, is similar to the expected changes between 2019 and 2069 under anticipated operations.

7.4.2.3 Operations Sensitivity

The third comparison was performed to evaluate the impact of Project operations on upstream water levels. The following section compares WSE impacts between 50 years of simulated *Baseline Operations* and 50 years of simulated *Anticipated Operations*. Sediment loading was identical for these simulations. Both simulations represent a future (2069) bed condition. The only difference was Project operation. The findings are summarized in Table 54.

Table 54
WSE Changes between *Anticipated Operations* and *Baseline Operations* Scenarios during Two Flow Events

Starting Stage (feet PD)	July 2007 (4-Year) Event				100-Year Event			
	Neosho River	Spring River	Elk River	Tar Creek	Neosho River	Spring River	Elk River	Tar Creek
Maximum Increase in WSE								
740	0.11	0.14	0.09	0.06	0.48	0.42	0.17	0.05
745	0.07	0.15	0.08	0.06	0.50	0.44	0.17	0.05
750	0.28	0.11	0.08	0.06	0.76	0.66	0.17	0.05
755	0.18	0.11	0.09	0.06	0.79	0.69	0.17	0.05
Max	**0.28**	**0.15**	**0.09**	**0.06**	**0.79**	**0.69**	**0.17**	**0.05**
Maximum Decrease in WSE								
740	-1.26	-1.28	-1.09	-0.04	-0.01	0.00	-0.02	0.00
745	-0.94	-0.94	-0.10	-0.06	-0.01	0.01	-0.02	0.00
750	-0.17	-0.29	-0.17	-0.05	-0.01	0.00	0.01	-0.01
755	-0.31	-0.31	-0.10	-0.05	0.00	0.00	0.01	0.00
Min	**-1.26**	**-1.28**	**-1.09**	**-0.06**	**-0.01**	**0.00**	**-0.02**	**-0.01**
Average Change in WSE (feet)								
740	-0.52	-0.48	-1.00	-0.02	0.13	0.22	0.04	0.01
745	-0.20	-0.37	-0.08	-0.03	0.14	0.24	0.03	0.01
750	-0.02	-0.01	-0.03	-0.03	0.14	0.30	0.04	0.00
755	-0.05	-0.12	0.00	-0.03	0.15	0.32	0.04	0.01

Notes: Positive values indicate increased WSE under *Anticipated Operations* compared to *Baseline Operations*.
"Max" provides the largest increase in WSE across all starting pool elevations and locations within a stream.
"Min" provides the largest decrease (or smallest increase) in WSE across all starting pool elevations and locations within a stream.

Figure 160 shows the changes in WSE from RM 130 to RM 140 on the Neosho River for the July 2007 event. It indicates that the changes in WSE near the City of Miami are generally negative during the July 2007 event simulation, meaning future geometry under *Anticipated Operations* predicts *lower* WSE as compared to future geometry under *Baseline Operations*. The largest positive change between RM 133 and RM 137 occurs with a starting pool elevation of 740 feet PD; the *Anticipated Operations* geometry resulted in water levels 0.01 foot higher at RM 136.30 upstream of the Highway 69 Bridge.

Figure 160
Changes in July 2007 Event WSE Due to 50 Years of Expected Sedimentation under *Anticipated* and *Baseline Operations* Conditions from RM 130 to RM 140

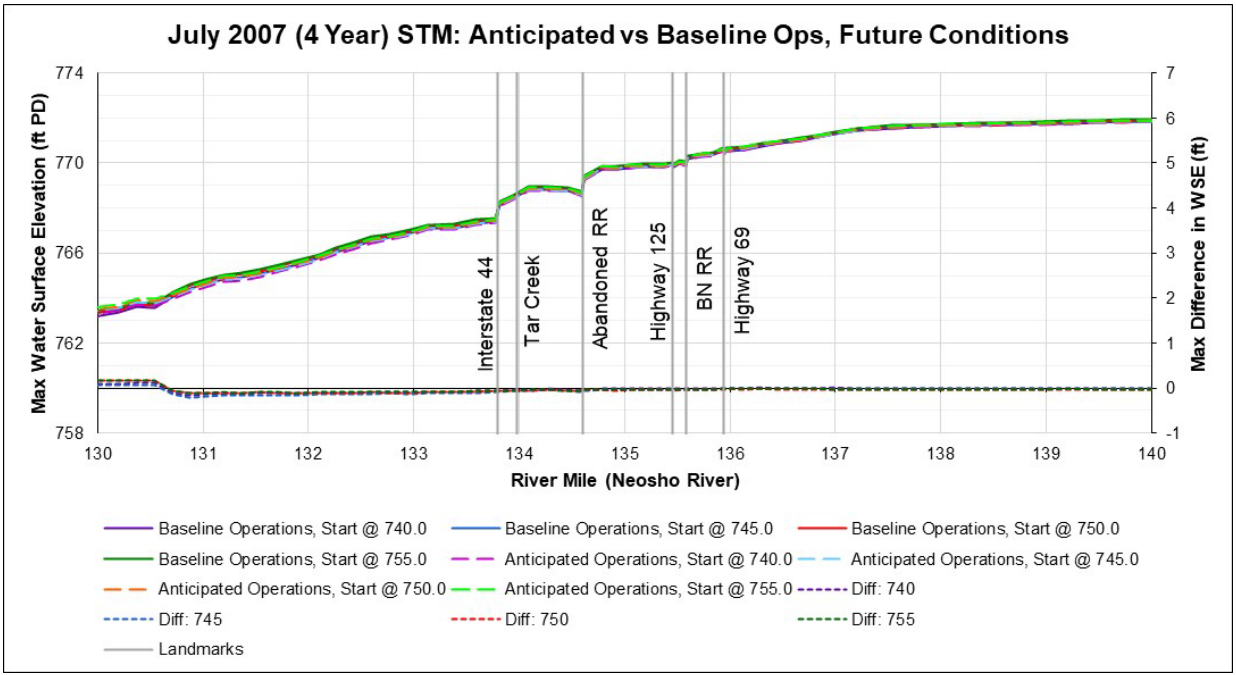

Figure 161 shows the changes in WSE from RM 130 to RM 140 on the Neosho River for the 100-year event. It indicates that average changes in WSE near the City of Miami are 0.01 foot during the 100-year event simulation, meaning future geometry under *Anticipated Operations* predicts similar WSE as compared to future geometry under *Baseline Operations*. The largest positive change between RM 133 and RM 137 occurs with starting pool elevations of 745 feet PD and 755 feet PD; the *Anticipated Operations* geometry resulted in water levels 0.02 foot higher at several locations.

Figure 161
Changes in 100-Year Event WSE Due to 50 Years of Expected Sedimentation under *Anticipated* and *Baseline Operations* Conditions from RM 130 to RM 140

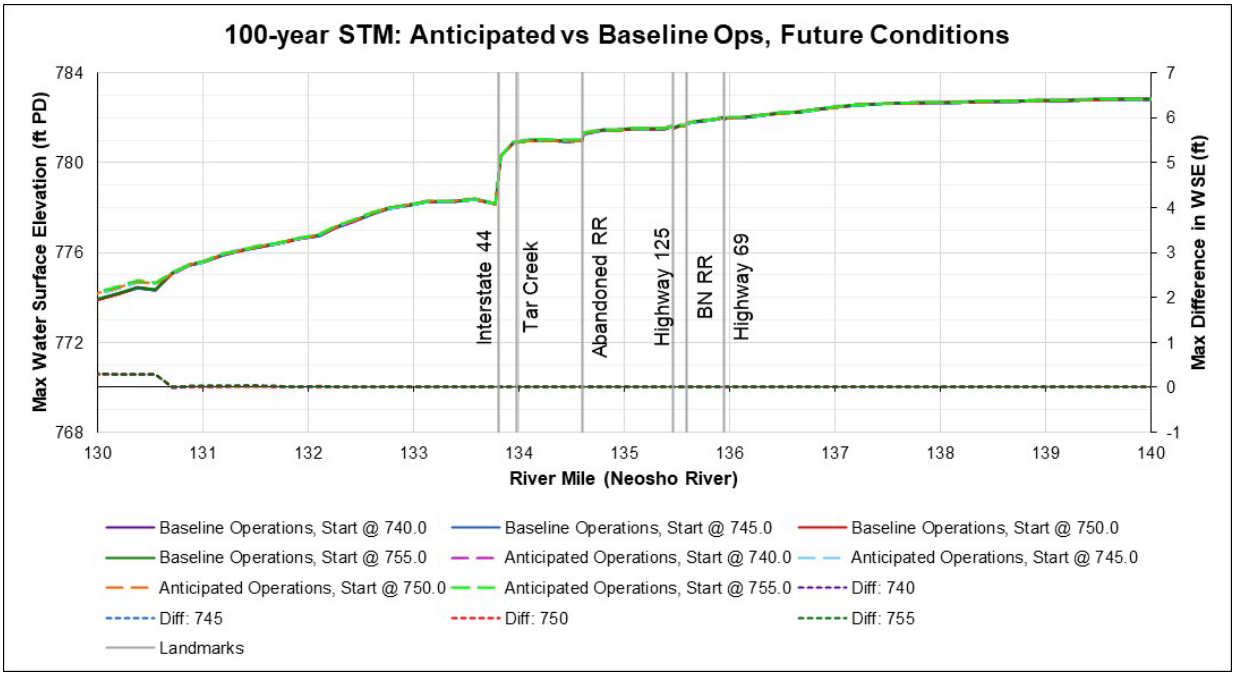

These results indicate that under both the July 2007 and 100-year flow events, water levels near Miami are expected to remain similar regardless of Project operations despite 50 years of future sediment deposition. In the smaller, more frequent July 2007 event, *Anticipated Operations* resulted in decreased average water levels near the urbanized areas of Miami.

Figure 162 shows the changes in WSE from RM 120 to RM 130 on the Neosho River for the July 2007 event. It indicates that the increases in WSE during the July 2007 event simulation are largest downstream of Miami, peaking between South 590 Road (Connors Bridge) and Twin Bridges. The largest positive change between RM 120 and RM 130 occurs with a starting pool elevation of 750 feet PD; the *Anticipated Operations* geometry resulted in water levels 0.28 foot higher at RM 125.56 downstream of Connors Bridge. It also indicates that water levels are typically *lower* under *Anticipated Operations* as compared to *Baseline Operations* with a maximum *decrease* of 1.26 feet at RM 122.25 at Twin Bridges with a starting pool elevation of 740 feet PD.

Figure 162
Changes in July 2007 Event WSE Due to 50 Years of Expected Sedimentation under *Anticipated* and *Baseline Operations* Conditions from RM 120 to RM 130

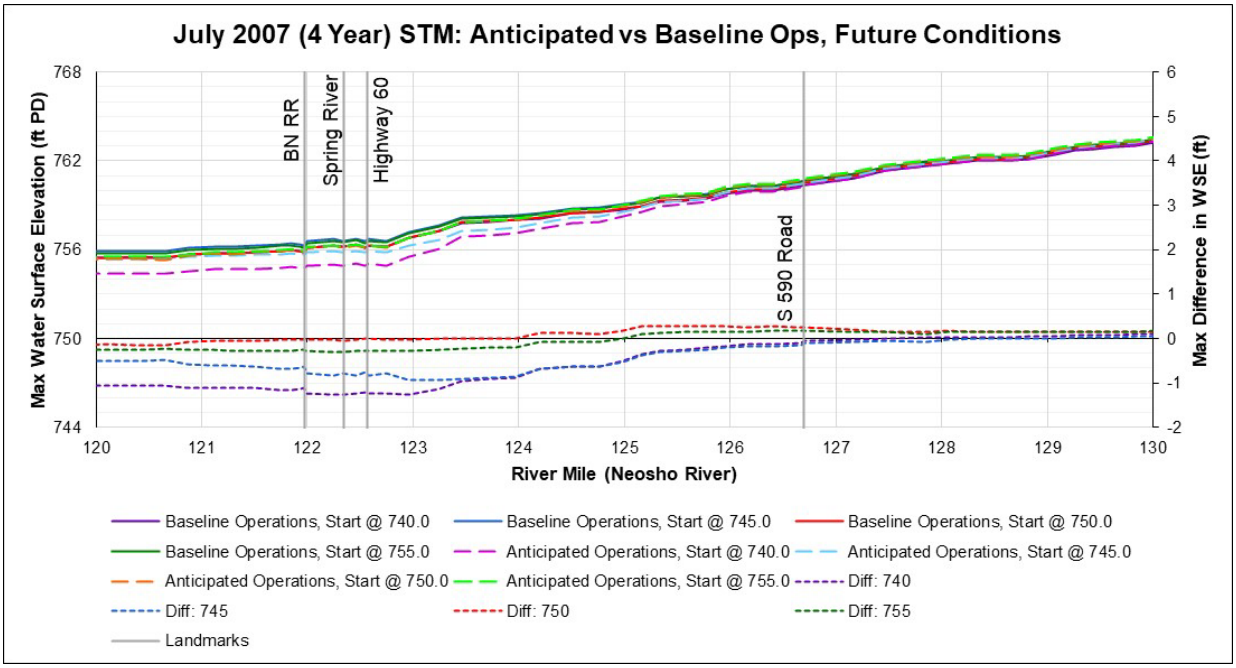

Figure 163 shows the changes in WSE from RM 120 to RM 130 on the Neosho River for the 100-year event. It indicates that the changes in WSE during the 100-year event simulation are largest downstream of Miami, peaking at Twin Bridges. The largest positive change between RM 120 and RM 130 occurs with a starting pool elevation of 755 feet PD; the *Anticipated Operations* geometry resulted in water levels 0.79 foot higher at RM 122.25 at Twin Bridges.

Figure 163
Changes in 100-Year Event WSE Due to 50 Years of Expected Sedimentation under *Anticipated* and *Baseline Operations* Conditions from RM 120 to RM 130

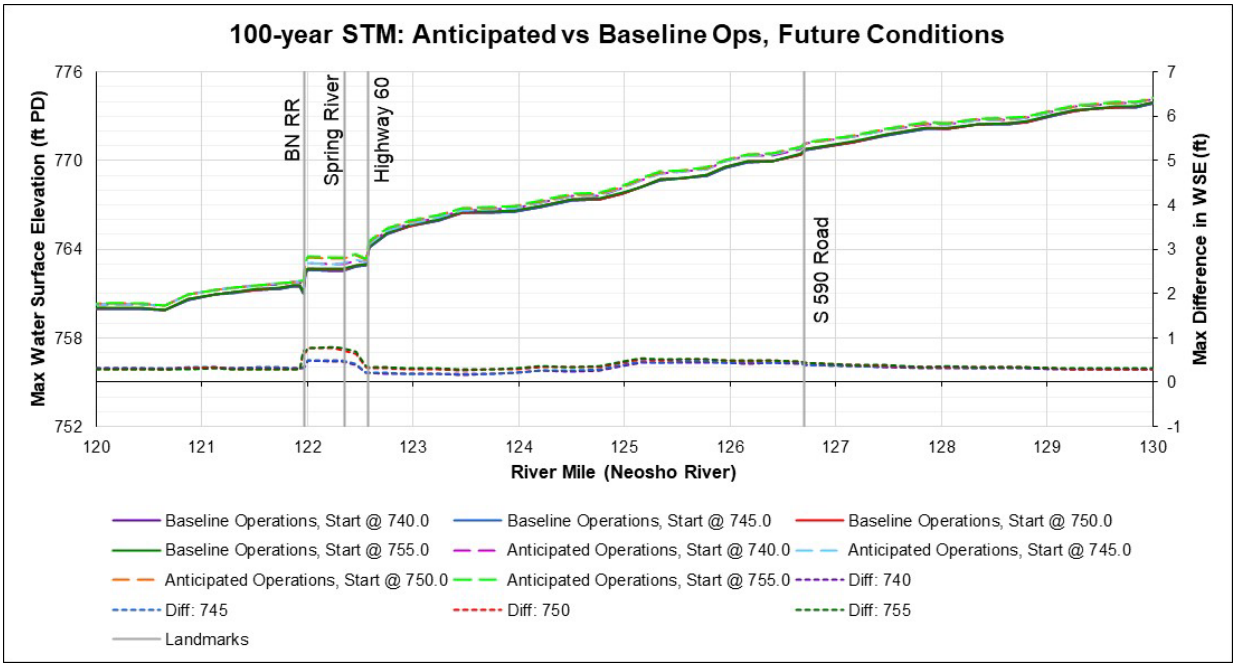

These results indicate that under the July 2007 event, average water levels on the Neosho River are expected to decrease, with a maximum decrease of 1.26 feet under *Anticipated Operations*. During 100-year flow events, average water levels on the Neosho River are expected to increase 0.15 foot or less under *Anticipated Operations*. There is no indication that the future Project operations will significantly impact inundation near heavily populated areas of Miami.

The impacts of Project operations on upstream water levels are limited and occur primarily downstream of the City of Miami. The results show that during the more typical 4-year flows such as the July 2007 event, *Anticipated Operations* will result in *lower* average water levels, and all expected changes in WSE near Miami are immaterial.

7.4.3 1D UHM Summary

The results show that potential impacts to WSE due to sedimentation are primarily the result of future sediment loading to the study area (Table 55).

Table 55
Maximum WSE Increases on the Neosho River during Simulated Events

Compared Scenarios	Maximum WSE Increase, July 2007 (feet)	Average WSE Increase, July 2007 (feet)	Maximum WSE Increase, 100-Year (feet)	Average WSE Increase, 100-Year (feet)
Future Geometry vs. Current Geometry	1.27	0.15	1.80	0.43
High Sedimentation vs. *Low Sedimentation*	1.29	0.14	0.84	0.15
Anticipated Operations vs. *Baseline Operations*	0.28	-0.20	0.79	0.14

The simulations show that sediment loading had the biggest impact on upstream water levels for the July 2007 event and expected sediment accumulation over the next 50 years will have the largest impact on WSEs during the 100-year event. Results indicate that the impact of sedimentation loading is approximately 4.6 times the impact of Project operations during the July 2007 event and approximately 1.1 times as large during the 100-year event.

In all evaluations, the average impacts to WSE on the Neosho River during large flow events are expected to be 0.43 foot or less. Operational changes produced smaller changes (or decreases) to water levels than comparisons between sediment-driven phenomena. This fact is unsurprising and confirms GRDA's statements that sediment loading (both comparative rates and cumulative 50-year inflows) drives changes in upstream water levels; GRDA has no ability to prevent sediment from flowing downstream, and the simulation results do not suggest Project operations are the driving contributor to water level impacts.

These results are similar to the findings of the H&H study, which quantified how *nature* plays the defining role in upstream water levels rather than Project operations. GRDA exerts no more control over incoming sediment than it does over incoming water, and the quantity of incoming sediment is the biggest driver of increases in upstream WSE over the 50-year license period.

Further, all scenarios indicated the impacts to WSE in the City of Miami due to sedimentation or Project operations are immaterial (Table 56). For the evaluations shown, "Vicinity of Miami, OK" was defined as the reach of the Neosho River from RM 133 to RM 137.

Table 56
Maximum WSE Increases on the Neosho River in the Vicinity of Miami, Oklahoma, during Simulated Events

Compared Scenarios	Maximum WSE Increase, July 2007 (feet)	Average WSE Increase, July 2007 (feet)	Maximum WSE Increase, 100-Year (feet)	Average WSE Increase, 100-Year (feet)
Future Geometry vs. Current Geometry	0.10	0.03	0.10	0.08
High Sedimentation vs. *Low Sedimentation*	0.12	0.01	0.00	-0.02
Anticipated Operations vs. *Baseline Operations*	0.01	-0.02	0.02	0.01

Notes: Vicinity of Miami is defined as between RM 133 and RM 137.

The results indicate that the impacts of sedimentation on WSE are immaterial in urbanized areas, regardless of loading rates, Project operations, or future versus current geometry. This finding further confirms the fact that Project operations are not a major contributor to increased upstream water levels in the City of Miami or other urbanized portions of the study area. Downstream of Miami, sediment loading, a natural phenomenon outside GRDA's control, has the biggest impact on WSE.

8 Conclusions

The Sedimentation Study produced several significant findings. The first major change in available information was that the sediment moving through the study area was dominated by cohesive material rather than sand and gravel as claimed by the City (2018). A second significant finding is that the delta feature apparent in the 2009 OWRB survey but not visible in bathymetry claimed by the City's consultant to be surveyed circa 1998 did *not* in fact form over a period of 11 years. The third major finding is that sedimentation is primarily driven by the amount of sediment conveyed into the system and *not* by Project operations.

The City argued in their 2018 response to GRDA's preliminary study plan that "The cohesive sediment is carried as wash load well downstream into the reservoir, and deposition and re-entrainment of that material has very little, if any effect, on upstream channel capacity and flooding." This statement implied that cohesive material was unimportant to understanding sediment transport within the study area, and that the only material of interest was the non-cohesive sands and gravels. Multiple sampling efforts of bedload and suspended sediment load by GRDA revealed virtually no coarse material moving through the system.

The importance of cohesive material complicated STM development. HEC-RAS is an excellent tool for evaluating hydraulics and non-cohesive sediment transport but is more limited in its ability to simulate cohesive sediment transport. As a result, it was necessary to model only the upper portions of the system rather than extending the model to Pensacola Dam where cohesive materials reduce the reliability of predictive HEC-RAS models. Calibration required more comprehensive inputs to evaluate critical shear stress, erosion rates, and mobility parameters with the cohesive sediments.

This increased relevance of cohesive materials also introduced uncertainty to the model. Spatial variations in erosive parameters are present in all sedimentation studies, but cohesive material introduces significant temporal variability as well. As cohesive material accumulates, it compresses and consolidates, increasing density and critical shear stress.

The second major discovery of the Sedimentation Study was that the terrain information initially proposed for use in the study was unreliable. This is covered in significant detail in Section 2.1.1, but the key takeaways are as follows:

- The 1998 REAS dataset did *not* extend downstream of RM 120.1 and the data below that point are from an unknown time period, likely circa 1940, despite the City's arguments that GRDA should be required to use the REAS terrain for the entire system (City 2022).
- There is limited information available from circa 1940 including topographic maps of varying quality and cross-sectional survey information within the study area.

As detailed above, the reliable portions of the available datasets were used for STM development. However, although the data used represent the best available information, they are imperfect and introduce uncertainty to any measurements, particularly the circa-1940 data.

These datasets were flawed but nonetheless are also the most complete available for the relevant time periods. The data were used to evaluate sedimentation and future impacts through two separate approaches as part of the three-level process: the quantitative analysis and the STM. The objective of the three-level approach is to ensure that reasonable and reliable results are obtained. This is achieved if there is consistency between the results of the quantitative analysis and the STM.

The quantitative analysis approach utilized the hydraulic component of HEC-RAS to compute hydraulic shear stresses for historical flows and operation and future scenarios. The historical change in bathymetry was then related to hydraulic shear stresses for historical flows and operation to develop a relationship between hydraulic shear stress and the sedimentation pattern. The HEC-RAS hydraulic component was then run for future flow and operation scenarios to compute the hydraulic shear stresses under these future conditions. The resulting shear stresses were then used in the relationship between hydraulic shear and sedimentation pattern to compute sedimentation for the future scenarios. The quantitative analysis (Section 4) concluded the following:

> The quantitative analysis of the future 50 years of hydrology and operation shows no significant sediment deposition on top of the delta feature that would adversely affect existing hydraulic control in upstream reaches. Most of the sediment delivered to the reservoir is transported past the top of the delta feature, farther downstream to the downstream face of the feature. Approximately 98 to 99 percent of the incoming sediment load is transported past RM 110.
>
> The quantitative analysis demonstrates that the top surface of the delta feature is in a state of dynamic equilibrium. This state of dynamic equilibrium is consistent with the fact that the average shear stress over the top of the delta feature is generally equal to or greater than the minimum critical shear from the SEDFlume analysis.
>
> This pattern of predicted sediment deposition, located downstream of the high point on the delta feature and at an elevation several feet below this high point, cannot reasonably be expected to adversely affect upstream hydraulics and flooding. Based on the relatively small change in effectiveness of moving sediment downstream with the comparison between the future flows with anticipated operation and baseline operation, as well as the USGS analysis of the effect of significant changes in water level resulting in very limited changes in sediment storage in John Redmond Reservoir; there is no basis to conclude that there would be any significant benefit in operating Grand Lake at a lower level.

It is important to remember that Grand Lake is under operational control of USACE when the water level approaches or exceeds elevation 745 feet PD and that under these conditions, which only occur 19.8% of the time, delivers 75.6% of the incoming sediment load to the reservoir. Neither the upstream sediment load nor operational control of Grand Lake is controlled by GRDA at that time.

The STM utilized the HEC-RAS model with available bathymetric data to describe the channel/reservoir geometry, analysis of sediment sampling to describe the physical characteristics of the sediment (including particle size distributions, erosion parameters, and sediment density), and inflow hydrology along with sediment inflow rates using sediment rating curves based on sediment transport and flow data. This was an extremely complex process due to the nature of the dominance of cohesive sediment (silt and clay) for which densities, critical shear, and erosion rates vary widely.

The uncertainties associated with both the sediment properties and the available topographic and bathymetric data contributed to difficulties in model calibration and validation. The Neosho River was captured with reasonable accuracy, but modeled changes on the Elk and Spring rivers were somewhat less reliable.

To manage the uncertainties associated with both the cohesive sediment and terrain information, the model evaluated *High Sedimentation* and *Low Sedimentation* scenarios in addition to the *Baseline Operations* and *Anticipated Operations* simulations. The *High* and *Low Sedimentation* scenarios provided bounding possibilities for future sediment deposition. Differences between those scenarios in terms of sediment deposition depths were larger than the differences between modeled Project operations. This also holds true for storage volume changes over time, with the operational scenarios showing relatively little difference and sediment loading playing a larger role.

Each of these scenarios used a high sediment loading condition based on older, higher sediment rating curves. This was the same loading used for calibration and validation, and it is considered a conservative evaluation. As discussed in Section 4.2.1 of this report, changes in land use, increased use of no-till, and cover crop agricultural practices, and the presence of John Redmond Dam, have all contributed to a *decrease* in total sediment loading to the system. It is almost certain that future sedimentation impacts will be *smaller* than those reported here.

The City has implied that the delta feature is solely attributable to Project operations and changes in those operations would remove it. However, there are a range of factors that influence the exact location of sediment deposition in this area. The presence of the Ozark Uplift changes the bed slope and increases the likelihood of deposition at that location, which coincides with the current delta feature. Sediment carried by the steeper Spring River empties into the Neosho River just upstream of the delta feature; the decreased sediment carrying capacity of the Neosho River below this point results in increased sedimentation downstream of that confluence. The fact that the stream is more

well-connected to the floodplain at this location means flows are able to spread laterally, decreasing stream velocity and allowing for deposition; upstream of this area, rocky cliffs prevent this lateral flow expansion and keep fine material in suspension until farther downstream in the system.

The City claimed that ongoing sedimentation would increase the height of the delta feature. The STM showed that is not the case, with simulations showing deposition on the downstream face of the delta feature rather than on the crest, which is typical of such formations as documented by Vanoni (2006) and others in scientific literature. This finding confirmed that the delta feature is not growing appreciably in height, and that neither Project operations nor incoming sediment is expected to have a significant impact on delta feature crest elevations.

The City's claims also neglect the role of bridges and associated embankments on flood risks. The Burlington Northern railroad bridge features an extensive embankment that constricts the flow from a width of 1.80 miles (9,500 feet) upstream of the bridge to just 770 feet at the bridge opening. Multiple bridges in the area also show large masses of debris trapped on piles. This debris reduces flow capacity at those bridges and creates backwater effects that increase water levels upstream. Disregarding these contributing factors and instead placing all blame for high water levels on Project operations is disingenuous and ignores basic hydraulic flow characteristics.

Results of the STM and 1D UHM demonstrate that **sedimentation rates in Grand Lake and the associated tributaries are dictated primarily by the future incoming sediment load rather than Project operations**. The differences in deposition rates and patterns for the *Baseline Operations* and *Anticipated Operations* scenarios are smaller than the differences between the *High Sedimentation* and *Low Sedimentation* scenarios. Furthermore, for all modeled scenarios, the sediment deposition follows typical reservoir deposition patterns, with sedimentation largely occurring downstream of the existing delta feature rather than continuing to increase the delta feature crest elevation.

The City claimed Project operations would increase the delta feature size, thereby raising water levels in Miami. To assess the impact of Project operations on the delta feature size and upstream water levels, geometry from the predicted future sedimentation pattern was imported to the 1D UHM to evaluate flooding events and the effect on flooding in upstream reaches of the Neosho River through the City of Miami. The findings did not support the City's claims. Sediment loading rates produced larger impacts to both storage volume change and upstream water levels, as compared to GRDA's operations. Furthermore, the STM showed most of the incoming material depositing on the downstream face of the delta feature as expected, and the 1D UHM results showed immaterial impacts to upstream water levels in the City of Miami.

In the City of Miami, **impacts to water levels due to Project operations are immaterial**. Neither operations nor sedimentation rates produce an appreciable difference in WSE between RM 133 and RM 137. Over a 50-year time period, there is virtually no increase to water levels in the City of Miami

due to Project operations, and average water levels were shown to decrease during the July 2007 flow event under anticipated operations. Further, in the vicinity of Miami, the impacts due to sediment loading, Project operations, and expected future deposition produce only immaterial changes to water levels. Any meaningful increase in water levels due to sedimentation is further downstream and is primarily driven by the incoming sediment load.

Sedimentation and associated impacts to water levels are not driven by Project operations. This finding is similar to that of the H&H study, which showed that Project operations have limited ability to dictate WSE upstream of Pensacola Dam. GRDA has no control over the incoming sediment loads, and adjusting Project operations does not have a meaningful impact to sediment depositional patterns. Impacts of future sedimentation are the result of incoming material, and *not* Project operations.

The Sedimentation Study has shown that the sediment moving through the system is fine, cohesive material. It has also evaluated a range of datasets for stream bathymetry and overland topography in the study area and concluded that significant portions of the 1998 REAS data are unreliable and that the circa-1940 data are limited. To bound the uncertainties of the available datasets, multiple sediment transport simulations were performed, and the study showed that nature, not Project operations, dictates the rate of sedimentation in Grand Lake. Any material impacts to upstream WSE during large flow events are the result of sediment loading, which GRDA does not control. Furthermore, when the water level in Grand Lake is above 745 feet PD or expected to rise beyond that level, USACE dictates operation of the reservoir to mitigate downstream flooding, and under these conditions most of the sediment (75.6%) is delivered to the reservoir.

9 References

Anchor QEA, LLC, Simons & Associates, and Mead & Hunt, 2022. *Updated Study Plan Sedimentation Study.* Prepared for Grand River Dam Authority. April 2022.

Andrews, W.J., M.F. Becker, S.L. Mashburn, and S.J. Smith, 2009. *Selected Metals in Sediments and Streams in the Oklahoma Part of the Tri-State Mining District, 2000–2006*. U.S. Geological Survey Scientific Investigations Report SIR 2009-5032. July 2009.

Aqua Survey, 2004. *Technical Report Environmental Dredging and Sediment Decontamination Technology Demonstration Pilot Study Lower Passaic River Restoration Project Magnetometer and Sub-Bottom Profiler Debris Survey*. December 3, 2004.

Arcement, G.K., and V.R. Schneider, 1989. *Guide for Selecting Manning's Roughness Coefficients for Natural Channels and Floodplains*. U.S. Geological Survey Water Supply Paper 2339.

Borrowman, T.D., E.R. Smith, J.Z. Gailani, and L. Caviness, 2006. *Erodibility Study of Passaic River Sediments Using USACE SEDflume*. Dredging Operations and Environmental Research Program. U.S. Army Engineer Research and Development Center, Vicksburg, Mississippi Environmental Laboratory. September 2006.

Byerly, R.D., 2012. *Chert Gravel Sources, Hydrology, Transportation, and Deposition within the Lower Neosho River, Southeastern Kansas.* Master's thesis. Emporia State University

City of Miami, 2018. Letter to: Kimberly D. Bose. Regarding: Comments of the City of Miami, Oklahoma on GRDA's Revised Study Plan Pensacola Hydroelectric Project, Project No. 1494-438. October 24, 2018.

City of Miami, 2022. Letter to: Kimberly D. Bose. Regarding: Pensacola Hydroelectric Project, FERC Project No. 1494-438; Supplemental Comments on GRDA's Untimely Request to Modify Sedimentation Study and Requests for Study Modifications to Conform with Approved Study Plan. March 28, 2022.

DeVries, R.N., 1996. *Rule 26 Expert Report: An Evaluation of the Water Surface Elevations of the Grand (Neosho) River Upstream of the Pensacola Dam*. March 14, 1996.

Dewberry, 2011. *USGS Grand Lake, OK LiDAR Project.* Prepared for the U.S. Geological Survey.

Duan, N., 1983. "Smearing estimate: A nonparametric retransformation method." *Journal of the American Statistical Associatio*n 78(383):605–610.

Edwards, T.K., and G.D. Glysson, 1999. "Field Methods for Measurement of Fluvial Sediment." *Technique of Water-Resources Investigations of the U.S. Geological Survey*. Book 3, Chapter C2. Denver, Colorado: U.S. Geological Survey.

Engineering-Environmental Management, Inc., 2013. *Final Supplement to the Final Environmental Statement Volume 1*. Prepared for Storage Reallocation John Redmond Dam and Reservoir, Kansas.

Fan, J., and G.L. Morris, 1992. "Reservoir sedimentation I. Delta and density current deposits." *Journal of Hydraulic Engineering* 118(3):354–69.

FERC (Federal Energy Regulatory Commission), 2022. *Determination on Request for Study Modifications for Project No. 1494-438*.

GRDA (Grand River Dam Authority), 2017. *Pensacola Hydroelectric Project, FERC No. 1494 Pre-Application Document*.

GRDA, 2018. Letter to: Kimberly D. Bose. Regarding: Pensacola Hydroelectric Project (FERC No. 1494-438); Filing of Revised Study Plan. September 24, 2018.

GRDA, 2022. GRDA Response Comments on Sedimentation Study Plan: Pensacola Hydroelectric Project No. 1494 FERC Relicensing.

Gupta, H.V., S. Sorooshian, and P.O. Yap, 1999. "Status of automatic calibration for hydrologic models: Comparison with multilevel expert calibration." *Journal of Hydrologic Engineering* 4(2) 135–143.

Huang, J., R.C. Hilldate, and B.P. Greiman, 2006. *Erosion and Sedimentation Manual*. US Department of the Interior. United States Bureau of Reclamation.

IHO (International Hydrographic Organization), 2008. *IHO standards for hydrographic surveys (5th ed.): International Hydrographic Organization Special Publication no. 44*, 28 p. Accessed April 20, 2022. Available at: https://iho.int/uploads/user/pubs/standards/s-44/S-44_5E.pdf.

Ingersoll, C.G., C.D. Ivey, W.G. Brumbaugh, J.M. Besser, N.E. Kemble, and S. Dudding, 2009. *Toxicity Assessment of Sediments from the Grand Lake O' the Cherokees with the Amphipod* Hyalella azteca. U.S. Geological Survey Administrative Report CERC-8335-FY09-20-01.

Integral Consulting, 2020. *Grand Lake Waterways SEDflume Analysis: Grand Lake o' the Cherokees, Oklahoma*. SEDflume Study, Grand Lake o' the Cherokees. Santa Cruz, California.

Juracek, K.E., and M.F. Becker, 2009. *Occurrence and Trends of Selected Chemical Constituents in Bottom Sediment, Grand Lake O' the Cherokees, Northeast Oklahoma, 1940-2008*. U.S. Geological Survey Scientific Investigations Report 2009-5258, 28 p.

Kramer, A.R., C.L. Peterman-Phipps, M.D. Mahoney, and B.S. Lukasz, 2021. *Sediment Concentrations and Loads Upstream from and through John Redmond Reservoir, East-Central Kansas, 2010–19.* Scientific Investigations Report 2021–5037. U.S. Geological Survey.

Krone R.B., 1962. "Flume studies of the transport of sediment in estuarial shoaling processes." Hydrologic Engineering Laboratory, University of California at Berkely.

Lane, E.W., and V.A. Koelzer, 1943. *Density of sediments deposited in reservoirs, a case study of methods used in measurement and analysis of sediment loads in streams*. Report No. 9, Interagency Committee on Water Resources.

Lee, C., and G. Foster, 2013. "Assessing the potential of reservoir outflow management to reduce sedimentation using continuous turbidity monitoring and reservoir modelling." *Hydrological Processes* v. 27, No. 10, p. 1426–1439.

Lewis, J., 2022. Regarding [EXTERNAL] 2009 OWRB Survey of Grand Lake O' the Cherokees. Email to: Brent Teske (Anchor QEA). April 20, 2022.

Lumborg, U., and H. Vested, 2008. *Modelling of Cohesive Sediment Dynamics* (Chapter 6).

McKnight, E.T., and R.P. Fischer, 1970. *Geology and Ore Deposits of the Picher Field Oklahoma and Kansas*. Geological Survey Professional Paper 588. U.S. Department of Interior.

McNeil, J., C. Taylor, and W. Lick, 1996. "Measurements of Erosion of Undisturbed Bottom Sediments with Depth." *Journal of Hydraulic Engineering* 122(6):316–324.

Moriasi, D.N., J.G. Arnold, M.W. Van Liew, R.L. Bingner, R.D. Harmel, and T.L. Veith, 2007. "Model Evaluation Guidelines for Systematic Quantification of Accuracy in Watershed Simulations." *Transactions of the American Society of Agricultural and Biological Engineers* 50(3): 885–900.

Mussetter, B., 1997. *Analysis of Backwater Conditions Caused by Pensacola Dam on the Neosho River in the Vicinity of Miami, Oklahoma*. Fort Collins, Colorado.

Mussetter, B., 1998. *Evaluation of the Roughness Characteristics of the Neosho River in the Vicinity of Miami, Oklahoma*. Fort Collins, Colorado.

Nash, J.E., and J.V. Sutcliffe, 1970. "River flow forecasting through conceptual models: Part 1. A discussion of principles." *Journal of Hydrology* 10(3): 282–290.

OWRB (Oklahoma Water Resources Board), 2009. *Hydrographic Survey of Grand Lake*.

Partheniades, E., 1962. "A study of erosion of cohesive soils in salt water." University of California at Berkely PhD Dissertation.

Pope, L.M., 2005. *Assessment of Contaminated Streambed Sediment in the Kansas Part of the Historic Tri-State Lead and Zinc Mining District, Cherokee County, 2004.* No. 2005-5251.

Science Applications International Corporation, 2001. *Results of the March 2001 Sub-Bottom Profiling and Sediment Profile Imaging of the Outer Gloucester Harbor*. SAIC Report 541. June 2001.

Simons, D.B., and F. Senturk, 1992. *Sediment Transport Technology Water and Sediment Dynamics*. Water Resource Publications.

Singh, J., H.V. Knapp, and M. Demissie, 2004. *Hydrologic modeling of the Iroquois River watershed using HSPF and SWAT*. ISCW CR 2004-08. Champaign, Ill.: Illinois State Water Survey.

Smith, D.C., 2016. *Occurrence, Distribution, and Volume of Metals-Contaminated Sediment of Selected Streams Draining the Tri-State Mining District, Missouri, Oklahoma, and Kansas, 2011*-12. U.S. Geological Survey Scientific Investigations Report 2016-5144, 86 p., Available at: http://dx.doi.org/10.3133/sir20165144.

Smith, S., S. Hunter, and C. Ashworth, 2017. *Bathymetric Surveys of the Neosho River, Spring River, and Elk River, Northeastern Oklahoma and Southwestern Missouri, 2016-2017.* Denver, Colorado: U.S. Geological Survey.

Strong, S., 2022. Regarding Lake O' the Cherokees (Grand Lake) gage questions. Email to: Jesse Piotrowski, Ryan Greif (Mead & Hunt); Jason Lewis (USGS). March 22, 2022.

Tetra Tech, 2015. *Hydraulic Analysis of the Effects of Pensacola Dam on Neosho River in the Vicinity of Miami, Oklahoma*. Prepared for City of Miami. December 9, 2015.

Tetra Tech, 2016. *Hydraulic Analysis to Evaluate the Impacts of the Rule Curve Change at Pensacola Dam on Neosho River Flooding in the Vicinity of Miami, Oklahoma*. Prepared for City of Miami. February 3, 2016.

Tetra Tech, 2018. *Pensacola hydropower project FERC Project No. 1494-438: Sedimentation Study Plan*. Fort Collins, Colorado: Tetra Tech, Inc.

USACE (U.S. Army Corps of Engineers), 1938. *Photostatic Copies of Plane Table Sheets of the Pensacola Reservoir Area Survey*.

USACE, 1941. *Pensacola Reservoir Computation Folder for Envelope Curve of Water Surface in Reservoir*.

USACE, 1942. *Pensacola Reservoir Computation Folder for Revised Envelope Curve of Water Surface in Reservoir*.

USACE, 1969. *Flood Plain Information, Neosho River and Tar Creek, Miami Oklahoma*. Tulsa, Oklahoma: USACE Tulsa District.

USACE, 1995. *Engineering Manual 1110-2-4000: Engineering and Design – Sedimentation Investigations of Rivers and Reservoirs*.

USACE, 1996. *Rule 26 Expert Report: An Evaluation of the Water Surface Elevations of the Grand (Neosho) River Upstream of the Pensacola Dam*. Prepared by Richard N. DeVries. March 14, 1996.

USACE, 1998. *Grand Lake, Oklahoma Real Estate Adequacy Study*.

USACE, 2002. *Engineering Manual 1110-2-1003: Engineering and Design – Hydrographic Surveying Version 3*.

USACE, 2016. *HEC-RAS River Analysis System User's Manual*. Davis: Hydrologic Engineering Center.

USACE, 2022. "Sediment Rating Curve Analysis Tool." Available at: Sediment Rating Curve Analysis Tool (army.mil).

USDA (U.S. Department of Agriculture), 1938. Aerial photography of McDonald County, MO. Aerial Photography Field Office, Washington, D.C.

USDA, 1939a. Aerial photography of Delaware County, OK. Aerial Photography Field Office, Washington, D.C.

USDA, 1939b. Aerial photography of Ottawa County, OK. Aerial Photography Field Office, Washington, D.C.

USDA, 1940. Aerial photography of Mayes County, OK. Aerial Photography Field Office, Washington, D.C.

USDA, 1990. *Engineering Field Manual, Chapter 4. Elementary Soil Engineering.* U.S. Department of Agriculture, Soil Conservation Service.

USGS (U.S. Geological Survey), 1907. *Wyandotte, OK-MO-KS Historical Map 125000-Scale*.

USGS, 2006. Collection of Water Samples (ver. 2.0). *U.S. Geological Survey Techniques of Water-Resources Investigations,* Book 9.

USGS, 2017. "National Geospatial Program." *The National Map Viewer*. Available at: https://www.usgs.gov/core-science-systems/national-geospatial-program/national-map.

USGS, 2020. *Bathymetric Map, Surface Area, and Capacity of Grand Lake O' the Cherokees, Northeastern Oklahoma, 2019*. Available at: https://pubs.er.usgs.gov/publication/sim3467.

USGS, 2021a. "USGS 07189000 Elk River near Tiff City, Mo." *National Water Information System*. Accessed February 5, 2021. Available at: https://waterdata.usgs.gov/mo/nwis/uv?site_no=07189000.

USGS, 2021b. "USGS 07185000 Neosho River near Commerce, OK." *National Water Information System*. Accessed February 5, 2021. Available at: https://waterdata.usgs.gov/nwis/uv?site_no=07185000.

USGS, 2021c. "USGS 07185080 Neosho River at Miami, OK." *National Water Information System*. Accessed February 5, 2021. Available at: https://waterdata.usgs.gov/ok/nwis/uv?site_no=07185080.

USGS, 2021d. "USGS 07185095 Tar Creek near Commerce, OK." *National Water Information System*. Accessed February 5, 2021. Available at: https://waterdata.usgs.gov/nwis/uv?site_no=07185090.

USGS, 2021e. "USGS 07185095 Tar Creek at 22nd Street Bridge at Miami, OK." *National Water Information System*. Accessed February 5, 2021. Available at: https://waterdata.usgs.gov/nwis/uv?site_no=07185095.

USGS, 2021f. "USGS 07188000 Spring River near Quapaw, OK." *National Water Information System*. Accessed February 5, 2021. Available at: https://waterdata.usgs.gov/nwis/uv?site_no=07188000.

USGS, 2021g. "USGS 07190000 Lake O' the Cherokees at Langley, OK." *National Water Information System*. Accessed February 5, 2021. Available at: https://waterdata.usgs.gov/ok/nwis/uv?site_no=07190000.

USSD (U.S. Society on Dams), 2015. *Modeling Sediment Movement in Reservoirs.* Prepared by the U.S. Society on Dams Committee on Hydraulics of Dams, Subcommittee on Reservoir Sedimentation, June 2015.

van Rijn, L.C., (n.d.). *Sedimentation of Sand and Mud in Reservoirs in Rivers*. Accessed April 11, 2022. Available at: https://www.leovanrijn-sediment.com/.

Vanoni, V.A. ed., 2006. *Sedimentation engineering*. American Society of Civil Engineers. March 2006.

Walling D.E., and D. Fang, 2003. "Recent trends in the suspended sediment loads of the world's rivers." *Global and Planetary Change* 39:111–126.

WEST (WEST Consultants), 2012. *Hydraulic and Sedimentation Modeling in HEC-RAS – Cochiti Baseline Study: Sediment Transport Modeling.* Prepared for the Pueblo de Cochiti and the U.S. Army Corps of Engineers, ABQ District.

WEST, 2022. Independent Technical Review of HEC-RAS Sediment Transport Model.

Zavala, C., 2020. "Hyperpycnal (over density) flows and deposits." *Journal of Palaeogeography 9*(1):1–21.